Diazonium salts induced anchoring process: mechanism, application(s)

Alice Mesnage

Thèse de doctorat de l'École Polytechnique

Spécialité : Science des matériaux

Présentée par

Alice MESNAGE

Diazonium salts induced anchoring process: mechanism, application(s)

Procédé d'ancrage induit par des sels de diazonium : mécanisme, application(s)

Soutenance prévue le 26 Septembre 2011 devant le jury composé de :

Pr. Etienne DUGUET	*Université Bordeaux 1*	Rapporteur
Dr. Mohamed CHEHIMI	*Université Paris Diderot*	Rapporteur
Dr. François OZANAM	*Ecole Polytechnique*	Examinateur
Pr. Claude CHEVROT	*Univeristé de Cergy-Pontoise*	Examinateur
Dr. Christine LAMOUROUX	*CEA Saclay*	Examinateur
Dr. Guy DENIAU	*CEA Saclay*	Directeur de thèse

Remerciements

Ce travail de thèse a été réalisé au Laboratoire de Chimie des Surfaces et Interfaces (LCSI) du Service de Physique et Chimie des Surfaces et Interfaces (SPCSI) du Commissariat à l'Energie Atomique et aux Energies Alternatives (CEA) de Saclay.

Je tiens tout d'abord à remercier Pr **Etienne Duguet** et Dr **Mohamed Chehimi**, les rapporteurs de ce travail, pour l'avoir jugé avec intérêt. Je suis également très reconnaissante à Pr **Claude Chevrot** et à Dr **Christine Lamouroux** d'avoir accepté de participer à ce jury ainsi qu'à Dr **François Ozanam** de l'avoir présidé.

Je tiens à exprimer ma profonde gratitude à **Serge Palacin**. Je ne saurais dire combien j'ai apprécié tes remarques et corrections aussi bien pour les articles que pour le manuscrit ainsi que ton soutien dans la « bataille finale ». Dans un tout autre contexte, merci de m'avoir (nous avoir) encouragée à pleine voix au bord du terrain !

Je remercie tout particulièrement mon directeur de thèse **Guy Deniau**. Merci pour ton optimisme, tes anecdotes croustillantes et tes histoires rocambolesques. Je croise les fesses pour que tu n'aies jamais à te mettre la rate au court-bouillon.

Je tiens également à remercier mes collègues du LCSI qui ont rendu, par leur bonne humeur, leur humour et leur esprit d'équipe, ces trois années si agréables.

Un merci tout particulier à **Alexandre**. Tu as été mon repère pendant ces trois ans, mon paramètre invariant tant au niveau de l'humeur que du caractère. Merci d'avoir accepté de partager ta chambre avec moi lors de nos conférences au Mexique et en Turquie ;-) !

Merci à **Romain** et **Federico** les « meilleurs » co-bureau … ou presque, d'avoir mis de la joie dans ce bureau par tous les moyens possibles et imaginables. N'oublions pas Toto Bat qui malheureusement nous a quittée depuis.

Je voudrais aussi adresser un énorme MERCI à **Lorraine**, **Nabila** et **Fanny** pour leur soutien mais surtout nos soirées « girls only ».

Merci à **Xavier** pour son aide inestimable ainsi qu'à tous les permanents du laboratoire qui m'ont tous soutenue et ont contribué de manière directe ou non à ce travail : **Bruno**, **Pascal**, **Pascale**, **Brigitte, Thomas**, **Julienne**, **Cécile**.

Un grand merci aussi à notre secrétaire **Catherine** grâce à qui toute démarche administrative paraît presque facile.

Merci aux stagiaires que j'ai pu encadrer pour leur travail et leur engagement : **Matthieu**, **Mohamed** et **Christophe**. J'espère avoir été à la hauteur de vos attentes.

Je remercie aussi tous ceux que j'ai croisés pendant ma thèse : **Frida**, **Adina**, **Amandine**, **Dimitri**, **Cédric**, **Olivier**, **Fabien**, **Cauê**, **Christian**, **Achraff**, **Corinne**, **Fabrice**, **Siddarth**, pour avoir contribué à la bonne ambiance au labo.

Je remercie également les collègues des laboratoires qui m'ont accueillie le temps de quelques expériences. Merci à **Diane L.**, **Vincent M.**, **Gilbert Z.**, **Stéphane E.**, **Stéphane C.**, **Pascale C.**, **Xavier S.** and **Géraldine H.** Merci également aux collègues du SPAM avec qui j'ai toujours gardé contact et que je suis venue embêter plus d'une fois : **Pardis**, **Vincent**, **Nathalie**, **Stéphanie**, **Yann**, **Olivier**, **Aurélie**, **Martine**, **Mathieu**, **Dominique**.

Je termine ces remerciements par adresser un grand merci à mes amis : **Nathalie**, **Génôme**, **Cécile**, **Fanny**, **Catherine**, … et à **ma famille** : mes parents, mes grands-parents, mon frère (je doute d'entendre un jour cette phrase : « Docteur Bouli, docteur Bouli, on le perd … »), mes tantes, mon parrain et sa famille ainsi que Mike (sorry, they did not give me a stethoscope) qui m'ont tous beaucoup soutenue. Enfin, je dédie ma thèse à « **Chapeau cloche** ». Merci pour tout ce que tu as toujours fait pour moi.

Table of contents

Abbreviations, notations & acronyms

A

ACN	Acetonitrile
AIBN	Azobisisobutyronitrile
AFM	Atomic force microscopy
ATRP	Atom transfer radical polymerization

B

BE	Binding energy

C

CE	Counter electrode
CNT	Carbone nanotube
CPS	Counts per second
CV	Cyclic voltammetry
CVD	Chemical vapor deposition

D

DFT	Density functional theory
DI	Deionized
DMF	N,N-dimethyl formamide
DNA	Deoxyribonucleic acid
DP_n	Number-average degree of polymerization
DSC	Differential scanning calorimetry

E

EPR	Electron paramagnetic resonance
ESI-MS	Electrospray ionization mass spectroscopy
eV	Electronvolt

F

FCC	Face-centred cubic
FET	Field effect transistor
FWHM	Full width at half maximum

G

GC	Glassy carbon
GCE	Glassy carbon electrode
GC-MS	Gas chromatography - mass spectroscopy

H

HEMA	Hydroxyethyl methacrylate
HF	Hydrofluoric acid
HFSC	Hyperfine splitting constant
HOPG	Highly ordered pyrolitic graphite

I

IR-ATR	Infrared-attenuated total reflection
IRRAS	Infrared reflection absorption spectroscopy
ITO	Indium tin oxide

L

LCSI	Chemistry of surfaces and interfaces laboratory
LFP	Francis Perrin laboratory

M

MBDT	4-methoxybenzene diazonium tetrafluoroborate
MCT	Mercury cadmium telluride
MNP	2-methyl-2-nitrosopropane

N

NBDP	4-nitrobenzene diazonium perchlorate
NBDT	4-nitrobenzene diazonium tetrafluoroborate
NEDA	N-(1-naphtyl-4-diazo-4-nitrobenzene) ethylenediamine
NHE	Normal hydrogen electrode
NMP	Nitroxide-mediated polymerization
NMR	Nuclear magnetic resonance

O

OCP	Open-circuit potential

P

PAA	Poly(acrylic acid)
PBMA	Poly(butyl methacrylate)
PE	Polyethylene
PHEMA	Poly(hydroxyethyl methacrylate)
PNP	Polynitrophenylene
PS	Polystyrene
PTFE	Poly(tetrafluoroethylene) or Teflon®

Q

QCM	Quartz crystal microbalance

R

RAFT	Reversible addition-fragmentation polymerization
RMS	Root mean square
ROMP	Ring-opening metathesis polymerization
RT	Room temperature

S

SAMs	Self-assembled monolayers
SCE	Saturated calomel electrode
SEC	Size exclusion chromatography
SECM	Scanning electrochemical microscopy
SEEP	Surface electroinitiated emulsion polymerization
SEM	Scanning electron microscopy
SERS	Surface-enhanced Raman scattering
SI-ATRP	Surface-initiated atom transfer radical polymerization
SI-NMP	Surface-initiated nitroxide-mediated polymerization
SIP	Surface-initiated polymerization
SIPP	Surface-initiated photopolymerization
SI-RAFT	Surface-initiated reversible addition-fragmentation polymerization
SWNT	Single-walled carbon nanotube

T

TEAP	Tetraethyl ammonium perchlorate
TEM	Transmission electron microscopy
TEMPO	2,2,6,6-Tetramethylpiperidin-1-yl)oxyl
TGA	Thermogravimetric analysis
THF	Tetrahydrofurane
ToF-SIMS	Time of flight-secondary ions mass spectroscopy

U

US	Ultrasonication
UV	Ultraviolet
UVO	UV-ozone

V

VC	Vitamin C or ascorbic acid

X

XRD	X-ray diffraction
XPS	X-ray photoelectron microscopy

Chemicals

1. Diazonium salts

Full name	Notation	Structure	Source
3,4,5-trichlorobezene diazonium salt tetrafluoroborate	-	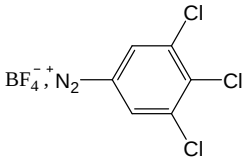	Homemade (LCSI)
4-bromobenzene diazonium tetrafluoroborate	-	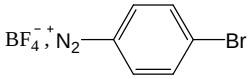	Aldrich, *96 %*
4-carboxybenzene diazonium tetrafluoroborate	-	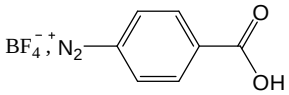	Homemade (LCSI)
4-methoxybenzene diazonium tetrafluoroborate	MBDT	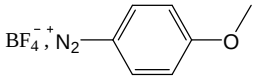	Aldrich, *98 %*
4-nitrobenzene diazonium perchlorate	NBDP	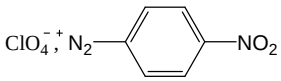	Homemade (LCSI)
4-nitrobenzene diazonium tetrafluoroborate	NBDT	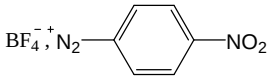	Aldrich, *97 %*
4-thiomethylbenzene diazonium tetrafluoroborate	-	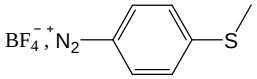	Homemade (LCSI)
4-trifluoromethylbenzene tetrafluoroborate	-	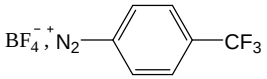	Homemade (LCSI)

2. Amines

Full name	Notation	Structure	Source
3,4,5-trichloroaniline	-	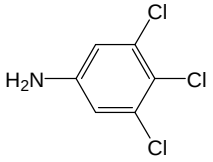	Aldrich, *97 %*
4-aminobenzoic acid	-	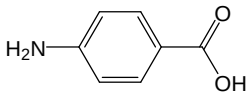	Aldrich, *99 %*
4-nitroaniline	-	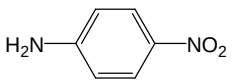	Aldrich, *>99 %*
4-(thiomethyl)aniline	-	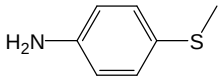	Aldrich, *98 %*
4-(trifluoromethyl)aniline	-	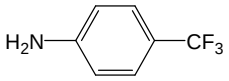	Aldrich, *99 %*

3. Reducing agents

Full name	Notation	Structure	Source
Ascorbic acid	VC	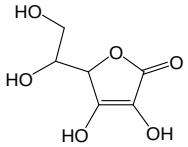	Aldrich, *>99 %*
Hypophosphorous acid	H_3PO_2	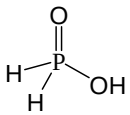	Aldrich, 50 wt%
Iron powder	Fe	-	VWR Prolabo

4. Solvents

Full name	Notation	Structure	Source
Acetonitrile	ACN	$CH_3–C\equiv N$	Aldrich, *>99 %*
Acetonitrile-d_3	-	$CD_3–C\equiv N$	Aldrich, *99.8 atom %*
Ammonium acetate	-	CH_3COO^-,NH_4^+	Aldrich, *>99.9 %*
Deionized water	H_2O DI	-	Millipore, *55MΩ*
Deuterium oxide	D_2O	-	Aldrich, *99.9 atom %*
Diethyl ether	-	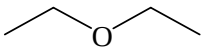	Aldrich
Ethanol	EtOH	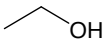	VWR, *96 %*
Fluoroboric acid	HBF_4	H^+,BF_4^-	Aldrich, 5*0 %*
Hydrochloric acid	HCl	H^+,Cl^-	VWR, *37 %*
Methanol	MeOH	$CH_3–OH$	Fluka
Nitric acid	HNO_3	H^+,NO_3^-	Aldrich, *>90 %*
N,N-dimethylformamide	DMF	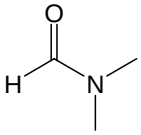	Carlo Erba reagent, *99.8 %*
Perchloric acid	$HClO_4$	H^+,ClO_4^-	Aldrich, 7*0 %*
Phosphoric acid	H_3PO_4	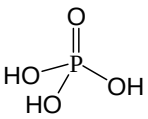	Aldrich, *>85 wt%*
Sulphuric acid	H_2SO_4	$2H^+,SO_4^{2-}$	Fischer Scientific, *>95 %*
Tetrahydrofuran	THF		AnalaRNormapur

5. Monomer/polymer

Full name	Notation	Structure	Source
2-hydroxyethyl methacrylate	HEMA	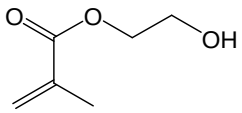	Aldrich, *97 %*
Poly(2-hydroxyethyl methacrylate)	PHEMA	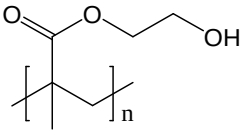	Aldrich, *Mv ca. 20,000*

6. Substrates

Full name	Notation	Structure	Source
Chromium	Cr	-	CERAC TM Inc, *99.99 %*
Germanium wafer	Ge	-	Neyco, *undoped, 1-30 Ω/cm*
Gold	Au	-	Williams Advanced Materials, *99.99 %*
Nickel	Ni	-	Marz, *99.995 %*
Polyethylene disk	PE	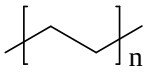	-
Platinum	Pt	-	Marz, *99.99 %*
Silicon wafer	Si	-	ITME, *N-type (100)*
Undoped and N-doped titanium oxide	TiO_2	-	Homemade (LFP)
Titanium oxide	P25 TiO_2	-	Evonik Degussa, *∅25nm, 80-20% anatase-rutile*

7. Supporting electrolytes

Full name	Notation	Structure	Source
Magnesium sulphate	$MgSO_4$	Mg^{2+},SO_4^{2-}	Aldrich
Potassium bromide	KBr	K^+,Br^-	Aldrich, *>99 %*
Potassium chloride	KCl	K^+,Cl^-	Fluka
Tetraethylammonium perchlorate	TEAP	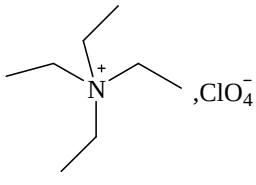	Acros

8. Others

Full name	Notation	Structure	Source
2-methyl-2-nitrosopropane	MNP	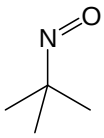	Homemade (LCSI)
2-methyl-2-nitrosopropane dimer	MNP dimer	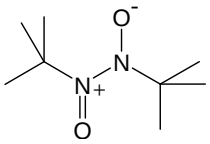	Aldrich
3-O-arenediazoascorbic acid	Diazoether	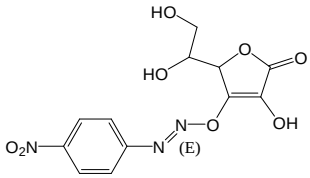	Homemade (LCSI)
4-hydroTEMPO	-	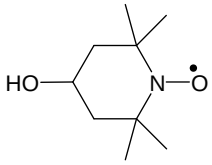	Aldrich, *97 %*
4-nitrophenol	-	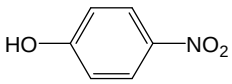	Aldrich, *>99 %*
Hydrobromic acid	HBr	H^+,Br^-	Aldrich, *48 %*
Hydrogen peroxide	H_2O_2	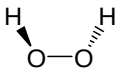	Aldrich, *35 wt%*
N-(1-naphthyl) ethylene diamine dihydrochloride	NEDA	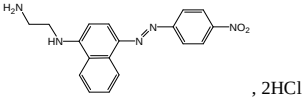 , 2HCl	Aldrich
Nitrobenzenethiol	-	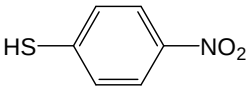	Aldrich, *80 %*
Nitrosonium tetrafluoroborate	$NOBF_4$	NO^+,BF_4^-	Aldrich, *95 %*
Sodium nitrite	$NaNO_2$	Na^+,NO_2^-	Fluka
Trifluoroacetic anhydride	-	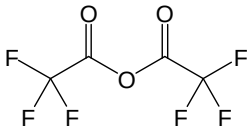	Aldrich, *>99.9 %*

INTRODUCTION

Products and materials coated with organic films are ubiquitous in everyday life. Indeed, the surface functionalization of materials is a very powerful tool since it permits to combine the bulk properties of materials and the properties of the coatings. It plays an important role in many industrial fields, for instance, paints and varnishes used in the automobile industry for preventing corrosion, non-toxic coatings in the food industry (e.g. non-stick cookware), lubricant coatings for electrical connectors, wear resistant and biocompatible coatings for medical devices and implants... In all applications, the coatings must be stable under harsh conditions, exhibit the required adhesive properties, protect substrates against corrosion for long periods, be either hydrophilic or hydrophobic and, last but not least, be safe for users.

Therefore, for almost a century, important work has been made in order to bring new properties to materials and nowadays surface modification of materials is more than ever a very attractive research subject related to a variety of promising industrial applications. In view of the increasing demand for surface-modified materials, various functionalization techniques were developed depending on the type of material to be modified and the nature of the coating to be added.

Numerous methods are commonly used for the formation of organic coatings on surfaces classified as physisorption and chemisorption techniques (respectively creating a weak chemical and a true chemical bonding between the organic components and the substrate) or classified as "*grafting to*" (polymer chains are initiated in solution and react with functional groups previously immobilized on the substrate) and "*grafting from*" (the polymerization is initiated on the surface from initiators previously attached on the substrate) processes. They include spin-coating, grafting of self-assembled monolayers (SAMs), cathodic electrografting, surface-initiated polymerizations and surface electroinitiated emulsion polymerization (SEEP). Most of these techniques generally require the use of organic solvents which make them poorly advisable from an environmental point of view. However, the recent development of the SEEP process was a real progress in the surface functionalization field. Indeed, deriving from cathodic electrografting of vinylic monomers, the SEEP process leads to the formation of grafted organic films on semi-conducting or conducting surfaces in water. It overcomes the limitations of the cathodic electrografting (drastic experimental conditions and restrictive range of monomers) and the other functionalization techniques by combining electroreduction of aryl diazonium salts and radical polymerization in dispersed aqueous medium. However, it still has some limitations related to its electrochemical nature, since the functionalized substrate has to be conductive.

In this context, in 2007, an innovative process for the functionalization of materials by organic coatings has been developed in our laboratory. Also based on the reduction of diazonium salts, it consists in performing this reaction chemically thanks to the addition of a reducing agent in solution (redox process) in presence or absence of a vinylic monomer. It is

thus no longer limited to semi-conducting or conducting substrates but can be applied to any type of materials. As a new technique, there was a real need for a better understanding of the grafting mechanism. Moreover, it was also interesting to test this process regarding applications. This study has been divided as follows:

In the first chapter presenting the context of this study, typical functionalization methods of organic coatings leading either to non-polymer layers or polymer films will be detailed. The principle, the substrates, the type of coating obtained as well as the advantages and limitations of each technique will be underlined.

The second chapter aims at presenting the genesis and the principle of the chemical anchoring process based on diazonium salts, to define and characterize its main components i.e. the diazonium salt, the reducing agent, the vinylic monomer and the substrates.

The following chapter is a study of the most basic reaction i.e. the spontaneous grafting (from solution only containing the diazonium salt). It will first deal with the various mechanisms proposed in the literature according to the substrate and to the work aiming at demonstrating the covalent nature of the substrate-surface bonds. Then, it will focus on our attempts to reveal such bonds and the explanation of the spontaneous grafting mechanism on gold substrates.

The fourth chapter, which is dedicated to the study of the reaction when a reducing agent is added in solution (redox-induced grafting), will start with the investigation of the chemical composition of the organic grafted films and the study of the effect of the variation of experimental parameters. Then, thanks to dual surface-solution analyses, an explanation of the grafting mechanism will be proposed.

In the fifth chapter, the redox-induced grafting in presence of a vinylic monomer (Graftfast^{TM} process) which leads to the grafting of polymer films on any type of materials will be investigated. The films will be deeply characterized in terms of composition, structure, morphology, homogeneity, thickness and a wide range of experimental conditions will be explored. Subsequently, by combining surface with solution analyses, a grafting mechanism for the formation of those polymer films will be established.

To finish, the last chapter will be devoted to a preliminary study consisting in evaluating the feasibility of grafting a polymer layer (by the Graftfast^{TM} process) on TiO_2 nanoparticles which will be used in sunscreen products for filtering UVA as well as UVB radiations.

CHAPTER I

Surface functionalization by organic coatings

The surface modification of materials is a way to combine bulk properties (e.g. mechanical, electrical or optical) with the appropriate surface properties (for instance protection against corrosion, hydrophobicity/hydrophilicity, biocompatibility, adhesion, wear resistance…). Tailoring the surface properties of materials by organic coatings is of great interest from an industrial point of view. Therefore, a wide range of techniques has been developed. Among requirements for organic coatings, the stability under usage conditions, which strongly depends on the actual bonding between the substrate and the coating, is the most frequent. The known methods producing organic films on substrates are thus usually classified according to the type of interactions (weak or strong) between the substrate and the organic film i.e. the kind of bonds provided at the interface. "Soft methods" giving only weak chemical bonds between the organic components and the substrate can be gathered as physisorption techniques. On the contrary, chemisorption methods include grafting techniques in which the organic layer is covalently bound to the substrate.

In this chapter presenting the context of our study, we will focus on the main surface functionalization techniques leading to either non-polymer organic films[a] or polymer films on flat surfaces.

I.1 - Non-polymer organic coatings

Various methods provide non-polymer organic films. We will in particular deal with the chemical vapor deposition technique or the Langmuir-Blodgett method which both give physisorbed films. Based on stronger interactions between the organic layer and the substrate, the formation of self-assembled monolayer will also be described. To finish, we will present oxidative as well as reductive electrograftings methods to prepare chemisorbed films.

I.1.1 - Vapor deposition

Physical or chemical vapor deposition[1, 2] (respectively PVD and CVD) is typically used for inorganic coatings (ceramics, silicon carbide, nitrides, metals) but can also be applied to small organic molecules, for example, in the fabrication of organic thin-film transistors, organic light-emitting diodes and organic photovoltaic cells.

In a typical CVD process, the substrate is exposed to precursors in gaseous phase which react and/or decompose at the surface of the substrate leading to the formation of the deposited film (Scheme 1). Soft conditions (low pressure, flash heating) are generally chosen to prevent thermal degradation of the organics during vaporization and retain the molecular properties in the final film. Hence, in the case of organic coatings, only weak interactions can be created between the molecular film and the substrate.

[a] In some cases, polymer-like films can also be obtained by those methods.

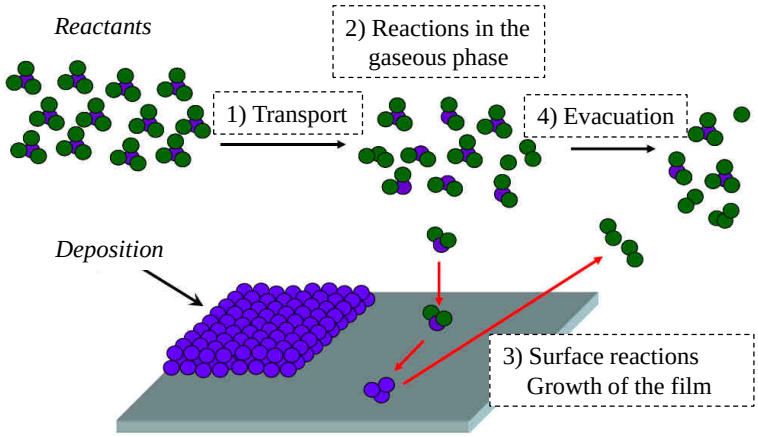

Scheme 1 – Principle of the chemical vapor deposition process extracted from Roucoules's work[3].

Vapor deposition works under vacuum and provides thin films from gaseous precursors. This technique is limited to organic coatings that are not prone to mechanical or thermal constraints. Moreover, vapor-deposited films can locally be highly crystalline but are often prone to defects such as grain boundaries or cracks.

I.1.2 - **Langmuir-Blodgett technique**

The Langmuir-Blodgett technique was developed in 1934 by I. Langmuir and K. Blodgett, pioneers in the field of surface functionalization by organic layers[4]. Historically used with fatty acids on glass, it was adapted to other amphiphilic systems (surfactants, lipids…). However, nowadays the use of Langmuir-Blodgett technique is widened to non-amphiphilic systems of different types such as nanoparticles, polymers[5] or biological objects.

This principle of this technique is based on the organisation of the amphiphilic molecules at the water surface according to the affinities of both parts of the molecules. The solution containing the molecules of interest is deposited in droplets at the water surface. The molecular density at the air-water interface is adjusted by manipulating PTFE moveable barriers. By moving closer the two barriers, the film is compressed which changes the surface tension of the air-water interface and leads to a vertical and ordered organisation of the molecules. The so-formed monolayer, called Langmuir film, can be transferred to a flat solid support by an upstroke of the immersed substrate through the monolayer (Scheme 2). During the vertical transfer, the surface pressure of the monolayer is kept constant by automatically compressing the film by the barriers to account for the material loss. According to the nature of the substrate (hydrophilic or hydrophobic), two types of structures can be obtained. In the case of hydrophilic substrates (glass, silicon wafers…), the monolayer will be transferred with the polar heads of the molecules in contact with the substrate (as represented on Scheme 2). Concerning hydrophobic substrates, the aliphatic tails get in contact with the substrate during the transfer step. By performing multiple immersions of the substrate, the two effects described above

combine. It conducts to the successive deposition of layers at the air-water interface when inserting or withdrawing the substrate and thus leads to the formation of multilayers films.

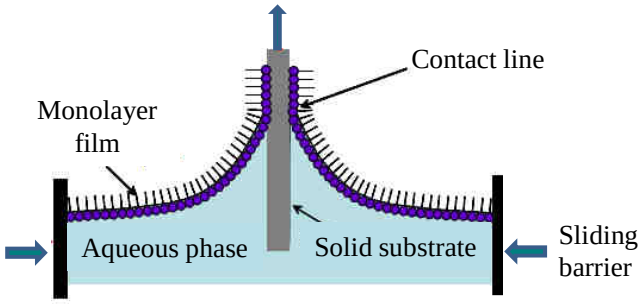

Scheme 2 – Hydrophilic Langmuir-Blodgett transfer onto a flat solid substrate extracted from Roucoules's work[3].

The Langmuir-Blodgett technique leads to thin and uniform organic films of controlled thickness and high degree of structural order with an excellent reproducibility. Such films can exhibit various properties (electrical, biological, photochemical…) and many possible applications have been suggested over years[6]. However, the main drawback of those films is linked to their weak mechanical and thermal resistance as well as the possibility to wash them off the substrate easily with usual organic solvents.

I.1.3 - **Self-assembled monolayers**

Since almost thirty years, an easy method to prepare thin and organized organic films called self-assembled monolayers (SAMs)[7] is available. Contrary to the Langmuir-Blodgett films obtained through a mechanical process, SAMs are formed spontaneously by simply immersing the appropriate substrate into a solution of the surface-active material[8]. Those precursor molecules have a characteristic structure leading to the molecular orientation of the films. As represented on Scheme 3, the molecules are usually composed of an interface group and a head group (capable of specific interactions with the substrate) linked by an alkyl chain (or other molecular skeleton). The driving force for the spontaneous formation of the 2D assembly includes chemical bond formation of molecules with the surface and Van der Waals interactions between neighboring chemisorbed molecules.

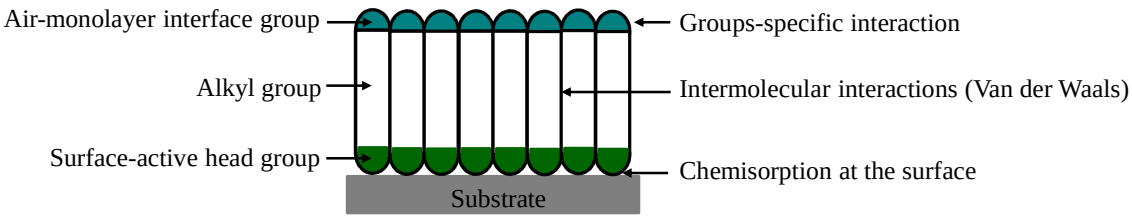

Scheme 3 – Representation of the theoretical structure of a SAM.

According to the nature of head group/substrate couple, various types of SAMs can be obtained. The most commonly studied are: alkanethiols (R-SH) or sulfides (R-S-S-R and R-S-R) on gold and silver[9], alkoxysilanes on oxides[10] and alkenes on silicon[11].

Since their discovery in 1983 by Nuzzo and Allara[12], SAMs of thiols and dialkyldisulfides on gold surfaces have constantly attracted a great interest. Investigations showed that long thiol chains (C18) tend to give film with a thickness close to molecular monolayer (<10 nm) and with a stable and organized structure (allowed from the weak Au-S bond). Moreover, it has been demonstrated that the alkyl chains form an inclination angle of 20-35° with the substrate[13] (Scheme 4). To date, the formation mechanism and the nature of the bond between the thiol and gold are not yet fully understood.

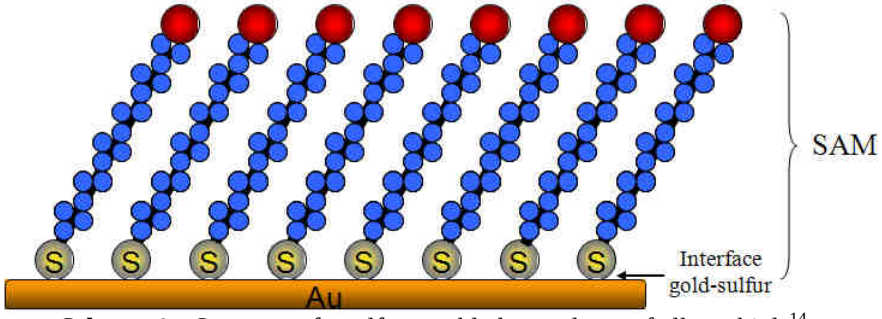

Scheme 4 – Structure of a self-assembled monolayer of alkanethiols[14].

In the case of SAMs of alkoxysilanes on oxides, the process can be decomposed in two steps[15] as represented on Scheme 5: (i) the organosilane is hydrolyzed by water which is either pre-adsorbed on the surface or present in the solvent and (ii) the hydrolyzed silanol is adsorbed via hydrogen bonds and can react with the surface silanol groups at the surface to form a siloxane Si-O-Si bond.

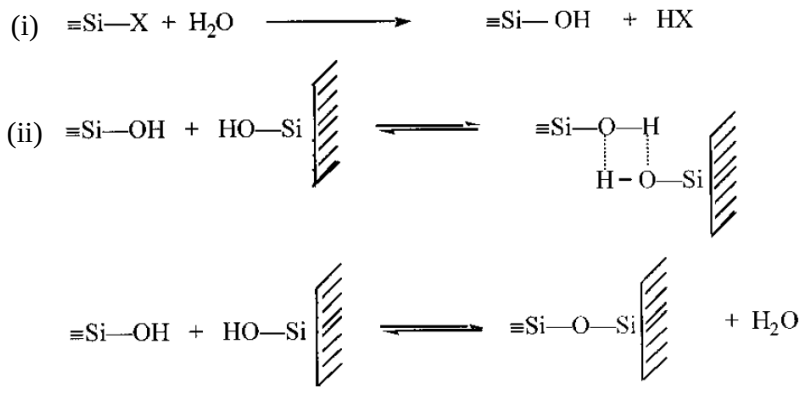

Scheme 5 – Formation mechanism of SAMs of alkoxysilanes on silica from Duchet's work[15].

Self-assembly is a very attractive technique for the formation of organic coatings. Indeed, it combines low-cost processes, soft conditions that prevent degradation of the coated molecules and spontaneous formation of chemical linkages between the molecules and the substrates. Very stable coatings are obtained with silanes on oxides and alkenes on silicon. In contrast, noble

metals with sulphur-containing molecules give weak bonds that can be easily broken under harsh conditions (high temperature, oxidative or reductive potentials, solvents...). Multilayers can be obtained by sequential steps but self-assembly is the method of choice for the synthesis of molecular-thick films for a use under moderate conditions with potential applications, for instance, in surface passivation, microlithography[16] or molecular electronics[17].

I.1.4 - **Oxidative electrograftings**

On top of the well-known methods for surface functionalization with non-polymer organic layers, oxidative electrograftings also appeared suitable for such purpose from different reagents: Grignard reagents, carboxylates, amines and alcohols. As deeply described in terms of mechanism as well as applications in the recent review by Bélanger and Pinson on electrografting[18], those methods for surface modification will be rapidly presented.

I.1.4.1 - Grignard reagents

Anodic electrografting of Grignard reagents (RMgX) has been investigated on silicon (SiH surface obtained by HF or NH_4F treatment). In order to avoid the oxidation of Si, experiments are performed in oxygen-free conditions. Moreover, as Grignard reagents react rapidly with water, work is performed is an anhydrous environment. Those particular experimental conditions constitute the main drawback of this technique. However, SiH surfaces have already been successfully modified by a large range of Grignard reagents with a methyl[19], alkyl[20], aryl[21] (giving polymer-like grafted films) or vinyl and ethynyl[22, 23] (giving polymer films) skeleton.

A simplified electrografting mechanism is presented on Scheme 6. The first step consists in the oxidation of the organomagnesium compound into a radical (Scheme 6i). The alkyl radical $R^{\bullet}$ may abstract a hydrogen atom from the hydrogenated silicon surface (Scheme 6ii). The so-formed radical at the surface can then react with the Grignard reagent or another $R^{\bullet}$ (Scheme 6iii).

(i) $RMgX + h^+ \rightarrow R^{\bullet} + MgX^+$

(ii) $\equiv SiH + R^{\bullet} \rightarrow \equiv Si^{\bullet} + RH$ (fast)

(iii) $\equiv Si^{\bullet} + RMgX + h^+ \rightarrow \equiv SiR + MgX^+$ (slow)

or $\equiv Si^{\bullet} + R^{\bullet} \rightarrow \equiv SiR$ (slow)

Scheme 6 – Oxidative electrografting of alkyl Grignard reagents on Si extracted from Etcheberry and coworkers' work[20], (h^+ = hole).

I.1.4.2 - Carboxylates

Only described on carbon (for instance glassy carbon, carbon fibers), the oxidative electrografting of carboxylates leads to the formation of an attached organic layer. The mechanism of this process is based on the Kolbe reaction (Scheme 7) which provides dimers by electrooxidation of carboxylates. However, the electrografting mechanism needs to be clarified.

Indeed, the growth mechanism of the layer has not been fully explained and questions remain on the involvement of radicals or carbocations in the grafting reaction.

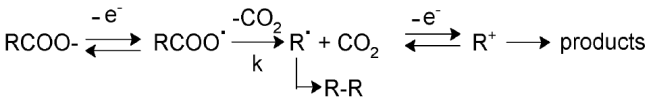

Scheme 7 – The Kolbe reaction extracted from Pinson's review[18].

I.1.4.3 - Alcohols

The oxidative electrografting of some alcohols (see references 82-100 herein Pinson's review[18]), for instance, 1-octanol, 1-ω-alkanediols, triethylene glycol, polyvinylalcohol), in acidic solution (Scheme 8) or aqueous $LiClO_4$ solution, leads to the formation of an organic layer on carbon (a polymer film is formed only when using the latter reactant).

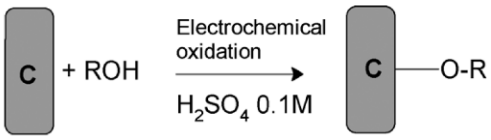

Scheme 8 – The electrooxidative grafting of alcohols on carbon extracted from Pinson's review[18].

Although not deeply investigated, the mechanism of this process may be based on the oxidation of the aromatic moieties at the surface of carbon which forms radical cations that undergo a nucleophilic attack by alcohols. This method has already been applied for instance to create sensors and limit the adsorption of proteins.

I.1.4.4 - Amines

The oxidative electrografting of amines is an irreversible one-electron redox process leading to the formation of covalently bound thin organic layers resisting to ultrasonic cleaning[24-26]. The efficiency of the electrografting is dependent on the redox potential of the amine, which means primary amines give better results than secondary and tertiary ones. Concerning the electrografting mechanism, recent investigations[24] have proposed that the initial radical cation (formed by oxidation at the electrode) deprotonates, thus providing a radical carbon and then an aminyl radical able to attach to the surface (Scheme 9).

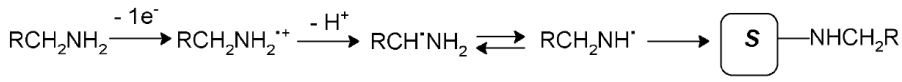

Scheme 9 – The oxidative electrografting mechanism of amines extracted from Pinson's review[18].

The large variety of amines commercially available and the possibility to work in many solvents make this process very versatile. N-modified surfaces have already been used for example to develop H_2O_2 biosensors, pH probes[27] or for the immobilization of DNA and proteins[28]. However, as for the oxidative electrografting of carboxylates and alcohols, the method suffers from the limited number of substrates adapted for the reaction i.e. substrates

withstanding harsh oxidative conditions (> 1 V/SCE for aliphatic amines in aprotic media[24]) which are, in this case, limited to carbon, gold and platinum.

I.1.5 - **Reductive electrograftings**

To finish the non-exhaustive presentation of the techniques of surface modification by non-polymer organic coatings, we will succinctly introduce the reductive electrografting methods of alkyl halides and various onium salts with a strong focus on the electrografting of diazonium salts.

I.1.5.1 - Alkyl halides

The electrochemical reduction of alkyl halides offers interesting possibilities for the synthesis of strongly attached alkyl layers. Efficient in aprotic medium, it was subject to many investigations with a large variety of molecules (mainly alkyl bromides and iodides) and on many substrates: glassy carbon, porous hydrogenated silicon and metals (Au, Fe, Cu, Ag, Pd). In particular, the alkylation of Si surface was shown to improve the chemical stability of the modified surfaces (against oxidation and corrosion)[29].

No general mechanism has unfortunately been proposed for that process, but a few assumptions can be made (see the electrografting review for a discussion on the mechanism according to the experimental conditions[18]). Briefly, the first step consists in the reduction of the alkyl halide at the electrode which forms the corresponding radical. The second step is likely to be the grafting of this radical onto the surface but in some cases, it could also be a reduction of the radical leading to the corresponding anion.

I.1.5.2 - Onium salts (in particular diazonium salts)

The electrochemistry of ammonium, phosphonium, sulfonium, bromonium, iodonium, xenonium, stilbonium and diazonium salts has been investigated in specific experimental conditions: solvents, substrates, potentials, temperatures, etc (references 665-699 in Pinson's review on electrografting[18]). Various mechanisms have been proposed according to the onium salts considered and the electrografting conditions. Xenonium salts are powerful oxidant, stronger than diazonium salts while phosphonium salts are the least oxidant of all. In the case of the electrografting of bromonium, iodonium salts and diazonium salts, it is likely that a similar mechanism is involved.

As aryldiazonium salts (N_2^+-ϕ-R) are the molecules at the heart of this work, their reductive electrografting will be more detailed. Since the first report in 1992 by Delamar, Hitmi, Pinson and Savéant on carbon surface[30], the electrografting of diazonium salts has been widely and deeply reviewed (Downard[31], Tessier[14], Pinson and coll.[18, 32] and references 233-243 herein the last review quoted). To date, the techniques have been extended to a large number of surfaces which can be classified in five groups:

- Carbon surfaces (glassy carbon, highly ordered pyrolytic graphite (HOPG), graphene, carbon fibres, carbon blacks, carbon nanotubes, etc)[31, 33-42],
- Metallic surfaces (noble metals[43-46]: Pt, Au and other metals[33, 47-54]: Co, Fe, Cu, Zn, Ni, Pd),
- Semi-conductors (Si[55-58], GaAs[55], diamond[59], TiO_2[60]),
- Organic surfaces (Teflon®[61]),
- Conductive oxides (ITO[62]).

In addition to the diversity of substrates, the method is also very interesting thanks to the large amount of functionalities available, the simplicity of synthesis of the precursors and their low potential of reduction (0.2 to -0.5 V/SCE according to the type of substituent of the aromatic ring in organic solvent). Indeed, diazonium salts are easy to synthesize (even *in situ*[36, 45, 63]) from the corresponding amines giving a large choice in substituents particularly *in para* of the aryldiazonium cation (see II.3.1.1 for more details).

According to the experimental conditions (solvent, substrate, reaction time, concentration in diazonium salt and potential), the thickness of the grafted films varies from a monolayer of aryl groups to a few hundred nanometer-thick film. In the latter case, the films obtained are multilayers of phenyl groups which can be considered tantamount to a polymer-like film of polyphenylene. In all cases, the film is strongly grafted on the substrate. The covalent nature of the interface aryl-substrate bond has been demonstrated several times by more or less direct techniques (see III.2.1.3 for an overview of those studies).

Usually performed in acetonitrile (ACN), this reaction can also be conducted in aqueous acidic solutions or ionic liquids. From a mechanistic point of view, it was demonstrated that the electrochemical reduction of the diazonium salt leads to the formation of aryl radicals able to graft on the electrode (Scheme 10). In the growth process of the films, the aryl radicals react on top of each other by radical aromatic substitutions (cf IV.2.3.2). Therefore, the electrografting of polyaryl films follows a chemical radical chain process equivalent to "*grafting from*". However, variations in grafting mechanism can be observed according to the nature of the substrate[18] (e.g. hydrogenated monocrystalline surface of Si(111)[56]).

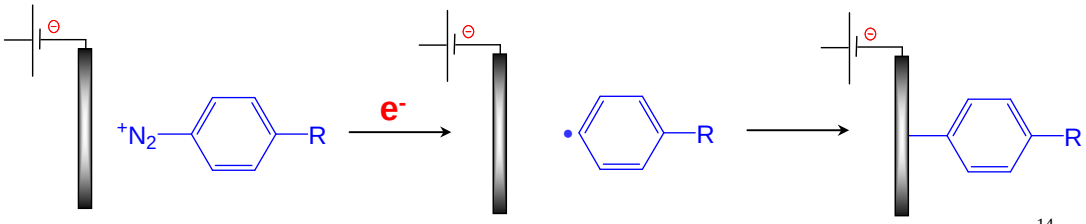

Scheme 10 – Principle of the reductive electrografting of diazonium salts from Tessier's work[14].

The molecular reductive electrografting of diazonium salts has been investigated with a view to numerous applications, for instance, protection against corrosion[49], chemical sensors, attachment of biomolecules, microelectronics (see references 473-650 in Pinson's last review[18]).

Recently, some authors have reported the spontaneous grafting (without the use of a potenstiostat) of aryl radicals on various substrates by simple immersion of the samples. This method will be described in details in chapter III.

To summarize, the covalent electrografting of diazonium salts has attracted considerable attention in the last few years due to the numerous advantages of this method: low cost, rapidity, easiness to set up, diversity of the functions to give to the substrate and large number of possible substrates.

I.2 - Polymer organic coatings

Let's now focus on the most common methods employed to modify the surface of materials with polymer coatings including physisorption as well as chemisorption techniques. We have split them in two parts depending on whether the presence of a primer layer on the substrate is required in the process or not.

I.2.1 - Direct methods

In this section, various methods allowing the direct formation of polymer films (i.e. straight on the substrate) will be presented such as the spin coating, dip coating, spray coating and layer by layer coating which all lead to physisorbed polymer films, but also plasma polymerization and electrochemical processes (electropolymerisation of conducting polymers, cathodic electrografting and diazonium based electrografting in presence of vinylic monomers) which provide covalently grafted polymer films.

I.2.1.1 - Spin coating

Spin-coating is the most widely used technique for organic coating based on polymer solutions particularly for industrial applications, for instance, photosensitive resins in lithography for microelectronics, antireflection coatings for flat-screen displays, television tubes and compact discs.

The technique is very simple to set up and its principle is explained on Scheme 11. An excess amount of the coating solution is deposited on the substrate which is then accelerated in order to spread the solution thanks to centrifugal force. Although the spreading phase only lasts a few seconds, the rotation is maintained longer in order to evacuate the solution at the edges of the substrate and to reach the desired thickness while the solvent simultaneously evaporates.

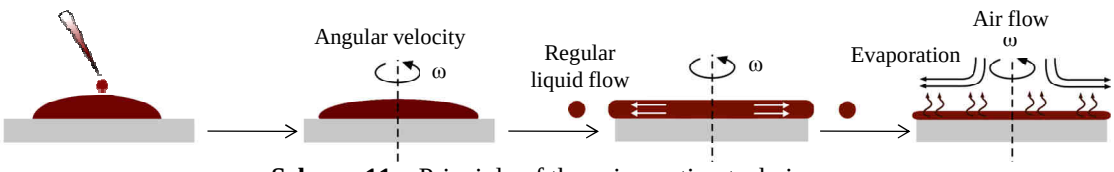

Scheme 11 – Principle of the spin-coating technique.

This technique reproducibly leads to thin polymer films on flat surfaces with controlled thicknesses. The characteristics of the deposited film (particularly the thickness and homogeneity) depend on parameters such as the rotation rate, the temperature, the concentration of the solution, its viscosity, the volatility of the solvent or the atmosphere. Typically, the film thickness ranges from 1 to 200 µm. However, thinner films can be produced with dilute solutions and high spinning rates. In comparison to other coating techniques, spin-coating has a major advantage since it can be performed on large surfaces (with limitations on high roughness substrates) while still giving continuous and homogenous films. Since the organic film is only physisorbed on the substrate and can be removed by rinsing in a good solvent of the polymer, the spin-coating technique is mainly ideal for temporary organic coatings as in the case of lithographic resins.

I.2.1.2 - Dip coating

The dip-coating technique is a very often used method to obtain thin polymer films (up to a few hundred micrometers) on flat or cylindrical substrates. It consists in simply immersing the substrate in a solution of the coating polymer. The polymer layer is deposited when the substrate is removed from the solution and the film is formed after evaporation of the volatile solvent (Scheme 12). This reproducible technique leads to the formation of homogeneous films. The thickness of the polymer layer can be controlled by taking into account the characteristics of the solution (viscosity forces, surface tension, evaporation speed of the solvent) as well as the withdrawing speed of the substrate from the solution. The faster the substrate is removed, the thicker the polymer film.

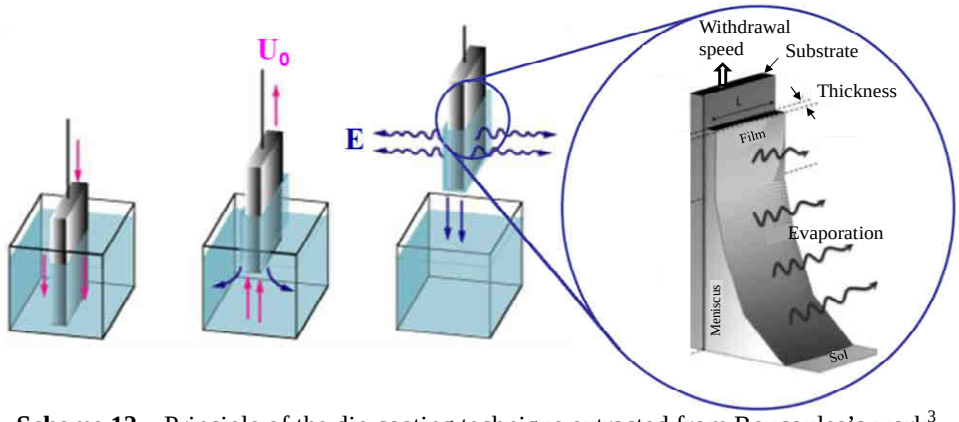

Scheme 12 – Principle of the dip coating technique extracted from Roucoules's work[3].

I.2.1.3 - Spray coating

Spray coating is a technique widely used in the industry to apply coatings, paints, disinfectants, cleaners, chemicals in particular polymers, powders or other industrial materials to surfaces with a high accuracy, reliability, repeatability and efficiency. However, similarly to the two methods presented above, the films can be removed from the substrate by simply washing it with the appropriated solvent.

In the case of spray coating of fluids, a spray gun is used to produce the spray by forcing the fluid under high pressure through a small nozzle. As a result of the friction between the fluid and the air, the fluid breaks into fragments and then droplets which are blasted on the substrate (Scheme 13). The factors affecting the deposition include the atomizer orifice size and shape, the fluid pressure and the fluid viscosity.

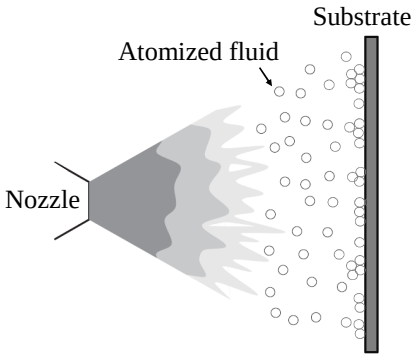

Scheme 13 – Fluid atomization process in spray coating.

I.2.1.4 - Layer by layer coatings

Layer by layer deposition was discovered by Decher in the early nineties[64, 65]. It leads to the formation of mixed polymer films by using a couple of polymers which can, in contact, develop specific interactions, for instance, hydrogen bonds or electrostatic interactions in the case of polyelectrolytes. Easy to set up, this process has been largely applied notably in the field of light-emitting diodes[66] and biomaterials[67].

The construction of films by the layer by layer technique lies on the alternate adsorption of two different compounds. The cohesion of the film is provided by the complementary chemical functions borne by the two polymers. In the most common case i.e. the formation of mutilayer films of polyelectrolytes by dipping, the film is obtained by the alternate immersion of the substrate in polyelectrolyte solutions (polyanion or polycation) and rinsing solutions (Scheme 14).

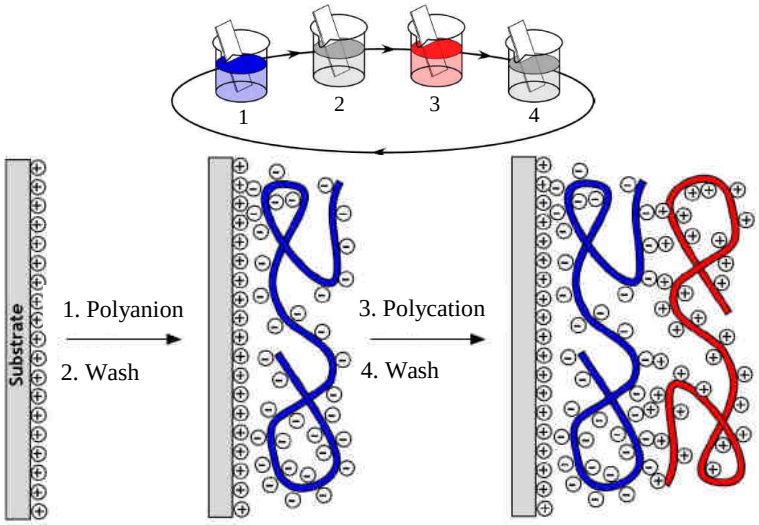

Scheme 14 – Formation of mutilayers film of polyelectrolytes by the layer by layer process (dipping) extracted from Decher's work[64].

The properties of the film depend on the dipping time, the concentrations of the solutions, the pH, the ionic strength and the temperature. The layers in contact are highly interpenetrated; hence, the polymer film is resistant to mechanical constraints which allows the formation of self-supported films by the specific dissolution of the substrate[68]. Such films are however sensitive to ionic solutions which may affect the coulombic interactions between the various layers.

I.2.1.5 - Plasma polymerization

Plasma polymerization (or glow discharge polymerization), known for more than 50 years[69, 70], produces highly robust polymeric coatings. This technique has been widely used for corrosion protection, scratch-resistant coatings and antisoiling applications[71]. However, the deposition rates are generally low and the process is costly.

The fast application of an increasing voltage between the two parallel plate electrodes in the system induces an abrupt increase in current which leads to the breakdown of the gases in between the electrodes (Scheme 15). The collisions of high-energy electrons with hydrocarbon molecules produce reactive species such as positive ions, excited molecular or atomic fragments, radicals, etc. The emission of photons by excited molecules creates the glow. Strong chemical linkages are then formed between the reactive species created in the glow and the substrate which leads to highly adherent films.

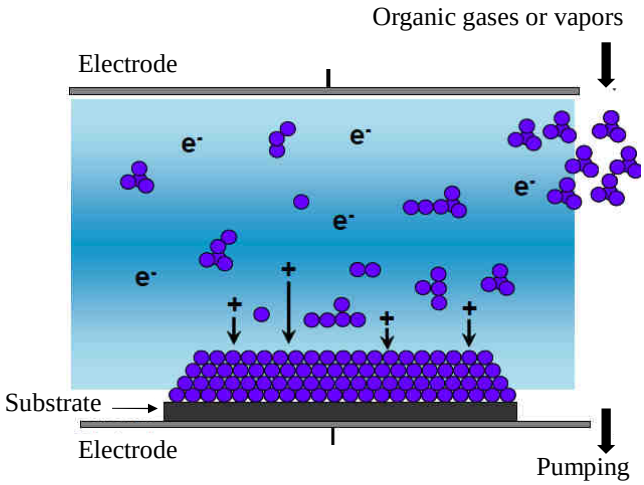

Scheme 15 – Principle of plasma polymerization extracted from Roucoules's work[3].

Plasma polymerization depends on the monomer flow rate, the system pressure and discharge power among other variable parameters such as the geometry of the system, the reactivity of the starting material, the frequency of the excitation signal and the temperature of the substrate. Since the glow discharge is very energetic, plasma polymerization can also be used to produce polymer films from organic gases or vapors that are not regarded as monomers for conventional polymerization. The final deposit is very different from a conventional polymer film: the plasma polymer does not contain regular repeated units but branched and

randomly terminated chains with a high degree of cross-linking. In some cases, free radicals remain trapped within the highly cross-linked structure and their subsequent recombination results in ageing of the coating.

I.2.1.6 - Electropolymerisation of conducting polymer

The electropolymerisation of conducting polymer presents some specific advantages: rapidity, simplicity, absence of catalyst, control of the thickness of the film and possibility to characterise the growth of the film *in situ* by electrochemical or spectroscopic techniques. Researches on conductive polymers were highly motivated with a view to their applications in technological fields as in photovoltaic cells[72] and field effect transistors[73].

Among the conducting polymers (characterised by a conjugated system of bonds) composed of aromatic units as benzene[74], aniline or pyrrole[75], the polythiophene[73, 76] and its derivatives are the most investigated polymers due to their stability and high conductivity.

The electropolymerization of thiophene occurs via the succession of electrochemical and chemical steps (Scheme 16). The primer electrochemical step consists in the oxidation of the monomer in a radical cation at the anode (when the potential is equal or higher than the oxidation potential of the monomer). The coupling of two radicals leads to the formation of the dihydrodimer dication which rearranges in the neutral dimer. The rearomatization is the driving force of the chemical step. The dimer, which can be oxidized more easily than its monomer, is converted in radical cation and the polymerization carries on until the oligomer becomes insoluble in the electrolytic medium and precipitates onto the electrode surface.

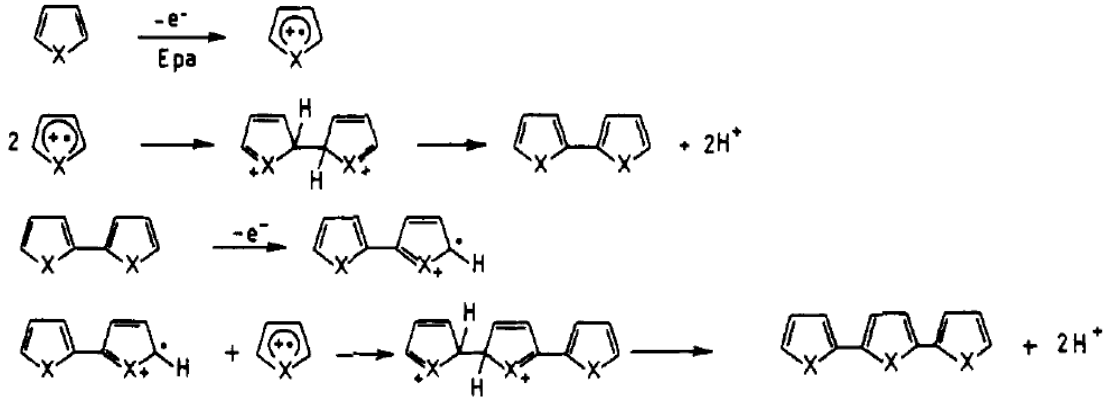

Scheme 16 – Mechanism of electropolymerization of conducting polymer (thiophene and pyrrole respectively when X=S and NH) extracted from Roncali's work[76].

I.2.1.7 - Cathodic electrografting of vinylic monomer

As originally shown by Lecayon from 1982 and reviewed by Palacin *et al.*[77], strongly adhesive polymer films are formed on any conductive surface by cathodic electrografting from anhydrous solutions of vinylic monomers such as acrylonitrile and acrylates.

It allows the deposition of very thin polymer films (typically between a monolayer and 500 nm) via very strong substrate-molecule links. Contrary to electropolymerization of

conducting polymers which requires a potential supply throughout deposition to fuel the redox processes, cathodic electrografting is an electron-initiated process which requires a charged electrode only for the grafting step, but not for thickening. As a cathodic process, it can generally be applied to various metallic and semi-conducting substrates without any concern over oxide formation.

This technique is based on an initiation of polymerisation by electrochemical activation of the monomer (reduction peak around -2.5 V/Ag/AgCl for acrylates and acrylonitrile). The reduction of the vinylic monomer gives a radical anion (Scheme 17i) that grafts to the cathode to give a metastable grafted anion (Scheme 17ii). The grafted anion can react with another monomer to propagate the grafted polymer chain (Scheme 17iii) or it may also be ejected from the surface (Scheme 17iv) which frees the radical anion in solution. Then, this free radical anion evolves by radical-radical coupling into a dianion that starts to polymerize in solution to give non-grafted polymer chains[78]. The propagation step is purely chemical and thus independent of the applied tension. Hence the final thickness of the grafted films only depends on the experimental conditions: concentration, solvent, temperature…

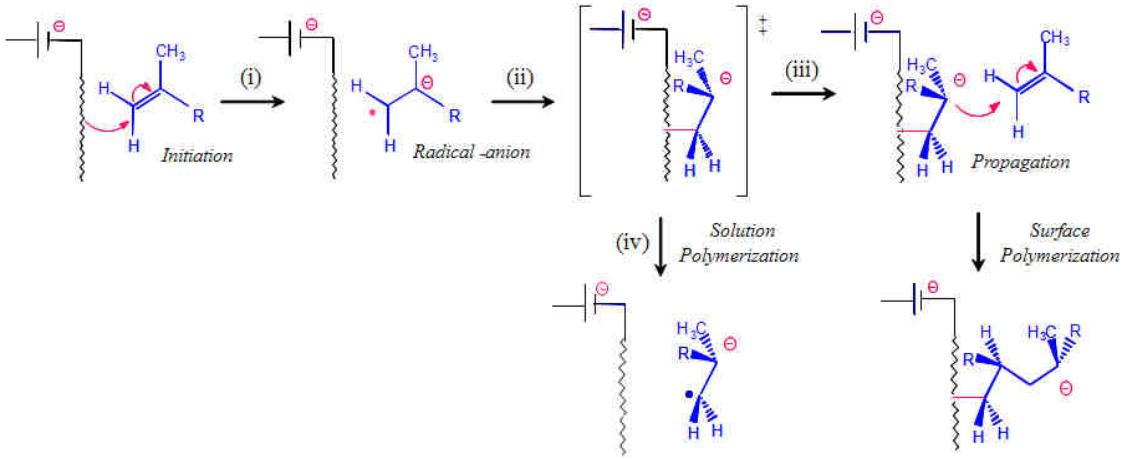

Scheme 17 – Proposed mechanism of the cathodic electrografting of methacrylic derivates. It shows the competition between grafting to the surface of the cathode and polymerization in solution[14].

The cathodic electrografting of vinylic polymers produces truly grafted polymer films and is a "*grafting from*" process as respectively demonstrated by Deniau *et al.*[79] (XPS observation of a carbon-metal interface bond) and Viel *et al.*[80]. Thanks to the local generation of active and short-living species, the cathodic electrografting of vinylic polymers can be localized which leads to a few applications for instance in the fabrication of composite surfaces[81], locally doped semiconductors[82], lubrication[83], heavy metal depollution[84] and biological purposes[85]. Although this process has significant advantages, it suffers from two main drawbacks which limit its application particularly in industrial conditions. First, due to its anionic mechanism, it requires drastic anhydrous conditions. Second, this technique is restricted to the use of vinylic monomer

bearing electron-withdrawing groups (to stabilize the carbanion formed during the polymerization) and resisting to highly cathodic potentials.

I.2.1.8 - Diazonium salt based cathodic electrografting in presence of vinylic monomers: the SEEP process

To overcome the previously mentioned limitations of the cathodic electrografting of vinylic monomers, several ways were investigated[86]. First, Deniau and coll.[87] demonstrated the possibility of adding some water to the reactive solution. Second, the synthesis of amphiphilic acrylic monomers by Jérôme and coworkers[88] (incorporation of a positive charge through an ammonium group and an alkyl chain to an acrylate compound) allowed extending the cathodic electrografting to aqueous solutions. Electrografted films on carbon surfaces of a few dozen nanometers were obtained from those molecules playing the role of monomer, surfactant (to form micellar solutions in water) and initiator at the same time. However, the long synthesis (several days) of those amphiphilic molecules is the main restriction on the wide use of this electrografting method. In parallel, a third alternative method was developed in our laboratory consisting in applying cathodic potentials to a mixture containing both a diazonium salt and a vinylic monomer either in homogeneous or in emulsion aqueous conditions depending on the solubility of the monomer[89].

This process, called SEEP for surface electroinitiated emulsion polymerization, is a real improvement of simple cathodic electrografting of vinylic monomers. It has recently been deeply investigated regarding the structure of the grafted films as well as the electrografting mechanism[14, 90]. In a general way, vinylic polymer chains can be grafted on the cathode after a few voltamperometric cycles (between the rest potential and -1.1 V/SCE in order to allow diazonium salt and proton reduction but avoid any vinylic double bond electroreduction) from acidic solutions containing a diazonium salt, the monomer and a surfactant, when the monomer is not fully soluble in water (Scheme 18).

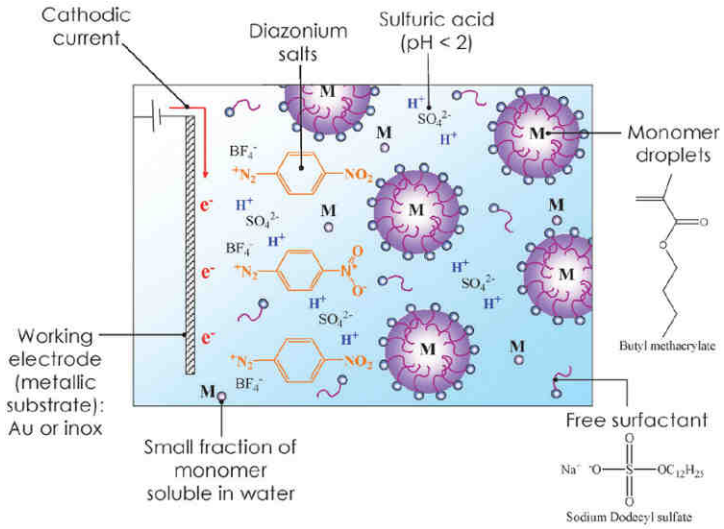

Scheme 18 – Composition of the initial miniemulsion system of the SEEP process from Deniau's work[90].

The SEEP process allows to switch from a direct anionic mechanism (classical cathodic electrografting of vinyl monomers) to a radical pathway thanks to the outstanding properties of diazonium salts. Indeed, it was demonstrated that aryl radicals (from the electroreduction of the aromatic diazonium salts) play a double role: (i) attaching onto the electrode surface to form an essential polyphenylene layer ("*grafting from*" process) and (ii) initiating the radical polymerization of the vinylic monomers in solution. It is important to underline that the initiation of polymerization can also take place through hydrogen radicals obtained by reduction of protons. The continuous supply in monomer required during the propagation step occurs via monomer diffusion from the droplets. The final grafted film results from the direct reaction between those macro-radicals and the primer polyphenylene layer ("*grafting to*" mechanism). It can be considered as a bilayered "co-polymer" with a primer layer almost entirely formed by the aryl moieties and a top-layer, whose thickness depends on the number of applied cycles, composed of vinylic polymer chains connected to the primer layer and likely cross-linked by aryl groups.

The SEEP process is an one-pot method working at room temperature, in aqueous medium, homogeneous or heterogeneous, from available reagents, with low reaction times and providing various polymer films (whatever the solubility of the initial monomer) strongly grafted but only on conducting or semi-conducting substrates. It was already successfully applied to a wide range of acrylate monomers such as acrylonitrile[89], acrylic acid[89], butyl methacrylate[14, 89, 90], hydroxyethyl methacrylate[14]. SEEP was even proved efficient for the modification of carbon nanotubes carpets[91] with a view to develop selective sensors and for the synthesis of micrometric hydrophobic/hydrophilic patterned surface[92] (Scheme 19).

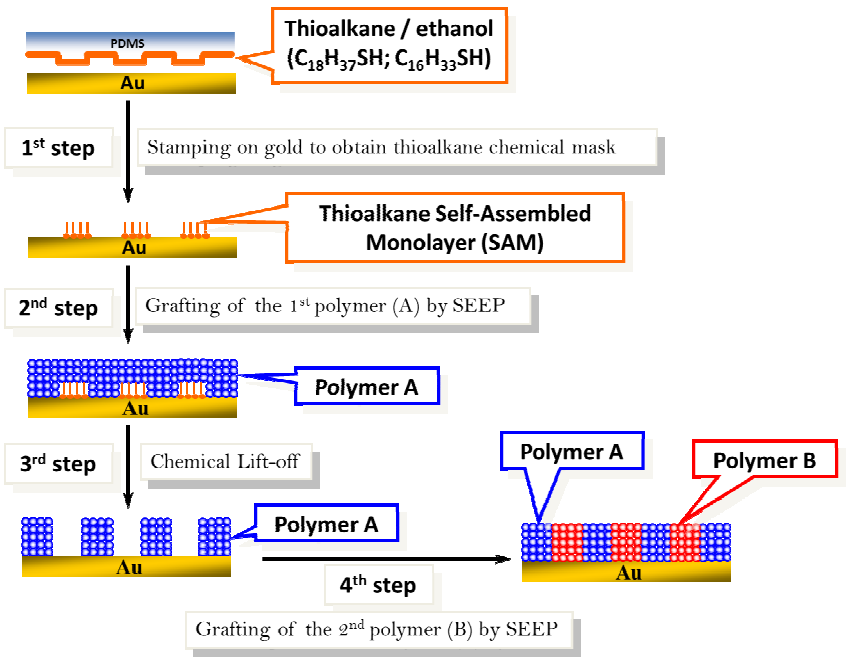

Scheme 19 – Strategy used to synthesize by SEEP a surface alternating hydrophobic (polymer A) and hydrophilic (polymer B) micro-areas extracted from Deniau's work[92].

Patterning of surfaces can also be achieved by slightly varying the SEEP experimental conditions. For example, it was possible to locally graft vinylic polymer coatings by using gel-electrolytes[93] (Scheme 20). In this case, agarose hydrogel was swelled with mixtures of diazonium salts and water-soluble vinylic monomers. After drying, the gel was brought into contact with two electrodes and, the reaction of polymerization occurred by applying a cathodic potential.

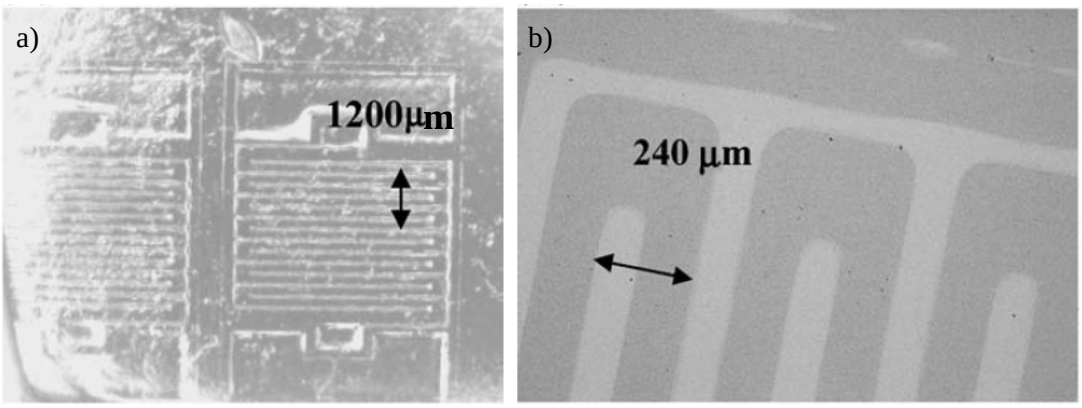

Scheme 20 – Optical micrographs of a) a patterned agarose gel and b) the pattern transferred by SEEP on the gold surface using the patterned gel containing HEMA as anode extracted from Palacin's work[93].

To finish, another way to localize the electrografting is to use a micro-electrode. By using a AFM-SECM system (atomic force microscope combined with a scanning electrochemical microscope), Charlier and coll.[94] managed to induce localized grafting of organic coatings on a conducting substrate. The only variation with the SEEP process is the use of a micro-electrode (AFM-SECM tip) as a counter-electrode CE (Scheme 21a). As deeply described in a recent study[95], in this configuration, it was possible to draw lines and curves with a submicrometer resolution using the tip as a pencil to direct the electrografting of the "co-polymer" film (Scheme 21b and c).

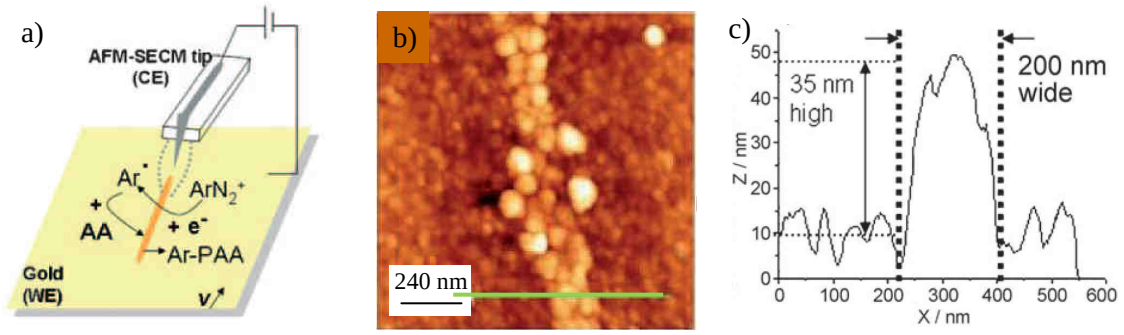

Scheme 21 – a) Schematic of the electrografting reaction mediated by the AFM-SECM tip with ArN_2^+: aryl diazonium salt, $Ar^\bullet$: aryl radical, AA: acrylic acid monomer, PAA: polyacrylic acid film; b) Phase AFM image of the line pattern drawn with the AFM-SECM tip on the gold surface in the case of the direct aryl diazonium salt/acrylic acid reduction; c) Thickness profile of the line pattern, extracted from Charlier's work[94].

I.2.2 - **Indirect methods**

A wide range of polymer grafting can be performed through primer layers (films already attached to the substrate). The substituents borne by the molecules initially grafted on the sample can be used as reacting sites to promote selective attachment or start controlled polymerization. In this part, we will focus on the presentation of techniques using primer layer of precursors to form polymer films. Therefore we will not develop post-functionalization techniques of those layers with various materials (molecules or nano-objects). The reader can refer to the reviews of Pinson[18] or Chehimi[96] for more information on the post-functionalization of substituted phenyl layers from diazonium salts. The indirect formation of polymer films on substrates can be achieved by the grafting of polymers to surfaces by a "*grafting to*" process or by surface-initiated polymerization (SIP). However, as Klok and coworkers[97] have recently published a very complete review on the synthesis, characterization, properties and applications of polymer brushes via surface-initiated controlled radical polymerization, we will not go into too many details in the presentation of those methods. Moreover, although the second step is a classical SIP, the formation of polymer coatings from polydopamine primer layer will be described in a separate part at the end of this chapter since, in our opinion, it constitutes a real breakthrough in the field of surface functionalization by polymer films.

I.2.2.1 - Grafting of polymers: "grafting to"

As example of "grafting to" procedures, Adenier and coworkers[98] presented the modification of an iron surface by polystryrene (PS) via an electrostatic bonding. On a substrate grafted with carboxyphenyl groups, Mg^{2+} ions and a solution containing a polymer (composed of carboxylates groups and a double bond) were mechanically deposited inducing the formation of an electrostatic bonding between the carboxylate groups on the surface and the polymer. Then, by adding styrene and irradiating the solution, it is possible to cross-link the polymer by copolymerization with styrene providing a PS strongly grafted to the iron surface (Scheme 22).

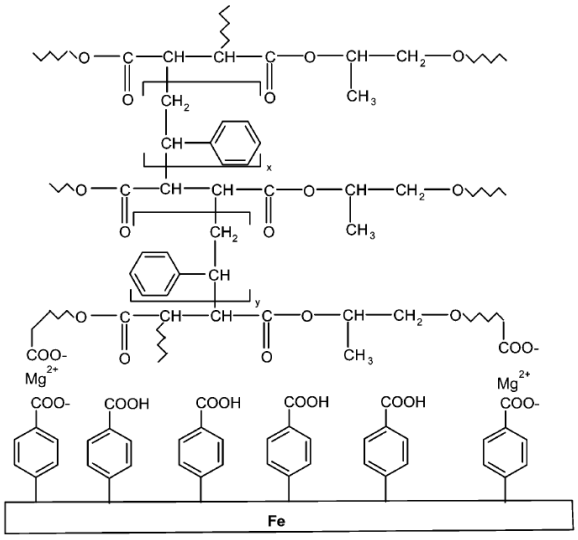

Scheme 22 – Structure of metal polymer composite presented by Adenier *et al.*[98].

Another indirect technique for "*grafting to*" surface modification by polymer films is click chemistry. As stated by Chehimi and coll.[96], "compared to various methods for binding thin films of preformed end-functionalized macromolecules onto surfaces, it is indeed simple, fast, selective and permits the incorporation of various functional polymers avoiding side reactions".

Li *et al.*[99] have successfully functionalized single-walled carbon nanotubes (SWNT) with polystyrene. Alkyne groups were introduced on the surface of single-walled carbon nanotubes while in parallel azide-terminated polystyrene was synthesized. The modified-PS was clicked to the alkynylated SWNT (Huisgen 1,3-cycloaddition catalysed by Cu(I)) leading to SWNT with a high polystyrene grafting density, a full control over polymer molecular weight and a good stability in organic solvents (Scheme 23).

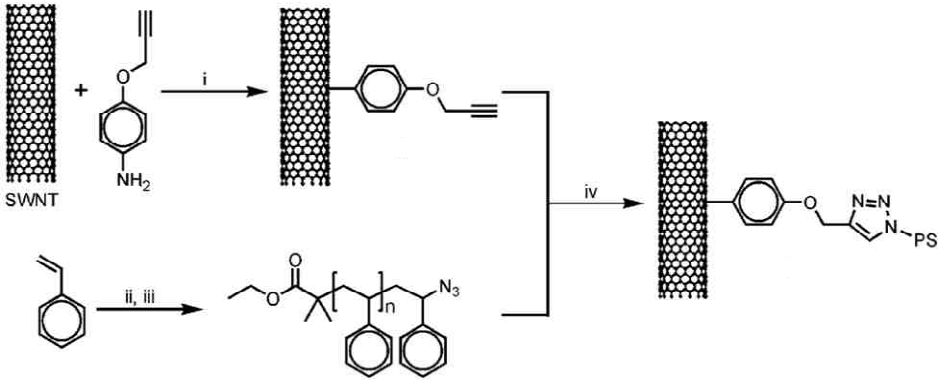

Scheme 23 – Principle of the grafting of polystyrene onto single-walled carbon nanotubes by click chemistry, (i) Isoamyl nitrite, 60 °C; (ii) EBiB, CuBr/BPy, DMF, 110 °C; (iii) NaN_3, DMF, room temperature; (iv) Cu(I), DMF extracted from Adronov's work[99].

In a similar way, a tandem diazonium salt/click chemistry process has been proposed to synthesize OEG (oligoethylene glycols) and FEG (perfluorinated ethylene glycol) polymer-modified gold surfaces[100]. However, contrary to the previous example, in this case, the azide group (obtained from Br by nucleophilic attack of N_3^-) is borne by the electrografted molecules from the primer layer whereas the polymers to attach are mono or bi-substituted with an alkyne group (Scheme 24).

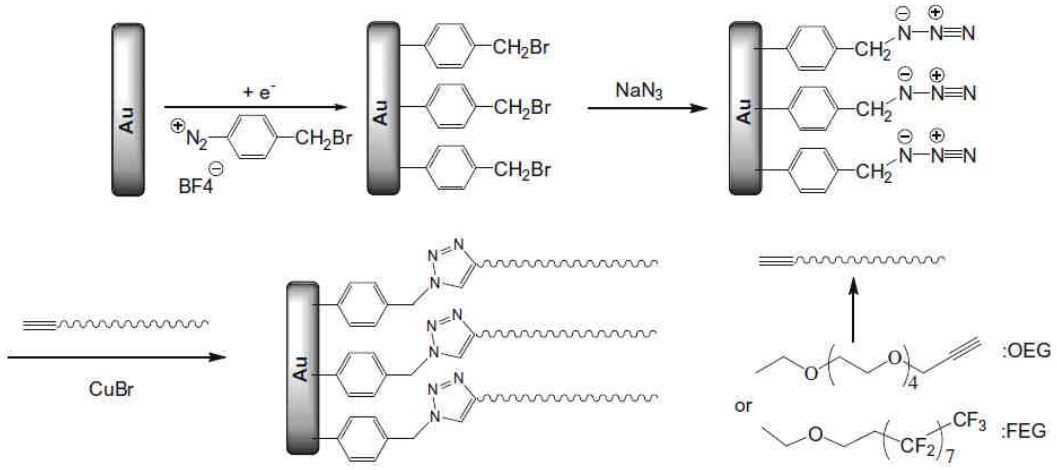

Scheme 24 – Principle of the functionalization of gold surface with OEG and FEG by tandem diazonium salt /click chemistry extracted from Chehimi's work[100].

I.2.2.2 - Surface-initiated polymerization (SIP): "grafting from"

An indirect method for surface functionalization with polymers can also be based on the promotion of the polymerization of monomers directly from initiators already attached to surfaces. Such process is called surface-initiated polymerization (SIP). It leads to the formation of polymer brushes i.e. polymer chains tethered by one end to a surface. Nearly all polymerization techniques that have been developed in solution have now been adapted for SIP. Polymer brushes can for example be prepared by: free radical polymerization[101], cationic polymerization[102], anionic polymerization[102], ring-opening metathesis polymerization (ROMP)[103], nitroxide-mediated polymerization (NMP)[104], reversible addition-fragmentation polymerization (RAFT)[104], atom transfer radical polymerization (ATRP)[104]. All these methods are suitable for polymerizing different types of monomers on a variety of surfaces and particles. Hence, we will restrict the presentation of SIP to a few examples of the most employed techniques.

Surface-initiated nitroxide-mediated polymerization (SI-NMP)

As ATRP and RAFT, NMP is a controlled radical polymerization process based on a dynamic equilibrium between dormant species and active radicals. In this case, alkoxyamine initiators can thermally dissociate in a carbonated initiator radical as well as a stable nitroxide radical and the control of the NMP process relies on the reversible capture of the propagating species by nitroxides with formation of dormant chains (alkoxyamines).

Husseman *et al.*[105] were the first, in 1999, to report the application of NMP to surface-initiated graft polymerization. From the attachment on the substrate of a TEMPO-derivated alkoxyamine (thanks to the reaction between a chlorosilane and surface silanol groups of silicon wafers or silica gel particles), they successfully grafted dense polystyrene polymer brushes. A free alkoxyamine was added to control the polymerization. The coating of the initiators on the surface is a key point in order to improve the polymer grafting density. Therefore, methods such as the Langmuir-Blogdgett technique[106] or cathodic electrografting[107] were also used to immobilize the initiating molecules. For example, Jérôme and coworkers prepared random copolymer brushes adherent to stainless steel by cathodic electrografting of an alkoxyamine containing acrylate followed with the nitroxide-mediated controlled radical copolymerization of styrene (Sty) (or n-butyl acrylate (BuA)) and 2-(dimethylamino ethyl)acrylate (DAEA) (Scheme 25).

SI-NMP is a method allowing the controlled fabrication of polymer brushes without the addition of further catalyst. However, it often requires the careful selection and the synthesis of the mediating radical, according to the monomer used.

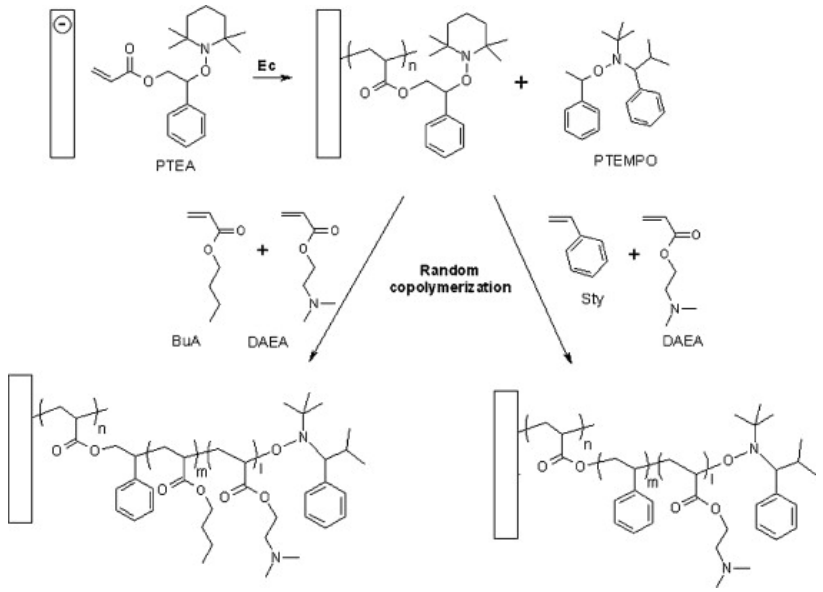

Scheme 25 – Combination of cathodic electrografting (Ec) and NMP extracted from Jérôme's work[108].

Surface-initiated reversible addition-fragmentation polymerization (SI-RAFT)

The first application of RAFT to surface-initiated polymerization was shown by Baum and Brittain[109]. They synthesized brushes of polystyrene, PMMA, poly(N,N-dimethylacrylamide) and their copolymers on silicate surfaces from a substrate-immobilized free azo initiator. As for SI-NMP, to control the graft polymerization, a chain transfer agent (dithiobenzoate) was added (Scheme 26). Like in solution RAFT polymerization, the introduction of a free initiator (AIBN) was found advantageous.

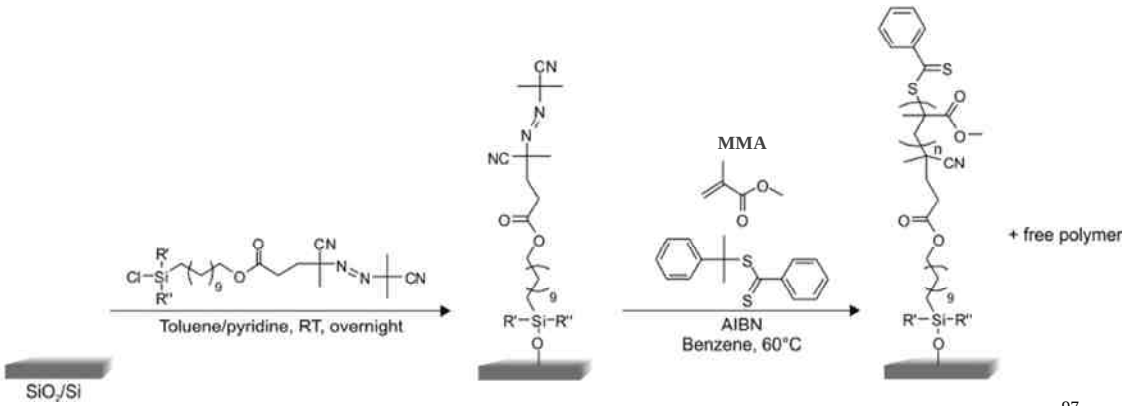

Scheme 26 – SI-RAFT polymerization from a free radical-modified surface from Klok's review[97].

The use of free radical initiator-modified substrates is not the only method to carry out SI-RAFT. Li and coworkers[110] have recently shown SI-RAFT from surface-immobilized RAFT agents on silica particles (Scheme 27). In this case, the immobilization of the chain transfer agent was performed by silane coupling. However, the RAFT agent can be immobilized by different ways including electrochemical processes as electrodeposition[111] and electropolymerization of thiophene[112]. The SI-RAFT polymerization has been recently used for the synthesis of water-soluble SWNTs (SWNT-polyacrylamide composite)[113] as well as protein and cell-resistant coatings for biomedical devices[111].

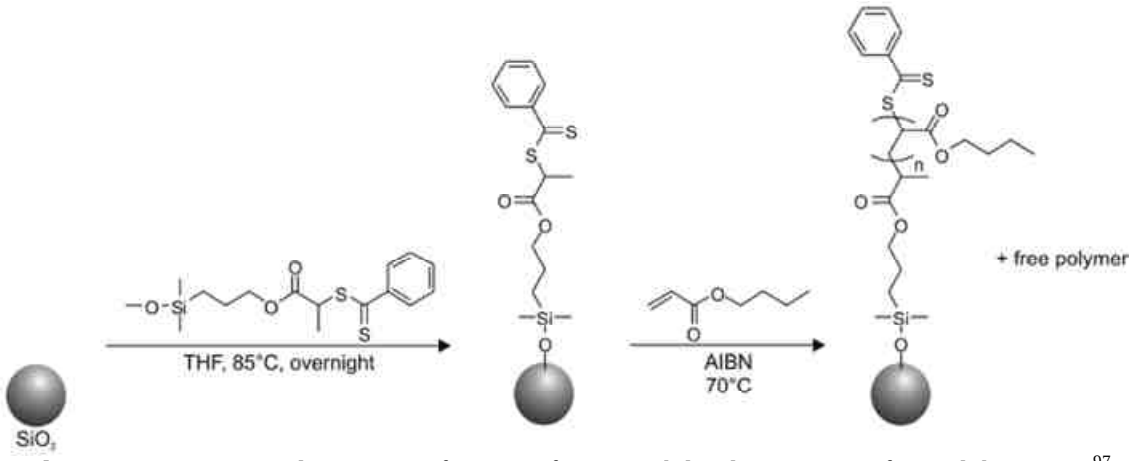

Scheme 27 – SI-RAFT polymerization from a surface-immobilized RAFT agent from Klok's review[97]

In comparison with other controlled radical polymerization techniques, RAFT polymerization is extremely versatile. However, it has a main drawback: the chain transfer agents are generally not commercially available and synthesized via multiple steps.

Surface-initiated atom transfer radical polymerization (SI-ATRP)

Controlled atom transfer radical polymerization is certainly the technique the most applied to SIP. Polymer brushes were obtained on a large variety of materials from flat surfaces to particles or porous materials. SI-ATRP relies on a reversible redox activation between immobilizing initiating dormant species (usually bearing Cl or Br) or grown dormant chains and a transition metal complex leading to a halogen transfer as illustrated by Scheme 28. Monomer units can attach on the so-formed propagating radical until it captures a halogen atom to be a dormant chain.

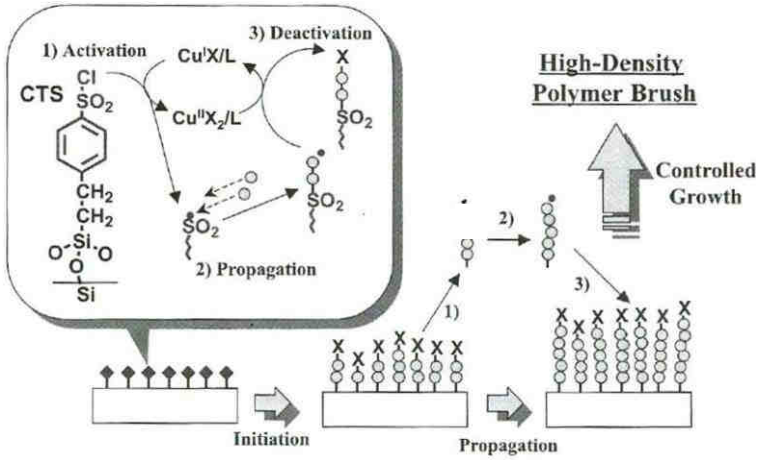

Scheme 28 – Illustration of ATRP extracted from *Surface-Initiated Polymerization I*[104].

Huang and Wirth were the first, in 1997, to report the formation of polymer brushes by SI-ATRP[114]. From a self-assembled benzyl chloride monolayer on silica gel, they successfully grafted polyacrylamide on the silica surface. They were closely followed by Ejaz and coworkers[115] who showed the growth of PMMA brushes on a silicon wafer initiated from ATRP initiators immobilized by the Langmuir-Blodgett technique. Gold substrates modified by

self-assembled monolayers (SAM) of thiols have also been used to achieve SI-ATRP. For instance, diblock polymer brushes on gold were obtained by SI-ATRP of the two monomers one after the other[116]. Through surface-initiated polymerization of methyl and glycidyl methacrylate in aqueous medium on gold, the authors demonstrated a linear relationship between initiator density and the growth rate of the polymer brush formed[117]. By comparing SI-ATRP initiated from SAM of thiols to cathodic electrografting, Palacin and coll.[118] concluded that those two techniques were valuable tools for the grafting of organic coatings on conductive surfaces but with different scope of applications due to differences in strengths and weaknesses of those two processes.

Lately, Matrab *et al.*[119] have opened a new route (Scheme 29) for the immobilization of ATRP initiators based on the electrochemistry of brominated aryldiazonium salts (see I.1.5.2). Such method can be applied to a wide range of materials (different from silica and gold) such as iron[119], stainless steel[120] and carbonated materials[120-122]. It gives primer-layers with high density of initiators, strongly adherent to the substrate and resistant to high temperature and ultrasonication. An investigation on the influence of several experimental parameters has recently been conducted by Iruthayaraj *et al.*[120]. From the variation of the thickness of the polymer brush as a function of the surface concentration of bromine reactive sites on the surface, they showed a gradual mushroom to brush transition of the chains grafted on the substrate. As detailed in Chehimi's review[96], this tandem diazonium salt/ATRP approach is suitable for the formation of polymer brushes in various fields of applications including stents (vascular prosthesis), capture of metal ions or optical sensors.

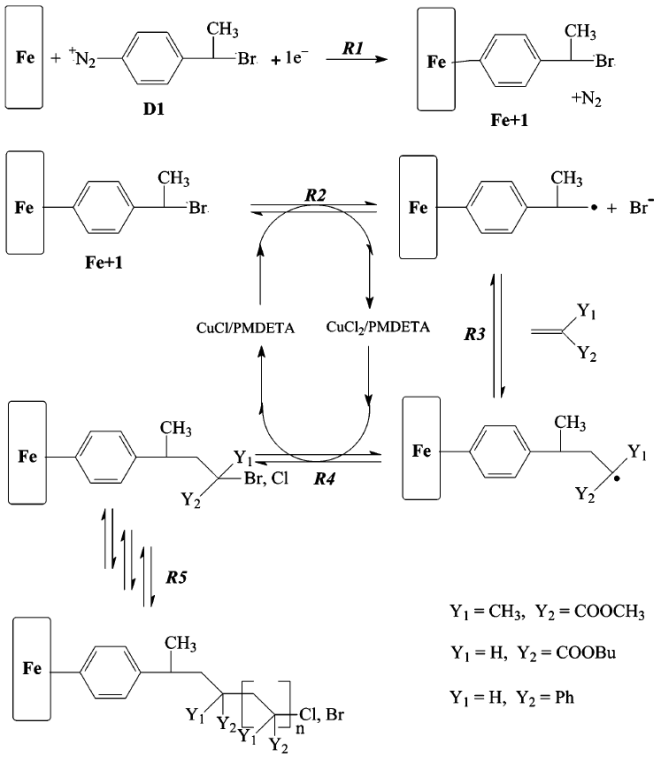

Scheme 29 – Principle of the tandem diazonium salt electrochemistry and ATRP from Matrab's work[119].

SI-ATRP not only provides the control of the chain length of polymer brushes but also high grafting densities. As summarized by Klok and coll.[97], SI-ATRP is well-adapted for the preparation of polymer brushes and very versatile since a large range of monomers and functional groups are compatible with this technique. It is still efficient when working with a high degree of impurities and avoids the formation of non-grafted chains in solution. Finally, ATRP initiators are in general commercially available or easy to synthesize. However, SI-ATRP presents some limitations. It cannot be used with monomers able to react or complex with the metal transition catalyst (pyridine or acidic monomers). Besides, it can be difficult to wash off this metal catalyst from the polymer brush which could be damaging to potential applications in biomedical or the electronics industry.

Surface-initiated photopolymerization (SIPP)

As deeply described by Dyer[123], surface initiated polymerization was carried out with a large range of common photoinitiators bonded to the substrate in particular peroxide, benzophenone[124] and AIBN-type[125] as well as on a wide variety of surfaces: gold, organic polymers, silicon oxide (including glass)... For instance, the SIPP of styrene[124, 126], methyl methacrylate[127], acrylonitrile[125] were reported on gold from SAMs of photoinitiators. An alternative approach has recently been proposed by Chehimi and coll.[128]. As represented on Scheme 30, from the electrografting of benzoylphenyl moieties (reduction of diazonium salt) on gold-coated silicon wafer in presence of tertiary amine in solution (photosensitizer added to abstract hydrogen atoms from the substrate), they obtained PS, PMMA and PHEMA grafted films. It is worth noting that, in the last case, a 100 nm-thick film was formed in chloroform in approximately 1h.

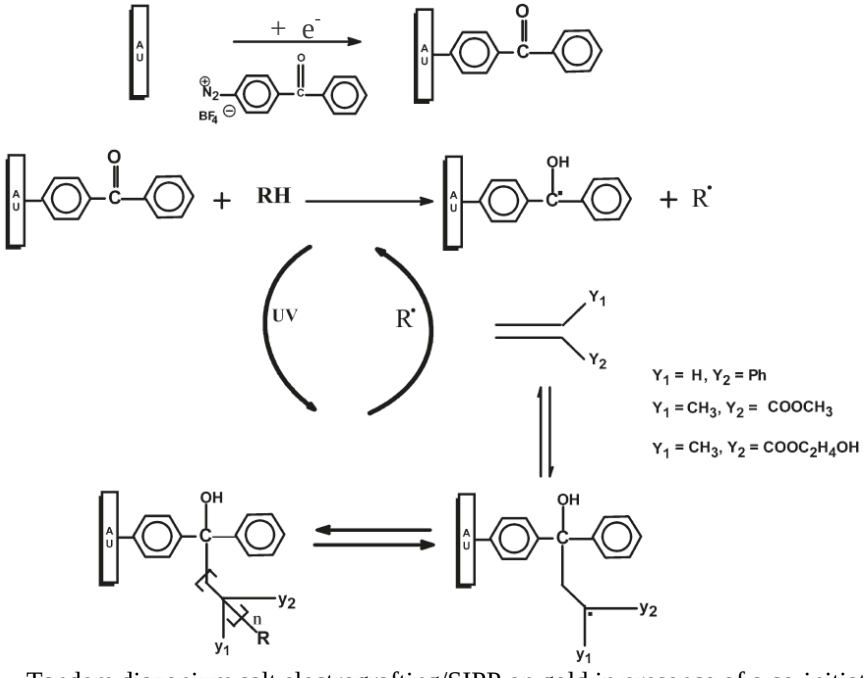

Scheme 30 – Tandem diazonium salt electrografting/SIPP on gold in presence of a co-initiator (RH) as extracted from Chehimi's work[128].

Surface-initiated photopolymerization shows several advantages. It is a fast process. It can be performed in a simple way at room temperature, applied to a wide range of monomers, on various types of substrates and from photoinitiators grafted or in solution. However, the potential occurrence of shaded regions might lead to defects in the grafted films.

I.2.2.3 - Process based on polydopamine functionalized substrates

In this section, we will focus on a recently discovered and a very powerful process to synthesize strongly adherent polymer films on any type of surfaces. It is a method based on the polymerisation of dopamine. Polydopamine coated layers could be used on their own. However, they are especially interesting for post-functionalization since it leads to the formation of coatings on any type of material combining a strong adhesion (from the primer layer) and the properties of the added film. Therefore, we will describe two-step methods based on the modification of polydopamine functionalized substrates.

The first step of this process is based on a recently reported work[129, 130] to obtain polydopamine coatings on any type of materials from noble metals, native oxide surfaces, oxides, semiconductors, ceramics to polymers. This method, inspired from mussels' adhesion properties to marine surfaces, relies on the spontaneous formation of a highly adhesive thin polymer films from simple immersion of the substrates in buffered solution or ammonium persulfate aqueous solution of dopamine (the latter oxidizing conditions favoring shorter reaction times[131]). Indeed, dopamine is a small molecule containing both alkylamine and catechol functionalities which mimic the structure of the mussels' foot protein. Although the exact mechanism for dopamine self-polymerization is still unknown, it is likely to involve oxidation of the catechol to quinone, followed by polymerization in a manner reminiscent of melanine formation (Scheme 31), which occurs through polymerization of structurally similar compounds (reference 25 herein Lee's work[129]).

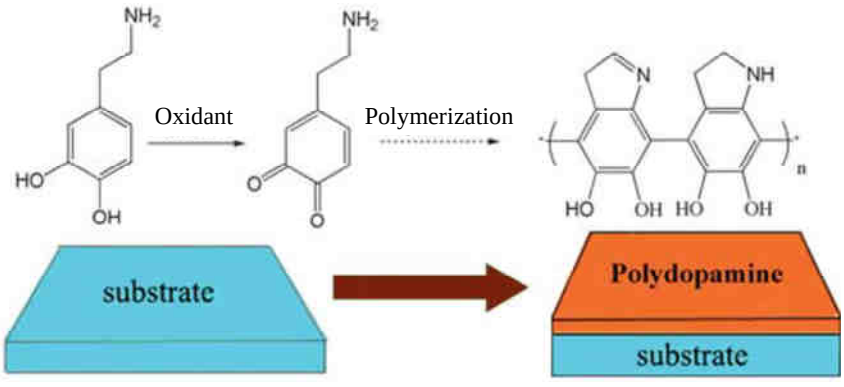

Scheme 31 – Multifunctional coating formation by oxidant-induced dopamine polymerization extracted from Zhao's work[131].

So far, this method has been demonstrated to be suitable for the patterning of surfaces[132] but also to constitute a very interesting reactive platform for further secondary treatments widening

the scope of applications. Particularly, the grafting of polymer ad-layers onto such surfaces has been achieved using thiol- or amine-functionalized polymers in the secondary step leading for example to the formation of fouling-resistant surfaces[129] or PEG coated capillaries for separation of proteins in capillary electrophoresis[133]. More recently, polydopamine coatings have been used by Wang *et al.*[134] to immobilize an ATRP initiator and perform the polymerization of poly(acrylic acid) adding a strong attachment of the polymer coating on top of the usual advantages of ATRP.

Summary

We have described the most common techniques used for the surface functionalization of materials by organic coatings including physisorption as well as chemisorption methods. In particular, the use of diazonium salts as coupling agent for bonding polymers to surfaces has permitted to significantly improve a few processes such as surface-initiated polymerization techniques or cathodic electrografting with the recent development of the SEEP process.

In this context, we have investigated a new approach, i.e. an anchoring process based on diazonium salts, for the chemical grafting of aryl layers but more important the surface modification by polymers of any type of materials. This recently developed technique is, to our opinion, very promising since it overcomes the main limitations or drawbacks of the methods previously presented such as weakly bonded coating (as for physisorption methods), restrictive conditions (in the case of cathodic electrografting), constraints in term of substrate (mainly for electrochemical techniques) and multiple steps (regarding surface-initiated polymerization).

References

1. J. E. Mahan, *Physical Vapor Deposition of Thin Films*, Wiley, New York, **2000**.
2. C. F. Powell, J. H. Oxley, J. M. Blocher, *Vapor Deposition*, Wliey, New York, **1966**.
3. V. Roucoules, *Stage pédagogique - Matériaux polymères en couches minces*, **2010**.
4. K. Blodgett, *Monomolecular films of fatty acids on glass*, ***Journal of the American Chemical Society***, **1934**, 56, 495-495.
5. V. V. Arslanov, *Polymer Monolayers and Langmuir-Blodgett-Films - The Influence of Polymer Chemical-Structure and External Conditions on Formation and Properties of the Planar Organized Ensembles*, ***Russian Chemical Reviews***, **1994**, 63 (1), 1-39.
6. H. Motschmann, H. Mohwald, *Handbook of Applied Surface and Colloid Chemistry - Chap 28 Langmuir-Blodgett films*, John Wiley & Sons, **2001**.
7. A. Ulman, *Formation and structure of self-assembled monolayers*, ***Chemical Reviews***, **1996**, 96 (4), 1533-1554.
8. A. Ulman, *An introduction of Ultra-thin Organic Films: From Langmuir-Blodgett to Self Assembly*, Academic Press, Boston, **1991**.
9. G. E. Poirier, E. D. Pylant, *The self-assembly mechanism of alkanethiols on Au(111)*, ***Science***, **1996**, 272 (5265), 1145-1148.
10. S. R. Wasserman, Y. T. Tao, G. M. Whitesides, *Structure and Reactivity of Alkylsiloxane Monolayers Formed by Reaction of Alkyltrichlorosilanes on Silicon Substrates*, ***Langmuir***, **1989**, 5 (4), 1074-1087.
11. M. R. Linford, P. Fenter, P. M. Eisenberger, C. E. D. Chidsey, *Alkyl Monolayers on Silicon Prepared from 1-Alkenes and Hydrogen-Terminated Silicon*, ***Journal of the American Chemical Society***, **1995**, 117 (11), 3145-3155.
12. R. G. Nuzzo, D. L. Allara, *Adsorption of Bifunctional Organic Disulfides on Gold Surfaces*, ***Journal of the American Chemical Society***, **1983**, 105 (13), 4481-4483.
13. R. G. Nuzzo, F. A. Fusco, D. L. Allara, *Spontaneously Organized Molecular Assemblies. 3. Preparation and Properties of Solution Adsorbed Monolayers of Organic Disulfides on Gold Surfaces*, ***Journal of the American Chemical Society***, **1987**, 109 (8), 2358-2368.
14. L. Tessier, *Greffage de Films Organiques par Polymerisation Radicalaire Electro-amorcée en Milieu Aqueux Dispersé*, Thèse de l'Université Pierre et Marie Curie, Paris, **2009**.
15. J. Duchet, B. Chabert, J. P. Chapel, J. F. Gerard, J. M. Chovelon, N. JaffrezicRenault, *Influence of the deposition process on the structure of grafted alkylsilane layers*, ***Langmuir***, **1997**, 13 (8), 2271-2278.
16. K. K. Berggren, A. Bard, J. L. Wilbur, J. D. Gillaspy, A. G. Helg, J. J. McClelland, S. L. Rolston, W. D. Phillips, M. Prentiss, G. M. Whitesides, *Microlithography by using Neutral Metastable Atoms and Self-Assembled Monolayers*, ***Science***, **1995**, 269 (5228), 1255-1257.
17. D. K. Aswal, S. Lenfant, D. Guerin, J. V. Yakhmi, D. Vuillaume, *Self assembled monolayers on silicon for molecular electronics*, ***Analytica Chimica Acta***, **2006**, 568 (1-2), 84-108.
18. D. Bélanger, J. Pinson, *Electrografting: a powerful method for surface modification*, ***Chemical Society Reviews***, **2011**, 40, 3995-4048.
19. A. Fidelis, F. Ozanam, J. N. Chazalviel, *Fully methylated, atomically flat (111) silicon surface*, ***Surface Science***, **2000**, 444 (1-3), L7-L10.
20. S. Fellah, A. Teyssot, F. Ozanam, J. N. Chazalviel, J. Vigneron, A. Etcheberry, *Kinetics of electrochemical derivatization of the silicon surface by Grignards*, ***Langmuir***, **2002**, 18 (15), 5851-5860.
21. S. Fellah, F. Ozanam, J. N. Chazalviel, J. Vigneron, A. Etcheberry, M. Stchakovsky, *Grafting and polymer formation on silicon from unsaturated grignards: I - Aromatic precursors*, ***Journal of Physical Chemistry B***, **2006**, 110 (4), 1665-1672.
22. S. Fellah, A. Amiar, F. Ozanam, J. N. Chazalviel, J. Vigneron, A. Etcheberry, M. Stchakovsky, *Grafting and polymer formation on silicon from unsaturated grignards: II. Aliphatic precursors*, ***Journal of Physical Chemistry B***, **2007**, 111 (6), 1310-1317.

23. F. Yang, R. Hunger, K. Roodenko, K. Hinrichs, K. Rademann, J. Rappich, *Vibrational and Electronic Characterization of Ethynyl Derivatives Granted onto Hydrogenated Si(111) Surfaces*, ***Langmuir***, **2009**, 25 (16), 9313-9318.

24. A. Adenier, M. M. Chehimi, I. Gallardo, J. Pinson, N. Vila, *Electrochemical oxidation of aliphatic amines and their attachment to carbon and metal surfaces*, ***Langmuir***, **2004**, 20 (19), 8243-8253.

25. R. S. Deinhammer, M. Ho, J. W. Anderegg, M. D. Porter, *Electrochemical Oxidation of Amine-containing Compounds - A Route to the Surface Modification of Glassy-Carbon Electrodes*, ***Langmuir***, **1994**, 10 (4), 1306-1313.

26. G. Herlem, C. Goux, B. Fahys, F. Dominati, A. M. Goncalves, C. Mathieu, E. Sutter, A. Trokourey, J. F. Penneau, *Surface modification of platinum and gold electrodes by anodic oxidation of pure ethylenediamine*, ***Journal of Electroanalytical Chemistry***, **1997**, 435 (1-2), 259-265.

27. A. H. Holm, K. H. Vase, B. Winther-Jensen, S. U. Pedersen, K. Daasbjerg, *Evaluation of various strategies to formation of pH responsive hydroquinone-terminated films on carbon electrodes*, ***Electrochimica Acta***, **2007**, 53 (4), 1680-1688.

28. H. Tang, J. H. Chen, K. Z. Cui, L. H. Nie, Y. F. Kuang, S. Z. Yao, *Immobilization and electro-oxidation of calf thymus deoxyribonucleic acid at alkylamine modified carbon nanotube electrode and its interaction with promethazine hydrochloride*, ***Journal of Electroanalytical Chemistry***, **2006**, 587 (2), 269-275.

29. C. Gurtner, A. W. Wun, M. Sailor, *Surface modification of porous silicon by electrochemical reduction of organo halides*, ***Angewandte Chemie-International Edition***, **1999**, 38 (13-14), 1966-1968.

30. M. Delamar, R. Hitmi, J. Pinson, J. M. Saveant, *Covalent Modification of Carbon Surfaces by Grafting of Functionalized Aryl Radicals Produced from Electrochemical Reduction of Diazonium Salts*, ***Journal of the American Chemical Society***, **1992**, 114 (14), 5883-5884.

31. A. J. Downard, *Electrochemically assisted covalent modification of carbon electrodes*, ***Electroanalysis***, **2000**, 12 (14), 1085-1096.

32. J. Pinson, F. Podvorica, *Attachment of organic layers to conductive or semiconductive surfaces by reduction of diazonium salts*, ***Chemical Society Reviews***, **2005**, 34 (5), 429-439.

33. A. Adenier, N. Barre, E. Cabet-Deliry, A. Chausse, S. Griveau, F. Mercier, J. Pinson, C. Vautrin-Ul, *Study of the spontaneous formation of organic layers on carbon and metal surfaces from diazonium salts*, ***Surface Science***, **2006**, 600 (21), 4801-4812.

34. P. Allongue, M. Delamar, B. Desbat, O. Fagebaume, R. Hitmi, J. Pinson, J. M. Saveant, *Covalent modification of carbon surfaces by aryl radicals generated from the electrochemical reduction of diazonium salts*, ***Journal of the American Chemical Society***, **1997**, 119 (1), 201-207.

35. S. Baranton, D. Belanger, *In situ generation of diazonium cations in organic electrolyte for electrochemical modification of electrode surface*, ***Electrochimica Acta***, **2008**, 53 (23), 6961-6967.

36. T. Breton, D. Belanger, *Modification of carbon electrode with aryl groups having an aliphatic amine by electrochemical reduction of in situ generated diazonium cations*, ***Langmuir***, **2008**, 24 (16), 8711-8718.

37. M. Delamar, G. Desarmot, O. Fagebaume, R. Hitmi, J. Pinson, J. M. Saveant, *Modification of carbon fiber surfaces by electrochemical reduction of aryl diazonium salts: Application to carbon epoxy composites*, ***Carbon***, **1997**, 35 (6), 801-807.

38. T. Itoh, R. L. McCreery, *In situ Raman spectroelectrochemistry of electron transfer between glassy carbon and a chemisorbed nitroazobenzene monolayer*, ***Journal of the American Chemical Society***, **2002**, 124 (36), 10894-10902.

39. B. Ortiz, C. Saby, G. Y. Champagne, D. Belanger, *Electrochemical modification of a carbon electrode using aromatic diazonium salts. 2. Electrochemistry of 4-nitrophenyl modified glassy carbon electrodes in aqueous media*, ***Journal of Electroanalytical Chemistry***, **1998**, 455 (1-2), 75-81.

40. M. Pandurangappa, T. Ramakrishnappa, *Derivatization and characterization of functionalized carbon powder via diazonium salt reduction*, ***Journal of Solid State Electrochemistry***, **2008**, 12 (11), 1411-1419.

41. M. S. Strano, C. A. Dyke, M. L. Usrey, P. W. Barone, M. J. Allen, H. W. Shan, C. Kittrell, R. H. Hauge, J. M. Tour, R. E. Smalley, *Electronic structure control of single-walled carbon nanotube functionalization*, ***Science***, **2003**, 301 (5639), 1519-1522.

42. P. Viel, X. T. Le, V. Huc, J. Bar, A. Benedetto, A. Le Goff, A. Filoramo, D. Alamarguy, S. Noel, L. Baraton, S. Palacin, *Covalent grafting onto self-adhesive surfaces based on aryldiazonium salt seed layers*, ***Journal of Materials Chemistry***, **2008**, 18 (48), 5913-5920.

43. M. C. Bernard, A. Chausse, E. Cabet-Deliry, M. M. Chehimi, J. Pinson, F. Podvorica, C. Vautrin-Ul, *Organic layers bonded to industrial, coinage, and noble metals through electrochemical reduction of aryldiazonium salts*, ***Chemistry of Materials***, **2003**, 15 (18), 3450-3462.

44. A. Laforgue, T. Addou, D. Belanger, *Characterization of the deposition of organic molecules at the surface of gold by the electrochemical reduction of aryldiazonium cations*, ***Langmuir***, **2005**, 21 (15), 6855-6865.

45. J. Lyskawa, D. Belanger, *Direct modification of a gold electrode with aminophenyl groups by electrochemical reduction of in situ generated aminophenyl monodiazonium cations*, ***Chemistry of Materials***, **2006**, 18 (20), 4755-4763.

46. A. Ricci, C. Bonazzola, E. J. Calvo, *An FT-IRRAS study of nitrophenyl mono- and multilayers electro-deposited on gold by reduction of the diazonium salt*, ***Physical Chemistry Chemical Physics***, **2006**, 8 (37), 4297-4299.

47. A. Adenier, E. Cabet-Deliry, A. Chausse, S. Griveau, F. Mercier, J. Pinson, C. Vautrin-Ul, *Grafting of nitrophenyl groups on carbon and metallic surfaces without electrochemical induction*, ***Chemistry of Materials***, **2005**, 17 (3), 491-501.

48. K. Boukerma, M. M. Chehimi, J. Pinson, C. Blomfield, *X-ray photoelectron spectroscopy evidence for the covalent bond between an iron surface and aryl groups attached by the electrochemical reduction of diazonium salts*, ***Langmuir***, **2003**, 19 (15), 6333-6335.

49. A. Chausse, M. M. Chehimi, N. Karsi, J. Pinson, F. Podvorica, C. Vautrin-Ul, *The electrochemical reduction of diazonium salts on iron electrodes. The formation of covalently bonded organic layers and their effect on corrosion*, ***Chemistry of Materials***, **2002**, 14 (1), 392-400.

50. C. Combellas, M. Delamar, F. Kanoufi, J. Pinson, F. I. Podvorica, *Spontaneous grafting of iron surfaces by reduction of aryldiazonium salts in acidic or neutral aqueous solution. Application to the protection of iron against corrosion*, ***Chemistry of Materials***, **2005**, 17 (15), 3968-3975.

51. C. Combellas, F. Kanoufi, J. Pinson, F. I. Podvorica, *Sterically hindered diazonium salts for the grafting of a monolayer on metals*, ***Journal of the American Chemical Society***, **2008**, 130 (27), 8576-8577.

52. P. Doppelt, G. Hallais, J. Pinson, F. Podvorica, S. Verneyre, *Surface modification of conducting substrates. Existence of azo bonds in the structure of organic layers obtained from diazonium salts*, ***Chemistry of Materials***, **2007**, 19 (18), 4570-4575.

53. B. L. Hurley, R. L. McCreery, *Covalent bonding of organic molecules to Cu and Al alloy 2024 T3 surfaces via diazonium ion reduction*, ***Journal of the Electrochemical Society***, **2004**, 151 (5), B252-B259.

54. Q. M. Pan, M. Wang, W. T. Chen, *Hydrophobization of metal surfaces by covalent grafting of aromatic layer via aryldiazonium chemistry and their application in the fabrication of superhydrophobic surfaces*, ***Chemistry Letters***, **2007**, 36 (11), 1312-1313.

55. M. P. Stewart, F. Maya, D. V. Kosynkin, S. M. Dirk, J. J. Stapleton, C. L. McGuiness, D. L. Allara, J. M. Tour, *Direct covalent grafting of conjugated molecules onto Si, GaAs, and Pd surfaces from aryidiazonium salts*, ***Journal of the American Chemical Society***, **2004**, 126 (1), 370-378.

56. C. H. deVilleneuve, J. Pinson, M. C. Bernard, P. Allongue, *Electrochemical formation of close-packed phenyl layers on Si(111)*, ***Journal of Physical Chemistry B***, **1997**, 101 (14), 2415-2420.

57. A. Ghorbal, F. Grisotto, M. Laude, J. Charlier, S. Palacin, *The in situ characterization and structuring of electrografted polyphenylene films on silicon surfaces. An AFM and XPS study*, ***Journal of Colloid and Interface Science***, **2008**, 328 (2), 308-313.

58. P. Allongue, C. H. de Villeneuve, G. Cherouvrier, R. Cortes, M. C. Bernard, *Phenyl layers on H-Si(111) by electrochemical reduction of diazonium salts: monolayer versus multilayer formation*, ***Journal of Electroanalytical Chemistry***, **2003**, 550, 161-174.

59. S. Q. Lud, M. Steenackers, R. Jordan, P. Bruno, D. M. Gruen, P. Feulner, J. A. Garrido, M. Stutzmann, *Chemical grafting of biphenyl self-assembled monolayers on ultrananocrystalline diamond*, ***Journal of the American Chemical Society***, **2006**, 128 (51), 16884-16891.

60. A. Merson, T. Dittrich, Y. Zidon, J. Rappich, Y. Shapira, *Charge transfer from TiO2 into adsorbed benzene diazonium compounds*, ***Applied Physics Letters***, **2004**, 85 (6), 1075-1076.

61. C. Combellas, F. Kanoufi, D. Mazouzi, A. Thiebault, P. Bertrand, N. Medard, *Surface modification of halogenated polymers. 4. Functionalisation of poly(tetrafluoroethylene) surfaces by diazonium salts*, ***Polymer***, **2003**, 44 (1), 19-24.

62. S. Maldonado, T. J. Smith, R. D. Williams, S. Morin, E. Barton, K. J. Stevenson, *Surface modification of indium tin oxide via electrochemical reduction of aryldiazonium cations*, ***Langmuir***, **2006**, 22 (6), 2884-2891.

63. M. Toupin, D. Belanger, *Thermal stability study of aryl modified carbon black by in situ generated diazonium salt*, ***Journal of Physical Chemistry C***, **2007**, 111 (14), 5394-5401.

64. G. Decher, *Fuzzy nanoassemblies: Toward layered polymeric multicomposites*, ***Science***, **1997**, 277 (5330), 1232-1237.

65. G. Decher, J. D. Hong, J. Schmitt, *Buildup of Ultrathin Multilayers Films by Self-Assembly Process. 3. Consecutively Alternating Adsorption of Anionic and Cationic Polyelecrolytes on Charged Surfaces*, ***Thin Solid Films***, **1992**, 210 (1-2), 831-835.

66. P. K. H. Ho, J. S. Kim, J. H. Burroughes, H. Becker, S. F. Y. Li, T. M. Brown, F. Cacialli, R. H. Friend, *Molecular-scale interface engineering for polymer light-emitting diodes*, ***Nature***, **2000**, 404 (6777), 481-484.

67. J. M. Garza, N. Jessel, G. Ladam, V. Dupray, S. Muller, J. F. Stoltz, P. Schaaf, J. C. Voegel, P. Lavalle, *Polyelectrolyte multilayers and degradable polymer layers as multicompartment films*, ***Langmuir***, **2005**, 21 (26), 12372-12377.

68. F. Caruso, *Colloids and colloids assemblies*, Wiley-VCH, Weinheim, **2003**.

69. H. Biederman, Y. Osada, *Plasma Polymerization Processes*, Elsevier, Amsterdam, **1992**.

70. M. Konuma, *Film Deposition by Plasma Techniques*, Springer Verlag, Berlin, **1992**.

71. S. Gaur, G. Vergason, *Plasma Polymerization: Theory and Practice*, ***SVC: Annual Technical Conference Proceedings - Denver***, **2000**.

72. S. Glenis, G. Tourillon, F. Garnier, *Influence of the Doping on the Photovoltaic Properties of Thin-Films of Poly-3-methylthiophene*, ***Thin Solid Films***, **1986**, 139 (3), 221-231.

73. A. Tsumura, H. Koezuka, T. Ando, *Macromolecular electronic device - Field-effect transistor with a polythiophene thin-film*, ***Applied Physics Letters***, **1986**, 49 (18), 1210-1212.

74. P. Kovacic, M. B. Jones, *Dehydro Coupling of Aromatic Nuclei by Catalyst Oxidant Systems - Poly(para-phenylene)*, ***Chemical Reviews***, **1987**, 87 (2), 357-379.

75. A. F. Diaz, J. C. Lacroix, *Synthesis of Electroactive Conductive Polymer-Films - Electrooxidation of Heteroaromatic-Compounds*, ***New Journal of Chemistry***, **1988**, 12 (4), 171-180.

76. J. Roncali, *Conjugated Poly(thiophenes) - Synthesis, Functionalization and Applications*, ***Chemical Reviews***, **1992**, 92 (4), 711-738.

77. S. Palacin, C. Bureau, J. Charlier, G. Deniau, B. Mouanda, P. Viel, *Molecule-to-metal bonds: Electrografting polymers on conducting surfaces*, ***ChemPhysChem***, **2004**, 5 (10), 1469-1481.

78. G. Deniau, P. Viel, C. Bureau, G. Zalczer, P. Lixon, S. Palacin, *Study of the polymers obtained by electroreduction of methacrylonitrile*, ***Journal of Electroanalytical Chemistry***, **2001**, 505 (1-2), 33-43.

79. G. Deniau, L. Azoulay, P. Jegou, G. Le Chevallier, S. Palacin, *Carbon-to-metal bonds: Electrochemical reduction of 2-butenenitrile*, ***Surface Science***, **2006**, 600 (3), 675-684.

80. P. Viel, C. Bureau, G. Deniau, G. Zalczer, G. Lecayon, *Electropolymerization of methacrylonitrile on a rotating disk electrode at high spinning rate*, ***Journal of Electroanalytical Chemistry***, **1999**, 470 (1), 14-22.

81. J. Charlier, S. Ameur, J. P. Bourgoin, C. Bureau, S. Palacin, *Mask-free localized grafting of organic polymers at the micrometer or submicrometer scale on composite conductors or semiconductor substrates*, ***Advanced Functional Materials***, **2004**, 14 (2), 125-132.

82. J. Charlier, L. Baraton, C. Bureau, S. Palacin, *Directed organic grafting on locally doped silicon substrates*, ***ChemPhysChem***, **2005**, 6 (1), 70-74.

83. A. Benedetto, M. Balog, P. Viel, F. Le Derf, M. Salle, S. Palacin, *Electro-reduction of diazonium salts on gold: Why do we observe multi-peaks?*, ***Electrochimica Acta***, **2008**, 53 (24), 7117-7122.

84. P. Viel, L. Dubois, J. Lyskawa, M. Sallé, S. Palacin, *New concept to remove heavy metals from liquid waste based on electrochemical pH-switchable immobilized ligands*, ***Applied Surface Science***, **2007**, 253 (6), 3263-3269.

85. S. Ameur, C. Bureau, J. Charlier, S. Palacin, *Immobilization of biomolecules on electrodes modified by electrografted films*, ***Journal of Physical Chemistry B***, **2004**, 108 (34), 13042-13046.

86. S. Palacin, J. Charlier, G. Deniau, P. Jegou, B. Jousselme, B. Mouanda, P. Viel, *Molecular and Organic Devices Chap 1*, Ed. D. K. Aswal and J. V. Yakhmi; Nova Sciences Publishers, **2010**.

87. C. Bureau, J. Gonzales, G. Deniau, *Procédé de formation d'un film polymère sur une surface conductrice ou semi-conductrice*, French Patent FR 2860523, **2005**.

88. M. Cecius, R. Jerome, C. Jerome, *New monomers tailored for direct electrografting onto carbon in water*, ***Macromolecular Rapid Communications***, **2007**, 28 (8), 948-954.

89. G. Deniau, L. Azoulay, L. Bougerolles, S. Palacin, *Surface electroinitiated emulsion polymerization: Grafted organic coatings from aqueous solutions*, ***Chemistry of Materials***, **2006**, 18 (23), 5421-5428.

90. L. Tessier, G. Deniau, B. Charleux, S. Palacin, *Surface Electroinitiated Emulsion Polymerization (SEEP): A Mechanistic Approach*, ***Chemistry of Materials***, **2009**, 21 (18), 4261-4274.

91. L. Tessier, J. Chancolon, P. J. Alet, A. Trenggono, M. Mayne-L'Hermite, G. Deniau, P. Jegou, S. Palacin, *Grafting organic polymer films on surfaces of carbon nanotubes by surface electroinitiated emulsion polymerization*, ***Physica Status Solidi A: Applications and Materials Science***, **2008**, 205 (6), 1412-1418.

92. A. Mesnage, G. Deniau, L. Tessier, V. Mevellec, S. Palacin, *Localized grafting through chemical lift-off*, ***Applied Surface Science***, **2011**, 257 (17), 7805-7812.

93. B. Mouanda, V. Eyeffa, S. Palacin, *Agarose-based hydrogel as an electrografting cell*, ***Journal of Applied Electrochemistry***, **2009**, 39 (3), 313-320.

94. A. Ghorbal, F. Grisotto, J. Charlier, S. Palacin, C. Goyer, C. Demaille, *Localized Electrografting of Vinylic Monomers on a Conducting Substrate by Means of an Integrated Electrochemical AFM Probe*, ***ChemPhysChem***, **2009**, 10 (7), 1053-1057.

95. F. Grisotto, *Localized Organic Electrografting on Conductive and Semiconductive Surfaces Induces by Local Probe Elecrochemical Microscopy*, Thèse de l'Ecole Polytechnique, Palaiseau, **2010**.

96. S. Mahouche-Chergui, S. Gam-Derouich, C. Mangeney, M. Chehimi, *Aryl diazonium salts: a new class of coupling agents for bonding polymers, biomacromolecules and nanoaprticles to surfaces*, ***Chemical Society Reviews***, **2011**, 40, 4143-4166.

97. R. Barbey, L. Lavanant, D. Paripovic, N. Schuwer, C. Sugnaux, S. Tugulu, H. A. Klok, *Polymer Brushes via Surface-Initiated Controlled Radical Polymerization: Synthesis, Characterization, Properties, and Applications*, ***Chemical Reviews***, **2009**, 109 (11), 5437-5527.

98. A. Adenier, E. Cabet-Deliry, T. Lalot, J. Pinson, F. Podvorica, *Attachment of polymers to organic moieties covalently bonded to iron surfaces*, ***Chemistry of Materials***, **2002**, 14 (11), 4576-4585.

99. H. M. Li, F. O. Cheng, A. M. Duft, A. Adronov, *Functionalization of single-walled carbon nanotubes with well-defined polystyrene by "click" coupling*, ***Journal of the American Chemical Society***, **2005**, 127 (41), 14518-14524.

100. S. Mahouche, N. Mekni, L. Abbassi, P. Lang, C. Perruchot, M. Jouini, F. Mammeri, M. Turmine, H. Ben Romdhane, M. M. Chehimi, *Tandem diazonium salt electroreduction and click chemistry as a novel, efficient route for grafting macromolecules to gold surface*, ***Surface Science***, **2009**, 603 (21), 3205-3211.

101. O. Prucker, J. Ruhe, *Synthesis of poly(styrene) monolayers attached to high surface area silica gels through self-assembled monolayers of azo initiators*, ***Macromolecules***, **1998**, 31 (3), 592-601.

102. R. Advincula, *Polymer Brushes by Anionic and Cationic Surface-Initiated Polymerization (SIP) - In: Surface-Initiated Polymerization I*, Springer-Verlag, Berlin, **2006**.

103. M. R. Buchmeiser, *Metathesis Polymerization To and From Surfaces - In: Surface-Initiated Polymerization I*, Springer-Verlag, Berlin, **2006**.

104. Y. Tsujii, K. Ohno, S. Yamamoto, A. Goto, T. Fukuda, *Struture and Properties of High-Density Polymer Brushes Prepared by Surface-Initiated Living Radical Polymerization - In: Surface-Initiated Polymerization I*, Springer-Verlag, Berlin, **2006**.

105. M. Husseman, E. E. Malmstrom, M. McNamara, M. Mate, D. Mecerreyes, D. G. Benoit, J. L. Hedrick, P. Mansky, E. Huang, T. P. Russell, C. J. Hawker, *Controlled synthesis of polymer brushes by "Living" free radical polymerization techniques*, ***Macromolecules***, **1999**, 32 (5), 1424-1431.

106. C. Devaux, J. P. Chapel, E. Beyou, P. Chaumont, *Controlled structure and density of "living" polystyrene brushes on flat silica surfaces*, ***European Physical Journal E***, **2002**, 7 (4), 345-352.

107. M. Ignatova, S. Voccia, B. Gilbert, N. Markova, P. S. Mercuri, M. Galleni, V. Sciannamea, S. Lenoir, D. Cossement, R. Gouttebaron, R. Jerome, C. Jerome, *Synthesis of copolymer brushes endowed with adhesion to stainless steel surfaces and antibacterial properties by controlled nitroxide-mediated radical polymerization*, ***Langmuir***, **2004**, 20 (24), 10718-10726.

108. C. Jerome, S. Gabriel, R. Jerome, *Cathodic electrografting of acrylics: From fundamentals to functional coatings*, ***Progress in Polymer Science***, **2010**, 35 (1-2), 113-140.

109. M. Baum, W. J. Brittain, *Synthesis of polymer brushes on silicate substrates via reversible addition fragmentation chain transfer technique*, ***Macromolecules***, **2002**, 35 (3), 610-615.

110. C. Z. Li, B. C. Benicewicz, *Synthesis of well-defined polymer brushes grafted onto silica nanoparticles via surface reversible addition-fragmentation chain transfer polymerization*, ***Macromolecules***, **2005**, 38 (14), 5929-5936.

111. M. C. R. Tria, C. D. T. Grande, R. R. Ponnapati, R. C. Advincula, *Electrochemical Deposition and Surface-Initiated RAFT Polymerization: Protein and Cell-Resistant PPEGMEMA Polymer Brushes*, ***Biomacromolecules***, **2011**, 11 (12), 3422-3431.

112. C. D. Grande, M. C. Tria, G. Q. Jiang, R. Ponnapati, R. Advincula, *Surface-Grafted Polymers from Electropolymerized Polythiophene RAFT Agent*, ***Macromolecules***, 44 (4), 966-975.

113. G. J. Wang, S. Z. Huang, Y. Wang, L. Liu, J. Qiu, Y. Li, *Synthesis of water-soluble single-walled carbon nanotubes by RAFT polymerization*, ***Polymer***, **2007**, 48 (3), 728-733.

114. X. Y. Huang, M. J. Wirth, *Surface-initiated radical polymerization on porous silica*, ***Analytical Chemistry***, **1997**, 69 (22), 4577-4580.

115. M. Ejaz, S. Yamamoto, K. Ohno, Y. Tsujii, T. Fukuda, *Controlled graft polymerization of methyl methacrylate on silicon substrate by the combined use of the Langmuir-Blodgett and atom transfer radical polymerization techniques*, ***Macromolecules***, **1998**, 31 (17), 5934-5936.

116. W. X. Huang, J. B. Kim, M. L. Bruening, G. L. Baker, *Functionalization of surfaces by water-accelerated atom-transfer radical polymerization of hydroxyethyl methacrylate and subsequent derivatization*, ***Macromolecules***, **2002**, 35 (4), 1175-1179.

117. D. M. Jones, A. A. Brown, W. T. S. Huck, *Surface-initiated polymerizations in aqueous media: Effect of initiator density*, ***Langmuir***, **2002**, 18 (4), 1265-1269.

118. B. Mouanda, E. Bassa, G. Deniau, P. Jegou, P. Viel, S. Palacin, *Comparison of two "grafting from" techniques for surface functionalization: Cathodic electrografting and surface-initiated atom transfer radical polymerization*, ***Journal of Electroanalytical Chemistry***, **2009**, 629 (1-2), 102-109.

119. T. Matrab, M. M. Chehimi, C. Perruchot, A. Adenier, A. Guillez, M. Save, B. Charleux, E. Cabet-Deliry, J. Pinson, *Novel approach for metallic surface-initiated atom transfer radical polymerization using electrografted initiators based on aryl diazonium salts*, ***Langmuir***, **2005**, 21 (10), 4686-4694.

120. J. Iruthayaraj, S. Chernyy, M. Lillethorup, M. Ceccato, T. Ron, M. Hinge, P. Kingshott, F. Besenbacher, S. U. Pedersen, K. Daasbjerg, *On Surface-Initiated Atom Transfer Radical Polymerization Using Diazonium Chemistry To Introduce the Initiator Layer*, ***Langmuir***, **2011**, 27 (3), 1070-1078.

121. T. Matrab, J. Chancolon, M. M. L'hermite, J. N. Rouzaud, G. Deniau, J. P. Boudou, M. M. Chehimi, M. Delamar, *Atom transfer radical polymerization (ATRP) initiated by aryl diazonium salts: a new route for surface modification of multiwalled carbon nanotubes by tethered polymer chains*, ***Colloids and Surfaces, A: Physicochemical and Engineering Aspects***, **2006**, 287 (1-3), 217-221.

122. T. Matrab, M. M. Chehimi, J. P. Boudou, F. Benedic, J. Wang, N. N. Naguib, J. A. Carlisle, *Surface functionalization of ultrananocrystalline diamond using atom transfer radical polymerization (ATRP) initiated by electro-grafted aryldiazonium salts*, ***Diamond and Related Materials***, **2006**, 15 (4-8), 639-644.

123. D. J. Dyer, *Photoinitiated Synthesis of Grafted Polymers - In: Surface-Initiated Polymerization I*, Springer-Verlag, Berlin, **2006**.

124. O. Prucker, C. A. Naumann, J. Ruhe, W. Knoll, C. W. Frank, *Photochemical attachment of polymer films to solid surfaces via monolayers of benzophenone derivatives*, ***Journal of the American Chemical Society***, **1999**, 121 (38), 8766-8770.

125. R. Paul, R. Schmidt, D. J. Dyer, *Synthesis of ultrathin films of polyacrylonitrile by photoinitiated polymerization from self-assembled monolayers on gold*, ***Langmuir***, **2002**, 18 (23), 8719-8723.

126. O. Prucker, J. Habicht, I. J. Park, J. Ruhe, *Photolithographic structuring of surface-attached polymer monolayers*, ***Materials Science & Engineering C-Biomimetic and Supramolecular Systems***, **1999**, 8-9, 291-297.

127. M. Niwa, M. Date, N. Higashi, *In situ photopolymerization of methacrylic acid at a self-assembled xanthate monolayer surface on gold. Formation of poly(methacrylic acid) brushes and their interaction with cytochrome c*, ***Macromolecules***, **1996**, 29 (11), 3681-3685.

128. S. Gam-Derouich, B. Carbonnier, M. Turmine, P. Lang, M. Jouini, D. Ben Hassen-Chehimi, M. M. Chehimi, *Electrografted Aryl Diazonium Initiators for Surface-Confined Photopolymerization: A New Approach to Designing Functional Polymer Coatings*, ***Langmuir***, **2010**, 26 (14), 11830-11840.

129. H. Lee, S. M. Dellatore, W. M. Miller, P. B. Messersmith, *Mussel-inspired surface chemistry for multifunctional coatings*, ***Science***, **2007**, 318 (5849), 426-430.

130. J. H. Waite, *Surface chemistry - Mussel power*, ***Nature Materials***, **2008**, 7 (1), 8-9.

131. Q. Wei, F. L. Zhang, J. Li, B. J. Li, C. S. Zhao, *Oxidant-induced dopamine polymerization for multifunctional coatings*, ***Polymer Chemistry***, **2010**, 1 (9), 1430-1433.

132. S. H. Ku, J. S. Lee, C. B. Park, *Spatial Control of Cell Adhesion and Patterning through Mussel-Inspired Surface Modification by Polydopamine*, ***Langmuir***, **2010**, 26 (19), 15104-15108.

133. R. J. Zeng, Z. F. Luo, D. Zhou, F. H. Cao, Y. M. Wang, *A novel PEG coating immobilized onto capillary through polydopamine coating for separation of proteins in CE*, ***Electrophoresis***, **2010**, 31 (19), 3334-3341.

134. W. C. Wang, J. Wang, Y. Liao, L. Q. Zhang, B. Cao, G. J. Song, X. L. She, *Surface Initiated ATRP of Acrylic Acid on Dopamine-Functionalized AAO Membranes*, ***Journal of Applied Polymer Science***, **2010**, 117 (1), 534-541.

CHAPTER II

Presentation of the chemical anchoring process

What is a chemical anchoring process based on diazonium salts? This chapter aims at answering this question. First of all, the progression that has led to the creation of the anchoring method based on diazonium salts and particularly the Graftfast™ process will be developed. The advantages of such process will be demonstrated. To finish, its principle will be detailed, the main components will be presented and characterized.

II.1 - Origin and principle of the chemical anchoring process

The grafting of polymers on surfaces is a major research topic of our laboratory and has thus been widely studied especially through the cathodic electrografting of vinylic monomers and, more recently, through a process called SEEP standing for Surface Electroinitiated Emulsion Polymerization. As mentioned in I.2.1.7, the cathodic electrografting of vinylic monomers[1] gives strongly adhesive polymer films on any conducting or semi-conducting surface from anhydrous solutions of vinylic monomers. Overcoming the limitations of this process coming from the inherent mechanism of the reaction (anionic polymerization) has led to work with diazonium salts and to invent the SEEP process[2-4] (see I.2.1.8). Indeed, this electroiniated radical polymerization process works in dispersed aqueous media and with a wide range of monomers. However, both processes, as electrochemical procedures, are limited in terms of substrates. To open the route towards the grafting of any type of surfaces from conductors to insulators, a method employing a reducing agent in solution was developed to activate the diazonium salts.

Such as its electrochemical counterpart process SEEP, this new procedure[5], called Graftfast™, is a radical polymerization process based on the reduction of diazonium salts generating radicals able to initiate the polymerization in solution of vinylic monomers. The nature of the films obtained ranges from poly(meth)acrylates (the main family of polymers grafted by cathodic electrografting) to all polymers that can be synthesized by radical polymerization. Graftfast™ leads to grafted polymer films from a short one-step reaction occurring at atmospheric pressure, at room temperature, in water and requiring no external energy source.

Literally, the name Graftfast™ is employed to describe the anchoring process mixing a diazonium salt, a reducing agent with or without a vinylic monomer in solution. However, for the sake of clarity, we will only call Graftfast™ the process involving a vinylic monomer. The anchoring process employing the diazonium salt uniquely in presence of a reducing agent will be simply named “redox-induced process” and the grafting using only the diazonium salt is a “spontaneous” process. Both were also studied and will be discussed in this thesis.

To date, only a few methods comparable to Graftfast™ exist. The closest one is a bioinspired method based on the self-polymerization of dopamine (cf I.2.2.3) which can be followed by a classical polymerization[6]. However, unlike Graftfast™, the formation of polymer films on the surface of materials using dopamine requires a two-step (at least) reaction and involves long reaction times.

II.2 - Advantages of the chemical anchoring process

In order to understand the interest of this work, it is important to have an overview of the potentialities of the process. Among the methods to functionalize materials by polymer films, Graftfast™ appears to be a powerful process since it was successfully applied to a large variety of materials and, as demonstrated by previous works[5, 7], it enables to control the thickness of the films, the surface properties of the substrates as well as the localization of the grafting.

II.2.1 - Type of materials

Theoretically, Graftfast™ can suit any type of surface, insulators or conductors. The process has been widely applied on conducting or semi-conducting substrates such as, for example, on nickel, zinc, platinum, stainless steel (inox), titanium, gold, carbon fibres and aluminium as illustrated in Figure 1 but also on nano-objects such as carpets of multiwalled carbon nanotubes[8] (Figure 2). Insulating materials from glass to Teflon® (PTFE), both detailed in II.2.2.2, including plastics, cellulose (wood, paper) or cotton have also been grafted by this method.

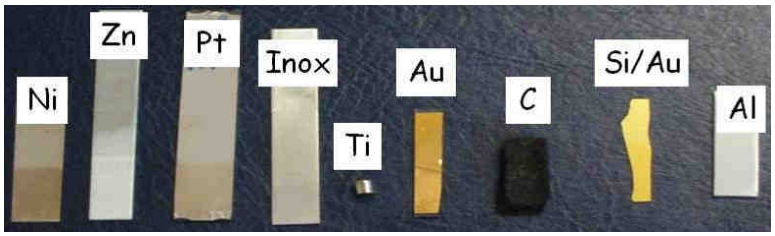

Figure 1 – Conducting or semi-conducting substrates successfully grafted by the Graftfast™ process[7]. Some of the grafted films are visible to the naked eye as for graftings on Ni or Pt where the films are located on the darkest area of the substrate.

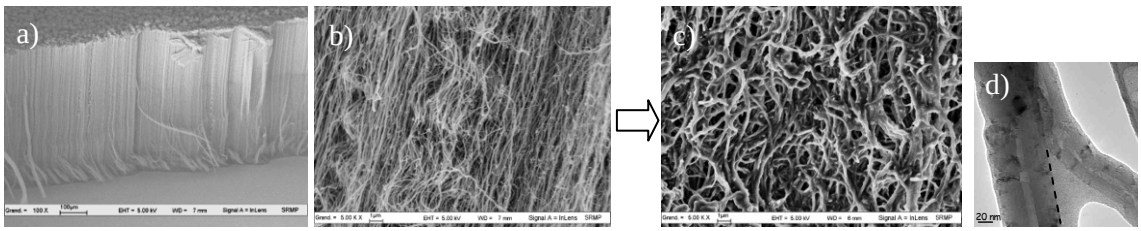

Figure 2 – SEM images a) and b) before grafting (different magnifications) and c) after grafting. TEM image of the grafted nanotubes is shown in d). The dashed line corresponds to the interface polymer/nanotube[7].

II.2.2 - **Parameters controlled in the process**

II.2.2.1 - Control of the thickness

The initial study on the Graftfast™ process conducted by Mévellec *et al.*[5] has demonstrated that the intensity of the IR band characteristic of the grafted polymer increased with the reaction time and has established a correlation between the intensity of the IR band and the film thickness. Therefore, they proved that by controlling the reaction time, the thickness of the grafted films can be tailored.

II.2.2.2 - Control of the surface properties

One of the main purposes of surface modification is, without any doubt, to tailor the surface properties of materials. As an example, for some industrial applications, the production of glass with a hydrophobic surface can be a major issue. With the Graftfast™ process, this transformation of the glass surface has been achieved by the grafting of an hydrophobic polymer (poly(butyl methacrylate) PBMA) as shown in Figure 3a. The opposite surface modification consisting in changing a hydrophobic surface into a hydrophilic one has also been successfully carried out on Teflon® (Figure 3b). The process is a very promising method for surface modifications. Thus, it is easy to understand why this chemically-initiated process attracts considerable attention in many fields of applications such as biomedical and biotechnologies, polymer metallization, lubrication...

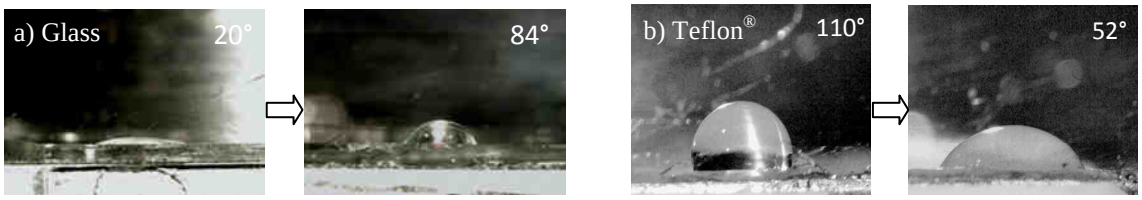

Figure 3 – Contact angle measurements of a) glass before and after modification with PBMA and b) Teflon® before and after modification with PAA[5].

II.2.2.3 - Simultaneous and sequential grafting

Thanks to this process, it is also possible to combine the characteristic properties of two or more polymers by either introducing them simultaneously or one after the other in solution. In the first case, by adding simultaneously various monomers, a non-ordered mixture of the two polymers grafted on the substrate can be obtained, bringing different surface groups with potentially different reactivity or properties. In the second case, a multilayer-like polymer film is built which allows combining the bulk properties of the first polymer introduced and the surface properties of the last one. In both cases the range of applications of such grafted materials is widen.

II.2.2.4 - Localized grafting

Another important asset of this anchoring process lies in the control of the localization of the grafting. Indeed, as the radical moieties involved in the process are prone to graft on any

surface, transient masking methods based on poorly adherent films can be used to prevent the covalent grafting in designated areas of the full substrate. First of all, in order to test the validity of lift-off processes, we demonstrated the possibility of using a commercial ink simply drawn on a metallic substrate as a chemical mask to protect designated areas from the chemical grafting of polymers by Graftfast™. Then we confirmed that using microcontact printed alkanethiols SAMs as sacrificial layers, gold surfaces can be patterned by the Graftfast™ process as illustrated in Figure 4. Therefore, using common lift-off techniques in addition to the Graftfast™ process, the localization of polymer grafting has been achieved which opens the route towards applications requiring patterned surfaces[9].

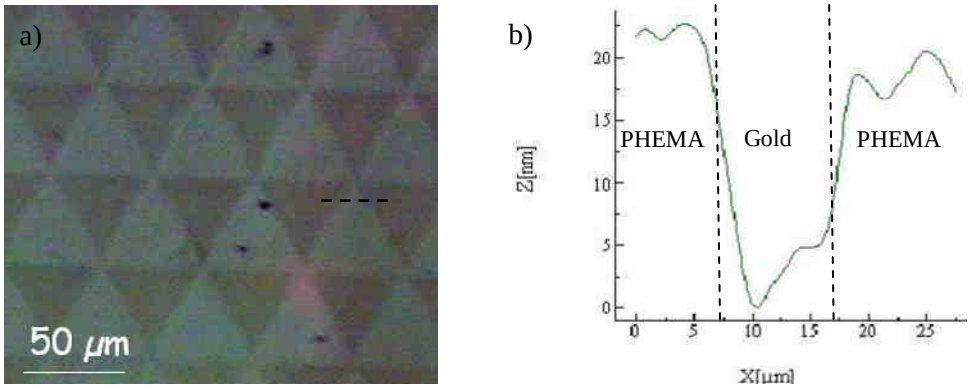

Figure 4 – The optical micrograph of a gold plate coated with a thiol mask with triangular patterns after treatment by Graftfast™ in the presence of HEMA and removal of a mask is shown in a). Dark zones correspond to the polymer while the clear ones correspond to non-covered gold. The graph (b) is the AFM profile obtained between covered and non-covered zones schematically represented in dashed line on a)[9].

II.3 - **Main components of the chemical anchoring process in details**

As illustrated by Scheme 32, carrying out a typical Graftfast™ experiment consists in choosing: the diazonium salt, the reducing agent, the vinylic monomer, the substrate, possibly the solvent and adjusting the concentration of each reactant, the reaction time but also, if necessary, the temperature, the atmosphere, the bubbling of the solution with different gases, its stirring, its exposure to light ... Each parameter can influence the film grafting and has thus to be selected carefully according to the aim of the work. Therefore, this section will focus on a general presentation of the main components of the Graftfast™ procedure as well as a detailed characterization of the selected compounds in this work. The data gathered from this part will have to be kept in mind for further considerations and interpretations of results obtained in the following studies.

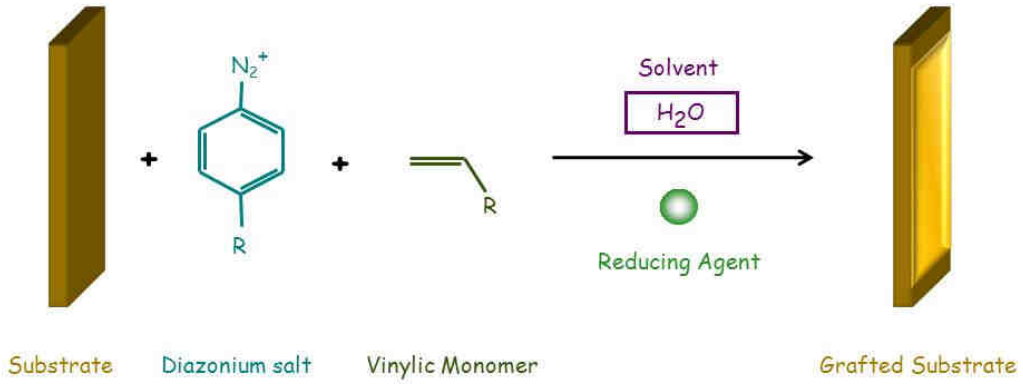

Scheme 32 – A typical Graftfast™ experiment.

II.3.1 - **Diazonium salt**

A diazo compound is an aliphatic, aromatic or heterocyclic compound in which a $-N_2$ group is attach to a carbon atom. In 1858, Peter Griess discovered aromatic diazonium compounds ($RN_2^+X^-$)[10]. Conjugation with the aromatic cycle π-electrons makes aryl diazonium ions much more stable[11] than their aliphatic counterparts which are potentially explosive when dry[12] and therefore rarely used in classic organic chemistry[13-15]. In contrast to all alkyl diazonium ions, aromatic diazonium salts are not Brønsted acids but Lewis acids[10]. The diazonium moiety (N_2^+) is reported to be the most electron-withdrawing substituent known[16]. Consequently, diazonium salts take part in a large variety of reactions[17-19] in particular nucleophilic additions on the β-nitrogen of the diazonium, nucleophilic substitutions[20] and azo coupling. Important industrial applications have arisen from those reactions including intermediates or end products such as azo dyes[10].

II.3.1.1 - Diazoniation reactions

A few para-substituted aromatic diazonium salts are commercially available among them 4-bromo, nitro or methoxy benzenediazonium tetrafluoroborate (BF_4^- is known to stabilize diazonium salts[10]). A range of di-substituted or complex aromatic diazonium salts can also be found. However, to synthesize and isolate aromatic diazonium compounds (diazoniation reaction), a number of distinct methods are known[18]. The more common one consists in the reaction of sodium nitrite on an aryl amine in acidic media at 0°C (Scheme 33)[10, 18].

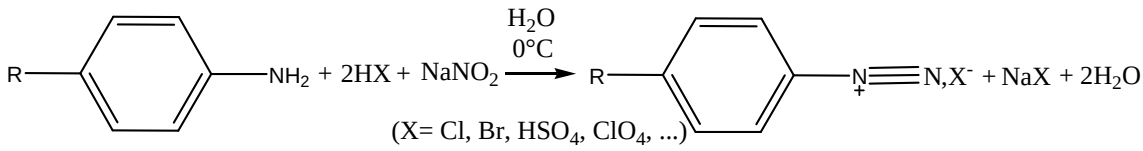

Scheme 33 – Typical diazoniation reaction.

Other methods such as $NOBF_4$ in ACN at 0°C or BF_3OEt_2/t-BuONO in THF at -40°C[21] in presence of the appropriated aryl amine can also be employed depending on the nature of the diazonium salt and its associated counterion desired. To finish, it is important to underline that

the first two diazoniation methods described above can be used to synthesize the diazonium salt *in-situ* i.e. in the reactive solution consuming the diazonium salt. This kind of method is known as *one-pot* reaction[22, 23].

II.3.1.2 - Dediazoniation reactions

Among the variety of reactions based on diazonium salts, dediazoniation reactions (referring to reactions involving the loss of dinitrogen) have attracted much interest. They may take place following either a heterolytic or a homolytic mechanism (Scheme 34)[10, 17].

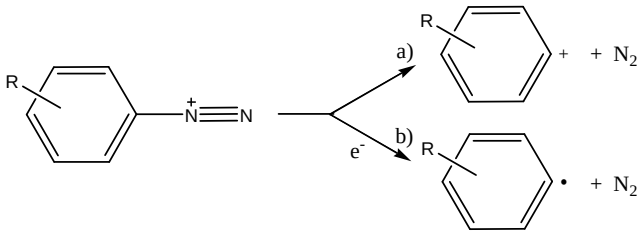

Scheme 34 – Dediazoniation through a a) heterolytic and b) homolytic mechanism.

The heterolytic dediazoniation pathway is the most likely mechanism in the degradation of diazonium salts in solution as it forms a very stable product N_2 in addition to a metastable intermediate, the aryl cation leading to, for example, phenols[24]. Heterolytic cleavage of the C-N bond can also be involved in solvolytic or thermal reactions[25, 26]. As known by organic chemists, carrying out a homolytic dediazoniation requires an electron transfer which can be induced, for instance, by photochemistry[27], by the solvent[17], by a reduction at an electrode[17, 28] or by reducing agents[29, 30] (metal cations[31], anions[10], H_3PO_2[32-34]...). However, according to the reaction conditions, a competition or coexistence of the two mechanisms is always possible.

To finish, for further understanding, it is important to be aware that an electron transfer (homolytic dediazoniation) from a reducing agent (Red) to an aryldiazonium salt may actually follow two fundamental mechanisms[17, 30]. Represented in Scheme 35, they are described as inner-sphere (or bonded electron transfer process proceeding through a linkage between the two redox partners) and outer-sphere electron transfer pathway (in which chemical moieties always remain separated species). The most likely mechanism strongly depends on experimental conditions. For instance, I^- and $H_2PO_2^-$ which are considered as good anionic reducing agents would favor direct electron transfers (outer-sphere) whereas nucleophilic anions would prefer forming an adduct (inner-sphere).

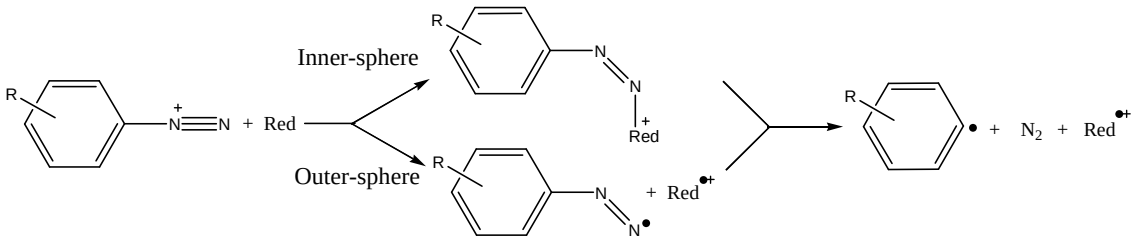

Scheme 35 – Electron transfer mechanism in homolytic dediazoniation.

II.3.1.3 - 4-nitrobenzenediazonium tetrafluoroborate

In order to study the mechanism of the anchoring process, we focused on experiments performed from the dediazoniation of, mainly, 4-nitrobenzene diazonium tetrafluoroborate (NBDT). Indeed, as NBDT is commercially available, we did not have to consider on top of the dediazoniation based reactions its *in-situ* formation. Furthermore, the nitro groups are easily identifiable by IR-ATR (see appendix 1 for more details on data acquisition), as the asymmetric and symmetric stretching vibration bands ν^{as}_{NO2} and ν^{s}_{NO2} are intense absorption bands and the binding energy of the N-O bond in nitro group in N 1s core level XPS spectra could not be confused with nitrogen contained in the substrates or eventual nitrogenous contaminations on their surfaces. In addition, no reducing agent or monomer bearing nitro groups was used. Hence, this group was characteristic of moieties only coming from the diazonium salt, which was an important asset in the understanding of the anchoring process mechanism. In addition, a study on the electrografting of diazonium salts conducted by Combellas[35, 36], consisting in sterically hindering different positions of the diazonium ions, has shown that using a para-substituted aromatic ring favors the growth of the grafted layer. To finish, NBDT has one of the highest reduction potential among known diazonium salts[37, 38] (i.e. with the greater affinity for electrons) which therefore allows a wider choice in the reducing agent. Therefore, the 4-nitrobenzene diazonium salt was selected and the main parameters having a potential influence on its reaction characterized. For instance, its reprecipitation was examined; its stability in various aqueous media was tested and its reduction potential was measured.

Reprecipitation

As received, the commercial 4-nitrobenzene diazonium tetrafluoroborate has a color varying from light to very dark orange. This variation of colour is likely to involve a change in the purity of the compound. Therefore, a classical reprecipitation procedure is employed to free it of any contaminant as described in the appendix 2 and leads to a pale yellow powder. NMR analyses as well as UV-visible spectra of the 4-nitrobenzene diazonium tetrafluoroborate (NBDT) before and after reprecipitation are found to be similar. Moreover, identical experiments carried out with the reprecipitated and non-reprecipitated diazonium salts roughly provided the same results. However, since the removal of traces of contaminants by this procedure may have shortened the list of species in solution, decreased the influence of interfering reactions and so simplified interpretations in solutions studies, the reprecipitation of the 4-nitrobenzene diazonium tetrafluoroborate was always undertaken prior to use.

Stability in various aqueous solvents

Diazonium salts are claimed to be perfectly stable in acidic aqueous solutions (pH < 2) and at low temperature (around 5°C). Therefore, in order to test the stability of NBDT at room temperature and in the solvents used in Graftfast™ experiments, UV-visible absorption

spectrometry was performed. The typical solvents used in the anchoring process tested were: deionized water (pH = 5.5), HCl (0.1 M – pH = 1) and H_2SO_4 (0.05 M – pH = 1). A typical UV-visible absorption spectrum of NBDT in water is shown in Figure 5. It displays two absorption bands: the main one centred at $\lambda = 260$ nm (for the more intense band) and a shoulder at $\lambda = 313$ nm[39-42]. First of all, the molar extinction coefficients at 260 nm in each solvent were experimentally determined using the Beer-Lambert law and four NBDT solutions with precise concentrations from 10^{-4} M to 10^{-5} M. They have been found in accordance with the values from the literature and are reported in Table 1.

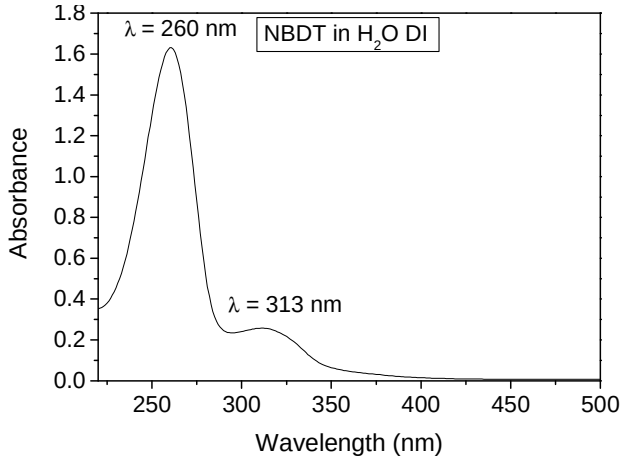

Figure 5 – Typical UV spectrum of NBDT in water.

Table 1 – Values of molar extinction coefficient at 260 nm (ε_{260}) of 4-nitrobenzene diazonium tetrafluoroborate at room temperature in various solvents determined from our experiments and from the literature.

Solvent	Molar Extinction Coefficient ($L.mol^{-1}.cm^{-1}$)	Value from the literature ($L.mol^{-1}.cm^{-1}$)
H_2O DI	17700 ± 60	-
HCl	17200 ± 55	16400[41]
H_2SO_4	15900 ± 50	-

Then, the decomposition of NBDT in those three solvents, at room temperature, ambient light and air was followed with time for 1 h, which corresponds to the usual reaction time of the anchoring experiments (Figure 6). A decrease in the NBDT concentration (determined from the peak at 260 nm) of 0.9 % of its initial value was calculated for the experiment performed in H_2O DI and 0.4 % when carried out in H_2SO_4. The evolution of the shape of the signal around 313 nm for the experiment in water will be discussed in the next paragraph. On the contrary, strong evidence of NBDT decomposition was found in HCl solution. Indeed, a drop of 6 % of the initial NBDT concentration was registered after 1 h. The most significant reason that leads to this drop-off is the possible involvement of the acid in an interfering reaction known to form chloroaryls[18]. However, this decomposition will be considered weak enough to be neglected when performing 1h experiments in HCl.

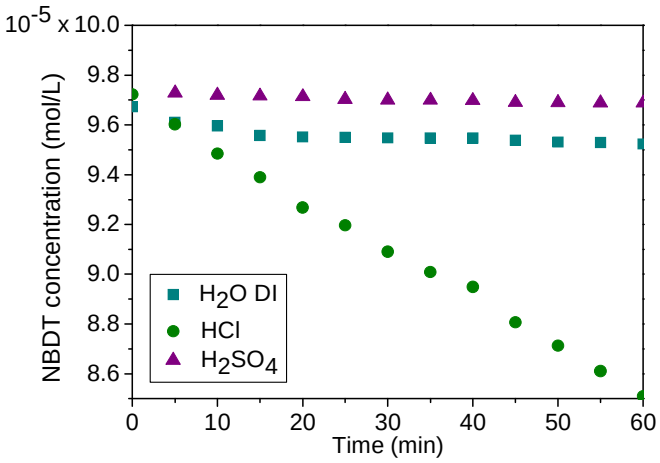

Figure 6 – Variations of the concentration (based on the absorbance value at 260 nm) over 1 h of NBDT ($C = 10^{-4}$ M) in H_2O DI, HCl (0.5 M – pH = 0.3) and H_2SO_4 (0.25M – pH = 0.3) solutions.

In order to evaluate the possibility of keeping NBDT solutions for several sets of experiments, the same experiments were performed over 7 h in the same solvents. A decrease of 5 % in H_2SO_4, 36 % in HCl and 39 % in H_2O DI of the initial NBDT concentration was detected. Figure 7 clearly represents this important degradation of the diazonium salt in H_2O DI. Besides, the drop of absorbance at 260 nm, a widening and an increase in intensity of the second absorption band at 313 nm was also observed on Figure 7 which stems from the creation of a compound absorbing in this range of wavelengths, assumed to be nitrophenol (Figure 8). The presence of an isosbestic point in Figure 7 indicates the direct transformation of the diazonium salt into nitrophenol. Finally, nucleophilic additions on the nitrogen atom leading to the formation of conjugated azo compounds as well as an azo coupling between the nitrophenol formed and the residual diazonium might be potential ways to explain the slight increasing absorption around 400 nm.

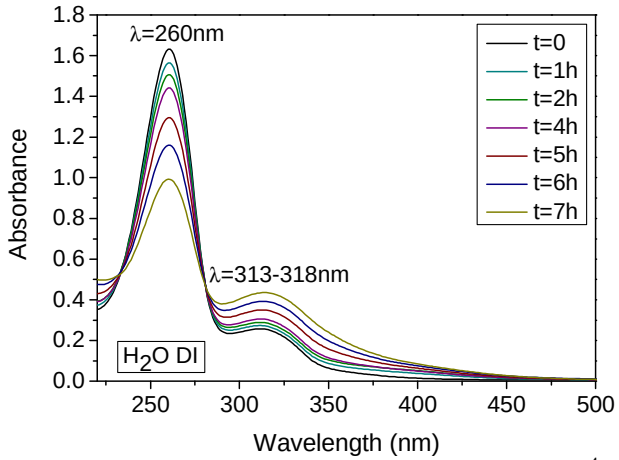

Figure 7 – Variations over 7 h of the UV-visible absorption of NBDT ($C = 10^{-4}$ M) in H_2O DI, (spectrum captured every hour).

Thus, nitrophenol is a likely product of degradation of NBDT since diazonium salts in aqueous solutions are well known to decompose into phenols[24, 43] by a heterolytic dediazoniation pathway as represented on Scheme 36.

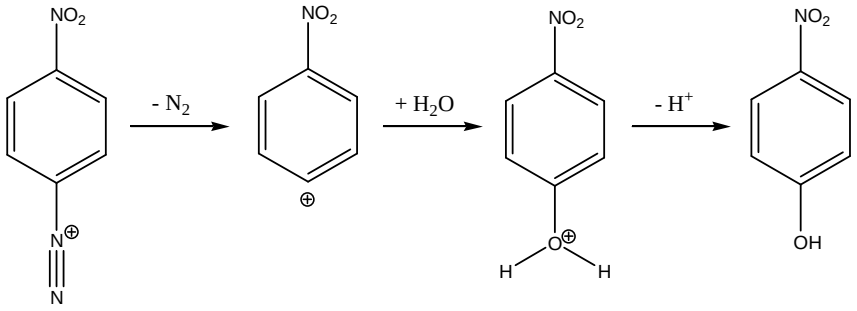

Scheme 36 – Decomposition of 4-nitrobenzene diazonium in aqueous solution.

The UV-visible spectrum of 4-nitrophenol in H_2O DI (Figure 8) displayed a main absorption band at 318 nm. Therefore, it is likely that this band contributes to the widening and increase of the signal in Figure 7 which confirms the formation of nitrophenol in the pathway of NBDT decomposition in H_2O.

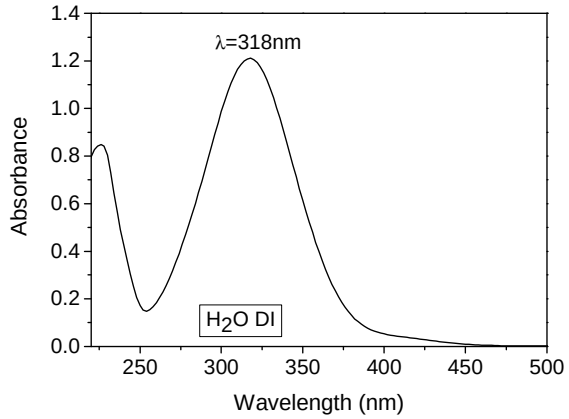

Figure 8 – UV-visible spectrum of 4-nitrophenol in H_2O DI.

With the purpose of investigating the rate law for the reaction of NBDT decomposition and particularly whether it is a first order reaction with respect to the diazonium salt, $\ln([NBDT]/[NBDT]_0)$ in H_2O DI and H_2SO_4 was plotted versus time in Figure 9. As the most likely reaction of degradation (conducting to nitrophenol) is a first order reaction with respect to NBDT, the following equations should be verified:

- reaction rate: $v = k.[NBDT].[H_2O] = k'.[NBDT]$ (since H_2O is the solvent) with k' the pseudo rate constant: $k' = k.[H_2O]$
- rate law: $\ln([NBDT]/[NBDT]_0) = -k'.t$
- half-life time: $t_{1/2} = \ln(2)/k'$.

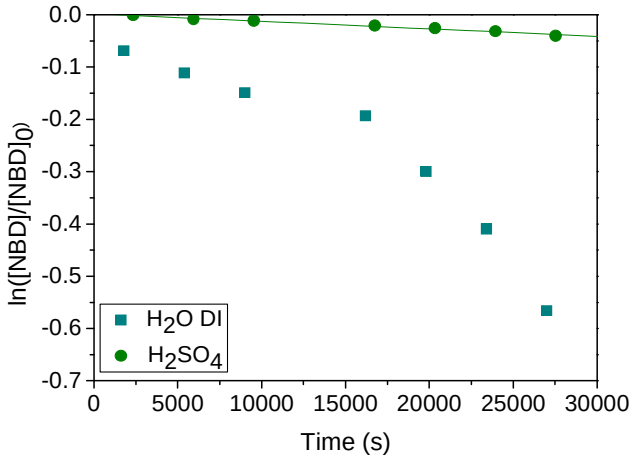

Figure 9 – Plots of ln([NBDT]/[NBDT]$_0$) versus time in H_2O DI and H_2SO_4 with [NBDT]$_0$ = 10^{-4} M

In the case of NBDT in H_2SO_4, the data formed a line which confirmed the involvement of a reaction following a first order rate law. A pseudo rate constant of 1.45x10^{-6} s^{-1} and a half-life time of 132 h were calculated. On the other hand, in H_2O DI, the decomposition of NBDT rate law did not match a first order reaction. This result suggested that other competitive reactions than the formation of nitrophenol might play a role in the diazonium salt degradation. Therefore, as described previously in the literature, diazonium salts are more stable in acid solutions (pH < 2) than in H_2O DI solutions as a drop of respectively only 5 % of the [NBDT] concentration and 40 % in 7 h were recorded (Figure 9).

In addition to nitrophenol detected in the UV-visible measurements, gas chromatography - mass spectroscopy (GC-MS) experiments performed on NBDT in deionized water demonstrated the presence of other products of degradation such as 1-fluoro-4-nitrobenzene and 4-nitrobenzene (cf IV.2.2.1). The former compound certainly comes from the Schiemann reaction (Scheme 37) which is a standard method for the preparation of fluoroaryl compounds[10, 17, 18, 44]. The formation of those products of degradation is probably due to the thermal decomposition of the diazonium salt in the GC-MS injector (heated at 250°C). Therefore, as most of the experiments in this thesis were carried out at room temperature, their presence should be limited and not influence the grafting.

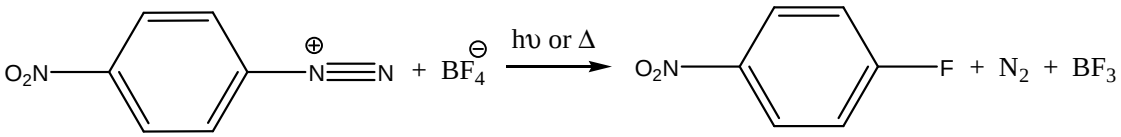

Scheme 37 – Formation of fluoroaryls by the Schiemann reaction.

Regarding all those results, experiments in H_2O DI or H_2SO_4 will be preferred since the NBDT solution remains fairly stable during the usual time of the experiments. Freshly made diazonium salt solutions will always be used in order to start with solutions with precise concentrations and containing a limited amount of nitrophenol.

Reduction potential

As the anchoring processes studied in this thesis are based on an electron transfer, it is important to get information on the reduction potential of the 4-nitrobenzene diazonium salt. NBDT solutions at various pH were electrochemically reduced. The data obtained for a series of three experiments for each pH are presented on Figure 10. The peak potential E_p tends to slightly increase with the pH, indicating an easier reduction of the diazonium salt in non-acidic media. Considering those results, we will consider that the NBDT reduction occurs between 0.25 V and 0.3 V (vs Saturated Calomel Electrode SCE) whatever the pH in the 0-6 range.

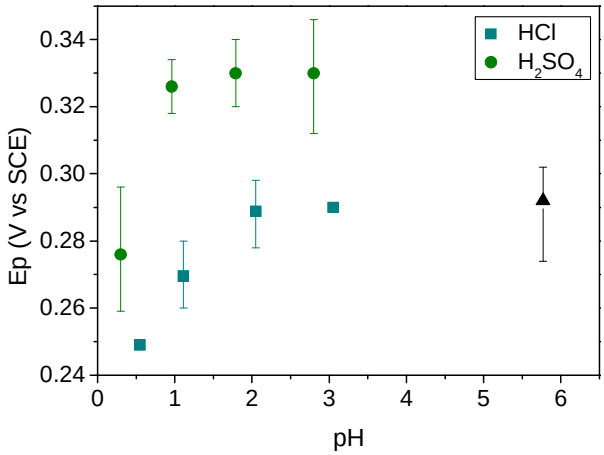

Figure 10 – Peak potential (E_p) for the 4-nitrobenzene diazonium tetrafluoroborate reduction in aqueous solutions (at 0.1 V/s scan rate, SCE, working electrode = gold plate, C = 5 mM) as a function of its pH (adjusted with HCl or H_2SO_4). E_p is the potential corresponding to the maximum of current (I_p) in absolute value. For each pH, the experiment has been repeated three times. Therefore, the dot stands for the average value of E_p and the error bar represents the range of values found.

II.3.2 - **Reducing agents**

Unlike the electrochemical processes, in this anchoring method the electron transfer at the origin of the diazonium salt reduction is not achieved by the application of an electrical potential but by a chemical oxidation-reduction (redox) reaction. Therefore, it follows the same rules as any redox reaction. As a first approximation, all reducing agents with a standard oxidation potential lower than the reduction potential of the diazonium salt are estimated to be suitable to operate the homolytic dediazoniation reaction. Among the possible reducing agents, two different types can be distinguished: the reducing agent acting in heterogeneous phases (composed by a liquid and a solid) and those operating in homogeneous phase (liquid phase).

II.3.2.1 - Heterogeneous phase

The reducing agents working in heterogeneous phase appropriated for the anchoring process of diazonium salts include all solid compounds fulfilling the requirements in terms of oxidation potential. Iron powder has been used as reducing agent in the original Graftfast™ experiments[5] and later for specific applications especially the grafting of cation exchange membranes to improve their selectivity[45], as a first step in an electroless plating process applicable to

polymers[46] and to create self-adhesive surfaces[47]. A lot of other compounds could also be suitable for instance all metals reductive enough (copper, nickel, zinc …).

II.3.2.2 - Homogeneous phase

The reduction of diazonium salts into aryl radicals in homogeneous phases is a well known reaction. It has been notably achieved with iodide[10, 17] and H_3PO_2[10, 48, 49]. It is only recently that this reaction has been considered as a way to functionalize the surface of materials. Up to now, hydroquinone[29], ferrocene (in organic media), H_3PO_2[50-54] and L-ascorbic acid[55] have been used to reduce diazonium salts in order to graft organic layers. Most of the work presented in this thesis was performed using L-acid ascorbic as a reducing agent. However, in some cases, for practical reasons, H_3PO_2 was employed.

In addition to its use in the reduction of arenediazonium salts, hypophosphorous acid (H_3PO_2) is commonly employed for electroless plating (deposition of metal films from solutions)[56, 57]. The study of H_3PO_2 as a reducing agent was only based on the values given in the Pourbaix diagram (pH-potential) represented in Figure 11. According to the pH of the solution, H_3PO_2 and $H_2PO_2^-$ were the species found in solution. The oxidation of both compounds occurs at potential lower than the reduction potential of NBDT meaning that H_3PO_2 and $H_2PO_2^-$ can undeniably work as reducer. However, their oxidation potential is also lower than zero, which means they are able to reduce protons in solution. These remarks have played an important role in understanding the mechanism.

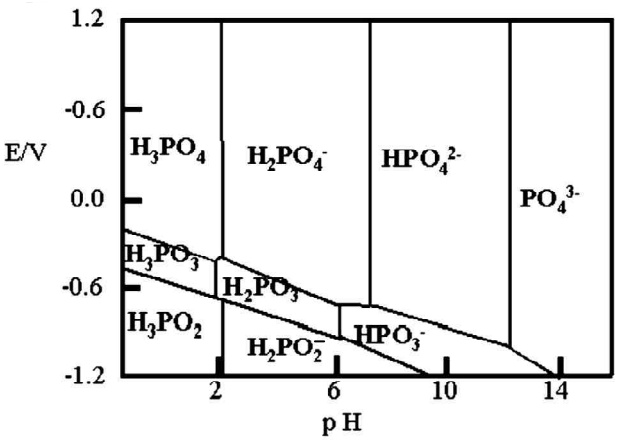

Figure 11 – The diagram of pH-potential of P-containing group at RT extracted from Lin's work[58].

L-ascorbic acid (Scheme 38), also named Vitamin C (VC), is a non-toxic molecule which has particularly attracted our attention. First, unlike iron, it works in homogeneous phase which is an essential criterion for a quantitative study. Second, unlike H_3PO_2, VC is a weak diacid which allows exploring broader experimental conditions as it does not limit too drastically the work in terms of pH. It has already been used as a reducer, for instance, in Sandmeyer reaction[59] or for the reduction of metal ions in solution[60, 61] particularly in the case of gold[62, 63] or silver[64, 65] nano-objects formation. In order to demonstrate the ability of VC to work as a reducing agent in

Graftfast™, the acid-base and redox reactions involving VC were defined, its Pourbaix (potential/pH) diagram was established and it was characterized in terms of oxidation potential.

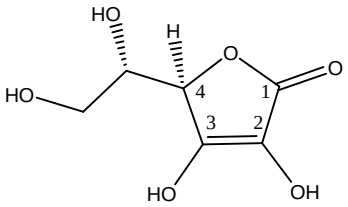

Scheme 38 – L-ascorbic acid or vitamin C (VC).

Acid-base and oxidation-reduction reactions

All the plausible reactions involving L-ascorbic acid and its derivates have been identified as reported in Scheme 39. The first acidity of VC (noted H_2A in some schemes) is due the presence of the acidic proton of the enol form (on carbon 3 of the cycle in Scheme 38) and its second acidity, much weaker, comes from the alcohol group on carbon 2 of the cycle represented in Scheme 38. The most likely redox reactions all lead to the formation of dehydroascorbic acid (noted A in Scheme 39). Experiments were always performed in aqueous solutions with pH lower than 5.5. Therefore, only the first acid-base and the top two redox reactions are likely to play a significant role[b].

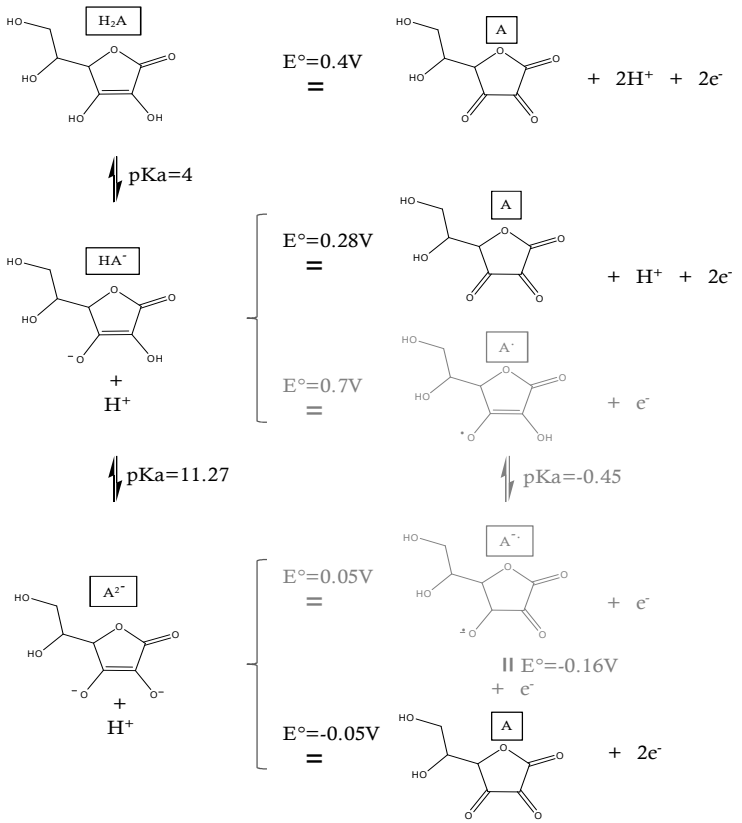

Scheme 39 – Acid-base and oxidation-reduction reactions involving L-ascorbic acid and its derivates[66, 67]. Black writing represents the most likely reactions.

[b] In a general way, the abbreviation VC will be used in this work to indifferently refer to ascorbic acid or its first base. However, when required, the distinction between the two compounds will be clearly made by using the abbreviation H_2A and HA^-.

Pourbaix diagram of L-ascorbic acid

From the data presented in Scheme 39 and the Nernst equation, the Pourbaix diagram of ascorbic acid was established (Figure 12). The diagram gives a visual representation of the main components present in the pH domain of our work (hatched area on Figure 12) and the experimental conditions required reaching the oxidation of the major stable derivatives of ascorbic acid. Therefore, it will be a helpful tool in the understanding of the reaction of ascorbic acid on diazonium salts.

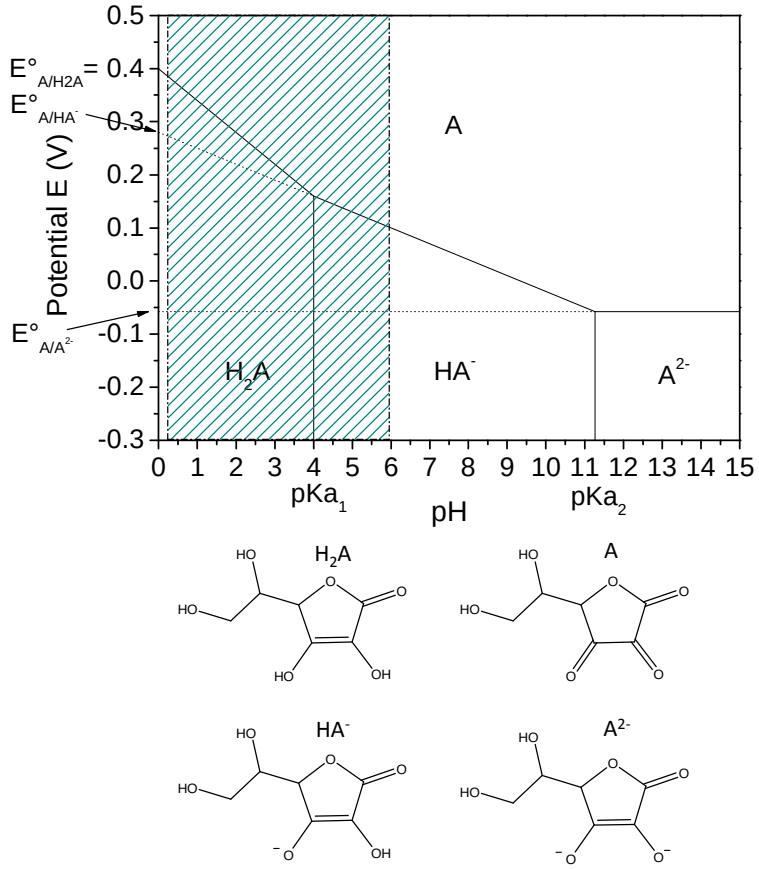

Figure 12 – Pourbaix diagram of ascorbic acid. The hatched lines represent the pH domain of our studies.

Oxidation potential

In order to demonstrate the ability of ascorbic acid to work as a reducing agent for the Graftfast^{TM} process, cyclic voltammetry (CV) was performed on acid ascorbic and 4-nitrobenzene diazonium salt separately, in aqueous solutions (Figure 13a). The cyclic voltammogram of VC displayed an oxidation peak, with a typical shape of a phenomenon driven by diffusion, likely to correspond to the oxidation of H_2A in A. On the contrary, the shape of the cyclic voltammogram of NBDT is well known by electrochemists and is due to the blocking of the surface coming from the grafting of the species formed by the reduction of the diazonium salt on the surface of the electrode. This also explained why the reduction peak of NBDT is only observed in the first cycle. According to the pH of the solution, the VC oxidation peak was spread over a large range of potentials. Indeed, as deducted from the Pourbaix

diagram (Figure 12), at a pH close to the first pKa of ascorbic acid, several redox couples may be active. Moreover, the oxidation process starts way before the maximum of the oxidation peak. This observation means that only taking into account the potential of the oxidation peak to determine the ability of VC to act as a reducing agent might be too restrictive. Consequently, a value more relevant of the start of the oxidation process, called the onset potential (E_{onset}), was calculated as described in Figure 13b.

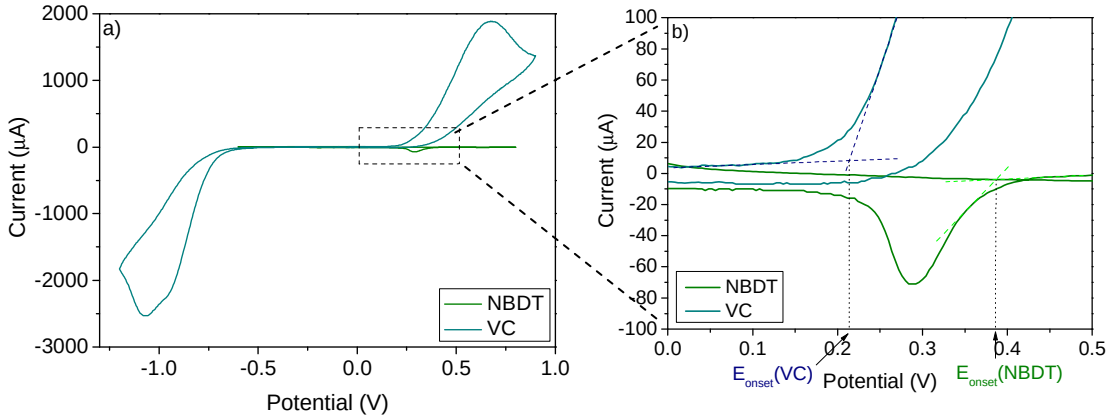

Figure 13 – Overlay cyclic voltammograms (0.1 V/s scan rate, SCE, working electrode = gold plate) of ascorbic acid (C = 3.10^{-2} M) and 4-nitrobenzene diazonium salt (C = 5.10^{-3} M) in HCl solutions (pH = 2) a) in full scale and b) zoomed in the area of interest.

The onset potentials of VC and NBDT were determined for aqueous solutions of various pH. The definition of "onset potential" is a bit arbitrary. However, it provides a first idea on the possibility of occurrence of the redox reaction between NBDT and VC. The curve E_{onset}(NBDT) versus pH plotted on Figure 14 is very similar to the E_p(NBDT) versus pH chart (Figure 10) but, as the reduction actually starts slightly before the reduction peak, the values are positively shifted. Concerning the ascorbic acid oxidation, it is clear from Figure 14 that the redox reaction is pH-dependent. The values E_{onset}(VC) do not strictly form a line with a slope of -0.06 V/pH (black line constructed on Figure 14) as we could expect from the Pourbaix diagram of VC (Figure 12). Nevertheless, by fitting linearly the data, the slope was found to be -0.07. This deviation can surely be attributed to uncertainties coming for the graphic determination of the onset potentials. In view of those results, it has been concluded that ascorbic acid is theoretically able to reduce 4-nitrobenzene diazonium salt whatever the pH of the solution.

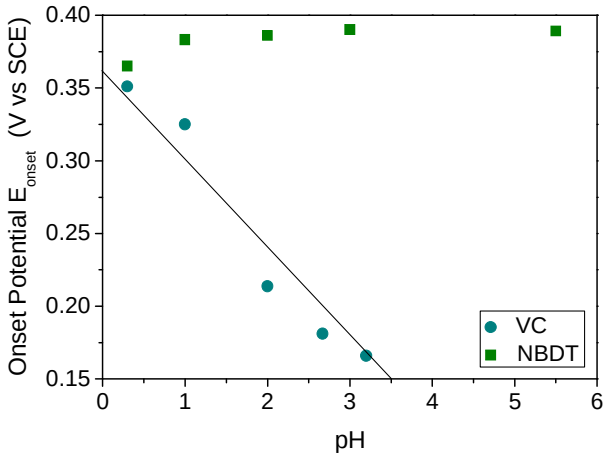

Figure 14 – pH dependence of the onset potential E_{onset} (obtained from CV, 0.1 V/s scan rate, SCE) for ascorbic acid (VC) and NBDT in aqueous solutions (adjusted with HCl). The E_{onset}(VC) at pH = 3.2 is simply obtained by mixing VC with H_2O DI. The line with a slope equal to -0.06 represents the theoretical evolution of the onset potential with pH.

In addition to the arguments mentioned above, ascorbic acid has also attracted all our attention in this work for another important reason. Unlike iron powder and as shown from the oxidation potential in Figure 14, VC is unable to reduce protons. This property has eased our interpretations of the mechanism by avoiding the formation of hydrogen radical from the reactive mixture, which could initiate as well as terminate the polymerization in solution of the vinylic monomer.

II.3.3 - **Vinylic monomers**

With the Graftfast™ anchoring process, all the vinylic monomers that can polymerize via a radical pathway are potentially usable. By analogy with the SEEP process, in the case of monomers with low solubility in water the anchoring method can be adapted by working in dispersed aqueous media (emulsion, miniemulsion). As a first work on the understanding of the grafting mechanism, we only considered monomers soluble in water and in particular the study was focused on the polymerization of hydroxyethyl methacrylate (HEMA, solubility = 1 mol.L^{-1} at 20 - 25°C). Indeed, the corresponding polymer PHEMA is biocompatible and easily identifiable by IR (intense absorption band at 1730 cm^{-1} attributed to the stretching vibration of C=O groups), by XPS (peak on the C 1s core level spectrum centred at 289.0 eV assigned to the carbonyl ester group COO) and by contact angle measurements (50 - 60° angle, very different from the contact angle of the pristine substrate, see II.3.4.3). To finish, PHEMA does not contain any nitrogen atom which makes the N 1s core level spectrum in XPS characteristic of the diazonium moieties.

II.3.4 - **Substrates**

Although this anchoring process allows working with a large range of substrates, in this thesis, the studies were mainly focused on the organic grafting on gold substrates. However,

other substrates have also been considered when required and particularly in chapter VI concerning the grafting on TiO_2 nanoparticles. As the main material of the studies, the gold substrate used was characterized in details since in processes such as Graftfast™, the surface condition of the substrate plays a key role in the grafting and can affect the reproducibility of the results as well as the homogeneity of the films.

II.3.4.1 - Why gold substrates?

In the framework of a fundamental study, gold substrates appeared to be very convenient for the three following main reasons. First of all, the evaporation technique employed to obtain gold substrates (described in the next paragraph) is fully mastered in the laboratory, very simple and quite cheap. Second, as a noble metal, gold is inert towards a lot of chemical compounds. Particularly, owing to its oxidation potential ($E°_{Au^{3+}/Au}$=1.5 V), gold is *a priori* unable to reduce any diazonium salt. Moreover, gold surfaces are prone to be less sensitive to surface contamination in comparison with other metallic substrates which, for instance, can be oxidized. To finish, gold substrates are adapted to surface studies by IR-ATR, XPS, AFM and ellipsometry.

II.3.4.2 - Preparation of gold substrates

Gold substrates were obtained by vacuum evaporation of pure gold (99.99 %) at room temperature on homemade cut glass plates. A 3 - 10 nm chromium sub-layer was first deposited to enhance gold adhesion on glass and then 50 - 150 nm of gold were evaporated as represented on Figure 15 under a residual pressure of 10^{-7} bar, at room temperature.

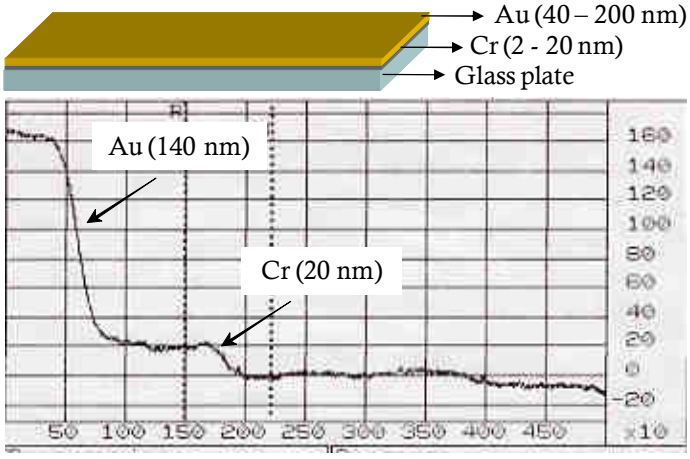

Figure 15 – Scheme (top) and thickness profile (bottom) of the chromium and gold layers deposited on glass plates by vacuum evaporation.

This process of vacuum evaporation leads to the formation of polycrystalline gold substrates made of multicrystals of 20 nm in average according to AFM measurements[68]. Due to its face-centered cubic (FCC) crystal structure, gold deposited on glass plates displays several crystalline faces: Au (111), Au (100), Au (110) and Au (311) as reported by Benedetto *et al*[69].

Contrary to monocrystalline epitaxial Au (111) on mica, gold grains clearly appear on "evaporated" gold surface as illustrated by SEM and AFM images in Figure 16. As expected, this gold surface has a higher roughness (RMS) than a surface prepared by epitaxial growth of gold on mica (0.1 nm[68]): the roughness values range from 4.5 nm (for calculations based on a 5 x 5 μm^2 AFM image) to 5.1 nm (1 x 1 μm^2 AFM image).

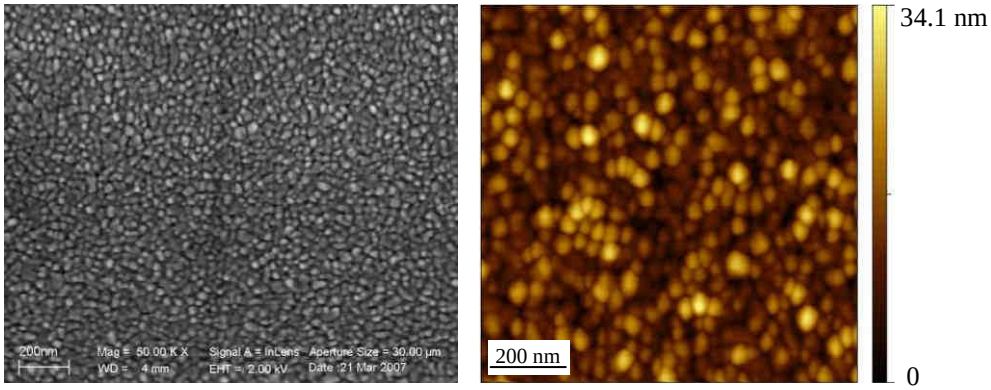

Figure 16 – SEM (left) and 1 x 1 μm^2 AFM (right) images of pristine gold substrate prepared by vacuum evaporation on a glass plate.

II.3.4.3 - Characterization of the pristine gold substrates

The surface condition of the substrate, particularly its contamination, is assumed to be a key parameter in the reproducibility of the experiments as well as in the homogeneity of the films. Therefore, the contamination, the storage and a treatment prior to use of the pristine substrates have been studied carefully.

Contamination of the gold substrates

Since the anchoring processes are likely to be influenced by the surface conditions of the substrates, an XPS analysis was performed on a pristine gold plate 8 days after evaporation in order to estimate and characterize its surface contamination. From the survey XPS spectrum (Figure 17), we observe, in addition to the characteristic Au 4f (84 and 88 eV), Au 4d (335 and 353 eV) and Au 4p (547 and 643 eV) peaks of gold, a C 1s signal at 285 eV and an O 1s signal at 531 eV. However, no nitrogen is detected and the pristine gold surface is also found alkali metals free. The contamination carbon (Figure 17) is mainly composed of aliphatic and/or aromatic carbons at 284.4 eV (91 %) and also of ca. 9 % of oxidized carbons at 286.0 and 287.4 eV. Therefore, purely organic contaminations are identified including hydrocarbons as well as oxidized hydrocarbons.

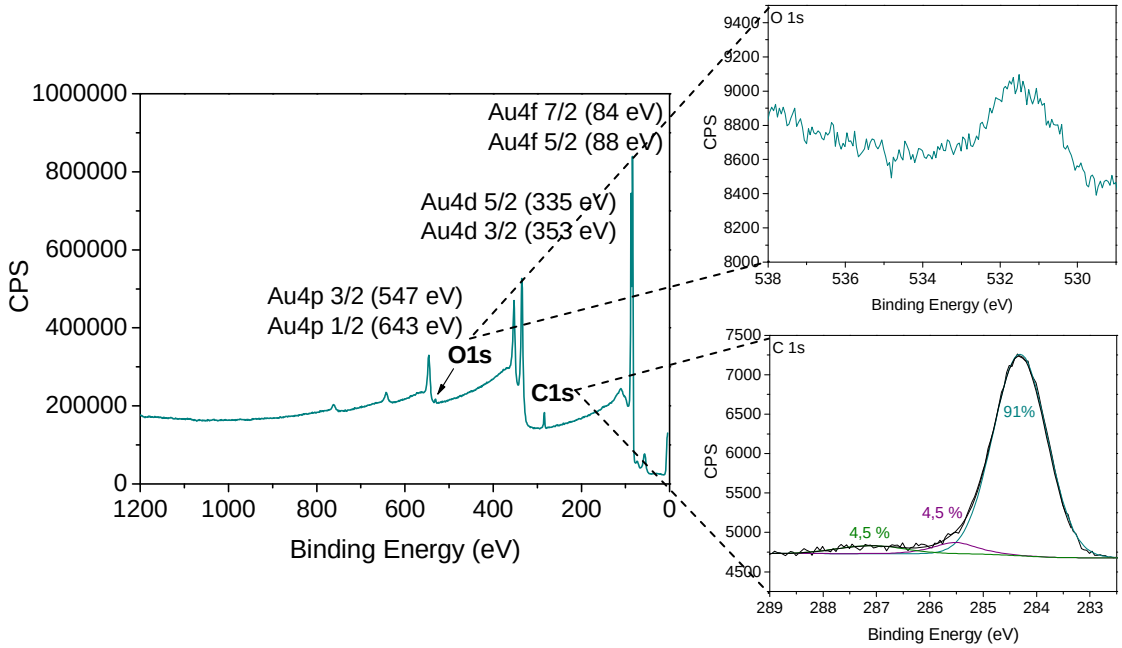

Figure 17 – XPS survey, O1s and C1s core level spectra of a pristine gold substrate eight days after evaporation.

The nature of the contamination was also confirmed by IR (Figure 18) since carbonyl groups and C-H stretching absorptions were detected, respectively, at 1727 and 2926 cm^{-1}. Indeed, those values are characteristic of fatty acids which are considered as the main surface contaminants[70].

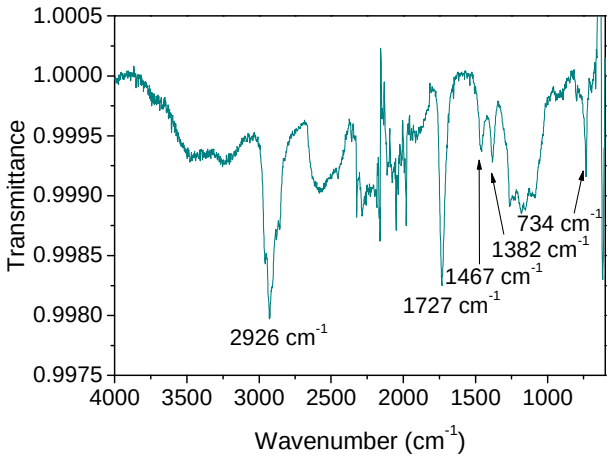

Figure 18 – IR-ATR spectrum of a contaminated pristine gold substrate eight days after evaporation.

To fully eliminate the contamination, an ionic abrasion under ultra-high vacuum inside the XPS can be performed. An area of 5 x 5 nm^2 of the substrate was bombarded with 4 keV Ar^+ ions by cycles of 2 min (analysis made on an area of 700 x 300 μm^2). As clearly shown by Figure 19, after 3 cycles of abrasion the surface is carbon and oxygen free. This method can also be employed to verify the purity of the deposited gold (as the substrate is normally only contaminated superficially). However it requires high vacuum, and cannot be applied on all our gold substrates.

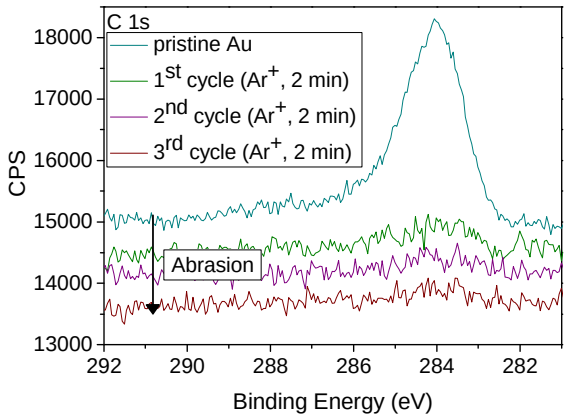

Figure 19 – C1s XPS spectrum of pristine gold substrate before and after successive ionic abrasions (Ar^+, 4 keV).

Two ways were considered to avoid or diminish as much as possible the contamination on gold substrates. First, a particular attention was given to their storage. Second, treatments prior to use were tested.

Storage of gold substrates

As previously demonstrated[71], after a 40-day storage at ambient air in plastic tubes, the contamination on gold substrates increased four times while keeping a C/O ratio of approximately 90/10. To limit this increase of contamination with storage time, the storage of gold plates in glass tubes in a nitrogen flow box was tested. As shown by Figure 20a and Figure 20b, the contamination of the substrates stored in the nitrogen flow box did not increase in intensity with the time of storage (see bands around 2900 cm^{-1}). As a result, all our gold substrates were kept in a nitrogen flow box in glass tubes. In addition, in order to minimize the influence of the contamination on the grafting, our substrates were used as soon as possible after evaporation (i.e. typically within the next three weeks).

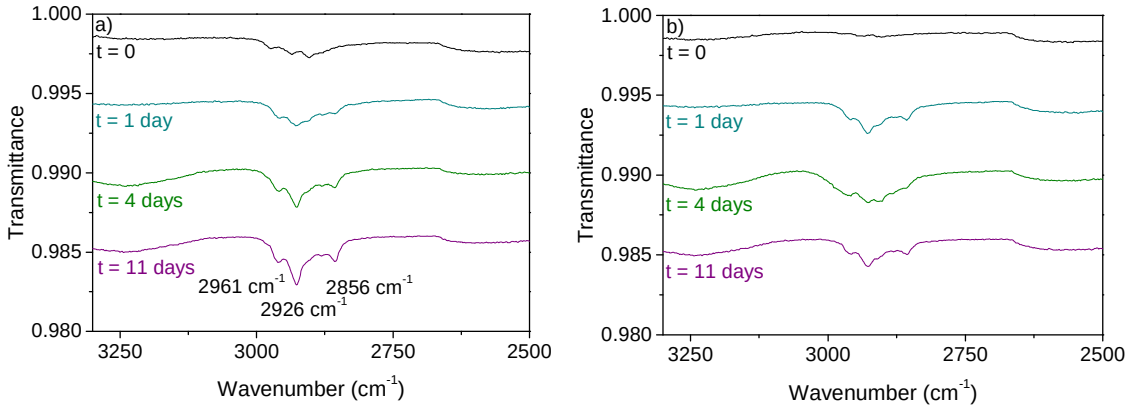

Figure 20 – IR-ATR spectra of pristine gold substrate with the time of storage in a) plastic tubes at ambient air and b) glass tubes in a nitrogen flow box.

Treatments prior to use of gold substrates

A common method to free the substrates from contamination is UV-ozone treatment. The UV-ozone method is a photo-sensitized oxidation process in which the contaminant molecules

coming from resins, human skin oils, cleaning solvent residues, silicone oils and so on are excited and/or dissociated by the absorption of short-wavelength UV radiation. Atomic oxygen is simultaneously generated when dioxygen molecules O_2 of the ambient air or ozone (formed from the combination of free oxygen atom and O_2 molecules) are dissociated. The products of excitation of contaminant molecules react with atomic oxygen to form simple, volatile molecules which desorb from the surface[70].

The effect of UV-ozone cleaning on gold substrate is clearly visible in Figure 21. Due to the hydrophobicity of adventitious carbon contaminants on gold surface, the average value of the contact angle reached 92° before cleaning. This value dropped to 5° after UV-ozone treatment. This result could be due to the oxidation of the contamination layer without evolution as gaseous species creating more hydrophilic oxidized species.

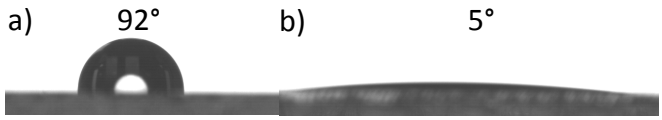

Figure 21 – Contact angle measurements (H_2O DI) on a pristine gold substrate a) before and b) after a 10 min UV-ozone cleaning.

The comparison of XPS analyses performed on gold substrates before and after a 10 min UV-ozone exposure (Figure 22) however reveals a two times higher carbon contamination (with an increase of oxidized carbons) and a three times higher oxygen contamination after cleaning. Those results appear in contradiction with the contact angle measurements, but could be explained by the increase in the surface reactivity of gold substrates after treatment which promotes their immediate recontamination in air. Indeed, the samples were manipulated a few minutes in the laboratory atmosphere between the UV-ozone chamber and the XPS.

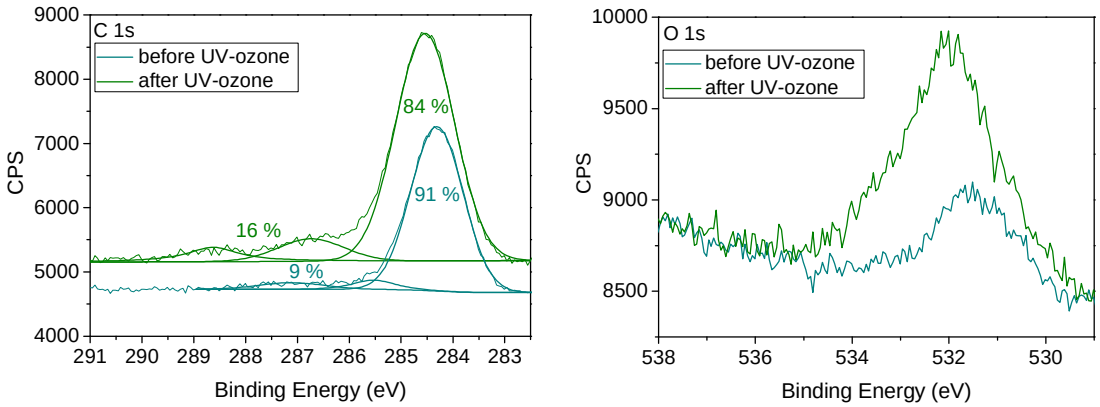

Figure 22 – C1s and O1s XPS spectra of a pristine gold substrate before and after a 10 min UV-ozone cleaning procedure.

Finally, after testing different ways of storage and various cleaning treatments including UV-ozone procedure and solvent rinsing (results not presented), it seemed that, except for the ionic abrasion in the XPS apparatus, no method can provide gold substrates fully free of

contamination. However, we have estimated that the best way to limit it consists in storing the gold substrates in glass tubes in a nitrogen flow box and using them without further cleaning treatment but as soon as possible after evaporation.

II.3.5 - **Typical Graftfast^{TM} experiment**

To sum up, for simplicity's sake, the study of the Graftfast^{TM} process was restricted, in case of most of the experiments, to the grafting of PHEMA on gold substrates through the reduction of 4-nitrobenzene diazonium salt in deionised water by either H_3PO_2 or ascorbic acid at room temperature, atmospheric pressure, with a magnetic stirring. Concerning the major part of the work, the reaction time was arbitrarily fixed at 60 min in order to be able to appreciate slow as well as fast phenomena. Unless otherwise mentioned, after the reaction, the substrates were rinsed according to the following rinsing procedure: water, ethanol and acetone then sonication in N,N-dimethylformamide (DMF) for 5 min. Indeed, no solvent is perfectly indicated to rinse poly(nitrophenylene) (films obtained from 4-nitrobenzene diazonium salt). However, unreacted NBDT as well as products of its degradation are soluble in those solvents. Moreover, in case of anchoring processes using monomers, unreacted HEMA was simply rinsed with water and physisorbed PHEMA was entirely removed with DMF (see V.3.2 for more details).

Summary

The anchoring process based on the reduction of diazonium salts has come from the evolution of the SEEP process towards the grafting of all type of materials. On top of this remarkable property, the process has shown other very interesting advantages such as a control on the thickness of the films, on the surface properties or on the localization of the grafting. In order to simplify further interpretations of the grafting mechanism, the main components entering in the process were precisely characterized. This anchoring process ranges from a simple reaction involving only the diazonium salt to more complex ones requiring a reducing agent as well as a vinylic monomer. Therefore, the study on the understanding of the mechanism will start in the next chapter by the easiest case i.e. the substrate-activated and spontaneous grafting of diazonium salts based on the simple use of a diazonium salt in solution.

References

1. S. Palacin, C. Bureau, J. Charlier, G. Deniau, B. Mouanda, P. Viel, *Molecule-to-metal bonds: Electrografting polymers on conducting surfaces*, ***ChemPhysChem***, **2004**, 5 (10), 1469-1481.
2. G. Deniau, L. Azoulay, L. Bougerolles, S. Palacin, *Surface electroinitiated emulsion polymerization: Grafted organic coatings from aqueous solutions*, ***Chemistry of Materials***, **2006**, 18 (23), 5421-5428.
3. L. Tessier, J. Chancolon, P. J. Alet, A. Trenggono, M. Mayne-L'Hermite, G. Deniau, P. Jegou, S. Palacin, *Grafting organic polymer films on surfaces of carbon nanotubes by surface electroinitiated emulsion polymerization*, ***Physica Status Solidi A: Applications and Materials Science***, **2008**, 205 (6), 1412-1418.
4. L. Tessier, G. Deniau, B. Charleux, S. Palacin, *Surface Electroinitiated Emulsion Polymerization (SEEP): A Mechanistic Approach*, ***Chemistry of Materials***, **2009**, 21 (18), 4261-4274.
5. V. Mevellec, S. Roussel, L. Tessier, J. Chancolon, M. Mayne-L'Hermite, G. Deniau, P. Viel, S. Palacin, *Grafting polymers on surfaces: A new powerful and versatile diazonium salt-based one-step process in aqueous media*, ***Chemistry of Materials***, **2007**, 19 (25), 6323-6330.
6. W. C. Wang, J. Wang, Y. Liao, L. Q. Zhang, B. Cao, G. J. Song, X. L. She, *Surface Initiated ATRP of Acrylic Acid on Dopamine-Functionalized AAO Membranes*, ***Journal of Applied Polymer Science***, **2010**, 117 (1), 534-541.
7. S. Roussel, *Préparation et greffage de molécules cages pour la captation d'ions lourds en pahse aqueuse*, Thèse de l'Université Paris XI, Paris, **2007**.
8. M. Pinault, V. Pichot, H. Khodja, P. Launois, C. Reynaud, M. Mayne-L'Hermite, *Evidence of sequential lift in growth of aligned multiwalled carbon nanotube multilayers*, ***Nano Letters***, **2005**, 5 (12), 2394-2398.
9. A. Mesnage, G. Deniau, L. Tessier, V. Mevellec, S. Palacin, *Localized grafting through chemical lift-off*, ***Applied Surface Science***, **2011**, 257 (17), 7805-7812.
10. H. Zollinger, *Diazo chemistry I: Aromatic and Heteroaromatic coumponds*, VCH: Weinheim, New York, **1994**.
11. J. B. Moffat, *The Chemistry of Diazonium and Diazo Compounds*, Ed. S. Patai John Wiley & Sons, New York, **1978**.
12. K. Forstinger, H. J. Metz, *Diazo Compounds and Diazo Reactions*, Ullmann's, **2001**, Encyclopedia of Industrial Chemistry.
13. T. Breton, D. Belanger, *Modification of carbon electrode with aryl groups having an aliphatic amine by electrochemical reduction of in situ generated diazonium cations*, ***Langmuir***, **2008**, 24 (16), 8711-8718.
14. F. Doctorovich, N. Escola, C. Trapani, D. A. Estrin, M. C. G. Lebrero, A. G. Turjanski, *Stabilization of aliphatic and aromatic diazonium ions by coordination: An experimental and theoretical study*, ***Organometallics***, **2000**, 19 (19), 3810-3817.
15. H. Zollinger, *Diazo chemistry II: Aliphatic, Inorganic and Organometallic Compounds*, VCH: Weinheim, New York, **1994**.
16. E. S. Lewis, M. D. Johnson, *The Substituent Constants of the Diazonium Ion Group*, ***Journal of the American Chemical Society***, **1959**, 81 (9), 2070-2072.
17. C. Galli, *Radical Reactions of Arenediazonium Ions - an Easy Entry into the Chemistry of the Aryl Radical*, ***Chemical Reviews***, **1988**, 88 (5), 765-792.
18. K. H. Saunders, *The Aromatic Diazo Compounds and their Technical Applications*, Edward Arnold, London, **1949**.
19. M. R. Heinrich, *Intermolecular Olefin Functionalisation Involving Aryl Radicals Generated from Arenediazonium Salts*, ***Chemistry-A European Journal***, **2009**, 15 (4), 821-833.
20. B. Andersson, B. Lamm, *Studies in Nucleophilic Aromatic Substitution Reactions .4. Replacement of Nitro Group in 2,6-Dichloro-4-Nitrobenzenediazonium and 2,4-Dichloro-6-Nitrobenzenediazonium Ions by Chlorideion*, ***Acta Chemica Scandinavica***, **1969**, 23 (9), 2983-2988.

21. M. Min, G. S. Bang, H. Lee, B. C. Yu, *A photoswitchable methylene-spaced fluorinated aryl azobenzene monolayer grafted on silicon*, ***Chemical Communications***, **2010**, 46 (29), 5232-5234.

22. B. Chen, A. K. Flatt, H. H. Jian, J. L. Hudson, J. M. Tour, *Molecular grafting to silicon surfaces in air using organic triazenes as stable diazonium sources and HF as a constant hydride-passivation source*, ***Chemistry of Materials***, **2005**, 17 (19), 4832-4836.

23. W. B. Lin, W. P. Lin, G. K. Wong, T. J. Marks, *Supramolecular approaches to second-order nonlinear optical materials. Self-assembly and microstructural characterization of intrinsically acentric [(aminophenyl)azo]pyridinium superlattices*, ***Journal of the American Chemical Society***, **1996**, 118 (34), 8034-8042.

24. U. Costas-Costas, R. Pazo-Llorente, E. Gonzalez-Romero, C. Bravo-Diaz, *Dediazoniations in water: An integrated physical organic chemistry experiment*, ***Journal of Chemical Education***, **2000**, 77 (3), 384-386.

25. P. S. J. Canning, K. McCrudden, H. Maskill, B. Sexton, *Rates and mechanisms of the thermal solvolytic decomposition of arenediazonium ions*, ***Journal of the Chemical Society-Perkin Transactions 2***, **1999**, (12), 2735-2740.

26. C. G. Swain, J. E. Sheats, K. G. Harbison, *Evidence for Phenyl Cation as an Intermediate in Reactions of Benzenediazonium Salts in Solution*, ***Journal of the American Chemical Society***, **1975**, 97 (4), 783-790.

27. W. Ando, *The Chemistry of Diazonium and Diazo Groups Part I*, Ed. S. Patai John Wiley & Sons, New York, **1978**.

28. M. Delamar, R. Hitmi, J. Pinson, J. M. Saveant, *Covalent Modification of Carbon Surfaces by Grafting of Functionalized Aryl Radicals Produced from Electrochemical Reduction of Diazonium Salts*, ***Journal of the American Chemical Society***, **1992**, 114 (14), 5883-5884.

29. K. C. Brown, M. P. Doyle, *Reduction of Arenediazonium Salts by Hydroquinone. Kinetics and Mechanism for the Electron-Transfer Step*, ***Journal of Organic Chemistry***, **1988**, 53 (14), 3255-3261.

30. M. P. Doyle, J. K. Guy, K. C. Brown, S. N. Mahapatro, C. M. Vanzyl, J. R. Pladziewicz, *Outer-Sphere One-Electron Reductions of Arenediazonium Salts*, ***Journal of the American Chemical Society***, **1987**, 109 (5), 1536-1540.

31. J. K. Kochi, *The Mechanism of the Sandmeyer and Meerwein Reactions*, ***Journal of the American Chemical Society***, **1957**, 79 (11), 2942-2948.

32. N. Kornblum, A. E. Kelley, G. D. Cooper, *The Chemistry of Diazo Compounds .3. The Reduction of Diazonium Salts by Phosphorous Acid*, ***Journal of the American Chemical Society***, **1952**, 74 (12), 3074-3076.

33. S. H. Korzeniowski, L. Blum, G. W. Gokel, *Reduction of Aryldiazonium Compounds in Nonpolar Media*, ***Journal of Organic Chemistry***, **1977**, 42 (8), 1469-1470.

34. L. K. Skrunts, L. A. Kiprianova, A. F. Levit, I. P. Gragerov, *Kinetics and Mechanism of the Reaction of N,N,N',N'-Tetramethyl-Para-Phenylenediamine with Diphenyliodonium Chloride and Phenyldiazonium Fluoroborate*, ***Zhurnal Organicheskoi Khimii***, **1979**, 15 (8), 1645-1649.

35. C. Combellas, F. Kanoufi, J. Pinson, F. I. Podvorica, *Sterically hindered diazonium salts for the grafting of a monolayer on metals*, ***Journal of the American Chemical Society***, **2008**, 130 (27), 8576-8577.

36. C. Combellas, D. E. Jiang, F. Kanoufi, J. Pinson, F. I. Podvorica, *Steric Effects in the Reaction of Aryl Radicals on Surfaces*, ***Langmuir***, **2009**, 25 (1), 286-293.

37. C. P. Andrieux, J. Pinson, *The standard redox potential of the phenyl radical/anion couple*, ***Journal of the American Chemical Society***, **2003**, 125 (48), 14801-14806.

38. S. Baranton, D. Belanger, *Electrochemical derivatization of carbon surface by reduction of in situ generated diazonium cations*, ***Journal of Physical Chemistry B***, **2005**, 109 (51), 24401-24410.

39. S. Baranton, D. Belanger, *In situ generation of diazonium cations in organic electrolyte for electrochemical modification of electrode surface*, ***Electrochimica Acta***, **2008**, 53 (23), 6961-6967.

40. E. M. Evleth, R. J. Cox, *Assignments of Electronic Transitions in Methoxy-Substituted Benzenediazonium Cations*, ***Journal of Physical Chemistry***, **1967**, 71 (12), 4082-4089.

41. C. Bravo-Diaz, L. S. Romsted, M. Harbowy, M. E. Romero-Nieto, E. Gonzalez-Romero, *Rates and pH-dependent product distributions of the CuCl2-catalyzed dediazoniation of p-nitrobenzenediazonium tetrafluoroborate in aqueous acid*, ***Journal of Physical Organic Chemistry***, **1999**, 12 (2), 130-140.

42. X. Zhang, J. P. Bell, *Studies of arenediazonium salts as a new class of electropolymerization initiator*, ***Journal of Applied Polymer Science***, **1999**, 73 (11), 2265-2272.

43. M. L. Crossley, R. H. Kienle, C. H. Benbrook, *Chemical Constitution and Reactivity. I. Phenyldiazonium Chloride and its Mono Substituted Derivatives*, ***Journal of the American Chemical Society***, **1940**, 62, 1400-1404.

44. A. F. Hegarty, *The Chemistry of Diazonium and Diazo Compounds*, Ed. S. Patai John Wiley & Sons, New York, **1978**.

45. X. T. Le, P. Viel, P. Jegou, A. Garcia, T. Berthelot, T. H. Bui, S. Palacin, *Diazonium-induced anchoring process: an application to improve the monovalent selectivity of cation exchange membranes*, ***Journal of Materials Chemistry***, **2010**, 20 (18), 3750-3757.

46. A. Garcia, T. Berthelot, P. Viel, J. Polesel-Maris, S. Palacin, *Microscopic Study of a Ligand Induced Electroless Plating Process onto Polymers*, ***ACS Applied Materials & Interfaces***, **2010**, 2 (11), 3043-3051.

47. P. Viel, X. T. Le, V. Huc, J. Bar, A. Benedetto, A. Le Goff, A. Filoramo, D. Alamarguy, S. Noel, L. Baraton, S. Palacin, *Covalent grafting onto self-adhesive surfaces based on aryldiazonium salt seed layers*, ***Journal of Materials Chemistry***, **2008**, 18 (48), 5913-5920.

48. N. Kornblum, G. D. Cooper, J. E. Taylor, *The Chemistry of Diazo Compounds .2. Evidence for a Free Radical Chain Mechanism in the Reduction of Diazonium Salts by Hypophosphorous Acid*, ***Journal of the American Chemical Society***, **1950**, 72 (7), 3013-3020.

49. L. K. Skrunts, L. A. Kiprianova, A. F. Levit, I. P. Gragerov, *Kinetics and Mechanism of the Reaction of N,N,N',N'-Tetramethyl-Para-Phenylenediamine with Diphenyliodonium Chloride and Phenyldiazonium Fluoroborate*, ***Zhurnal Organicheskoi Khimii***, **1979**, 15 (8), 1645-1648.

50. M. Pandurangappa, T. Ramakrishnappa, *Derivatization and characterization of functionalized carbon powder via diazonium salt reduction*, ***Journal of Solid State Electrochemistry***, **2008**, 12 (11), 1411-1419.

51. M. Pandurangappa, N. S. Lawrence, R. G. Compton, *Homogeneous chemical derivatisation of carbon particles: a novel method for funtionalising carbon surfaces*, ***Analyst***, **2002**, 127 (12), 1568-1571.

52. A. T. Masheter, G. G. Wildgoose, A. Crossley, J. H. Jones, R. G. Compton, *A facile method of modifying graphite powder with aminophenyl groups in bulk quantities*, ***Journal of Materials Chemistry***, **2007**, 17 (29), 3008-3014.

53. G. G. Wildgoose, N. S. Lawrence, H. C. Leventis, L. Jiang, T. G. J. Jones, R. G. Compton, *X-Ray photoelectron spectroscopy studies of graphite powder and multiwalled carbon nanotubes covalently modified with Fast Black K: evidence for a chemical release mechanism via electrochemical reduction*, ***Journal of Materials Chemistry***, **2005**, 15 (9), 953-959.

54. P. Abiman, G. G. Wildgoose, R. G. Compton, *A mechanistic investigation into the covalent chemical derivatisation of graphite and glassy carbon surfaces using aryldiazonium salts*, ***Journal of Physical Organic Chemistry***, **2008**, 21 (6), 433-439.

55. A. Mesnage, S. Esnouf, P. Jegou, G. Deniau, S. Palacin, *Understanding the Redox-Induced Polymer Grafting Process: A Dual Surface-Solution Analysis*, ***Chemistry of Materials***, **2010**, 22 (23), 6229-6239.

56. G. F. Cui, H. Liu, G. Wu, J. W. Zhao, S. Q. Song, P. K. Shen, *Electrochemical impedance spectroscopy and first-principle investigations on the oxidation mechanism of hypophosphite anion in the electroless deposition system of nickel*, ***Journal of Physical Chemistry C***, **2008**, 112 (12), 4601-4607.

57. M. Charbonnier, A. Romand, Y. Goepfert, D. Leonard, F. Bessueille, A. Bouadi, *Palladium (+2) reduction: A key step for the electroless Ni metallization of insulating substrates by a tin-free process*, ***Thin Solid Films***, **2006**, 515 (4), 1623-1633.

58. S. C. Lin, S. Y. Chen, S. Y. Cheng, J. C. Lin, *Synthesis and magnetic properties of highly arrayed nickel-phosphate nanotubes*, ***Solid State Sciences***, **2005**, 7 (7), 896-900.

59. C. Galli, *Stimulation by SN^{+2} or Ascorbic Acid on Diazonium Salts Reactions*, ***Tetrahedron Letters***, **1980**, 21 (47), 4515-4516.

60. A. McAuley, T. Oswald, R. I. Haines, *Kinetics and Mechanisms of The Oxidation of Ascorbic-Acid and Benzene Diols by Nickel(III) Tertaazamacroccyles in Aqueous Perchloric-Acid*, ***Canadian Journal of Chemistry***, **1983**, 61 (6), 1120-1125.

61. U. S. Mehrotra, M. C. Agrawal, S. P. Mushran, *Kinetics of The Reduction of Hexacyanoferrate(III) by Ascorbic Acid*, ***Journal of Physical Chemistry***, **1969**, 73 (6), 1996-1999.

62. W. Ahmed, E. S. Kooij, A. van Silfhout, B. Poelsema, *Controlling the morphology of multi-branched gold nanoparticles*, ***Nanotechnology***, **2010**, 21 (12), 125605.

63. I. Medina-Ramirez, M. Gonzalez-Garcia, J. L. Liu, *Nanostructure characterization of polymer-stabilized gold nanoparticles and nanofilms derived from green synthesis*, ***Journal of Materials Science***, **2009**, 44 (23), 6325-6332.

64. A. L. Wang, H. B. Yin, C. Ge, M. Ren, Y. M. Liu, T. S. Jiang, *Synthesis of hollow silver spheres using poly-(styrene-methyl acrylic acid) as templates in the presence of sodium polyacrylate*, ***Applied Surface Science***, **2010**, 256 (8), 2611-2615.

65. J. Zhou, G. Zhou, R. Wang, M. Lu, *Synthesis in aqueous phase and characterization of silver nanorods and nanowires*, ***Materials Science-Poland***, **2009**, 27 (1), 73-78.

66. C. Creutz, *The Complexities of Ascorbate as a Reducing Agent*, ***Inorganic Chemistry***, **1981**, 20 (12), 4449-4452.

67. Y. I. Turyan, R. Kohen, *Formal Redox Potentials of The Dehydro-L-Ascorbic Acid System*, ***Journal of Electroanalytical Chemistry***, **1995**, 380 (1-2), 273-277.

68. A. Benedetto, *Grafting of Organic Thin Films for the Lubrication of Electrical Contacts,* Thèse de l'Université d'Orsay Paris-Sud, Paris, **2008**.

69. A. Benedetto, M. Balog, P. Viel, F. Le Derf, M. Salle, S. Palacin, *Electro-reduction of diazonium salts on gold: Why do we observe multi-peaks?*, ***Electrochimica Acta***, **2008**, 53 (24), 7117-7122.

70. J. R. Vig, *Uv Ozone Cleaning of Surfaces*, ***Journal of Vacuum Science & Technology A: Vacuum Surfaces and Films***, **1985**, 3 (3), 1027-1034.

71. L. Tessier, *Greffage de Films Organiques par Polymerisation Radicalaire Electro-amorcée en Milieu Aqueux Dispersé*, Thèse de l'Université Pierre et Marie Curie, Paris, **2009**.

CHAPTER III

Spontaneous grafting of diazonium salts

As described in chapter II, the anchoring processes based on the reduction of diazonium salts are very easy to set up. However, the more chemical species are involved, the more complicated the mechanism of the grafting. Therefore, in this chapter, constituting a first step in the understanding of the grafting mechanism, we will deal with the most basic case of chemical grafting involving diazonium salts i.e. the spontaneous grafting (where only the diazonium salt is present in solution). This type of process as well as electrochemical methods is supposed to give highly robust films in comparison to physisorption methods since it has been claimed to form a covalent chemical bond between the substrate and the film. Therefore, numerous teams have worked on demonstrating the covalent nature of the interface bond on the simple case of polyphenylene grafting[a]. Thus, after presenting the spontaneous anchoring process of diazonium salts, we will discuss the existence of a covalent surface-carbon interface bond and describe our attempts to demonstrate it. To finish, we will focus on the study of similar graftings that have been recently observed on gold. The occurrence of this phenomenon on gold will be examined in details since it has been chosen as the main substrate of all this work and an explanation of the grafting mechanism will be proposed.

III.1 - **Spontaneous grafting in general**

The attachment of aryl groups to surfaces on a large range of materials has been widely described in the literature mainly via the electrochemical grafting of diazonium salts[1] (see I.1.5.2). However, it has also been achieved by non-electrochemical methods. The grafting of similar groups promoted by heat[2], UV radiation[3], ultrasonication[3, 4], ball milling[5] or chemical reducing agents has been reported. The last one will constitute the topic of chapter IV whereas the others will not be detailed in this work. More simply, similar graftings, called spontaneous graftings, have been performed at open-circuit potential (OCP) without any external source of energy.

This spontaneous process, reviewed by Barriere *et al.*[6], occurs by simple dipping in acetonitrile or aqueous solutions of diazonium salts on semiconductors (silicon[7, 8], GaAs[7] and more recently germanium[9]) or metals[10] such as copper[11], palladium[7], aluminium[12], titanium[12], nickel[13], iron[13, 14] and zinc[13]. The resulting films have been found very similar to those obtained by an electrochemical reduction. However, comparison studies have shown that, in general, films formed by the spontaneous route are thinner and are formed more slowly[15]. The spontaneous grafting has appeared to be a very interesting method since it operates under simple and environmental friendly experimental conditions (when performed in aqueous solution). It

[a] This term is used to describe the grafting of substituted phenyl moieties on the surface forming monolayer as well as multilayers films. However, we are aware that in the case of mono or bilayers graftings, this is a misuse of language.

was proved suitable for the modification of surface properties of materials. For instance, surface protection against corrosion[14] as well as iron and zinc superhydrophobic surfaces have been achieved[16]. Therefore, the investigation of the spontaneous grafting mechanism has attracted much interest.

It has been reported that if the substrate is reducing enough then it can operate itself the reduction of the diazonium salt into the corresponding aryl radical and react with it[13, 14]. The redox properties of both the diazonium salt and the metal have been shown to play a key role in the occurrence of this spontaneous grafting. For a given reducing substrate, the more difficult is the reduction of the diazonium salt, the less efficient is the grafting[13]. Consequently, with metals less reducing, this reaction should not occur. However, a spontaneous grafting of diazonium salt was observed on gold by Downard and coll.[17] in acidic media and by Pinson and coworkers[18] in acidic as well as in basic solution. As gold was selected as the substrate of our study on the anchoring processes, this phenomenon will be investigated in details in III.3 as it could have a significant influence on the redox-induced processes studied in chapters IV and V. The spontaneous one-electron reduction of diazonium salts was also demonstrated in the case of the grafting on hydride-terminated porous and planar silicon by conducting radical trapping experiments based on the reaction of surface Si radicals with, for instance, reagents such as arylselenoether or arylthioether[8].

The spontaneous grafting procedure was firstly introduced by Belmont. The modification of carbon black was the subject of numerous patents registered by Cabot Corporation (detailed in reference 4 therein Bélanger's work[19]) and used for interesting industrial applications in the manufacturing of inks. Later, works were performed on the aryl modification of carbon black[20] by reaction with diazonium salts and focused on the investigation of the grafting mechanism[19]. A concerted decarboxylation reaction where the diazonium cation would act as an electrophile replacing the oxygenated functionalities (leaving as CO_2) was suggested as illustrated in Scheme 40. The spontaneous grafting on other forms of carbon such as graphite[21], glassy carbon[10, 15, 21-23], graphene[24-30] and diamond[31, 32] was also reported and various grafting mechanisms were proposed.

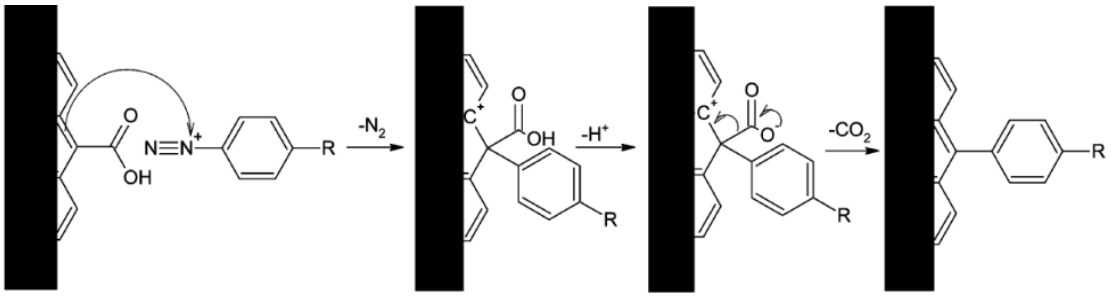

Scheme 40 – Proposed mechanism of the spontaneous grafting on carbon black extracted from the work of Toupin *et al.*[19].

Concerning the spontaneous grafting on graphite and glassy carbon in pure water, Abiman *et al.*[21, 22] suggested a heterolytic dediazoniation of the diazonium salt. The so formed aryl cation intermediate (see II.3.1.2) was considered to either react with the carbon surface itself or with surface carboxylic groups to form an aryl ester linkage. In contrast to this mechanism, from the study conducted by Bidan and coll.[23] on glassy carbon a spontaneous grafting mechanism involving an electron transfer initiation of the diazonium salt was proposed. Indeed, a jump of the open circuit potential was observed when NBDT was introduced in solution. In addition, NBDT appeared to be the only diazonium salt (among the diazonium salts tested) permitting a spontaneous grafting on glassy carbon, certainly because of its easy reduction.

In regards to the spontaneous grafting of graphene sheets, the covalent attachment of the aryl groups to the basal carbon atoms was also considered to be due to an electron transfer from the graphene layer to the diazonium salt[24, 28]. However, Raman spectroscopy measurements suggested a two-step reaction pathway presumably consisting in the adsorption of the diazonium salt on single (Scheme 41-(2)) or bi-layer (Scheme 41-(4)) graphene followed by its decomposition to form a covalent C-C bond with the substrate (Scheme 41-(3)&(5))[27]. Besides, the simple adsorption of nitrobenzene, arising from the spontaneous decay of the diazonium salt, could always be a possibility (Scheme 41-(7)). To finish, the spontaneous modification of graphene was demonstrated to be faster for single-layer graphene with enhanced reactivity at its edge[27, 28], as supported by theoretical calculations[33]. The electrical characteristics[26] of graphene devices treated with a diazonium salt and particularly the field effect transistor (FET) characteristics[25] were also investigated with a view to potential applications.

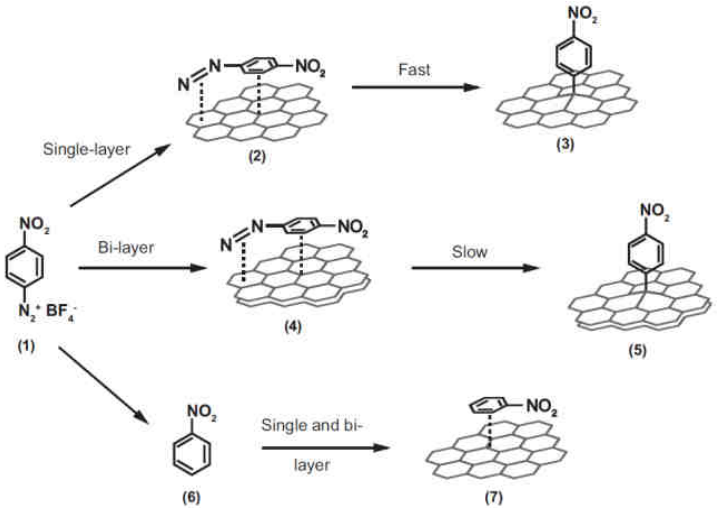

Scheme 41 – Spontaneous grafting mechanism of NBDT on graphene surfaces proposed by Koehler *et al.*[27].

In the case of carbon nanotubes[2, 22, 34], the spontaneous grafting was used notably to improve their dispersion in various environments[35] but also to selectively functionalize metallic CNT (i.e. preferentially to semiconducting CNT) in aqueous solution[36]. Concerning the mechanism,

Dyke *et al.*[37] refuted the possibility of an electron transfer initiation step for the spontaneous grafting reaction since it would lead to a multiple substitution pathway occurring with a very unlikely accumulation of charges on the CNT. Such as for graphene, a two-step mechanism consisting in a chemical adsorption step and a covalent bond forming step was also proposed[38] and supported by theoretical calculations[39]. However, this proposition seems unlikely when working in basic conditions since only diazoates can be present in solution at these pH. Therefore, the most likely mechanism to date which explains the spontaneous grafting in neutral or alkaline solutions was suggested to be based on the formation of a diazonium anhydride (Gomberg-Bachmann reaction) which can decompose in a homolytic cleavage into an aryl radical[37, 40] able to react with a CNT as illustrated by Scheme 42.

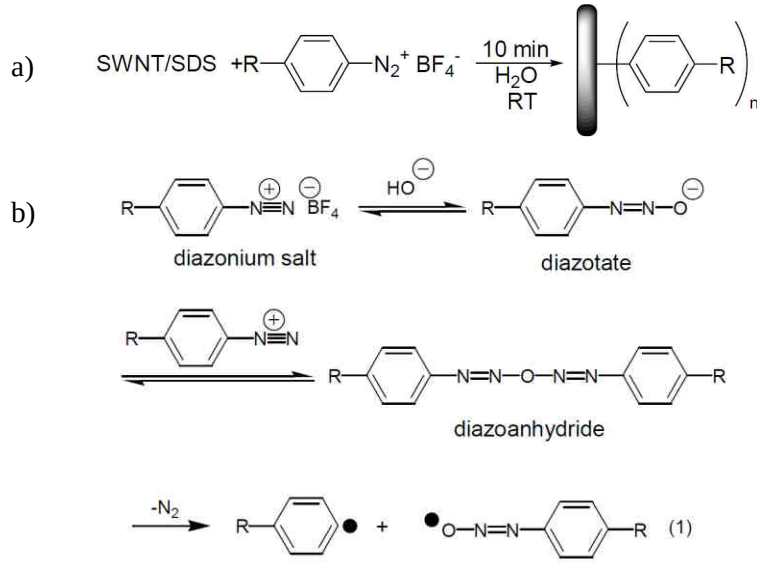

Scheme 42 – a) Generation of funtionalized SWNTs and b) mechanism of the spontaneous grafting at neutral or alkaline pH extracted from the work of Dyke *et al.*[37].

To summarize, it is likely that the mechanism is dependent on the diazonium salt used as well as on the substrate employed and its physical forms (in the case of carbon). No general mechanism of the spontaneous grafting could possibly be established and the spontaneous reaction pathway is still subject of much debate and investigations. However, since it is a very simple process forming robust films grafted on the substrate, the spontaneous grafting of diazonium salts is often employed for the surface modification of materials with aryl groups.

III.2 - **Towards the proof of existence of a covalent interface bond**

All the anchoring processes based on diazonium salts within this thesis are claimed as grafting methods of organic films leading to the formation of a covalent bond between the film and the substrate. Since it constitutes one of the main characteristics of those processes, special attention was paid to demonstrate the existence of such a bond.

The grafting methods described in this work lead either to the formation of polyphenylene layers or of polymer films. As it will be revealed in chapter V, the structure of the polymer films obtained by the Graftfast™ method is mainly composed, at the interface film-substrate, of an essential primer layer of polyphenylene on which the polymeric chains are grafted. Thus, the polyphenylene layer is assumed to be responsible for the covalent linkage between the substrate and the polymer film. Consequently, to establish the existence of a covalent bond at the interface surface-coating in the anchoring processes, we will uniquely focus on the study of polyphenylene grafted films. As such organic layers have already been obtained by various methods, we will first report the results obtained in previous studies and then describe our attempts to demonstrate the existence of a covalent bond.

III.2.1 - **Previous works**

As previously mentioned, methods permitting the covalent attachment of aryl groups to various surfaces have already been reported and range from spontaneous grafting (described above) to chemically induced (chapter IV) or electrochemical (see I.1.5.2 and I.2.1.8) graftings. For all of them, studies have already been performed to demonstrate the existence of a substrate-film bond and the most relevant ones will be detailed below.

III.2.1.1 - In spontaneous grafted films

As getting evidence of the presence of a bond between the surface and the organic layer is not easy, some teams described indirect proofs. The resistance of the films to simple treatments, such as cleaning[7] or sonication[14] in various solvents showing the chemical stability of the films were commonly admitted as an indirect evidence of the existence of a covalent bonding. Indeed, if the molecules were only physisorbed on the surface, these treatments would likely remove most of the organic residue. Indeed, full elimination of the grafted polyphenylene-like films has only been achieved by abrasion techniques[41].

Direct evidences of a covalent substrate-film bond was however reported. First of all, Hurley *et al.*[11] provided, thanks to XPS analysis, evidence of the establishment of both a Cu-O-C linkage and a Cu-C bond between grafted aryl moieties and a copper substrate. Then, ToF-SIMS analyses of polyphenylene films on glassy carbon plates, performed by Combellas *et al.*[15] permitted the detection of C-aryl fragments as well as O-aryl ones; the former testifying of the bond between the carbon plate and aryl groups. Therefore, in addition to providing evidences of the presence of a covalent surface-carbon bond, both studies demonstrated that the bonding between the substrate and the organic film could also occur through oxygenated functions.

Very recently, McDermott and coll.[42] provided the first direct evidence for the existence of a Au-C covalent bond by surface-enhanced Raman scattering (SERS) and high-resolution

electron energy loss spectroscopy (HREELS). The modifications of 40 nm gold nanoparticles and Au(111) with nitrobenzene moieties (from the corresponding diazonium salt) were obtained spontaneously in acetonitrile. Similarly to other teams dealing with carbon-gold bonds, the authors detected a band at 412 cm^{-1} in the SERS spectrum of the grafted gold nanoparticles (Figure 23) and a weak band at 420 cm^{-1} in the HREELS spectrum of modified Au(111) that they assigned to a Au-C stretch. The attribution of that bond was confirmed by calculations (DFT modelling).

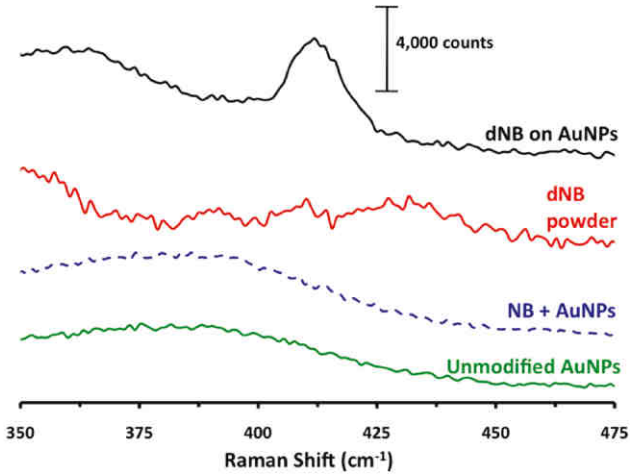

Figure 23 – Raman spectrum of solid NBDT (dNB, solid red line) and SERS spectra of unmodified 40 nm gold nanoparticles (AuNPs, solid green line), of NBDT-modified AuNPs (solid black line) and of AuNPs reacted with nitrobenzene (dashed blue line) expanded near 400 cm^{-1} extracted from the work of McDermott[42].

III.2.1.2 - In chemically induced grafted films

Although claimed by all the authors working on the chemical reduction of diazonium salts by H_3PO_2 on various forms of carbons, no clear evidence of a covalent grafting has been shown[19, 21, 22, 43, 44]. The assumption of such a characteristic of the films seems to only be based on analogy with the results obtained for the electrochemical and the spontaneous grafting.

III.2.1.3 - In electrochemically grafted films

Most of the studies dealing with the existence of an aryl-substrate interface bond concern electrochemically grafted films. As for the spontaneously grafted films, the first and most common argument for a covalent grafting relies on the chemical stability of the polyphenylene layers. First, as described in the very first publications[45, 46] on the electrochemical grafting of diazonium salts, the films remain stable after six months at air exposure. The layers were also observed to resist to severe rinsing procedures[47] (such as HF rinsing in the case of the grafting on Si) and to sonication procedures[1, 48-50] (long[51] or in various solvents[45]). The stability of the films was also investigated electrochemically by applying very negative or positive potentials at the grafted electrode. D'Amours *et al.*[52] demonstrated that the electrochemical polarization of the modified electrode could remove some aggregates generated during the process but could not completely free the electrode from the polyphenylene film. To finish, the mechanical

stability of the Si-C bond was tested by AFM[53]. After scratching the film with the AFM tip, a very thin layer of polyphenylene was still detected (by XPS). Moreover, Charlier and coworkers[53] determined that the grafted polyphenylene film is composed of a strongly adherent first layer, covalently linked to the substrate with on top a weakly bonded overlayer.

By comparing self-assembled monolayers (SAMs) of thiols to polyphenylene layers electrochemically grafted through the reduction of diazonium salts on gold, Shewchuk *et al.*[54] concluded that under certain conditions, electrochemically formed aryl films were more strongly bonded to gold surfaces than the thiol analogue. A recent study[55], using first principles density functional theory (DFT) simulations, predicted a higher value of binding energy for aryl C-Au(111) than aryl S-Au(111) which is in agreement with the experiments described above.

Other computational investigations[56] brought support to the evidence of bonds between a metallic surface and aryl groups from the organic film. For Fe, Cu, Pd or Au substrate, the C-Metal bond energy was shown to depend on the selected metal indicating a lower binding energy for C-Au(111) than for the three other metals mentioned. In addition, Jiang and coworkers established the most stable structures for upright or tilted configurations which, in the case of a gold substrate, consist in the aryl group linked to the surface by a single carbon atom (Scheme 43).

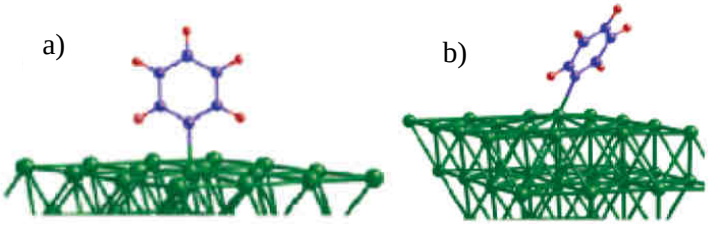

Scheme 43 – Optimized structures for phenyl groups on gold surfaces in a) upright and b) tilted configurations extracted from Jiang's work[56].

Using spectroscopy techniques, much stronger evidences of the existence of a covalent interface bond were detailed. The results, obtained by the in situ monitoring of the Raman spectra, over a wide range of potentials, of 4-nitrobenzene as a free molecule as well as a chemisorbed monolayer on glassy carbon electrode (GCE) surface, were consistent with strong electronic coupling across a conjugated phenyl-phenyl bond at the film-GC interface[57]. However, the most direct evidence of the nature of the interface bond was recently provided by McDermott and coworkers[42] using high-resolution electron energy loss spectroscopy (HREELS) on electrochemically modified Au(111). As a continuation of their work presented above on the spontaneous grafting on gold nanoparticles, from the observation of a band at 420 cm^{-1}, the authors concluded that a Au-C covalent bond is formed upon typical electrochemical grafting of NBDT on Au(111). A few teams also attempted to demonstrate the existence of a metal-carbon interface bond using XPS spectroscopy. On electrochemically modified iron surfaces[58], a minor

component centred at 283.3 eV was observed on the C 1s core level spectrum and assigned to the XPS signature of a carbide type of carbon that originates from the formation of a covalent Fe-C bond. Similar XPS characterizations were attempted on other metals. Nevertheless, on Si, only an indirect proof of the Si-C bond was found[47] whereas on gold substrates, closer results to those on Fe presented above by Laforgue *et al.*[49] were obtained. As illustrated in Figure 24, a small shoulder, at low energy, in the C 1s core level spectrum of a 4-carboxyphenyl modified gold electrode was observed which could be fitted with a Au-C component at 283.5 eV. However, the authors admitted that this result did not constitute an irrefutable evidence of the existence of a covalent film-gold interface bond since its signature was very weak.

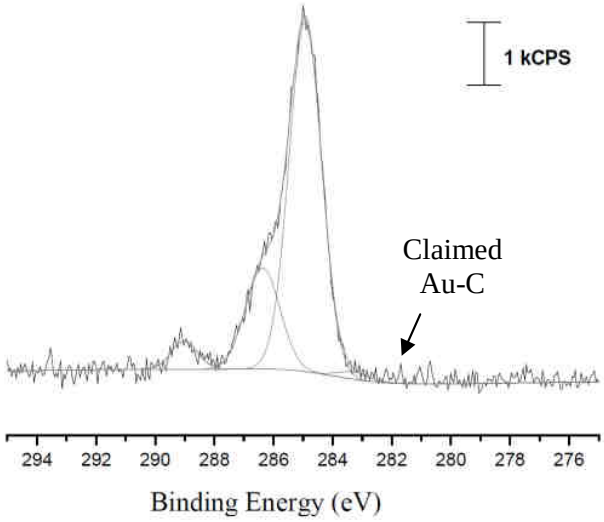

Figure 24 – C 1s core level spectrum of a polycarboxyphenylene thin layer electrochemically grafted on gold electrode extracted from the supporting information of Laforgue's work[49].

III.2.2 - **Our experiments**

The anchoring processes based on diazonium salts including the spontaneous grafting process are considered as covalent grafting methods of polymer or polymer-like films in the case of polyphenylene layers. In contrast to electrochemically grafted films, no direct evidence of covalent substrate-film bond in our films was established. To date, only indirect proofs of the existence of a covalent bond were found consisting in a resistance of the layers to sonication in solvents, 30 min in DMF at 60°C as well as Soxhlet extraction in EtOH overnight (cf V.3.2). As the formation of a bond between the surface and the organic layer represents one of the main characteristic of the processes studied in this work, particular efforts were made in order to demonstrate it from polyphenylene grafted substrates.

One of the most direct techniques to observe a surface-film bond is XPS, for which the studied substrate has to be chosen carefully. Although, as reported above, Laforgue and coworkers attempted such a study on gold[49], this metal is not very adapted. First, the electronegativities of gold and carbon are very close (χ_c = 2.55 and χ_{Au} = 2.54 using the Pauling

scale) which indicates that the signal from potential Au-C bonds would be difficult to distinguish from C-C bonds on the C 1s spectrum. Second, the small amount of Au-C bonds in the films in comparison to the C-C bonds (at best one carbon atom from each grafted aromatic ring should be involved in Au-C bond versus five contributing to C-C signal) would make the signal of interest very weak and merged in the peak of C-C at 285 eV. Consequently, the experiments were carried out on substrates such as germanium (χ_{Ge} = 2.01) and nickel (χ_{Ni} = 1.91) since (i) their electronegativities are lower than the one of carbon, (ii) the values of their oxidation potential[59] ($E°_{Ge2+/Ge}$ = 0.24 V and $E°_{Ni2+/Ni}$ = -0.257 V) are low enough to reduce most of the diazonium salts and (iii) methods are known to remove the oxide from their surfaces. In order to remain as close as possible to the experimental conditions employed in our classical experiments, germanium wafer was the first substrate of interest since its oxide can be removed in aqueous solutions. In addition to the commercially available NBDT, 4-methoxybenzenediazonium tetrafluoroborate (MBDT) was tested to determine the influence of the electronic effects of the substituent groups on the detection of the interface bond. Another compound, the 3,4,5-trichlorobezene diazonium salt, was likewise employed in order to enhance the detection of Au-C since it would sterically limit the layer growth and increases the ratio Au-C/C-C. Those three diazonium salts should be spontaneously reduced by germanium and nickel. Indeed, the redox potentials of NBDT and MBDT are respectively of 0.49 V (/NHE) (see II.3.1.3) and 0.25 V (/NHE)[60]. Concerning the trichlorobenzene diazonium salt, the redox potential value has not been measured yet. However, the existence of a linear relationship between the Hammett coefficients for *para* substituents of diazonium cations and the redox potential was reported in organic media[61] as well as in acidic solutions[60]. As the Hammett coefficient of a chloro substituent is likely to lie between the nitro and methoxy ones, this third diazonium salt could therefore potentially be reduced by the two substrates of interest.

III.2.2.1 - On germanium wafer

The first experiments aiming at proving the existence of the covalent interface bond were performed on undoped (100) germanium wafers spontaneously grafted with a diazonium salt. As silicon, germanium is a very reactive material forming, at air exposure, oxides on its surface. In order to observe the Ge-C XPS signature, prior treatments had to be carried out to remove these oxides. To date, a few methods were reported to be efficient at removing the germanium oxide including a UV-ozone oxidation in air followed by thermal desorption in ultrahigh vacuum[62], a wet chemistry methodology (hydrohalogenic acids etching)[63] or electrochemical pulses.

Hydrohalogenic acids etchings were identified as an advantageous route not only to remove the oxide and contamination but also to enhance the stability of the resulting Ge surface, making it suitable for wet functionalization. This treatment consists in the repetition of the three

following steps: oxidation (by H_2O_2) – rinsing (by H_2O DI) – etching (by HBr)[63]. With a view to functionalize the substrate, the diazonium salts mentioned above were directly added in the HBr solution during the last cycle of treatment. From IR and XPS analyses performed on the grafted germanium samples, it is difficult to conclude on the grafting of the methoxy diazonium salt since there is no marker such as nitrogen or chlorine in this molecule. Moreover, since no C-O bond can be distinguished in the C 1s spectrum, we considered that the grafting was unsuccessful. Nevertheless, strong evidences of a successful grafting in the case of the trichloro- and nitro- benzene diazonium salts were found. But, as illustrated in Figure 25, no evidence of a component at low energy in the C 1s core level spectra could be observed in those two cases. Since the observed Ge 2p spectra are characteristic of oxidized Ge substrates, it can be assumed that no Ge-C bond can be identified due to a poor removal of the oxide leading to the diazonium salt grafting on top of this oxide layer. However, this hypothesis has to be discarded. Indeed, the same etching method followed by the grafting of C9 thiols has led to the formation of a grafted SAMs on oxide free germanium, thus demonstrating the efficiency of this wet chemistry methodology to remove the germanium oxide. The presence of oxide on the sample can simply be explained by the transfer from the glove box to the XPS, at air exposure, of the non-passivating polyphenylene films after their synthesis. Therefore, it is likely that the detection of a Ge-C bond is prevented due to a very low grafting density of aryl groups on the surface from which results a too small amount of Ge-C bond in comparison with the number of C-C bonds and an easy reoxidation of the Ge surface.

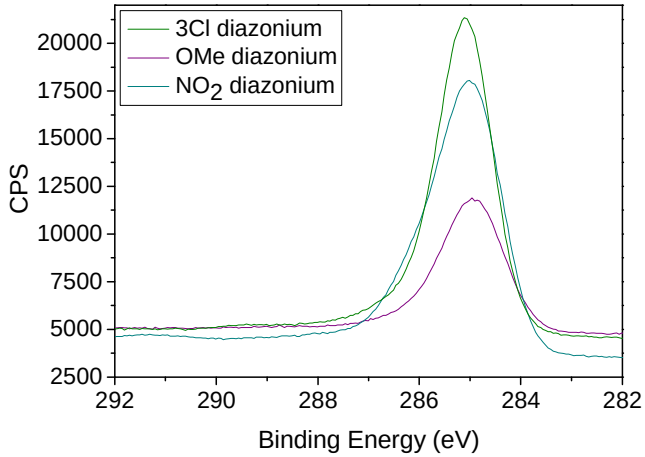

Figure 25 – C 1s XPS spectra of nitro, methoxy and trichloro benzene diazonium salts (0.001M) spontaneously grafted on germanium wafer after oxidation-rinsing-etching cycles.

Similar results were obtained for germanium wafers initially treated by electrochemical pulses in order to remove the oxide layer and then spontaneously grafted with diazonium salt. The electrochemical treatment, using the germanium wafer as working electrode, proceeded through a first electrochemical pulse at -4 V for 10 min followed by 10 cycles from 0 to -2 V in a 50:50 saturated KBr and HCl (10 %) solutions. As in the previous case, the methoxy diazonium salt was not successfully grafted on the substrate and no evidence of Ge-C bond was

obtained in the other cases, which can certainly be explained by the same reasons mentioned above.

To conclude, germanium wafers did not work out to be very adapted substrates to demonstrate the existence of a covalent film-surface bond. Therefore, our attention turned to nickel surfaces.

III.2.2.2 - On nickel plates

Nickel was already used for the observation of metal-carbon bonds resulting from the direct electrografting of vinylic monomers in aprotic conditions[64], mainly because (i) nickel oxide is electroreducible in organic media, and (ii) nickel electronegativity is far enough from the carbon one to allow a specific XPS signal to be observed. The electroreduction of nickel oxide operates under a controlled argon atmosphere and consists in performing a cyclic voltammetry in anhydrous acetonitrile, with tetraethyl ammonium perchlorate (TEAP) as supporting electrolyte and using nickel plates as the working electrode[65]. The spontaneous grafting of the three previously mentioned diazonium salts was carried out in three steps:

1. The nickel oxide was reduced by cyclic voltammetry in anhydrous acetonitrile in the argon atmosphere of a glove box. The potential was cycled between the rest potential of the electrochemical cell and a variable final potential (10 mV/s scan rate – 1 cycle).
2. The nickel working electrode was then disconnected from the power supply and introduced rapidly in the ACN diazonium salt solution (0.046 M) for 30 min.
3. The substrates were rinsed with ACN and transferred at air exposure from the glove box (controlled atmosphere) to the XPS chamber (high vacuum).

Thanks to a rapid study of the grafting of the three diazonium salts, we decided to focus on the spontaneous grafting of methoxybenzenediazonium salt (MBDT) since it gave the most promising results with a view to detect the Ni-C bond. As mentioned in the literature[65], the electroreduction of the nickel oxide starts at -1.9 V/SCE. In the same time, cathodic electrografting of the supporting electrolyte TEAP derivatives is observed on metallic electrodes at potentials below -2.2 V/SCE[64]. A redox mechanism for this grafting was proposed by Buriak and coll.[66]. Since those two values are close, it is likely that a compromise has to be found between those two phenomena. Therefore, we tested a wide range of final potential values during the electro-stripping of nickel oxide. In each case, one sample analysed directly after the electro-stripping was used as a reference for the corresponding sample subjected to the spontaneous grafting of MBDT diazonium salts. For instance, the C 1s XPS spectra corresponding to MBDT grafted nickel substrates as well as to pristine nickel plates after cyclic voltammetry reaching -2.2 V are shown in Figure 26. The most intense peaks around 285.1 eV is typical of carbon atoms such as in $–CH_2–$ and $–CH_3–$ groups. The components near 286.5 eV is indicative of C-O and C-N bonds whereas at 288.7 eV COO oxidized structures are identified.

In addition, at low binding energy, a shoulder was observed in the case of the grafting with MBDT. As already reported in the literature[64, 67, 68], this minor component, centred at 283.5 eV, can be attributed to carbon atoms involved in a bond with surface nickel atoms. In this case, the difference with the reference sample is clear but the peak is still very weak. Besides, the O 1s spectra, not shown here, indicate that the nickel oxide was only partially reduced. Hence, the weakness of the peak at 283.5 eV could either be explained by a low grafting density, or by that partial nickel oxide reduction.

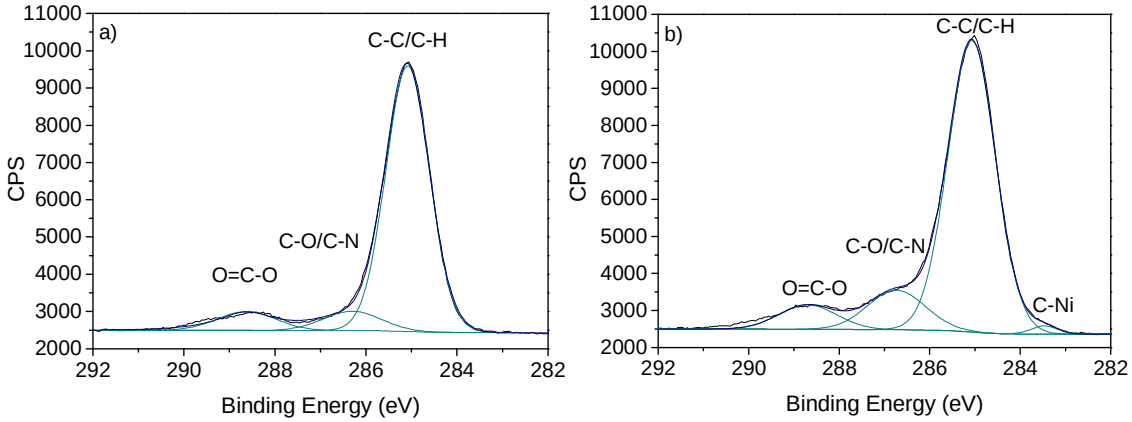

Figure 26 – C 1s XPS spectra of a) pristine and b) MBDT (0.046M) spontaneously grafted on nickel plates after cyclic voltammetry (between the rest potential of the electrochemical cell to -2.2 V/SCE, at 10 mV/s scan rate).

The area values of the Ni-C component in the C 1s XPS spectra as a function of the final potential used for the removal of the nickel oxide are listed in Table 2. No value in the table means that a satisfactory fit of the C 1s XPS spectrum could be obtained without any Ni-C component (as shown in Figure 26a) and therefore that no Ni-C bond was observed. Three different regimes can be distinguished from the results gathered in Table 2:

1. When the final potential of the stripping step is below -2.3 V, Ni-C bonds are observed on the reference samples, indicating some grafting from TEAP. Moreover, the more negative the final potential during the stripping step, the more Ni-C is observed Therefore, from and below that threshold, only an increase of the Ni-C amount when comparing the pristine nickel plate and the "grafted" one could demonstrate the efficiency of the spontaneous grafting from the diazonium salts. Unfortunately, no difference of area values of the Ni-C components is detected between pristine and grafted samples previously treated at potentials lower than -2.4 V. These results are consistent with an increase of the TEAP grafting at lower potentials preventing the grafting of the diazonium salt.
2. In contrast, for final potentials above -2.2 V, no signal from Ni-C is detected, neither on pristine nor on "diazonium treated" samples. The absence of Ni-C signature means that the potentials used are neither negative enough to reduce TEAP nor to remove the nickel oxide from the surface.

3. The most relevant experiments to demonstrate the existence of a covalent substrate-film bond concerned samples for which the stripping step reached -2.2 V/SCE. Indeed, no grafting of TEAP is detected in this case, but a signal from Ni-C bonds at 283.5 eV could be detected after contact with diazonium salts. Therefore, even if that signal is not very intense in comparison to the one reported by Deniau *et al.*[64], it can entirely be attributed to a metal-carbon bond at the interface (Figure 26b).

Table 2 – Area Values of the Ni-C peak observed in the C 1s core level spectra of pristine or grafted by the methoxybenzene diazonium salt (0.046 M) nickel substrate according to final potential (/SCE) reached during the cyclic voltammetry (10 mV/s scan rate) performed to remove the oxide.

	Area of the carbide component (a.u)						
Lowest CV potential	-1.7 V	-2 V	-2.2 V	-2.3 V	-2.4 V	-2.6 V	-2.9 V
Reference	-	-	-	118	137	139	192
OMe diazonium	-	-	164	157	142	147	193

The nitrogen content was also analysed in that latter case (stripping at -2.2 V, followed by treatment with MBDT). The corresponding N 1s XPS core level spectra are displayed in Figure 27. A nitrogen peak centred at 400 eV in the spectrum of the pristine nickel plate is clearly present and assumed to correspond to surface organic contamination. The N 1s signal observed on the sample treated with the diazonium salt contains a similar component, arising from the same contamination as well as azo groups from the spontaneously formed poly(methoxyphenylene) film grafted on nickel. An additional component was also detected at low binding energy (397.7 eV), which could be assigned to Ni-N bonds from the substrate-film interface[67]. Therefore, this result reveals the existence of a second type of grafting of the diazonium salt on the nickel surface likely to come from the formation of Ni-*N*=N-Φ-OMe. The probable origins of this grafting will be discussed in III.3.1.3. In addition to the presence of a new peak, the contribution of the second nitrogen atom in the following structure: Ni-N=*N*-Φ-OMe may be accounted within the main N1s peak at 400 eV.

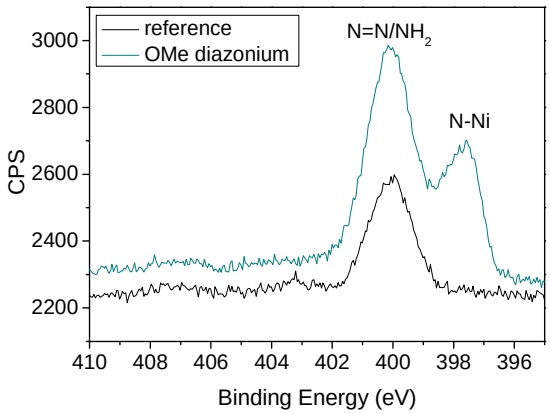

Figure 27 – N 1s XPS spectra of a) pristine and b) methoxybenzene diazonium salts (0.046 M) spontaneously grafted on nickel plates after cyclic voltammetry (between the rest potential of the electrochemical cell to -2.2 V/SCE, at 10 mV/s scan rate).

To conclude, by scanning a wide range of final potentials during the electro-stripping of nickel oxide, Ni-C as well as metal nitride bonds, formed by the spontaneous grafting of methoxybenzene diazonium salt and characteristic of the film-substrate interface, have been successfully observed. However, only spontaneous grafted films from this specific diazonium salt provide those interface signatures. We have no explanation for that at the moment.

We did not perform further experiments on nickel to demonstrate the existence of this interface bond with other grafting conditions. Indeed, the experimental conditions we used in this study are quite remote from those typically employed in these anchoring processes; particularly, working in organic media is not satisfactory since one of the main interests of these anchoring methods is to occur in aqueous solutions. However, we believe that a similar behaviour, even in aqueous solutions, would be observed on other substrates able to reduce diazonium salts as long as they are oxide free.

In the case of gold substrate, the detection of such a bond is not very likely for the reasons mentioned in III.2.2. Nevertheless, although gold cannot *a priori* reduce diazonium salts ($E°_{Au^{3+}/Au}$=1.5 V[59]), a polyphenylene film has also been detected after immersion of gold plates in aqueous solutions of diazonium salts.

III.3 - **Spontaneous grafting on gold**

Given that gold was chosen as the main substrate of interest in this work, typical films obtained by the spontaneous grafting of NBDT on gold were characterized in details. Then, we examined the mechanism of the spontaneous formation of polyphenylene films on gold.

III.3.1 - **Typical films**

To study the composition of spontaneously grafted films, gold plates were immersed for 1h in an aqueous solution (H_2O DI pH = 5.5) containing only the NBDT diazonium salt. The substrates were analyzed by contact angle measurements, IR-ATR and XPS, after a rinsing procedure consisting in a simple wash with water, ethanol and acetone followed by 5 min sonication in DMF (as described in II.3.5) supposed to remove all the non-grafted species from the surface. The usual settings for the acquisition of data are detailed in appendix 1.

IR-ATR is a usual technique for the determination of the chemical composition of materials particularly adapted for studies on thin films and flat reflective surfaces. The spectrum corresponding to the spontaneous grafting of NBDT on gold is shown in Figure 28 and the assignment of the peaks is summarized in Table 3[69]. It exhibits two absorption bands at 1525 and 1350 cm^{-1} attributed to, respectively, the asymmetric and symmetric stretching of NO_2 groups linked to aryl and a third weak one at 1600 cm^{-1} consistent with the presence of aromatic rings in the organic layer. Moreover, it is noteworthy that no band in the 2300-2130 cm^{-1} region

for the stretching of the N≡N bond in the diazonium cation[14, 69] is present in the spectrum, which indicates the loss of the diazonium group during the process. According to previous results on the electrochemical grafting of NBDT on gold electrodes[54, 60, 70], it can be concluded that this IR spectrum is characteristic of a polynitrophenylene-like (PNP) layer.

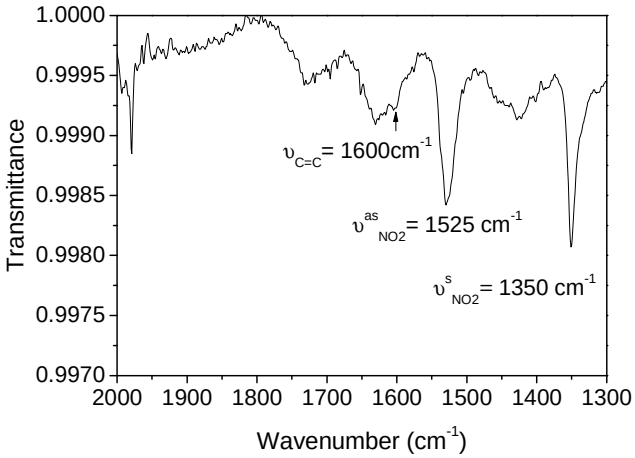

Figure 28 – IR-ATR spectrum of PNP layer spontaneously grafted on gold plates obtained by immersion in a 0.046 M NBDT solution for 60 min.

Table 3 – Attribution of the IR absorption bands of a spontaneously grafted film on gold plate from a NBDT aqueous solution.

Wavenumber (cm^{-1})	Vibrations	Assignments
1600	$\nu_{C=C}$	aryl group
1525	ν^{as}_{NO2}	nitro group
1350	ν^{s}_{NO2}	nitro group

The presence of an organic film on gold substrate after spontaneous reaction is also supported by static water contact angle measurements. Pristine gold substrate gives an angle of 94 ± 6° and this value decreases to 72 ± 3° after grafting as illustrated in Figure 29. However, a value of 58 ± 4° for a PNP layer was reported[60, 71]. The difference in contact angle could be explained by a low grafting density of polynitrophenylene on the surface giving an intermediate value between the bare substrate and a typical PNP film.

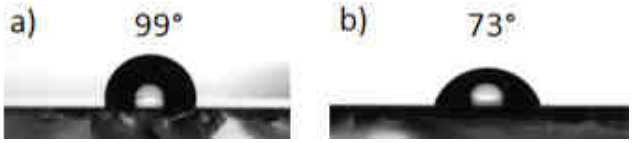

Figure 29 – Static water contact angle of a) pristine gold substrate and b) after spontaneous grafting of NBDT.

The N 1s core level XPS analysis (Figure 30) confirms the presence of the PNP layer on the gold substrates. No peak that would be attributed to nitrogen atoms in diazo group can be observed indicating a transformation of the diazonium cations[7]. First, the peak centered at 405.8 eV is attributed to nitro groups[60, 72, 73]. Since it has a large FWHM (full width at half

maximum), the broad peak around 400 eV can be decomposed in two peaks (corresponding to NH_2 or/and N=N groups) as it will be discussed below. Finally, the peak at a lower binding energy (397.5 eV) is assumed to indicate the presence of Au-N bonds since a similar binding energy peak was found when studying gold nitrite[74] or electrochemical oxidation of aliphatic amines[75]. To the best of our knowledge, this is the first time that such a bond, characteristic of the interface, is observed in the case of the grafting of diazonium salts on gold. The most similar results dealing with the existence of substrate N=N bonds at the interface concerns the grafting of diazonium salts on carbon (detailed in III.3.1.3). The C 1s core level analysis (not presented here) also confirms the presence of a PNP layer on the gold substrate.

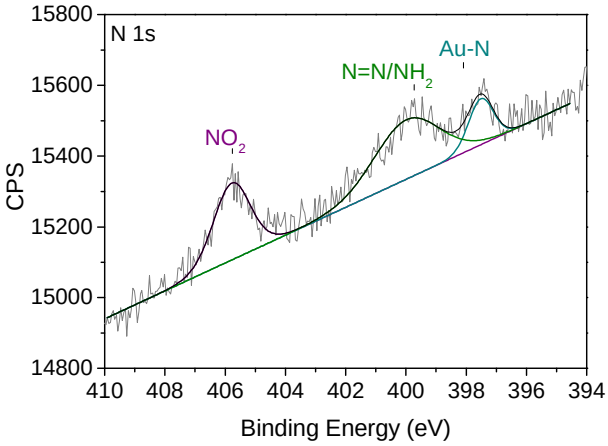

Figure 30 – Typical XPS N 1s core level spectrum of PNP layer spontaneously grafted on gold plates obtained by immersion of the substrates in a 0.046 M NBDT solution for 60 min.

Owing to similar IR intensities and XPS spectrum than thiol derivated nitrobenzene monolayers on gold (the total N 1s peak area is 350 a.u. in case of diazonium salt derivated nitrobenzene layers and 460 a.u. in case of thiol derivated nitrobenzene monolayers), we assume that this polynitrophenylene-like layer is very thin. However, we did not manage to get a relevant measurement of the thickness of the films. Indeed, the roughness of the gold substrate (cf II.3.4.2) in the case of measurements with both profilometer and ellipsometer in addition to the lack of adequate models of organic layers on gold in the latter case were the main obstacles. Therefore, the comparison of the graftings will only be based on the variation in IR absorption intensity of the characteristic nitro bands and on XPS measurements. However, in the case of IR-ATR, in view of the range of absorption values we will deal with in this case (between 0 and 1 %), it is important to be aware of the limits of this technique. The limiting factor in the comparison of the samples is not the sensitivity threshold of the equipment (close to 0.05%) but the variability of the ATR measurements. Indeed, IR-ATR measurements are influenced by environmental factors (for instance the pressure applied on the sample ensuring a good contact with the ATR crystal) as well as parameters inherent to the sample (for example its roughness). Regarding the spontaneous grafting of NBDT in H_2O DI, the variation on the intensity of the symmetric stretching of NO_2 groups (ν^s_{NO2}) around the average value reaches ± 0.02 % when

considering measurements taken on the same sample (based on three points of measurements along the substrate), approximately ± 0.03 % for measurements on three different samples grafted in the same reactive solution (coming from the same evaporation batch of gold) and ± 0.08 % if comparing measurements on films synthesized separately (over two years). As a result, we will only compare samples first obtained during the same gold evaporation then, when possible, grafted in the same solutions or made of the same reactants. Moreover, in the case of XPS measurements, comparisons of grafting will only be undertaken for samples analysed in a row.

Before going into further details in the study of the spontaneous grafting on gold, we will describe the assignments of the broad XPS peak in the N1s spectra and discuss the origins of the corresponding groups which presence could be useful for the understanding of the mechanism of this process.

III.3.1.1 - Assignments of the peak at 400 eV

The attribution of the large peak at 400.0 eV was achieved using a parallel with PNP films synthesized by the electrochemical reduction of NBDT. Although the first team to have successfully grafted NBDT on GC plates did not mention any peak around 400 eV in their study, the existence of such a peak was later observed by Allongue and coworkers[47] who, at the time, considered it as contamination. That interpretation of the peak was however quickly discarded and changed for the presence of amine ($-NH_2$)[10, 76], azo (–N=N–)[11, 20, 77, 78] groups or both[14, 52, 71] as detailed by Downard and coll.[71]. Even though some of the authors do not fit this signal with two peaks in the case of the grafting of NBDT[53], it is likely that the component around 400 eV is constituted by both types of groups since the signal is broad.

The most relevant study aiming at attributing the components of N 1s XPS signal was recently conducted by Tessier and coworkers[60]. Through the analysis of physisorbed films on gold substrates from aromatic molecules bearing nitro, amine, azo groups or combinations of those groups, they clearly assigned the peak around 400 eV from the results summarized in Table 4.

Table 4 – XPS analyses of reference molecules and the assignments of their nitrogen groups extracted from the work of Tessier[60].

Name	Molecule	Binding Energy (eV)	Assignments
1,4-phenylenediamine	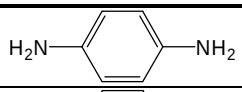	399.7	$–NH_2$
4-nitroaniline	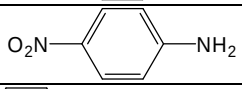	399.7 405.9	$–NH_2$ $–NO_2$
Azobenzene	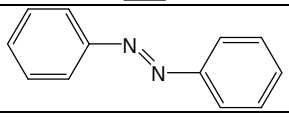	400.1	–N=N–
Disperse orange	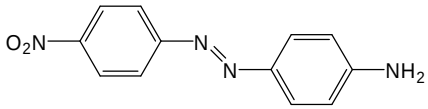	399.5 400.9 402.2 406.0	$–NH_2$ –N=N– *N1s* $–NO_2$

Therefore, in accordance with those results, when the N1s peak at 400 eV is broad, we will fit it with two components: one slightly below 400 eV corresponding to $–NH_2$ groups and another a little above 400 eV attributed to –N=N–. However, the origin of those peaks remains unclear and will hence be discussed now.

III.3.1.2 - Origin of amino groups

Several papers on the spontaneous grafting or on the electrografting of NBDT reported the presence of a XPS peak corresponding to $–NH_2$ groups in the grafted films on gold[17, 50, 51, 79] as well as on iron[14], carbon[31], copper and zinc[10, 77]. To date, two main explanations have been proposed: the electrochemical reduction of the NO_2 group in protic media or its reduction under exposure to X-ray irradiation.

Electroreduction of nitro $–NO_2$ groups

Aminophenyl groups are known to be formed by the reduction of nitrophenyl groups on the surface of the substrate in acidic media in presence of electrons as represented in Scheme 44.

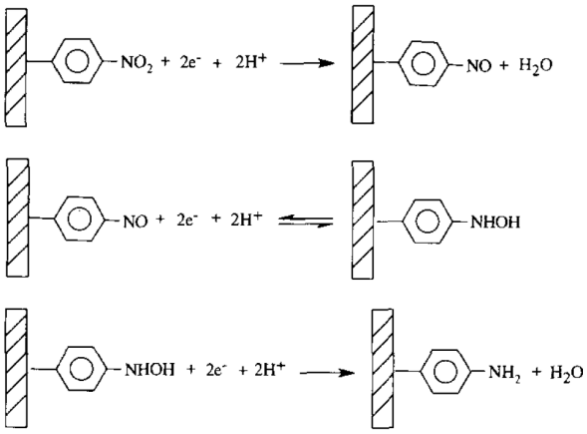

Scheme 44 – Reduction of nitro groups into amino groups in acidic media extracted from Delamar's work[80].

Such a reduction was studied by Delamar *et al.*[80] in protic (10/90 v/v EtOH/H_2O) and in acidic (10 % H_2SO_4) media on PNP electrografted carbon fiber electrodes. In both cases, they managed to observe the reduction peak of NO_2. Later, by XPS analysis of aryl-modified glassy carbon electrodes after polarization, Bélanger and coworkers[52] demonstrated that according to the selected potential, the nitro groups could be partially or totally reduced in amino groups. More recently, a study on the electrochemical response of reduced PNP films on glassy carbon also confirmed the conversion of nitro into amino groups in protic media[71].

Regarding the spontaneous grafting, experiments were performed in acidic media. Nevertheless, an electron transfer has not been demonstrated. In the case of the process induced by a reducing agent (described in chapters IV, V and VI), involving electron transfer, a similar pathway for the formation of amino groups as the one proposed by Delamar could be contemplated. However, the experimental conditions in such experiments are quite far from those commonly used and $–NH_2$ groups were also observed in H_2O DI (pH = 5.5) which is the main solvent in this work. Therefore, it is very unlikely that the reaction described above can occur in our case. Exposure to X-ray irradiation will be thus considered as another pathway to explain of the presence of the amino groups in the PNP films.

Exposure to X-ray irradiation

The degradation effects of XPS on terminal groups were already observed in the case of Br-, CH_3- and COOH-terminated alkylsilane self-assembled monolayers principally on silicon[81, 82]. Hence, as mentioned in electrochemical grafting studies of PNP layers, the reduction of nitro groups in the films under the effect of X-ray irradiation during XPS analysis was considered[14, 71, 77].

The first evidence of the transformation of surface NO_2 groups to amino groups upon photoelectron irradiation was shown by Grunze and coll.[83] during their work on biphenylthiol monolayers on gold. A new peak at 399.3 eV in the N1s XPS spectrum and the disappearance of the peak characteristic of nitro groups at 406.0 eV was observed. Later, Mendes and coworkers[84] demonstrated a similar behaviour in the case of arylnitro-terminated silane multilayers grafted on silicon substrate and proved a partial desorption of nitrogen groups, since the total nitrogen signal was slightly decreasing upon X-ray exposure. The results obtained by Iqbal *et al.*[85] on an X-ray study of SAMs with irradiation time suggested that such a reduction was essentially observed on nitro groups attached to an aromatic ring.

However, although this phenomenon was frequently observed, only a few authors suggested a possible mechanism of the X-ray-induced reduction of nitro groups into amino groups, for which electrons and protons are *a priori* required. Secondary photoelectrons emitted during the XPS analysis constitute the source of electrons. As for the hydrogen atoms required, Grunze and

coworkers[83] suggested that they were generated by the electron-induced dissociation of the C-H bonds in the biphenyl units whereas for Han *et al.*[86] it is more likely that hydrogen atoms come from water or solvent molecules trapped within the monolayer.

To conclude, PNP films are prone to substantial chemical transformations during XPS measurements. However, as the XPS spectra presented in Figure 30 displays both nitro and amino groups, it is likely that the reduction of $-NO_2$ to $-NH_2$ groups is only partial and mainly involves nitro groups from the outer surface of the film. Since the presence of amino groups in the films may come from an undesirable reaction during the XPS analysis, experiments were performed in order to make sure that no amino groups were present prior to the XPS characterization of the films.

Investigation of the presence of amino groups in PNP films before XPS analysis

A priori, the presence of NH_2 groups could be detected easily by performing the IR analysis of the PNP films. The characteristic bands of NH_2 groups should be found between 3300 and 3500 cm^{-1} in the case of ν_{NH2} and in the 1580-1650 cm^{-1} range for ν_{CNH}. However, the former band is hidden by the presence of a large signal attributed to liquid water in the MCT detector (condensation phenomenon at low temperature) and the latter band could be mistaken for the $\nu_{C=C}$ absorption from the aromatic cycle. Consequently IR-ATR cannot be used in this case to characterise the presence of amino groups in the films. Therefore, we concentrated on alternative ways based on the reaction of $-NH_2$ groups and the detection of the induced changes in the film composition.

The first reaction tested was an acetylation reaction consisting in immersing, for a few minutes, the PNP grafted samples in a trifluoroacetic anhydride solution (0.4 M) in THF[83] in order to form an amide bond. Spontaneously grafted films as well as layers synthesized through the induced reduction of NBDT by a reducing agent were studied. In both cases, no absorption band typical of an amide bond (around 1690 cm^{-1}) was detected in the corresponding IR spectra. Therefore, the presence of amino groups in grafted films seems unlikely. In order to confirm this hypothesis, we performed a diazoniation reaction. Indeed, as described in II.3.1.1, diazonium salts can be synthesized from aromatic amino compounds. Such a transformation of a polyaminophenylene films grafted on gold into a layer with terminated diazonium groups was already achieved by Viel *et al.*[87]. After 1 min in a $NOBF_4$ solution (10^{-3} M) in ACN, the two types of PNP films mentioned above were characterized by IR. The spectra remains the same than prior to the oxidizing treatment. No additional band around 2300 cm^{-1} that could be assigned to aryldiazonium stretching was observed.

From those results, it can be concluded that the presence of amino groups in the film directly after synthesis is very unlikely. Consequently the presence of NH_2 signals on the XPS spectrum

can be most likely attributed to the reduction of nitro groups into amino groups under exposure to X-ray irradiation during the XPS analysis. Therefore, in the following XPS analyses, the amount of nitro groups in the films will be calculated by adding, on top of the observed area of the NO_2 peak, the area of the peak attributed to the amino groups and sometimes to protonated amine NH_3^+ as described in IV.1.2. Let us now deal with the origin of the other nitrogen contribution in the XPS peak at 400 eV identified as azo groups.

III.3.1.3 - Origin of azo groups

The presence of azo groups in grafted films from diazonium salts was studied by XPS[14, 60] as well as ToF-SIMS[77]. As in the case of NH_2 groups, the origin of azo groups in the films was widely discussed in the literature and to date is still under debate[14, 51, 71]. The main mechanisms proposed so far describing azo bridges at the surface and within the film will be detailed below.

Bélanger and coll.[20, 78] were the first to propose a mechanism for the existence of azo groups in such organic layers. By undertaking a study of the spontaneous reaction between carbon black and aryldiazonium salts in aqueous solution, they assumed that the linkage arises from a diazonium coupling reaction between the phenolic functionalities on the carbon surface and the diazonium cation as represented in Scheme 45b. In our case, although azo bridges are observed, the substrate employed (gold plates) is very unlikely to display such functionalities. Moreover, such a mechanism suggests that azo groups are only located at the film-substrate interface. However, according to the XPS area ratio of Au-N/–N=N– found in typical films such as the one shown in III.3.1, it is likely that azo groups are present within the whole film thickness. Therefore, it is very probable that another mechanism is involved in the case of graftings on gold.

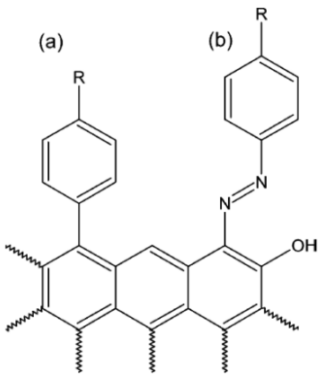

Scheme 45 – Possible linkage between aryl groups and a carbon surface by a) a C-C bond and b) an azo bridge in ortho of a phenolic functionality extracted from the work of Bélanger *et al*[20].

An alternative explanation involves the formation of an intermediate diazenyl (or azophenyl) radical during the reduction of the diazonium cation. Indeed, according to Galli[88], when a diazonium salt acquires an electron it creates a diazenyl radical (R-Φ-N=N•), a rather labile species, that can gives up dinitrogen to form an aryl radical (R-Φ•). The reaction of this diazenyl radical on an aromatic ring previously attached on the surface or directly on the surface, as in

Scheme 46, was considered by Laforgue and coworkers[49] to explain the presence of azo groups inside the layer as well as the film-substrate interface (whatever the substrate).

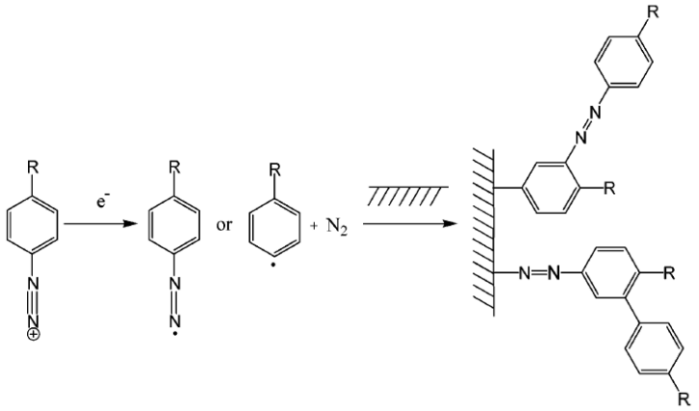

Scheme 46 – Potential mechanism involving diazenyl radical to explain the presence of azo groups extracted from the work of Laforgue *et al.*[49].

The previous mechanism implies the existence of a diazenyl radical. However, according to Doppelt *et al.*[77], it is a very unlikely mechanism since such intermediate species can only be produced at high driving force (pulse radiolysis) or at very negative potentials. Consequently, they proposed another mechanism, summarized in Scheme 47b, for the formation of azo bonds in those organic films derived from the growth mechanism of electrochemically grafted polyphenylene layers.

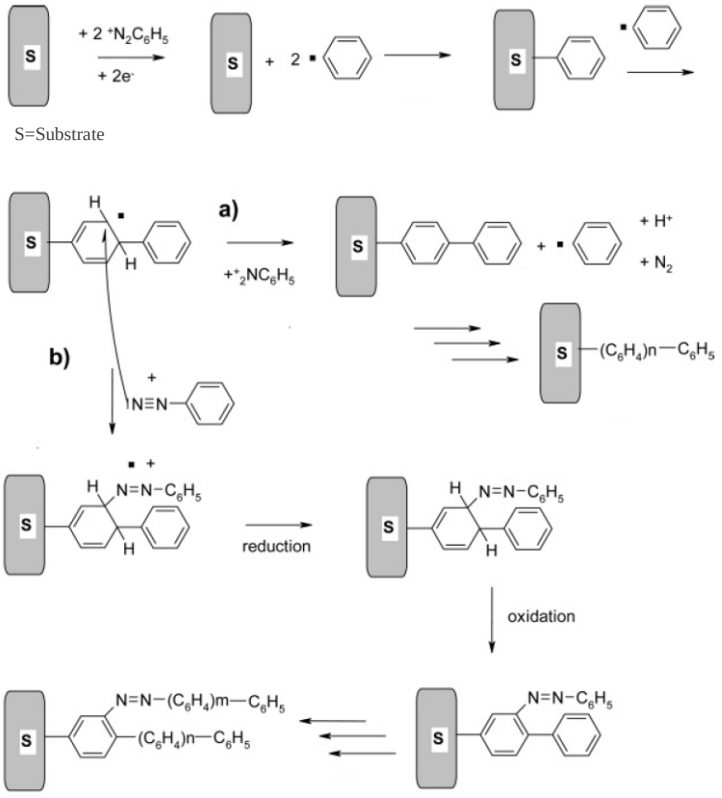

Scheme 47 – Proposed mechanism for the formation of azo bonds extracted from the work of Doppelt *et al.*[77].

That mechanism cannot however explain the presence of azo bridges at the film-substrate interface. Although the existence of Cu-N=N-Φ structures was reported to be very unlikely since the two nitrogen atoms were expected to give separate peaks in the XPS analysis, in our case, we have clearly identified the presence of Au-N bonds. Therefore, a mechanism in agreement with this latter result has still to be determined.

III.3.1.4 - Conclusion on the structure and chemical composition of the films

To sum up, from the IR and XPS characterizations, the structure of spontaneously grafted films on gold from NBDT has been deduced and is represented in Scheme 48. The presence of expected C=C bonds (IR: ν=1600 cm^{-1}) as well as nitro groups (IR: ν^{as}_{NO2}=1525 cm^{-1}, ν^{s}_{NO2}=1350 cm^{-1}; XPS: $BE_{NO2} \approx$ 406.0 eV) has been detected. The XPS analysis has also revealed the existence of NH_2 groups ($BE_{NH2} \approx$ 399.5 eV). Since amino groups are certainly due to the reduction of nitro groups under X-ray irradiation during the XPS analysis, those amino groups will be counted with the NO_2 groups upon quantitative comparisons. Azo bridges inside the films ($BE_{N=N} \approx$ 400.5 eV) and Au-N bonds from the film-substrate interface ($BE_{Au-N} \approx$ 397.5 eV) have also been identified in the PNP films. To date, no mechanism can fully explain the presence of both species in the spontaneously grafted PNP films.

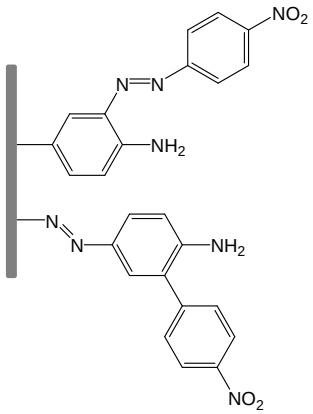

Scheme 48 – Structure of NBDT spontaneously grafted films on gold deduced from surface characterizations.

III.3.2 - **Previous mechanisms proposed**

The spontaneous grafting of a polyphenylene layer on gold has already been reported in 2002 by Fan *et al.*[89] in acetonitrile and explored later in various media[17, 18] by different techniques including scanning electrochemical microscopy (SECM)[90] and surface-enhanced Raman scattering (SERS)[42]. However, the mechanism involved in this phenomenon remains unclear although the following propositions were made.

As mentioned above, gold should, *a priori*, not be able to reduce diazonium salts into the corresponding aryl radicals. However, according to Downard and coll.[17], the spontaneous

reaction in aqueous acid solutions can proceed via an electron transfer from the gold to the diazonium cation. Indeed, Downard and coworkers described a jump in the open-circuit potential (OCP) of the gold working electrode upon the introduction of the diazonium salt in solution, followed by a slow decay of the OCP. As the increase in the OCP of conductive surfaces could indicate the accumulation of positive charges on its surface, they assigned this behavior to an electron transfer from the gold to the diazonium cation. The slow decrease of OCP was associated with the discharge of accumulated positive charges, perhaps through slow oxidation of adventitious impurities in the reaction solution. Hence, aryl radical species should be produced from that spontaneous electron transfer. However, when we immersed gold substrates in a NBDT/HEMA aqueous mixture (without any reducing agent), we did not observe any grafted PHEMA on the gold surface. Owing to the expected mechanism of Graftfast™ experiments (briefly described in II.1), we can state either that no aryl radicals initiated the radical polymerization of the vinylic monomer or that the amount of radical species produced was too low to end up grafted on the surface or simply to be detected on the surface by XPS. Therefore, our experiments are not in agreement with this spontaneous or "gold-activated" homolytic dediazoniation of diazonium salts.

A second mechanism going through a heterolytic pathway could also be envisaged. Such a dediazoniation would lead to the formation of nitrobenzene cations (known to be intermediate species in the degradation of the diazonium salt into nitrophenol[91]) able to graft spontaneously on electron rich surfaces such as metals. Nevertheless, this mechanism involving cationic species would not be consistent with the grafting in basic solution observed by Podvorica *et al.*[18] assumed to occur at pH 10 via the spontaneous homolytic dediazoniation of diazoates producing aryl radicals.

Therefore, as concluded from a solution study conducted by Pazo-Llorente and coworkers[92], a variation of the dediazoniation mechanism according to the solvent is very likely. We have thus focused in the understanding of the mechanism in the case of the spontaneous grafting in the main media used in the anchoring processes described in this work i.e. in aqueous solutions (unless otherwise mentioned in the case of very particular experiments). First, the conditions required in order to observe an organic layer on the gold substrates will be explored and then, several mechanisms will be investigated in order to find the grafting mechanism fitting the best our experimental results.

III.3.3 - **Occurrence of the spontaneous grafting**

In this part, the main parameters of the grafting such as the nature of the diazonium salt and the influence of its concentration on the grafting but also various solvents will be investigated

with a view to determine whether specific conditions are required to observe a spontaneously grafted film.

III.3.3.1 - Diazonium salt

The spontaneous grafting on gold has mainly been reported in the literature in the case of NBDT[17, 18] and more rarely MBDT[17] and bromobenzenediazonium salts[18]. We decided to test such a grafting with diazonium salts bearing groups with a large range of inductive and mesomeric effects, such as nitro, carboxy, bromo, thiomethyl and methoxy-benzene diazonium salts. Since some of those groups do not have a clear IR signature, the grafted samples were analysed by XPS. In all cases, a successful spontaneous grafting was identified thanks to the presence of a component around 406 eV (N1s) attributed to nitro groups in the case of NBDT, of a COO component (at 288.6 eV C1s) in the case of carboxy benzene diazonium salt, of a bromine signature in the case of Br diazonium salt, of a sulphur signal in the case of SCH_3 compound and of a more intense area of C-O bonds in the case of the grafting of MBDT. The N1s XPS spectra of the films obtained from all the diazonium salts tested are represented in Figure 31.

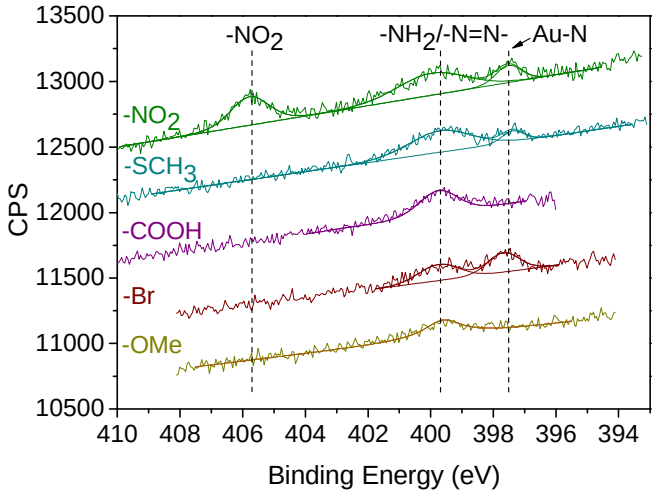

Figure 31 – XPS N 1s core level spectrum of spontaneously grafted layers on gold plates obtained by immersion in a 0.046 M NO_2, COOH, Br, CH_3S, CH_3O-benzene diazonium salt solution for 60 min.

In all cases, a component attributed to –N=N– bonds was identified (see III.3.1.3 for formation mechanisms). As previously observed in the case of the grafting of NBDT on gold, Au-N bonds were also detected when the Br- and CH_3S- diazonium salts were used, which suggests the presence of azo bonds at the film-substrate interface. No Au-N bonds could be observed in the spectra corresponding to the grafting of carboxy or methoxy benzenediazonium salts. It is however possible that both salts led to the formation of thicker or denser phenylene films than the other studied ones. Indeed, an Au-N signal could be hidden by the much larger N=N one, preventing its detection. Therefore, the spontaneous grafting is a process that seems to occur whatever the diazonium salt. However, no clear effect of the nature of the para

substituent could be found: groups with theoretically similar electronic effects such as thiomethyl and methoxy groups gave different results. Moreover, in three cases (nitro, carboxy, and thiomethyl-benzene diazonium salts), the observed spontaneous grafting mechanism comes with the formation of Au-N bonds.

In all those cases, we attempted to estimate the thickness of the grafted layers by using the decrease of the Au 4f 7/2 XPS signal upon the presence of the film (as detailed in V.2.6.1). However, the calculated thickness values were found identical to those of a pristine gold substrate (around 5 – 6 nm) which is possibly attributable to the fact that the value of the electron attenuation lengths employed in the formula was determined for flat and perfectly clean substrates which is far from being our case.

Since the nitro groups can be easily identified by IR and XPS, the study on the spontaneous grafting will be principally conducted with NBDT. To go further, we studied the influence of the concentration of NBDT in the spontaneous grafting on gold in aqueous solution (H_2O DI). The results of the IR-ATR analysis of the films after the rinsing procedure as a function of the amount of NBDT in solution are presented in Table 5. The absorption band corresponding to the symmetric stretching of aryl-NO_2 group was chosen to compare the samples since, among the three main characteristic bands of PNP films, this one gives the highest intensities.

Table 5 – Intensity of the ν^s_{NO2} absorption band from the IR-ATR analysis of the spontaneous grafted films obtained after 1h immersion of gold plates in H_2O DI solutions of various concentrations of NBDT.

[NBDT] (M)	n (mol)	I ν^s_{NO2} (%)
$4.6\ 10^{-2}$	$2.5\ 10^{-3}$	0.23
$2.3\ 10^{-2}$	$1.3\ 10^{-3}$	0.21
10^{-2}	$5.5\ 10^{-4}$	0.219
$4.6\ 10^{-3}$	$2.5\ 10^{-4}$	0.24
10^{-3}	$5.5\ 10^{-5}$	0.22
10^{-4}	$5.5\ 10^{-6}$	0.25
10^{-5}	$5.5\ 10^{-7}$	0.20
10^{-6}	$5.5\ 10^{-8}$	0.10
10^{-7}	$5.5\ 10^{-9}$	0.01
10^{-8}	$5.5\ 10^{-10}$	-

These results show that similar amounts of grafted nitro groups are observed when the concentration of diazonium salt is higher than 10^{-5} M. The same value decreases with the concentration below that threshold and is negligible for a concentration of 10^{-8} M. Lehr *et al.*[17] calculated a packing density of 12×10^{-10} mol.cm^{-2} for a close-packed layer of nitrophenyl groups on a flat surface. In our experiments, the gold plates had a surface area of 2.1 cm^2, which means that 3×10^{-9} mol of diazonium salt should be enough to obtain a compact layer of

nitrophenyl groups on the surface of the substrate. Our experiments however demonstrated that working with at least 5.5 x 10^{-8} mol of NBDT in solution, corresponding in this case to a NBDT concentration in solution of 10^{-6} M, was required to obtain a detectable grafted film. Therefore, such a reaction on gold is likely to occur (almost) whatever the concentration in diazonium salts provided it is higher than 10^{-6} - 10^{-7} M. Moreover, it indicates that all the diazonium salt in solution did not contribute to the formation of the film.

III.3.3.2 - Solvents

Another important parameter of the spontaneous grafting system lies in the solvent of the reaction. We first tested the influence of the pH (with HCl and H_2SO_4) of the solutions. The results obtained are summarized in Table 6, but they are difficult to analyse since the observed differences are quite low, and the IR intensities belong to the range of variations that can be attributed to the IR-ATR measurement itself (see III.3.1). However, by analogy with works carried out in acidic media by Downard[17] and Pinson[18], such IR intensities are estimated to correspond to thicknesses from 1.3 to 1.7 (± 0.5) nm. Whatever the acid (HCl or H_2SO_4), the main tendency, extracted from Table 6 and in comparison with the IR absorption values obtained in H_2O DI, is the lower the pH, the lower the amount of grafted matter. Some spontaneous grafting from NBDT is however observed whatever the pH and the acid used to control this pH.

Table 6 – Intensity of the ν^s_{NO2} absorption band from the IR-ATR analysis of the spontaneous grafted films obtained after 1h immersion of gold plates in 0.046 M NBDT HCl and H_2SO_4 solutions of various pH at room temperature.

Solvent	pH	I ν^s_{NO2} (%)	Solvent	pH	I ν^s_{NO2} (%)
HCl	0.3	0.07	***H_2SO_4***	0.30	0.12
	1.10	0.06		1.32	0.13
	1.96	0.17		1.88	0.19
	3.05	0.17		2.68	0.20

To go further in the study of the reactive medium and to conclude on the role of aqueous solutions on the reaction, the spontaneous grafting process was also tested in acetonitrile with NBDT. The signal from the IR analysis of the samples grafted in ACN was very weak: 0.07 % for the symmetric stretching of NO_2 groups. Although Lehr *et al.*[17] found no evidence for such reaction in ACN, the N1s XPS spectrum of our gold substrate after rinsing (Figure 32), proves the grafting of a PNP layer in this solvent. The peak centered at 400.0 eV is very large. Therefore, its decomposition in two peaks attributed to NH_2 and N=N groups (see III.3.1.1) is justified. As for the spontaneous grafting of NBDT in H_2O DI, Au-N bonds are present in the film and in very similar proportions to nitrogen atoms involved in –N=*N*– bonds (XPS area of

Au-N ~ 339 a.u. and of –N=*N*– ~ 381 a.u.) indicating that almost all the azo bonds are located at the film-substrate interface.

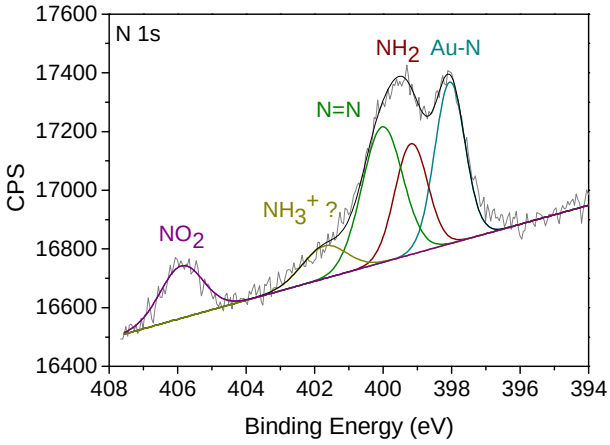

Figure 32 – XPS N 1s core level spectrum of PNP layer spontaneously grafted on gold plates obtained by immersion of the substrates in ACN with 0.005 M NBDT for 60 min.

In order to confirm the existence of a spontaneous grafting of diazonium salts in organic media and to widen the range of diazonium salts tested, the same reaction was carried out with 4-trifluoromethylbenzene diazonium (see appendix 2 for its synthesis). Indeed this salt can only be used in organic media because of its solubility and, due to steric effects of the CF_3 in *para* position, is assumed to limit the growth of the layer. Since the expected grafted film does not present any good marker for IR-ATR measurements, the sample was only characterized by XPS (Figure 33). The two components at 292.6 eV (C1s) and 687.9 eV (F1s)[73] can be attributed to C-F bonds from the trifluoromethyl group. The normalized XPS area of those two bands are in accordance since A(C1s C-F) ≈ A(F1s C-F)/3 ≈ 150 a.u. The other peak in the F1s spectrum is assumed to come from inorganic fluorides (BF_4^-)[9, 14]. The N1s spectrum is also very rich. It contains gold nitrides (398.1 eV), azo groups both from the interface and the film (400.0 eV) and an unknown peak at 401.6 eV. That latter component could be assigned to unreacted diazonium groups[32, 49, 51]. Once again, it is interesting to compare the XPS areas. It seems that there is more azo bonds inside the films than at the interface ($A(N=N)_{interface}$ = A(Au-N) = 40 a.u. and $A(N=N)_{inside} = (A(N=N)_{total} - A(N=N)_{interface})/2$ = 82 a.u.). Moreover, from the comparison of XPS areas, it can be deduced that around 80 % of the trifluoromethylphenyl groups are linked by an azo bond to the substrate (surface or organic moieties already grafted) whereas the rest is directly attached to it. To conclude, all these results indicate that a poly(trifluoromethylphenylene) film was successfully grafted. The spontaneous grafting on gold in ACN is therefore confirmed and the resulting films contain Au-N bonds, as grafted films from NBDT.

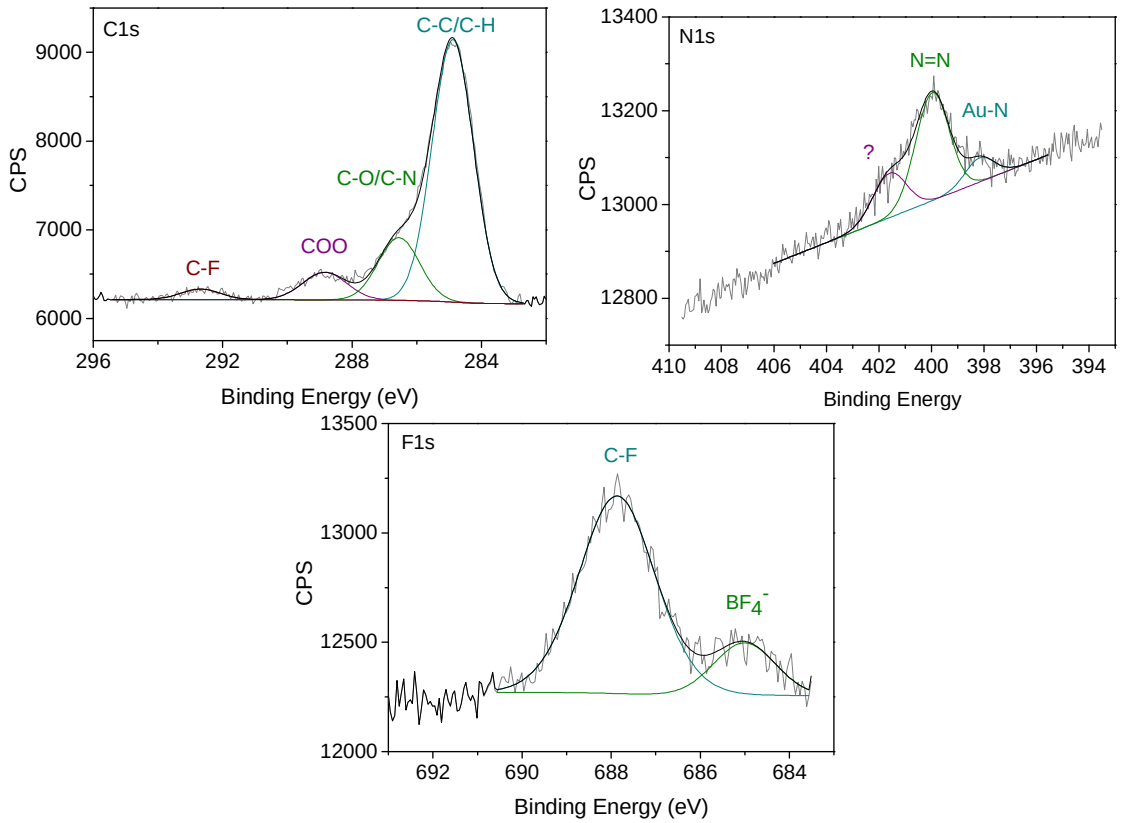

Figure 33 – XPS C 1s, N 1s and F1s core level spectra of spontaneously grafted layers on gold plates obtained by immersion in a 0.046 M F_3C-benzene diazonium salt solution for 60 min after rinsing and 30 s US in acetonitrile.

III.3.4 - **Investigation of the mechanism of the spontaneous grafting on gold**

We showed above that spontaneous grafting can be achieved with various diazonium salts, in aqueous or in organic media. We will now focus on finding a mechanism fitting all our experimental results. The first mechanism to be considered is simple and consists in a mechanical anchorage of the diazonium salts on the surface. Then, we will deal with more common pathways such as cationic and radical mechanisms. To finish, we will propose the involvement of another type of mechanism.

III.3.4.1 - A mechanical anchoring?

Due to the roughness of the substrate, the possibility of a mechanical anchoring of diazonium salts where phenyl molecules are embedded on the surface was our first assumption.

Quartz crystal microbalance (QCM) could have been an interesting tool to characterise the spontaneous grafting on low roughness gold substrate (golden quartz crystal resonators RMS roughness of 1.6 nm). Indeed, the addition of molecules at the surface of the resonator induces a change in resonance frequency of the crystal allowing determining the mass of grafted or deposited film per unit area. However, the sensitivity of the microbalance in water[93] is around 180 µg.cm^{-2}. Consequently, with a packing density of 12 x 10^{-10} mol.cm^{-2} i.e. 0.15 µg.cm^{-2} for a

close-packed layer of nitrophenyl groups on a flat surface, the spontaneously grafting is certainly not detectable.

Therefore, we concentrated on the surface study of the spontaneous grafting on gold substrates with a lower roughness than glass/Cr/Au plates. Mica/Au substrates could not be employed in this study since such gold layer is very fragile in aqueous solutions. Thus, only the grafting on Si/Cr/Au substrates was investigated. As calculated from the 1 x 1 µm² AFM image in Figure 34, Si/Cr/Au wafers have a RMS roughness of 2.9 nm whereas glass/Cr/Au plates displayed a roughness of 5.1 nm (as shown in II.3.4.2).

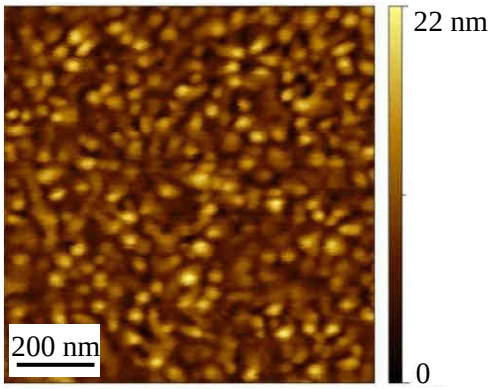

Figure 34 – 1 x 1 µm² AFM image of pristine Si/Cr/Au substrate.

IR-ATR analysis showed that grafted Si/Cr/Au sample contains less nitrophenyl groups than glass/Cr/Au plates ($I\nu^{s}_{NO2\text{-}Si/Cr/Au}$ = 0.1 % and $I\nu^{s}_{NO2\text{-}glass/Cr/Au}$ = 0.25 %). XPS measurements confirmed this tendency (Table 7). The XPS area corresponding to NO_2+NH_2 groups is approximately twice smaller in the case of Si/Cr/Au samples but the corresponding film still contains Au-N bonds as well as azo bridges. However, from IR and XPS, there is no evidence of diazonium groups ($–N_2^+$). Hence, the grafting does not seem to come from a mechanical anchoring of the diazonium salts on the surface. The differences observed between glass/Cr/Au and Si/Cr/Au samples can be simply explained by a higher specific surface area for the higher roughness samples, i.e. glass/Cr/Au, which involves a variation of reactivity of the surface. Another mechanism is therefore likely to take part in the spontaneous grafting of diazonium salts on gold.

Table 7 – XPS areas of the nitrogen components of PNP layers spontaneously grafted on Si/Cr/Au and glass/Cr/Au substrates obtained by immersion (1h) in 0.005 M NBDT H_2O DI.

Area of the N 1s components (a.u)		
	Si/Cr/Au	glass/Cr/Au
Au-N	44	72
N=N	121	76
NO_2+NH_2	222	413

III.3.4.2 - A cationic mechanism?

The hypothesis of a cationic pathway in the spontaneous grafting of diazonium salts on gold was tested by varying several parameters such as the exposure to light or dark, the acidification of the media and the temperature.

The effect of light is gathered in Table 8 at room temperature as well as at 2°C. Carrying out the reaction in the dark gives less grafted nitrophenyl groups than under light exposure, but a grafted film was anyway obtained. Besides, photochemical decomposition of diazonium salts in water was reported in the literature to lead to aryl cations[94]. Therefore, we assumed that a cationic mechanism plays a role in the spontaneous grafting on gold. The corresponding grafting mechanism could be described as followed: first, due to the short lifetime of aryl cations in water, only those formed near the substrate would attach to it and then, aryl cations could contribute to the growth of the films by their addition on aromatic rings already grafted on the gold surface followed by the elimination of H^+.

Table 8 – Intensity of the ν^s_{NO2} absorption band from the IR-ATR analysis of the spontaneous grafted films obtained after 1h immersion of gold plates in 0.046 M NBDT H_2O DI solutions at light exposure or in the dark at room temperature and 2°C.

	RT		**2°C**	
	Light	*Dark*	*Light*	*Dark*
I ν^s_{NO2} (%)	0.21	0.12	0.19	0.12

Such hypothesis of a cationic mechanism is confirmed by the previously described experiments on the influence of the pH on the grafting (cf III.3.3.2). From the results presented in Table 6, we concluded that the lower the pH, the less nitrophenyl groups are detected on the surface. This is also in good agreement with the data collected in the case of the spontaneous formation of films in phosphate buffer solutions of various pH (Table 9). Indeed, diazonium salts are claimed to be more stable in acidic solutions since it limits their decomposition into aryl cations *via* a heterolytic pathway[95, 96]. However, in HCl solution, Cl^- can act as a quencher of phenyl cations which would thus explain the observation of less nitrophenyl groups in the films in comparison with films synthesized in H_2SO_4. Therefore, the involvement of a cationic mechanism in the spontaneous grafting of diazonium salts on gold is likely.

Table 9 – Intensity of the ν^s_{NO2} absorption band from the IR-ATR analysis of the spontaneous grafted films obtained after 1h immersion of gold plates in phosphate buffer solutions of 0.046 M NBDT.

pH	**2.1**	**3.7**	**7.2**
I ν^s_{NO2} (%)	0.15	0.2	0.43

The thermal decomposition of diazonium salts was also reported to form aryl cations[94]. Therefore, the influence of the temperature on the reaction has been evaluated. It is clear from

the results shown in Figure 35 that beyond 40°C, the temperature favors the grafting of diazonium salts. Such a reaction cannot be considered as a spontaneous reaction since the grafting is thermally assisted. Below 40°C, the influence of the temperature seems negligible, although the experimented temperature range was limited. Therefore, the role of the thermal decomposition of diazonium salts in aryl cations is difficult to evaluate. However, the existence of a threshold temperature delimitating two different behaviours is not surprising since DSC experiments in NBDT water solutions show an exothermic peak around 45°C corresponding to the decomposition of the diazonium salt.

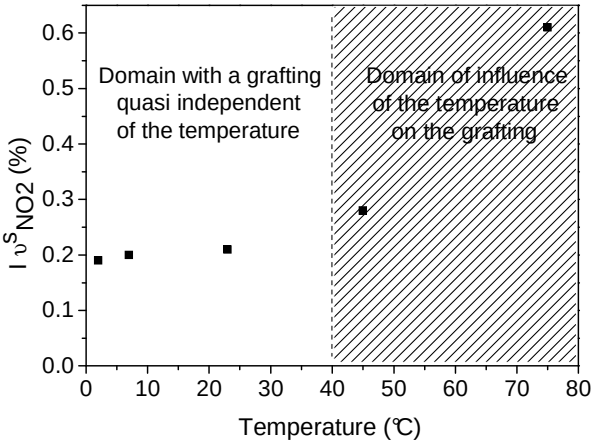

Figure 35 – Intensity of the ν^{s}_{NO2} absorption band from the IR-ATR analysis of the spontaneous grafted films obtained after 1h immersion of gold plates in 0.046 M NBDT H_2O DI solutions as a function of the temperature.

To sum up, exposure to light as well as perhaps temperature was demonstrated to take part in the spontaneous grafting of diazonium salts on gold in water through the formation of aryl cations. To confirm the role of these parameters on the spontaneous reaction in general, their influence was also tested in ACN since aryl cations have also been reported in this solvent[97]. Moreover, working in ACN allows reaching much lower temperature than in water. By combining precautions such as working in the dark and at low temperature (-18°C), the grafting of NBDT as well as its trifluoromethyl counterpart was tested. Since experiments in the case of both diazonium salts lead to similar conclusions, only the results obtained for the former diazonium salt will be discussed. As shown in Figure 36, the data summarized in the table indicate that in both conditions (light exposure at room temperature or dark at -18°C) films can be obtained but their composition is slightly different. Indeed, although both films contain azo bonds mainly located at the interface as previously described (III.3.1.4), there are more nitrophenyl groups not linked through those bridges in the film formed under light exposure at room temperature than in the film obtained in the dark at -18°C. Besides, even after taking all the precautions possible to avoid the decomposition of the diazonium salts into aryl cations, a non-negligible grafting of NBDT is still observed on gold at -18°C in the dark (corresponding to 4/5 of the total amount of nitrogen detected on the film formed at room temperature under light

exposure). Therefore, it seems that exposure to light and to a lesser extent the temperature have an only small influence on the grafting and are responsible for the presence of some nitrophenyl groups (not linked via an azo bond) in the films. Consequently, we concluded that the involvement of a cationic mechanism in the spontaneous grafting of diazonium salts on gold is only partial; another mechanism has to be considered.

a)

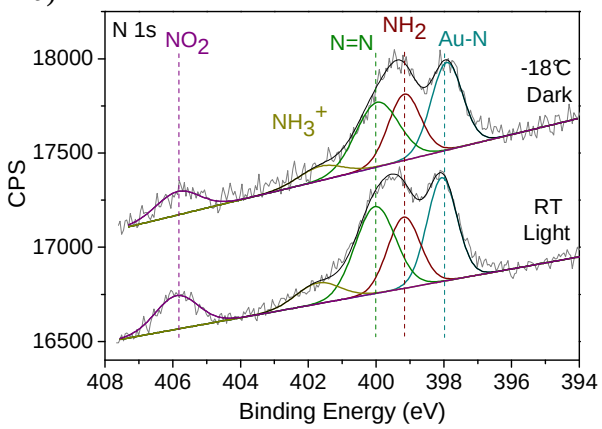

b)

Area of the N 1s components (a.u)		
	Dark	Light
	-18°C	RT
Au-N	300	339
N=N	303	381
NO_2+NH_2+ NH_3^+	410	506
N total	1013	1226

Figure 36 – XPS analyses a) N 1s core level spectra and b) area of the nitrogen components of PNP layer spontaneously grafted on gold plates obtained by immersion (1h) of the substrates in 0.005 M NBDT ACN at -18°C and room temperature after rinsing and 30 s US in acetonitrile.

III.3.4.3 - A radical mechanism?

As a parallel with the mechanisms proposed in the case of the spontaneous grafting of diazonium salts on reductive metals, a radical mechanism was considered to explain the spontaneous grafting on gold.

The most common technique to study organic free radicals is the electron paramagnetic resonance (EPR). Particularly, short lifetime free radicals can be detected and identified by a spin-trapping technique. It consists in the addition of nitroso or nitrone compounds which give stable nitroxide radicals as a result of spin-trapping the organic free radicals at stake. In our case, 2-methyl-2-nitrosopropane MNP (Scheme 49) was used (see IV.2.2.2 and appendix 4). The EPR study of a NBDT solution containing an excess of MNP spin-trap revealed no radicals. Therefore, it tends to prove that no homolytic dediazoniation of the diazonium salt occurred. However, this result has to be carefully considered. Indeed, as mentioned above in our experiments, 3×10^{-9} mol of diazonium salt would be enough to obtain a close-packed layer of nitrophenyl groups on our gold plates. The concentration detection limit of the EPR in our experimental conditions has been estimated at 4×10^{-7} mol. Thus, it seems that the very low concentration of aryl radicals needed to insure the grafting of a packed monolayer of PNP cannot be detected by EPR. Therefore, it is difficult to conclude with this experiment on the involvement of aryl radicals in the spontaneous grafting mechanism.

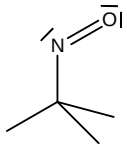

Scheme 49 – Structure of the 2-methyl-2-nitrosopropane spin-trap.

An indirect way to demonstrate the presence of aryl radicals during the spontaneous reaction consists in performing the grafting with an inhibitor of radical species in solution. Using dioxygen as radical killer was discarded because the influence of O_2 on the reaction was found to be complex. Therefore, we focused on MNP from the EPR experiments as inhibitor. From the IR-ATR data (Table 10), it seems that the grafting in absence or presence of MNP is different since the intensity of the band associated to symmetric stretching of NO_2 groups is weaker in the latter case. This result could be explained by the formation of a less dense or thinner organic layer i.e. with less NO_2 groups.

Table 10 – Intensity of the IR-ATR ν^{s}_{NO2} absorption band of the spontaneous grafted films (1h immersion of gold plates in 0.046 M NBDT H_2O DI) with or without MNP spin-trap, in a nitrogen flow glove box.

	NBDT	**NBDT + MNP**
I ν^{s}_{NO2} (%)	0.34	0.14

To go into further details, the substrates were characterized by XPS. **Figure 37** shows clearly that the amount of NO_2+NH_2+NH_3^+ in the film is higher for the reaction performed without MNP, which is in agreement with the IR-ATR results. In addition, by studying carefully the area of each nitrogen component present in the film, we found that the compositions of the two samples are different. With MNP in solution, there are more Au-N bonds (i.e. azo bridges between the surface and the film) but less azo inside the film. Moreover, most of the nitrophenyl groups are attached to the substrate (surface or already grafted moieties) by an azo bond. This suggests that, in contrast to what was observed for samples grafted in absence of MNP, almost no nitrophenyl moieties have been directly grafted on the substrate in the case of the reaction in presence of MNP. Therefore, according to the differences observed, a partial involvement of a radical mechanism in the spontaneous grafting of diazonium salts on gold seems possible. However, as a grafted film is still observed despite the presence of a spin-trap in the diazonium salt solution, a radical mechanism alone cannot fully explain this spontaneous grafting. Before looking for a complementary mechanism, the origin of the aryl radicals formation remains to be investigated. Therefore, several hypotheses have been considered.

a)

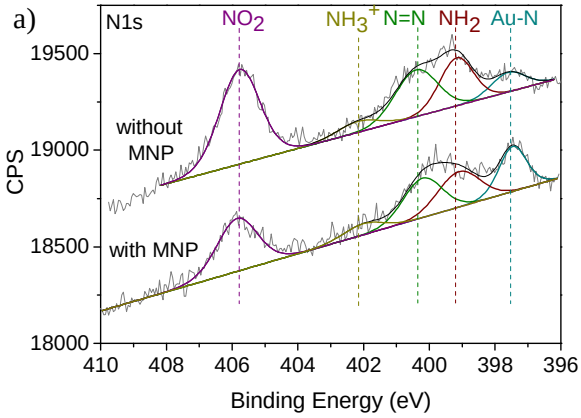

b)

Area of the N1s components (a.u)		
	NBDT	NBDT MNP
Au-N	72	138
N=N	215	168
NO_2+NH_2+ NH_3^+	653	448

Figure 37 – XPS analyses a) N 1s core level spectra and b) area of the nitrogen components of PNP layer spontaneously grafted on gold plates obtained by immersion (1h) of the substrates in 0.046 M NBDT H_2O DI solutions in absence or presence of the MNP spin-trap, in a nitrogen flow glove box.

First, the spontaneous formation of the aryl radical could come from a homolytic dediazoniation. However, the spontaneous formation of these radicals by this pathway is very unlikely since it would lead to the formation of $N_2^{+\bullet}$. Indeed, as outlined by Galli[88], the formation of aryl radicals from diazonium salts requires an electron transfer. Second, the formation of those radicals in solution could be due to the reduction of the diazonium salts by the chromium ($E°_{Cr2+/Cr}$ = 0.34 V) edges of the gold plates (cf II.3.4.2). The hypothesis was however quickly eliminated because the containment of the reaction only on the gold surface has given similar results as those obtained without these precautions. Hence, since no sensible explanation could be given for the presence of aryl radicals in this reaction, we reconsidered our experiment in presence of a spin-trap and attempted to answer the following question: is the MNP spin-trap really selective of aryl radicals? Considering the availability of the lone pair of its nitrogen atom, MNP may also react with aryl cations present in solution as demonstrated above. Thus, we concluded that the decrease in nitrophenyl moieties in the case of films grafted in presence of MNP was probably due to the unwanted reaction of the spin-trap with aryl cations in solutions. Therefore, a radical mechanism does not seem to take part into the spontaneous grafting.

III.3.4.4 - Another type of mechanism?

None of the previously described mechanisms can completely explain by itself the spontaneous grafting of diazonium salts on gold. The main puzzling result is the presence of Au-N bonds at the film-substrate interface. However, on the one hand, the diazonium salt is electron deficient and its resonance structure presents a 2p vacant orbital on the terminal nitrogen. On the other hand, gold is a d^9 electron rich metal. Thus, the 5d orbitals of gold are almost full and can possibly interact with other low energy vacant orbital such as the one of the diazonium salt. Therefore, we assumed that diazonium cations could directly interact with the gold surface *via* the diazonium group. Such a hypothesis is in agreement with experimental

results. First, it explains the presence of Au-N bonds as well as azo groups at the interface. Second, it is in accordance with the formation of "remaining" organic film whatever the temperature, light exposure, the roughness of the gold surface, the medium, the presence of quenchers and, in some extent, the concentration of the diazonium salt.

III.3.5 - **Conclusion on the mechanism of the spontaneous grafting**

The spontaneous grafting of diazonium salts on gold, resulting from the simple immersion of gold substrates in a diazonium salt solution under ambient conditions (room temperature, light exposure...), leads to very thin polyphenylene films. The growth of such film is assumed to come from complementary mechanisms represented on Scheme 50 and seems to be limited to only mono or bilayers. The first mechanism is likely to involve a direct reaction of diazonium cations with the gold surface and forms Au-N=N-Φ-R bindings. The absence of Au-N bond XPS signatures in the case of the grafting of COOH or MeO-benzene diazonium salts can be attributed to the formation of thicker films in those cases, preventing the detection of the interface bonds. The other phenyl groups in the spontaneously grafted layer are assumed to come from the interaction of aryl cations, from the decomposition of the diazonium salt mainly by light, with the surface or the other phenyl groups already bonded to the substrate. To finish, since no aryl radical seems to be formed during this reaction, azo groups inside the film are attributed to a diazonium coupling on the previously attached *para* substituted phenyl moieties.

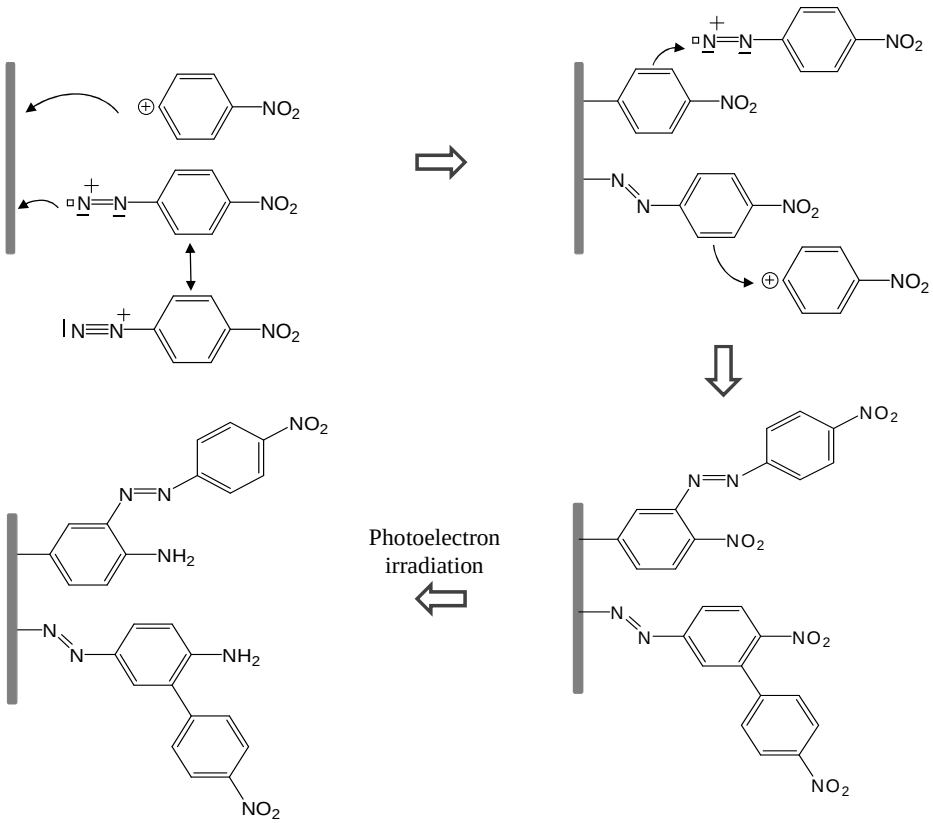

Scheme 50 – Mechanism proposed for the spontaneous grafting of NBDT on gold substrate.

Summary

The spontaneous reaction of diazonium salts has been used for the grafting on various substrates such as metals reducing enough to reduce themselves the diazonium cations into aryl radicals but also on semiconductors and on carbon for which the grafting mechanism proposed varies from diazonium coupling reaction to adsorption/decomposition pathways or homolytic cleavage of diazonium anhydride according to the type of carbon used. It has been widely employed since it consists in a simple immersion of the substrate in the diazonium salt solution. As electrochemical processes, the spontaneous grafting is assumed to give covalently bonded films. Resistances to solvents and to ultrasonication are commonly accepted as indirect proofs of the existence of a covalent bond. However, the most relevant attempts to demonstrate a metal-C interface bond were obtained by SERS on gold and by an XPS investigation of spontaneously grafted films on copper. Similarly, our experiments give evidence of such a bond in spontaneously grafted films on nickel substrates in acetonitrile. In the case of gold substrate, the formation of a spontaneous film was unexpected but reported in the literature in parallel to our observations. However, the detection of an Au-C bond by XPS is technically very unlikely. Propositions to explain the grafting mechanism on gold have been made. Nevertheless, none of them was fitting with our experimental results showing the presence of a Au-N bond. After testing the most probable mechanisms, we have concluded in favor of the involvement of complementary mechanisms which are the direct reaction of diazonium cations with the gold surface as well as a cationic mechanism leading to the formation of aryl cations able to graft on the substrate. However, it is important to underline that such process leads to films with a limited thickness. Therefore, in order to obtain thicker polyphenylene films on any type of substrates (including non-metals), the introduction of a reducing agent in solution has been investigated and the mechanism of the grafting is discussed in the following chapter.

References

1. J. Pinson, F. Podvorica, *Attachment of organic layers to conductive or semiconductive surfaces by reduction of diazonium salts*, ***Chemical Society Reviews***, **2005**, 34 (5), 429-439.
2. J. L. Bahr, J. M. Tour, *Highly functionalized carbon nanotubes using in situ generated diazonium compounds*, ***Chemistry of Materials***, **2001**, 13 (11), 3823-3824.
3. C. Bureau, J. Pinson, *Method for modifying insulating or semi-conductive surfaces, and resulting products.*, FR 2892325, EU 1948720, **2007**.
4. C. Mangeney, Z. Qin, S. A. Dahoumane, A. Adenier, F. Herbst, J. P. Boudou, J. Pinson, M. M. Chehimi, *Electroless ultrasonic functional ization of diamond nanoparticles using aryl diazonium salts*, ***Diamond and Related Materials***, **2008**, 17 (11), 1881-1887.
5. M. Pandurangappa, T. Ramakrishnappa, R. G. Compton, *Functionalization of glassy carbon spheres by ball milling of aryl diazonium salts*, ***Carbon***, **2009**, 47 (9), 2186-2193.
6. F. Barriere, A. J. Downard, *Covalent modification of graphitic carbon substrates by non-electrochemical methods*, ***Journal of Solid State Electrochemistry***, **2008**, 12 (10), 1231-1244.
7. M. P. Stewart, F. Maya, D. V. Kosynkin, S. M. Dirk, J. J. Stapleton, C. L. McGuiness, D. L. Allara, J. M. Tour, *Direct covalent grafting of conjugated molecules onto Si, GaAs, and Pd surfaces from aryidiazonium salts*, ***Journal of the American Chemical Society***, **2004**, 126 (1), 370-378.
8. D. Wang, J. M. Buriak, *Trapping silicon surface-based radicals*, ***Langmuir***, **2006**, 22 (14), 6214-6221.
9. G. Collins, P. Fleming, C. O'Dwyers, M. A. Morris, J. D. Holmes, *Organic Functionalization of Germanium Nanowires using Arenediazonium Salts*, ***Chemistry of Materials***, **2011**, 23, 1883-1891.
10. A. Adenier, E. Cabet-Deliry, A. Chausse, S. Griveau, F. Mercier, J. Pinson, C. Vautrin-Ul, *Grafting of nitrophenyl groups on carbon and metallic surfaces without electrochemical induction*, ***Chemistry of Materials***, **2005**, 17 (3), 491-501.
11. B. L. Hurley, R. L. McCreery, *Covalent bonding of organic molecules to Cu and Al alloy 2024 T3 surfaces via diazonium ion reduction*, ***Journal of the Electrochemical Society***, **2004**, 151 (5), B252-B259.
12. A. M. Mahmoud, A. J. Bergren, R. L. McCreery, *Derivatization of Optically Transparent Materials with Diazonium Reagents for Spectroscopy of Buried Interfaces*, ***Analytical Chemistry***, **2009**, 81 (16), 6972-6980.
13. A. Adenier, N. Barre, E. Cabet-Deliry, A. Chausse, S. Griveau, F. Mercier, J. Pinson, C. Vautrin-Ul, *Study of the spontaneous formation of organic layers on carbon and metal surfaces from diazonium salts*, ***Surface Science***, **2006**, 600 (21), 4801-4812.
14. C. Combellas, M. Delamar, F. Kanoufi, J. Pinson, F. I. Podvorica, *Spontaneous grafting of iron surfaces by reduction of aryldiazonium salts in acidic or neutral aqueous solution. Application to the protection of iron against corrosion*, ***Chemistry of Materials***, **2005**, 17 (15), 3968-3975.
15. C. Combellas, F. Kanoufi, J. Pinson, F. I. Podvorica, *Time-of-flight secondary ion mass spectroscopy characterization of the covalent bonding between a carbon surface and aryl groups*, ***Langmuir***, **2005**, 21 (1), 280-286.
16. Q. M. Pan, M. Wang, W. T. Chen, *Hydrophobization of metal surfaces by covalent grafting of aromatic layer via aryldiazonium chemistry and their application in the fabrication of superhydrophobic surfaces*, ***Chemistry Letters***, **2007**, 36 (11), 1312-1313.
17. J. Lehr, B. E. Williamson, B. S. Flavel, A. J. Downard, *Reaction of Gold Substrates with Diazonium Salts in Acidic Solution at Open-Circuit Potential*, ***Langmuir***, **2009**, 25 (23), 13503-13509.
18. F. I. Podvorica, F. Kanoufi, J. Pinson, C. Cornbellas, *Spontaneous grafting of diazoates on metals*, ***Electrochimica Acta***, **2009**, 54 (8), 2164-2170.
19. M. Toupin, D. Belanger, *Spontaneous functionalization of carbon black by reaction with 4-nitrophenyldiazonium cations*, ***Langmuir***, **2008**, 24 (5), 1910-1917.
20. M. Toupin, D. Belanger, *Thermal stability study of aryl modified carbon black by in situ generated diazonium salt*, ***Journal of Physical Chemistry C***, **2007**, 111 (14), 5394-5401.

21. P. Abiman, G. G. Wildgoose, R. G. Compton, *A mechanistic investigation into the covalent chemical derivatisation of graphite and glassy carbon surfaces using aryldiazonium salts*, ***Journal of Physical Organic Chemistry***, **2008**, 21 (6), 433-439.
22. P. Abiman, G. G. Wildgoose, R. G. Compton, *Investigating the mechanism for the covalent chemical modification of multiwalled carbon nanotubes using aryl diazonium salts*, ***International Journal of Electrochemical Science***, **2008**, 3 (2), 104-117.
23. F. Le Floch, J. P. Simonato, G. Bidan, *Electrochemical signature of the grafting of diazonium salts: A probing parameter for monitoring the electro-addressed functionalization of devices*, ***Electrochimica Acta***, **2009**, 54 (11), 3078-3085.
24. E. Bekyarova, M. E. Itkis, P. Ramesh, C. Berger, M. Sprinkle, W. A. de Heer, R. C. Haddon, *Chemical Modification of Epitaxial Graphene: Spontaneous Grafting of Aryl Groups*, ***Journal of the American Chemical Society***, **2009**, 131 (4), 1336-1337.
25. X. Y. Fan, R. Nouchi, L. C. Yin, K. Tanigaki, *Effects of electron-transfer chemical modification on the electrical characteristics of graphene*, ***Nanotechnology***, **2010**, 21 (47), 475208.
26. D. B. Farmer, R. Golizadeh-Mojarad, V. Perebeinos, Y. M. Lin, G. S. Tulevski, J. C. Tsang, P. Avouris, *Chemical Doping and Electron-Hole Conduction Asymmetry in Graphene Devices*, ***Nano Letters***, **2009**, 9 (1), 388-392.
27. F. M. Koehler, A. Jacobsen, K. Ensslin, C. Stampfer, W. J. Stark, *Selective Chemical Modification of Graphene Surfaces: Distinction Between Single- and Bilayer Graphene*, ***Small***, **2010**, 6 (10), 1125-1130.
28. R. Sharma, J. H. Baik, C. J. Perera, M. S. Strano, *Anomalously Large Reactivity of Single Graphene Layers and Edges toward Electron Transfer Chemistries*, ***Nano Letters***, **2010**, 10 (2), 398-405.
29. Y. Zhu, A. L. Higginbotham, J. M. Tour, *Covalent Functionalization of Surfactant-Wrapped Graphene Nanoribbons*, ***Chemistry of Materials***, **2009**, 21 (21), 5284-5291.
30. A. Sinitskii, A. Dimiev, D. A. Corley, A. A. Fursina, D. V. Kosynkin, J. M. Tour, *Kinetics of Diazonium Functionalization of Chemically Converted Graphene Nanoribbons*, ***ACS Nano***, **2010**, 4 (4), 1949-1954.
31. S. Q. Lud, M. Steenackers, R. Jordan, P. Bruno, D. M. Gruen, P. Feulner, J. A. Garrido, M. Stutzmann, *Chemical grafting of biphenyl self-assembled monolayers on ultrananocrystalline diamond*, ***Journal of the American Chemical Society***, **2006**, 128 (51), 16884-16891.
32. S. Szunerits, R. Boukherroub, *Different strategies for functionalization of diamond surfaces*, ***Journal of Solid State Electrochemistry***, **2008**, 12 (10), 1205-1218.
33. D. E. Jiang, B. G. Sumpter, S. Dai, *How do aryl groups attach to a graphene sheet?*, ***Journal of Physical Chemistry B***, **2006**, 110 (47), 23628-23632.
34. F. G. Brunetti, M. A. Herrero, J. D. Munoz, A. Diaz-Ortiz, J. Alfonsi, M. Meneghetti, M. Prato, E. Vazquez, *Microwave-induced multiple functionalization of carbon nanotubes*, ***Journal of the American Chemical Society***, **2008**, 130 (25), 8094-8100.
35. X. H. Chen, H. F. Wang, W. B. Zhong, T. Feng, X. G. Yang, J. H. Chen, *A scalable route to highly functionalized multi-walled carbon nanotubes on a large scale*, ***Macromolecular Chemistry and Physics***, **2008**, 209 (8), 846-853.
36. M. S. Strano, C. A. Dyke, M. L. Usrey, P. W. Barone, M. J. Allen, H. W. Shan, C. Kittrell, R. H. Hauge, J. M. Tour, R. E. Smalley, *Electronic structure control of single-walled carbon nanotube functionalization*, ***Science***, **2003**, 301 (5639), 1519-1522.
37. C. A. Dyke, M. P. Stewart, F. Maya, J. M. Tour, *Diazonium-based functionalization of carbon nanotubes: XPS and GC-MS analysis and mechanistic implications*, ***Synlett***, **2004**, (1), 155-160.
38. M. L. Usrey, E. S. Lippmann, M. S. Strano, *Evidence for a two-step mechanism in electronically selective single-walled carbon nanotube reactions*, ***Journal of the American Chemical Society***, **2005**, 127 (46), 16129-16135.
39. H. M. Wang, J. S. Xu, *Theoretical evidence for a two-step mechanism in the functionalization single-walled carbon nanotube by aryl diazonium salts: Comparing effect of different substituent group*, ***Chemical Physics Letters***, **2009**, 477 (1-3), 176-178.
40. G. Schmidt, S. Gallon, S. Esnouf, J. P. Bourgoin, P. Chenevier, *Mechanism of the Coupling of Diazonium to Single-Walled Carbon Nanotubes and Its Consequences*, ***Chemistry-A European Journal***, **2009**, 15 (9), 2101-2110.

41. C. Combellas, F. Kanoufi, D. Mazouzi, A. Thiebault, P. Bertrand, N. Medard, *Surface modification of halogenated polymers. 4. Functionalisation of poly(tetrafluoroethylene) surfaces by diazonium salts*, ***Polymer***, **2003**, 44 (1), 19-24.
42. L. Laurentius, S. R. Stoyanov, S. Gusarov, A. Kovalenko, R. B. Du, G. P. Lopinski, M. T. McDermott, *Diazonium-Derived Aryl Films on Gold Nanoparticles: Evidence for a Carbon-Gold Covalent Bond*, ***ACS Nano***, **2011**, 5 (5), 4219-4227.
43. A. T. Masheter, G. G. Wildgoose, A. Crossley, J. H. Jones, R. G. Compton, *A facile method of modifying graphite powder with aminophenyl groups in bulk quantities*, ***Journal of Materials Chemistry***, **2007**, 17 (29), 3008-3014.
44. M. Pandurangappa, T. Ramakrishnappa, *Spectroscopic and thermal characterization of carbon nanotubes functionalized through diazonium salt reduction*, ***Materials Chemistry and Physics***, **2010**, 122 (2-3), 567-573.
45. P. Allongue, M. Delamar, B. Desbat, O. Fagebaume, R. Hitmi, J. Pinson, J. M. Saveant, *Covalent modification of carbon surfaces by aryl radicals generated from the electrochemical reduction of diazonium salts*, ***Journal of the American Chemical Society***, **1997**, 119 (1), 201-207.
46. J. L. Bahr, J. P. Yang, D. V. Kosynkin, M. J. Bronikowski, R. E. Smalley, J. M. Tour, *Functionalization of carbon nanotubes by electrochemical reduction of aryl diazonium salts: A bucky paper electrode*, ***Journal of the American Chemical Society***, **2001**, 123 (27), 6536-6542.
47. C. H. deVilleneuve, J. Pinson, M. C. Bernard, P. Allongue, *Electrochemical formation of close-packed phenyl layers on Si(111)*, ***Journal of Physical Chemistry B***, **1997**, 101 (14), 2415-2420.
48. A. Chausse, M. M. Chehimi, N. Karsi, J. Pinson, F. Podvorica, C. Vautrin-Ul, *The electrochemical reduction of diazonium salts on iron electrodes. The formation of covalently bonded organic layers and their effect on corrosion*, ***Chemistry of Materials***, **2002**, 14 (1), 392-400.
49. A. Laforgue, T. Addou, D. Belanger, *Characterization of the deposition of organic molecules at the surface of gold by the electrochemical reduction of aryldiazonium cations*, ***Langmuir***, **2005**, 21 (15), 6855-6865.
50. M. C. Bernard, A. Chausse, E. Cabet-Deliry, M. M. Chehimi, J. Pinson, F. Podvorica, C. Vautrin-Ul, *Organic layers bonded to industrial, coinage, and noble metals through electrochemical reduction of aryldiazonium salts*, ***Chemistry of Materials***, **2003**, 15 (18), 3450-3462.
51. J. Lyskawa, D. Belanger, *Direct modification of a gold electrode with aminophenyl groups by electrochemical reduction of in situ generated aminophenyl monodiazonium cations*, ***Chemistry of Materials***, **2006**, 18 (20), 4755-4763.
52. M. D'Amours, D. Belanger, *Stability of substituted phenyl groups electrochemically grafted at carbon electrode surface*, ***Journal of Physical Chemistry B***, **2003**, 107 (20), 4811-4817.
53. A. Ghorbal, F. Grisotto, M. Laude, J. Charlier, S. Palacin, *The in situ characterization and structuring of electrografted polyphenylene films on silicon surfaces. An AFM and XPS study*, ***Journal of Colloid and Interface Science***, **2008**, 328 (2), 308-313.
54. D. M. Shewchuk, M. T. McDermott, *Comparison of Diazonium Salt Derived and Thiol Derived Nitrobenzene Layers on Gold*, ***Langmuir***, **2009**, 25 (8), 4556-4563.
55. E. de la Llave, A. Ricci, E. J. Calvo, D. A. Scherlis, *Binding between Carbon and the Au(111) Surface and What Makes It Different from the S-Au(111) Bond*, ***Journal of Physical Chemistry C***, **2008**, 112 (45), 17611-17617.
56. D. E. Jiang, B. G. Sumpter, S. Dai, *Structure and bonding between an aryl group and metal surfaces*, ***Journal of the American Chemical Society***, **2006**, 128 (18), 6030-6031.
57. T. Itoh, R. L. McCreery, *In situ Raman spectroelectrochemistry of electron transfer between glassy carbon and a chemisorbed nitroazobenzene monolayer*, ***Journal of the American Chemical Society***, **2002**, 124 (36), 10894-10902.
58. K. Boukerma, M. M. Chehimi, J. Pinson, C. Blomfield, *X-ray photoelectron spectroscopy evidence for the covalent bond between an iron surface and aryl groups attached by the electrochemical reduction of diazonium salts*, ***Langmuir***, **2003**, 19 (15), 6333-6335.
59. P. Vanysek, CRC Handbook of Chemistry and Physics, *Revision of Tables of Electrochemical Series*, 79th ed.; CRC Press: **1998**; (8-21)-(8-31).
60. L. Tessier, *Greffage de Films Organiques par Polymerisation Radicalaire Electro-amorcée en Milieu Aqueux Dispersé*, Thèse de l'Université Pierre et Marie Curie, Paris, **2009**.

61. R. M. Elofson, F. F. Gadallah, *Substituent Effects in Polarography of Aromatic Diazonium Salts*, ***Journal of Organic Chemistry***, **1969**, 34 (4), 854-857.

62. X. J. Zhang, G. Xue, A. Agarwal, R. Tsu, M. A. Hasan, J. E. Greene, A. Rockett, *Thermal-Desorption of Ultraviolet-Ozone Oxidized Ge(001) for Substrate Cleaning*, ***Journal of Vacuum Science & Technology a-Vacuum Surfaces and Films***, **1993**, 11 (5), 2553-2561.

63. P. Ardalan, Y. Sun, P. Pianetta, C. B. Musgrave, S. F. Bent, *Reaction Mechanism, Bonding, and Thermal Stability of 1-Alkanethiols Self-Assembled on Halogenated Ge Surfaces*, ***Langmuir***, **2010**, 26 (11), 8419-8429.

64. G. Deniau, L. Azoulay, P. Jegou, G. Le Chevallier, S. Palacin, *Carbon-to-metal bonds: Electrochemical reduction of 2-butenenitrile*, ***Surface Science***, **2006**, 600 (3), 675-684.

65. P. Viel, *Etude de la modification d'une surface métallique par greffage et croissance d'un film de polyacrylonitrile électropolymérisé sous polarisation cathodique*, Thèse de l'Université de Paris VI, Paris, **1990**.

66. D. Wang, J. M. Buriak, *Electrochemically driven organic monolayer formation on silicon surfaces using alkylammonium and alkylphosphonium reagents*, ***Surface Science***, **2005**, 590 (2-3), 154-161.

67. P. Bebin, R. E. Prud'homme, *Comparative XPS study of copper, nickel, and aluminum coatings on polymer surfaces*, ***Chemistry of Materials***, **2003**, 15 (4), 965-973.

68. G. Deniau, P. Viel, G. Lecayon, J. Delhalle, *Ups and Xps Study of the Polymer Metal Interface of Poly(2-Methyl-2-Propenenitrile) Electropolymerized on an Oxidized Nickel Surface Cathode*, ***Surface and Interface Analysis***, **1992**, 18 (6), 443-447.

69. G. Socrates, *Infrared Characteristic Group Frequencies*, Wiley Interscience, New York, **1980**.

70. A. Ricci, C. Bonazzola, E. J. Calvo, *An FT-IRRAS study of nitrophenyl mono- and multilayers electro-deposited on gold by reduction of the diazonium salt*, ***Physical Chemistry Chemical Physics***, **2006**, 8 (37), 4297-4299.

71. S. S. C. Yu, E. S. Q. Tan, R. T. Jane, A. J. Downard, *An electrochemical and XPS study of reduction of nitrophenyl films covalently grafted to planar carbon surfaces*, ***Langmuir***, **2007**, 23 (22), 11074-11082.

72. C. M. Elliott, R. W. Murray, *Chemically Modified Carbon Electrodes*, ***Analytical Chemistry***, **1976**, 48 (8), 1247-1254.

73. G. Beamson, D. Briggs, *High Resolutin XPS of Organic Polymers*, John Miley & Sons, **1992**.

74. L. Siller, L. Alves, A. C. Brieva, Y. V. Butenko, M. R. C. Hunt, *Gold Nitride: Preparation and Properties*, ***Topics in Catalysis***, **2009**, 52 (11), 1604-1610.

75. A. Adenier, M. M. Chehimi, I. Gallardo, J. Pinson, N. Vila, *Electrochemical oxidation of aliphatic amines and their attachment to carbon and metal surfaces*, ***Langmuir***, **2004**, 20 (19), 8243-8253.

76. B. Ortiz, C. Saby, G. Y. Champagne, D. Belanger, *Electrochemical modification of a carbon electrode using aromatic diazonium salts. 2. Electrochemistry of 4-nitrophenyl modified glassy carbon electrodes in aqueous media*, ***Journal of Electroanalytical Chemistry***, **1998**, 455 (1-2), 75-81.

77. P. Doppelt, G. Hallais, J. Pinson, F. Podvorica, S. Verneyre, *Surface modification of conducting substrates. Existence of azo bonds in the structure of organic layers obtained from diazonium salts*, ***Chemistry of Materials***, **2007**, 19 (18), 4570-4575.

78. C. Saby, B. Ortiz, G. Y. Champagne, D. Belanger, *Electrochemical modification of glassy carbon electrode using aromatic diazonium salts .1. Blocking effect of 4-nitrophenyl and 4-carboxyphenyl groups*, ***Langmuir***, **1997**, 13 (25), 6805-6813.

79. L. Tessier, G. Deniau, B. Charleux, S. Palacin, *Surface Electroinitiated Emulsion Polymerization (SEEP): A Mechanistic Approach*, ***Chemistry of Materials***, **2009**, 21 (18), 4261-4274.

80. M. Delamar, G. Desarmot, O. Fagebaume, R. Hitmi, J. Pinson, J. M. Saveant, *Modification of carbon fiber surfaces by electrochemical reduction of aryl diazonium salts: Application to carbon epoxy composites*, ***Carbon***, **1997**, 35 (6), 801-807.

81. P. C. Rieke, D. R. Baer, G. E. Fryxell, M. H. Engelhard, M. S. Porter, *Beam Damage of Self-Assembled Monolayers*, ***Journal of Vacuum Science & Technology a-Vacuum Surfaces and Films***, **1993**, 11 (4), 2292-2297.

82. E. Frydman, H. Cohen, R. Maoz, J. Sagiv, *Monolayer damage in XPS measurements as evaluated by independent methods*, ***Langmuir***, **1997**, 13 (19), 5089-5106.

83. W. Eck, V. Stadler, W. Geyer, M. Zharnikov, A. Golzhauser, M. Grunze, *Generation of surface amino groups on aromatic self-assembled monolayers by low energy electron beams - A first step towards chemical lithography*, ***Advanced Materials***, **2000**, 12 (11), 805-808.

84. P. Mendes, M. Belloni, M. Ashworth, C. Hardy, K. Nikitin, D. Fitzmaurice, K. Critchley, S. Evans, J. Preece, *A novel example of X-ray-radiation-induced chemical reduction of an aromatic nitro-group-containing thin film on SiO2 to an aromatic amine film*, ***ChemPhysChem***, **2003**, 4 (8), 884-889.

85. P. Iqbal, K. Critchley, D. Attwood, D. Tunnicliffe, S. D. Evans, J. A. Preece, *Chemical Manipulation by X-rays of Functionalized Thiolate Self-Assembled Monolayers on Au*, ***Langmuir***, **2008**, 24 (24), 13969-13976.

86. S. W. Han, I. Lee, K. Kim, *Patterning of organic monolayers on silver via surface-induced photoreaction*, ***Langmuir***, **2002**, 18 (1), 182-187.

87. P. Viel, X. T. Le, V. Huc, J. Bar, A. Benedetto, A. Le Goff, A. Filoramo, D. Alamarguy, S. Noel, L. Baraton, S. Palacin, *Covalent grafting onto self-adhesive surfaces based on aryldiazonium salt seed layers*, ***Journal of Materials Chemistry***, **2008**, 18 (48), 5913-5920.

88. C. Galli, *Radical Reactions of Arenediazonium Ions - an Easy Entry into the Chemistry of the Aryl Radical*, ***Chemical Reviews***, **1988**, 88 (5), 765-792.

89. F. R. F. Fan, J. P. Yang, L. T. Cai, D. W. Price, S. M. Dirk, D. V. Kosynkin, Y. X. Yao, A. M. Rawlett, J. M. Tour, A. J. Bard, *Charge transport through self-assembled monolayers of compounds of interest in molecular electronics*, ***Journal of the American Chemical Society***, **2002**, 124 (19), 5550-5560.

90. S. Griveau, S. Aroua, D. Bediwy, R. Cornut, C. Lefrou, F. Bedioui, *Spontaneous adsorbed layers of 4-nitrobenzenediazonium salt on gold and glassy carbon: Local characterization by SECM and electron-transfer kinetics evaluation*, ***Journal of Electroanalytical Chemistry***, **2010**, 647 (1), 93-96.

91. U. Costas-Costas, R. Pazo-Llorente, E. Gonzalez-Romero, C. Bravo-Diaz, *Dediazoniations in water: An integrated physical organic chemistry experiment*, ***Journal of Chemical Education***, **2000**, 77 (3), 384-386.

92. R. Pazo-Llorente, C. Bravo-Diaz, E. Gonzalez-Romero, *pH effects on ethanolysis of some arenediazonium ions: Evidence for homolytic dediazoniation proceeding through formation of transient diazo ethers*, ***European Journal of Organic Chemistry***, **2004**, (15), 3221-3226.

93. L. Rodriguez-Pardo, J. Farina, C. Gabrielli, H. Perrot, R. Brendel, *Resolution in quartz crystal oscillator circuits for high sensitivity microbalance sensors in damping media*, ***Sensors and Actuators B-Chemical***, **2004**, 103 (1-2), 318-324.

94. P. S. J. Canning, K. McCrudden, H. Maskill, B. Sexton, *Rates and mechanisms of the thermal solvolytic decomposition of arenediazonium ions*, ***Journal of the Chemical Society-Perkin Transactions 2***, **1999**, (12), 2735-2740.

95. M. L. Crossley, R. H. Kienle, C. H. Benbrook, *Chemical Constitution and Reactivity. I. Phenyldiazonium Chloride and its Mono Substituted Derivatives*, ***Journal of the American Chemical Society***, **1940**, 62, 1400-1404.

96. K. H. Saunders, *The Aromatic Diazo Compounds and their Technical Applications*, Edward Arnold, London, **1949**.

97. S. Milanesi, M. Fagnoni, A. Albini, *Cationic arylation through photo(sensitised) decomposition of diazonium salts. Chemoselectivity of triplet phenyl cations*, ***Chemical Communications***, **2003**, (2), 216-217.

CHAPTER IV

Redox-induced grafting of diazonium salts

As mentioned in II.3.2.2, the reduction of diazonium salts, by a reducing agent in solution, into aryl radicals is a well known reaction[1] and has been used during the last ten years as a way to functionalize the surface of materials[2-5]. This redox-induced grafting of diazonium salts is an anchoring method assumed to be based on an electron transfer reaction. First, with H_3PO_2 as a reducing agent, the common functionalization of carbon materials will be reviewed, the influence of most experimental conditions including reaction time on the grafting of polyphenylene films on gold will be determined and possible grafting mechanisms will be discussed. Then, to understand better this mechanism, another reducing agent, ascorbic acid, will be studied to reduce the diazonium salts. Thanks to a dual surface-solution analysis and a deep investigation of the composition of the reactive solution, a precise mechanism constituting a first step towards the understanding of more complex mechanisms (i.e. in presence of a vinylic monomer cf chapter V) will be proposed. To finish, we will compare the graftings that can be obtained with those two reducing agents as well as iron powder (redox compound at the origin of the Graftfast™ process) and discuss the parameters to consider in order to choose the appropriate reducing agent for a given work.

IV.1 - **Hypophosphorous acid (H_3PO_2)**

H_3PO_2 has been commonly used in the reduction of diazonium salts in solution[6-8] and more recently with a view to functionalize carbon materials. Therefore, after description of previous work on that latter topic, we will investigate the role of hypophosphorous acid and particularly the influence of experimental parameters on the grafting of polyphenylene films on gold substrates.

IV.1.1 - **Grafting with H_3PO_2 in the literature**

Among the techniques of functionalization available[9], the homogeneous reduction of diazonium salts by H_3PO_2 appeared to be an easy route for the derivatisation of a wide range of carbon materials such as carbon powder[10, 11], carbon particles[4], carbon black[5], glassy carbon[12], graphite[12-14] and lately carbon nanotubes[15-18]. Indeed, this procedure allows avoiding electrochemical methods as well as oxidative conditions and offers large possibilities in terms of substituted aryl groups that can be grafted on the carbon surfaces.

On carbon electrodes and CNT, the chemical reduction by H_3PO_2 and grafting of diazonium salts with anthraquinonyl and nitro groups was widely investigated. Indeed, carbon electrodes are inexpensive compared to metallic ones (gold, platinum) and are also relatively inert in most solutions and when functionalized, their properties can be tailored providing distinct advantages for catalysis, analysis and biological applications[13, 19]. For example, the modification of electrode surfaces by quinones enhances the rate of oxygen reduction[16]. Concerning CNT, their

functionalization by organic molecules or functional groups aims at improving the properties of the tubes such as their solubility in particular media or their binding ability to other materials and are contemplated to be used, for instance, in polymeric nanocomposites[20].

IV.1.2 - **Our typical films**

In the same way, we employed H_3PO_2 with a view to graft gold substrates with polyphenylene films and we investigated the composition of the resulting layers, their homogeneity as well as the influence of the main experimental parameters on the film in order to conclude on the H_3PO_2-induced grafting mechanism.

As widely discussed in chapter III, a spontaneous grafting was observed on gold samples by simple immersion in a solution containing the diazonium salt. Therefore, in order to evaluate the influence of H_3PO_2 on the grafting, we will compare this redox-induced grafting with the corresponding spontaneous reaction. Figure 38 shows clearly that the redox-induced grafting technique gives polynitrophenylene films of similar composition than those spontaneously grafted. Indeed, IR spectrum (Figure 38a) indicates the presence of nitro groups (ν^{as}_{NO2} = 1525 cm^{-1} and ν^{s}_{NO2} = 1350 cm^{-1}) as well as aryl groups ($\nu_{C=C}$ = 1600 cm^{-1}). Moreover, XPS spectrum (Figure 38b) confirms the existence of NO_2 in the film but also of amino groups assumed to come from the degradation of the nitro groups under exposure to photoelectron irradiation during the XPS measurements as detailed in III.3.1.2. As in the spontaneously grafted films, azo groups inside the film (N=N bonds) but also at the film-substrate interface (Au-N bonds) were detected in the samples synthesized by redox activation. Another component at 402.1 eV was also observed and attributed, in this situation, to protonated amino groups (NH_3^+) as widely described in the literature[21-23]. Indeed, such groups can be seen when working in an acidic medium which is the case here since the introduction of H_3PO_2 in solution induces a drop in pH from 5.5 (H_2O DI) to 0.55 ($pKa_{H3PO2/H2PO2-} \approx 2$ according to the pH-potential diagram in III.3.2.2). To finish, according to the comparison of the IR intensities of NO_2 groups as well as the XPS areas of NO_2 and related groups (NH_2 and NH_3^+), the amount of grafted nitrophenyl molecules is three to four times higher in the case of the H_3PO_2-induced grafted films than spontaneous-ones for the same starting concentration.

In addition, contact angle measurements (Figure 39) confirmed that more nitrophenyl groups were grafted on the surface by the redox-induced process since a classical value[22, 23] (for a PNP layer) of 59 ± 4° was measured, which is very different from the unusual value of 72 ± 3° found after the spontaneous grafting. Nevertheless, we cannot precise whether the H_3PO_2-induced process gives denser or thicker films since a relevant measurement of the thickness of the films is still complicated for the reasons mentioned in III.3.1. The change in the color of the solution with reaction time (starting from a pale yellow and reaching a dark brown) going with

precipitation of some compounds also indicates a reaction process different from the spontaneous grafting and will be discussed in IV.2.2.

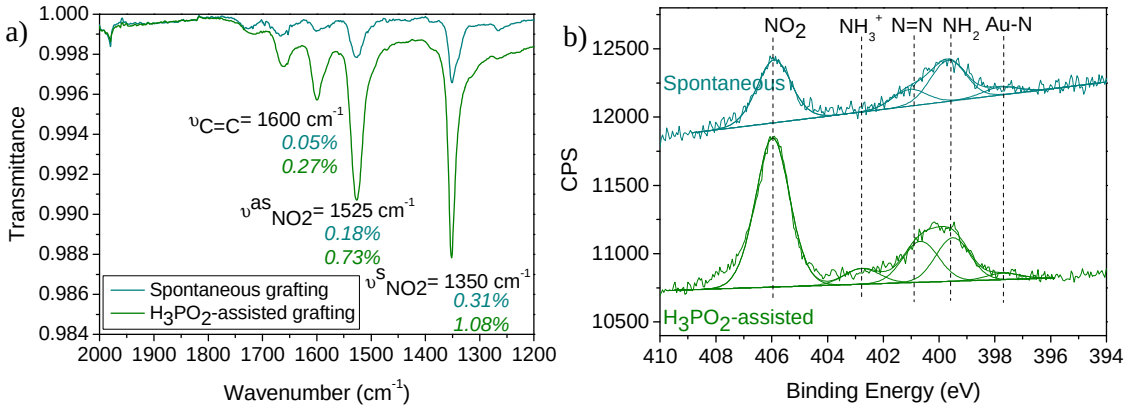

Figure 38 – Typical a) IR-ATR and b) XPS N 1s core level spectra of a PNP layer grafted by redox activation (H_2O DI, NBDT 0.046 M, H_3PO_2, 60 min) compared to the corresponding spontaneously grafted film.

Figure 39 – Static water contact angle of a) pristine, b) spontaneously grafted and c) H_3PO_2-induced grafted with NBDT gold substrates.

IV.1.2.1 - Homogeneity of the films

The influence of experimental parameters on the grafting was mainly studied by comparing IR intensities of the symmetric stretching of NO_2 groups on twelve different locations along the same substrate, as represented on Figure 40. We voluntarily disregarded the two values measured at the very top of the gold plates. Indeed, since the substrate was not fully immersed in the solution, it is not surprising that these values do not fit at all with the other values. Therefore, an average intensity value (ν^{S}_{NO2}) of 0.84 ± 0.08 % was calculated. This variation is certainly partially due to the variability of the ATR measurements (cf III.3.1) but mainly to the homogeneity of the grafting which could be linked, for instance, to the stirring of the solution, to variations in the surface reactivity, to the position of the sample in the beaker, etc. However, it is interesting to notice that if we consider measurements performed at the same height on the substrate the variation is smaller (0.01 % at the maximum). Consequently, with a view to minimize as much as possible the influence of the homogeneity in comparative studies, we arbitrarily chose to carry out all the IR-ATR measurements on the middle of all our samples.

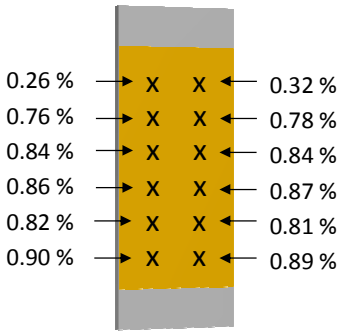

Figure 40 – Intensity of the ν^{s}_{NO2} absorption band from the IR-ATR analysis of the PNP films obtained by the reduction, in water, of NBDT (0.046 M) with H_3PO_2 along the gold substrate.

To go into further details, the homogeneity of the film was evaluated at a smaller scale by using IRRAS (infrared reflection absorption spectroscopy, see appendix 1) mapping focused on the more intense band of NO_2 groups at 1350 cm^{-1} (Figure 41). This particular technique should naturally give intensity values different from IR-ATR and also suppress the uncertainty in measurement due to the contact of the sample with the ATR crystal. As shown in Figure 41 (mapping on 6 mm^2), the average ν^{s}_{NO2} absorption intensity value is 0.16 ± 0.02 %, which indicates a 10 % systematic variation in the signal.

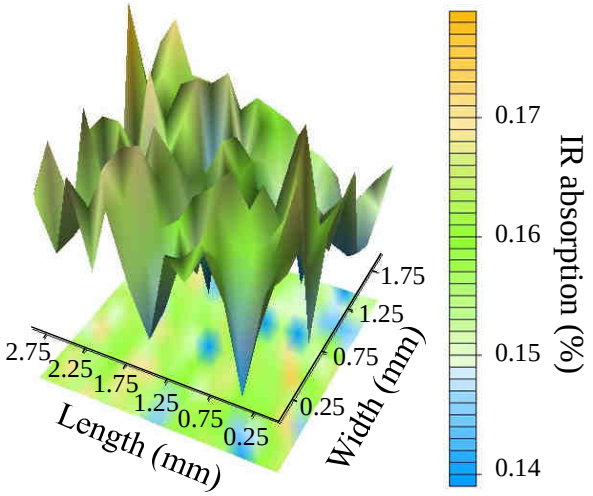

Figure 41 – IRRAS mapping (6 mm^2) of the ν^{s}_{NO2} band (1350 cm^{-1}) from a typical PNP layer grafted by redox activation in H_2O DI.

To sum up, in order to avoid variations due to the homogeneity of the grafting, the IR-ATR measurements were always performed in the middle of the substrate. Moreover, since in the case of the redox-induced grafting of diazonium salts a 10 % variation of the IR average value were monitored on the same sample, only a higher difference is considered relevant to evaluate the influence of an experimental parameter on the grafting.

IV.1.2.2 - Rinsing procedure

To finish on the study of typical films grafted by the H_3PO_2 redox-induced process, the efficiency of the rinsing procedure was evaluated. Indeed, it is important to ensure the removal of all physisorbed matter to check the chemisorption process. The rinsing procedure used in this

work (described in II.3.5) is composed of three main steps: a first wash in deionized water, a second which alternates ethanol and acetone washes and a last one consisting in a 5 min ultrasonic treatment in DMF. The IR-ATR spectrum of a PNP layer synthesized in water by the H_3PO_2 redox activation of NBDT was recorded after each rinsing step (Figure 42). 93 % of the pristine deposited matter was removed after the three rinsing steps, with 90 % of the drop in the ν^{s}_{NO2} intensity observed after the water rinsing. This large decrease upon a mild rinsing treatment is attributed without any doubt to the removal of physisorbed or unreacted nitro compounds on the surface on the sample. Therefore, the remaining molecules on the surface after the full rinsing process can be considered as chemically grafted since they resist to ultrasonication treatment. Moreover, these results prove the importance of performing this rinsing procedure on all the samples in order to be able to compare them.

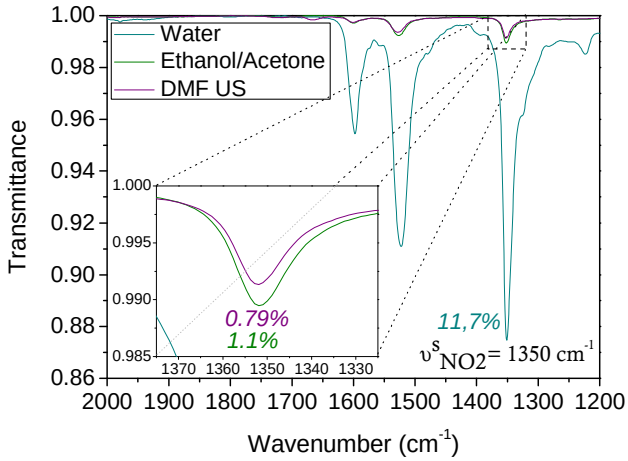

Figure 42 – IR-ATR spectra of a PNP layer grafted by redox activation (60 min, H_2O DI, NBDT 0.046 M, H_3PO_2) after rinsing with water, ethanol/acetone and DMF US.

IV.1.3 - **Variation of experimental parameters**

The redox-induced process using H_3PO_2 as reducing agent is clearly more efficient than the spontaneous one for grafting nitrophenyl groups on the substrate; we will now investigate the influence of experimental conditions on that grafting.

IV.1.3.1 - Substrates

First of all, we focused on the redox-induced grafting on various substrates from metallic (Au, Pt, Ni) to polymeric ones (polyethylene PE) in comparison with the corresponding spontaneous grafting. The results summarized in Table 11 show that the H_3PO_2-induced grafting of diazonium salts is definitely influenced by the nature of the substrate. Indeed,

(1) no spontaneous grafting was observed on polymeric substrates;

(2) whatever the substrate, more nitrophenyl groups were detected for redox-induced grafting than for the spontaneous one. The redox/spontaneous ratio was around 3 for gold and platinum substrates and close to 6 for nickel. In the latter case, the IR intensity of the

spontaneous grafting is higher than for the other metals; certainly due to the redox properties of nickel which is able to reduce the diazonium salt itself.

(3) the grafting on polyethylene disks with a PNP film was successfully achieved which opens a route towards the functionalization of insulators.

To conclude on this study, we have proved that H_3PO_2 has a real influence on the grafting and particularly regarding polymeric samples since without reducing agent no grafting at all can be achieved in this kind of substrate.

Table 11 – Intensity of the ν^s_{NO2} absorption band from the IR-ATR analysis of the PNP films obtained spontaneously or by the reduction, in water, of NBDT (0.046 M) with H_3PO_2 on gold, platinum, nickel and polyethylene substrates.

	I ν^s_{NO2} (%)	
	Spontaneous	***H_3PO_2-induced***
Au	0.25	0.86
Pt	0.32	0.87
Ni	0.4	2.31
PE	-	1.31

IV.1.3.2 - Solvent

Since the solvent was shown to have an influence on the spontaneous grafting on gold, we studied the influence of the acidity of the reactive solution as well as the nature of the acid on the redox-induced grafting in comparison to the spontaneous process. The results summarized in Table 12 are average values of the ν^s_{NO2} absorption band intensity between samples performed at various times in this work (over a year). Once again, these values indicate that the introduction of H_3PO_2 in the solution has a significant influence on the grafting since more nitrophenyl moieties are detected in H_3PO_2-induced processes than in spontaneously grafted layers whatever the pH conditions. Table 12 shows that the H_3PO_2-induced process in H_2O DI or H_2SO_4 give similar results, while less nitrophenyl groups are detected in the presence of HCl; this could be explained by the existence of the interfering reaction of the chloro ions with the diazonium salt (see II.3.1.3). However, in this latter case, the amount of such groups is still seven times higher than in the corresponding spontaneous grafting. Therefore, it seems that the redox grafting of diazonium salts induced by H_3PO_2 gives more nitrophenyl groups grafted than the spontaneous process and can be indifferently carried out in pure water or acidic solutions.

Table 12 – Intensity of the ν^s_{NO2} absorption band from the IR-ATR analysis of the PNP films obtained spontaneously or by the reduction with H_3PO_2, in HCl 0.5 M, in H_2SO_4 0.25 M or in water, of NBDT (0.046 M) on gold plates.

		HCl (0.5 M)	**H_2SO_4 (0.25 M)**	**H_2O DI**
I ν^s_{NO2} (%)	Spontaneous	0.07 ± 0.03	0.12 ± 0.03	0.23 ± 0.03
	H_3PO_2-induced	0.49 ± 0.06	0.83 ± 0.07	0.86 ± 0.08

IV.1.3.3 - [Red]/[NBDT] ratio

According to experimental conditions used to graft carbon materials by a H_3PO_2-induced process (cf IV.1.1), the relative amounts of the main reactants (NBDT and H_3PO_2) were reported to range from stoichiometric[5] ratio to extremely large excess of the reducing agent (up to 9200 equivalents of H_3PO_2 against NBDT[13, 14, 18]). Therefore, it is likely that the $[H_3PO_2]$/[NBDT] ratio is a parameter to adjust in each particular case. We thoroughly studied this parameter and found an 'ideal' ratio giving an optimum grafting, which will be kept for the rest of that work[a].

The redox-induced process is, *a priori*, based on the reduction of a diazonium salt by a reducing agent in solution forming aryl radicals able to graft on the surface of the substrate. However, the grafting mechanism is still unclear. For instance, is the actual reductive compound H_3PO_2 or its first base $H_2PO_2^-$? According to a few teams[6-8, 24], the hypophosphite ion $H_2PO_2^-$ is considered to be able to reduce diazonium salts *via* a possible mechanism represented in Scheme 51.

Initiation step: $ArN_2^+ + H_2PO_2^- \rightarrow Ar^\bullet + N_2 + H_2PO_2^\bullet$

Chain propagation: $Ar^\bullet + H_3PO_2 \rightarrow ArH + H_2PO_2^\bullet$

$H_2PO_2^\bullet + ArN_2^+ \rightarrow Ar^\bullet + N_2 + H_2PO_2^+$

$H_2PO_2^+ \xrightarrow{H_2O} H_3PO_3 + H^+$

Scheme 51 – Proposed mechanism for the reduction of aryldiazonium salt by hypophosphorous acid extracted from the review of Galli[6].

IV.1.3.4 - Reaction time

Finally, the influence of the reaction time on the H_3PO_2-induced grafting was investigated by a solution analysis and surface measurements. In most of the works on the grafting of carbon materials with this process (cf IV.1.1), a typical reaction time of 30 min was used (except when stoichiometric amounts of the reactants were employed for which an overnight reaction was performed[5]). However, that average reaction time was not optimized in our conditions. Indeed, according to Table 13, the maximum amount of grafted matter is reached after 15 min. Therefore, we tried to understand why the grafting of PNP films seems somewhat "self-limited".

Table 13 – Intensity of the ν^s_{NO2} absorption band from the IR-ATR analysis of the PNP films obtained by the reduction, in HCl 0.5 M, of NBDT (0.046 M) with H_3PO_2 on gold versus reaction time.

Reaction Time (min)	**5**	**10**	**15**	**20**	**25**	**30**	**45**	**60**
I ν^s_{NO2} (%)	0.15	0.37	0.52	0.56	0.55	0.57	0.55	0.54

[a] The details of this study as well as the value of the 'ideal' ratio cannot be given here for industrial property reasons.

First, this phenomenon could be explained by a complete consumption of the diazonium salt after 15 min by its reduction or in interfering reactions. In order to use non-diluted reactive solutions, its concentration was not evaluated directly by following the decrease in absorbance of the UV absorption peak of the diazonium salt at 260 nm but by an indirect method consisting in following the absorbance of the colored product formed from the specific diazo coupling reaction of NBDT with NEDA (appendix 4). Figure 43 shows that the NBDT concentration decreases similarly during the redox-induced process in H_2O DI or HCl solution. However, respectively 28 % and 40 % of the initial NBDT concentration obviously remains in H_2O DI and HCl solutions after 15 min of reaction thus discarding the complete consumption of diazonium salts as a reason for the observed limited grafting. Moreover, these values indicate that the decrease in diazonium salt is faster in the redox-induced reaction than its spontaneous degradation in water or HCl medium (see II.3.1.3). Therefore, it is likely that the reduction of the diazonium salt still occurs 15 min after the initiation of the reaction.

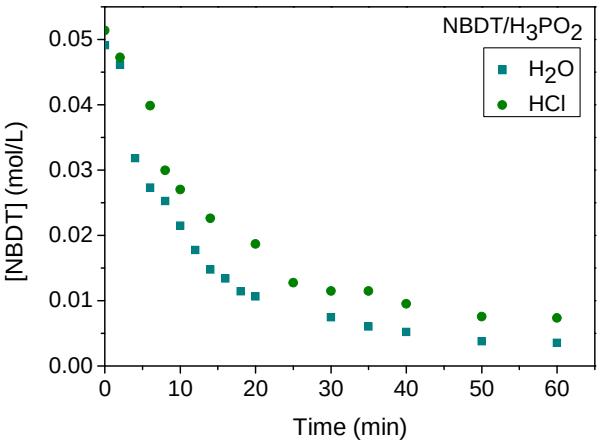

Figure 43 – Evolution of the NBDT concentration in solution during its reduction by H_3PO_2 in H_2O DI or HCl 0.5 M. The concentrations were determined from UV study of the diazo coupling reaction between NBDT and NEDA (appendix 4).

In order to estimate the "activity" of the solution during the whole reaction time, gold plates were introduced at different time of the reaction but only for five minutes. The results of the IR measurements performed on the so-formed films are presented in Figure 44. In both cases, H_2O DI or HCl solution, the maximum of nitrophenyl groups grafted is obtained for samples introduced in the solution 10 min after the beginning of the reaction. After that threshold time, the grafting slightly decreases with the time of introducing the sample in the reacting bath. This also shows that, even after a reaction time of 60 min, the reduction of the diazonium salt by the reducing agent still occurs and produces radical species able to initiate the grafting. To conclude, the limitation of the grafting observed when increasing steadily the reaction time cannot be explained by the lack of "activity" of the solution after 15 min since the solution can be used to graft the substrates for at least 60 min.

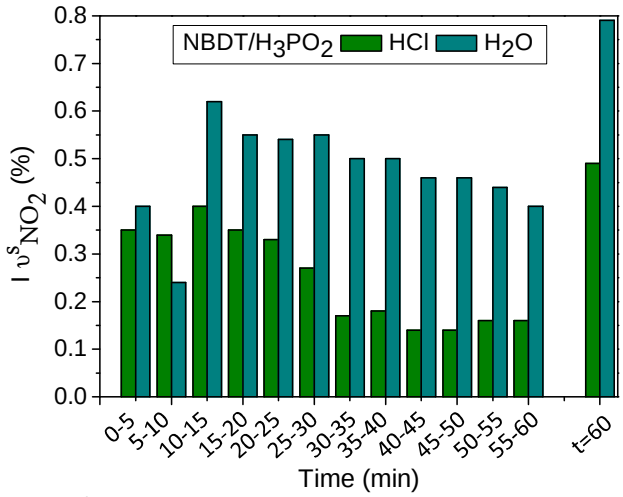

Figure 44 – Intensity of the ν^{s}_{NO2} absorption band from the IR-ATR analysis of the PNP films obtained by the reduction, in HCl 0.5 M as well as in water, of NBDT (0.046 M) with H_3PO_2 on gold substrate as a function of the 5 min chosen to graft the sample over the 60 min reaction. The last value on the right of the graph indicates the intensity obtained in the case of a substrate immersed in the same solution for the whole 60 min.

A first part of explanation of that "self-limitation" in the grafting was found by looking at changes occurring in the reactive solution. Indeed, we noticed that after ca. 30 min of reaction, the samples were slightly covered with brown compounds before rinsing, probably arising from non-soluble products formed during the reaction, which precipitated on the surface. Such precipitation on the substrate is likely to block its access for reactive species thus limiting the grafting. However, the threshold times do not match, since Table 13 gives 15 min as critical reaction time for the self-limited grafting. Therefore, the precipitation spotted on the surface cannot be the only reason for the limitation of the PNP films. Moreover, such result would mean that if the substrate was free of precipitated matter, the film could linearly grow with reaction time.

To test this hypothesis, an experiment consisting in immersing the substrates in a freshly initiated redox-induced reaction for 15 min and this, four times in a row (in order to reach a total reaction time of 60 min), with water, ethanol and acetone rinsings in between each reaction, was performed. After the four successive reactions, the intensity of the ν^{s}_{NO2} absorption band is very similar (0.43 ± 0.04 %) to the average value of 0.49 ± 0.06 % measured for films grafted in HCl solution for 60 min (Table 12). Therefore, the limitation on the grafting of nitrophenyl groups cannot really be explained, in this case, by the precipitation of non-soluble compounds on the surface. It is likely that this behaviour can be explained by the properties of the film itself. Indeed, the wettability of the layer influencing the penetration of the solvent in the film is a key parameter in film growth. As previously determined, a maximum polynitrophenylene film is formed after around a 15 min. However, no adequate rinsing solvent of this film is known and the wettability of this layer by water is certainly quite low. Thus this might prevent most of the reactive species to attach on it during the rest of the reaction and hence limits the grafting.

IV.1.3.5 - Conclusion on the experimental conditions

To sum up, after an indispensable rinsing of the substrates, the H_3PO_2-induced graftings were similar in terms of chemical composition to those obtained with the spontaneous method but they were clearly more abundant. In order to obtain as much nitrophenyl groups grafted on gold substrates as possible, it seems that:

- the reaction can be indifferently performed in H_2O DI or in H_2SO_4,
- An 'ideal' ratio of $[H_3PO_2]$/[NBDT] exists,
- a reaction time of 15 min is enough.

Depending on the applications, various other conditions such as, for instance, working in HCl solutions or with reaction times of a few minutes (any time during at least the first 60 min after the initiation of the reaction) can still remain efficient enough to obtain a grafted PNP layer.

IV.1.4 - **Mechanistic view**

Even if adequate experimental grafting conditions can be found, the mechanism involved in this grafting process is still unclear but is assumed to involve an electron transfer from the reducing agent to the diazonium salt[14, 17]. According to the discussion in IV.1.3.3, it has been suggested that $H_2PO_2^-$ is responsible for this redox reaction leading to the formation of aryl radicals. As a parallel with the electrochemical reduction of diazonium salts, aryl radicals are potentially able to graft on substrates but also on already grafted aromatic rings to form a polyphenylene film. Nevertheless, no real evidence of such a radical mechanism has ever been produced. EPR is the best characterization tool to get a confirmation of the presence of radicals in solution particularly using the spin-trapping technique, well adapted method in the case of short lifetime radicals. The spin-trapping investigation of free aryl radicals from aryldiazonium salts has already been carried out using nitroso compounds[25]. However, this particular spin-trap is only stable in non-acidic media. Therefore, in order to prove the involvement of aryl radicals and so to understand the mechanism of the redox-induced grafting process, another reducing agent (ascorbic acid) was chosen, allowing the reaction to be performed at a pH suitable for the spin-trapping agent.

IV.2 - **Ascorbic acid (VC)**

Already employed for its redox properties in Sandmeyer reaction[26], ascorbic acid allowed us to explore broader experimental conditions than hyphosphorous acid as its pH-range of use is larger. Consequently, it is suitable for EPR measurements with our chosen spin-trap. Prior to investigate the composition of the reactive solutions which will lead to a better understanding of the grafting mechanism, the VC-induced grafting of polyphenylene films will be characterized thanks to surface analyses and the influence of experimental parameters on the grafting will be studied.

IV.2.1 - **Variation of experimental parameters followed by surface analyses**

Since in the case of the H_3PO_2-induced reaction it was established that the value of the $[H_3PO_2]$/[NBDT] ratio has a substantial effect on the grafting, variations of the [VC]/[NBDT] ratio will be operated. Then, the influence of two main diazonium salts and then of various metallic substrates on the synthesis will be investigated.

IV.2.1.1 - [VC]/[NBDT] ratio

As for H_3PO_2-induced grafting, the [VC]/[NBDT] ratio was varied while keeping [NBDT] constant. First, regarding the pH, whatever the ratio, the addition of VC induces a drop of the pH down to 4.1. This value corresponds to the pKa of the first acid-base couple of VC (H_2A/HA^-). Therefore, there is an equilibrium between those two species in solution. Second, for all the ratios tested, the pale yellow solution of NBDT diazonium salt turned instantaneously into a lemon yellow mixture when VC was added. The higher [VC], the more intense the yellow color of the solution. In the same time, less bubbles (which arise from dinitrogen evolution from the reduction of the diazonium salt by the reducing agent) were observed when increasing [VC]. Therefore, it is likely that, for some ratios, VC reacts in a non-redox way. This observation is important and will orientate our further analysis of the grafting mechanism. By varying the [VC]/[NBDT] ratio, a tendency seems to come out of the IR-ATR spectra (Figure 45). Indeed, it appears that a slightly higher absorbance value is observed at 1525 and 1350 cm^{-1} for the 1/10 ratio (i.e. ten times less ascorbic acid than NBDT). Nevertheless, it is difficult to conclude on any “best” PNP grafting conditions from those experiments, for two main reasons. First, the observed differences in IR absorption intensity are similar to the sensitivity threshold of the IR-ATR equipment and to the variability of the measurements (cf III.3.1). Second, those absorption values are also close to those observed for a spontaneous grafting of NBDT (0.23 ± 0.08 % as previously described in III.3.3.1). This is confirmed by Figure 46 showing comparable grafting of nitrophenyl (NO_2 + NH_2) groups in the case of the spontaneous and induced process using a ratio 1/10. However, it is possible that, using other experimental conditions i.e. by changing the substrate or the diazonium salt, we will attest a real influence of ascorbic acid on the grafting.

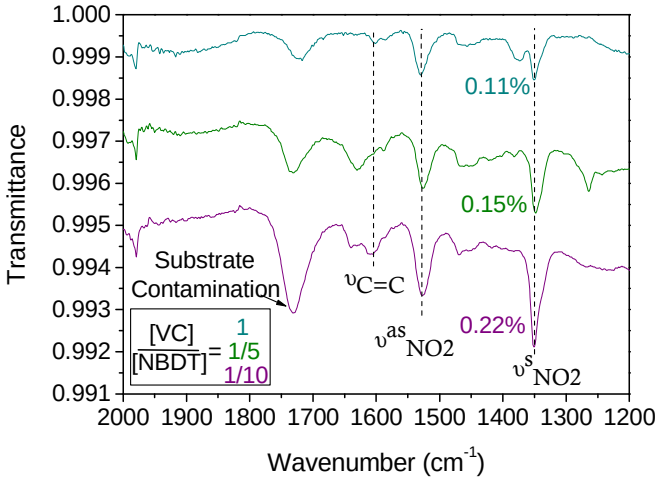

Figure 45 – IR-ATR spectra of PNP layers grafted on gold plates by VC-induced process (H_2O DI, NBDT 0.046 M and different ratio [VC]/ [NBDT] = 1, 1/5, 1/10).

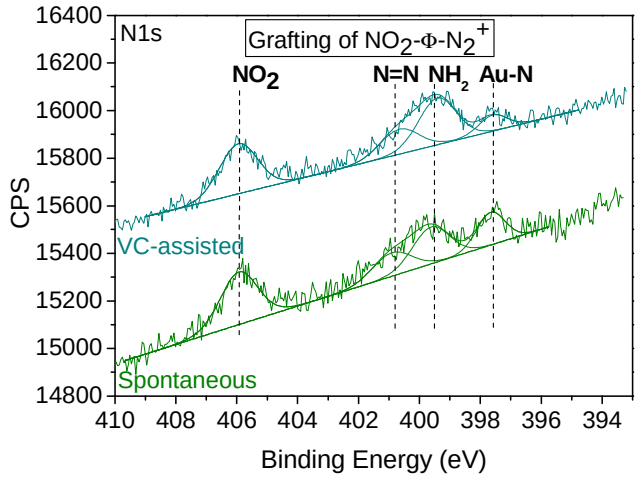

Figure 46 – N 1s core level spectra of layers grafted by VC redox activation of NBDT (H_2O DI, NBDT 0.046 M, VC 0.1 eq, 60 min) compared to the corresponding spontaneously grafted films.

IV.2.1.2 - Modifications according to the substrate or the diazonium salt

To carry on with the study of the effect of the diazonium salts reduction by ascorbic acid on the grafting, the reaction was performed on platinum and nickel plates. A slightly higher intensity of the main IR characteristic absorption band of nitro groups was measured in the case of the redox-induced grafting than for the spontaneous reaction on platinum (Table 14). However, surprisingly, the same comparison on nickel shows less nitrophenyl groups in the films synthesized in presence of VC than without. It is likely that reactions interfered strongly in this case preventing any type of grafting of the nickel surface. Therefore, it is obvious that the VC-induced grafting is widely dependent of the substrate. Is it also influenced by the nature of the diazonium salt?

Table 14 – Intensity of the ν^{s}_{NO2} absorption band from the IR-ATR analysis of the PNP films obtained by the reduction, in H_2O DI, of NBDT (0.046 M) with VC (0.1 eq) on platinum and nickel in comparison with the corresponding spontaneous grafting.

	I ν^{s}_{NO2} (%)	
	Spontaneous	***VC-induced***
Pt	0.32	0.39
Ni	0.40	0.05

To answer this question, we tested the behaviour of carboxybenzene diazonium salts and compared it with the corresponding spontaneous grafting. As illustrated by Figure 47, it is evident that a grafting of polyphenylene films was achieved with both processes. However, we observed more carboxyl (COO) groups grafted on the gold substrate when the reaction is induced with VC. Therefore, in this case, there is no doubt of an actual benefit of the introduction of VC in the reaction.

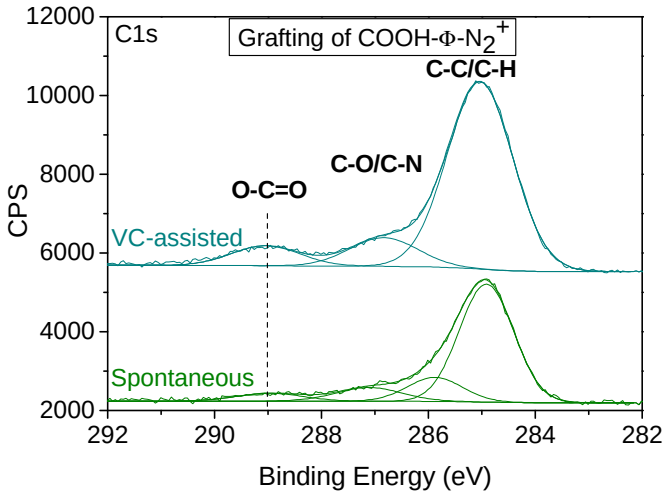

Figure 47 – Typical a) C 1s and b) N 1s core level spectra of layers grafted by VC redox activation of respectively carboxybenzene and nitrobenzene diazonium salts (H_2O DI, diazonium salt 0.046 M, VC 0.1 eq, 60 min) compared to the corresponding spontaneously grafted films.

To conclude on this study, it seems that in particular conditions (with COOH-Φ-N_2^+), ascorbic acid has a real influence on the grafting whereas with other parameters, results are not so clear (NBDT on gold and platinum) or even very unexpected (NBDT on nickel). If in the first case, it is likely that the grafting of polyphenylene-like layers in presence of VC is actually due to a combination of the spontaneous and the redox-activated process, in the others, it is possible that the redox reaction interferes somehow with the spontaneous process which inhibits the grafting. Consequently, in terms of grafting on the surface, ascorbic acid might not be the best reducing agent to use upon these non-optimized experimental conditions. However, considering the results obtained in presence of vinylic monomer (detailed in the next chapter) and the fact that it is a perfectly suitable compound for a solution study, particularly by EPR, we will still work in the rest of this chapter with ascorbic acid as a reducing agent.

IV.2.2 - **Study of the reaction by solution analyses**

With a view to get key information for the understanding of the redox-induced grafting mechanism, it is likely that the study of the reactive solution will be helpful. Since, according to the surface analysis of the grafting, the [VC]/[NBDT] ([NBDT] constant) value plays an important role in the grafting, most of the analyses will be performed by varying this ratio. First, in order to determine the compounds formed in solution, a gas chromatography - mass spectroscopy (GC-MS) study of the reactive solution with time was undertaken. Then, we focused on the demonstration of the presence of aryl radicals in solution using EPR. To finish, as results suggest the formation of an intermediate compound coming from the direct reaction of ascorbic acid with the diazonium salt, we characterized it and showed to what extent its presence fits our observations.

IV.2.2.1 - GC-MS

By studying the reactive solution with a technique combining the features of gas-liquid chromatography and mass spectrometry (appendix 1), we are able to detect some of the products present in solution and follow their evolution as a function of the reaction time. A typical GC-MS spectrum of a NBDT solution activated by VC is given in Figure 48. We can clearly identify the main products of decomposition of the diazonium salt in solution i.e. 4-fluoro,2-nitrobenzene, 4-nitrobenzene and 4-nitrophenol (cf II.3.1.3).

The three compounds with the longest retention times, i.e., in decreasing order of retention time, 4,4’-dinitroazobenzene, 4,4’-dinitrobiphenyl and one of its structural isomer, are also definitely coming from reactions involving NBDT. However, if there is no doubt concerning the assignment of the 4,4’-dinitroazobenzene, it is difficult to determine which structural isomer is in solution. Indeed, in order to assign compounds to mass spectra, a data base was used. It shows the more likely products susceptible to give the obtained mass spectrum. Nevertheless, in this case, only the isomer represented on Figure 48 is known from the data base and its corresponding probability of fitting is only of 45 %. The mass peaks observed do indicate that a structural isomer of the 4,4’-dinitrobiphenyl is present but we did not manage to determine precisely which one. Whatever the actual attribution of that derivative, both products clearly result from the dimerization of aryl radicals, which gives a first proof of a potential reduction of the diazonium salt into radicals. In the case of the formation of the azo compound, a diazo coupling reaction between nitrobenzene and the diazonium salt is probable. More surprisingly, according to the mass analysis, it is likely that the two non-attributed peaks correspond to benzoic acid and nitroaniline. It is assumed that benzoic acid is formed in the column by quenching of nitrobenzene with CO_2. As for nitroaniline, it could either be due to remaining traces from the synthesis of the diazonium salt or the degradation of azobenzene. The latter

explanation is certainly more probable since important variations in the intensity of the nitroaniline peak were observed according to experimental conditions.

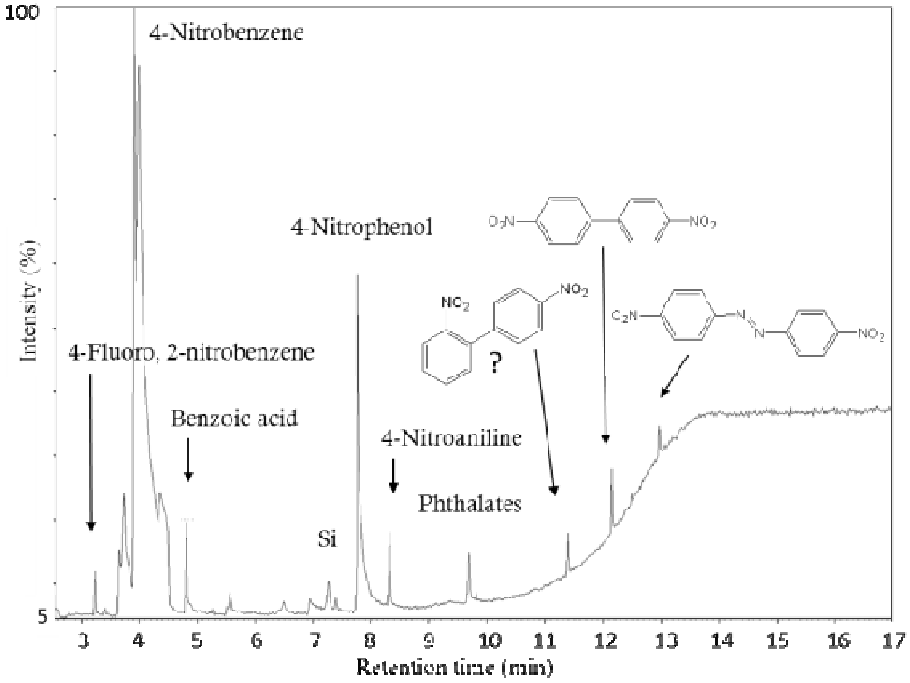

Figure 48 – Typical GC-MS spectrum obtained from a H_2O DI solution of NBDT (0.046 M) and VC (0.1 eq).

To go further, the reaction of NBDT in presence of ascorbic acid was followed by GC-MS with time and for three different [VC]/[NBDT] ratios. In order to compare the results, we normalized the intensity values according to all the identified compounds mentioned above containing nitrobenzene moieties (Figure 49). First of all, no nitrobenzene dimer was detected when a stoichiometric ratio was used meaning that, in these conditions, the presence of aryl radicals is very unlikely. This is in good agreement with the IR results showing, for stoichiometric amounts of reactants, a very weak signal characteristic of a polynitrophenylene layer which may therefore only be attributed to the spontaneous grafting of diazonium salts on gold. In view of the two other cases, it seems that the more ascorbic acid is added, the more dimers are formed. However, this behaviour remains to be explained since these results do not fit with the surface analyses showing that more nitrophenyl groups are grafted with the lower ratios.

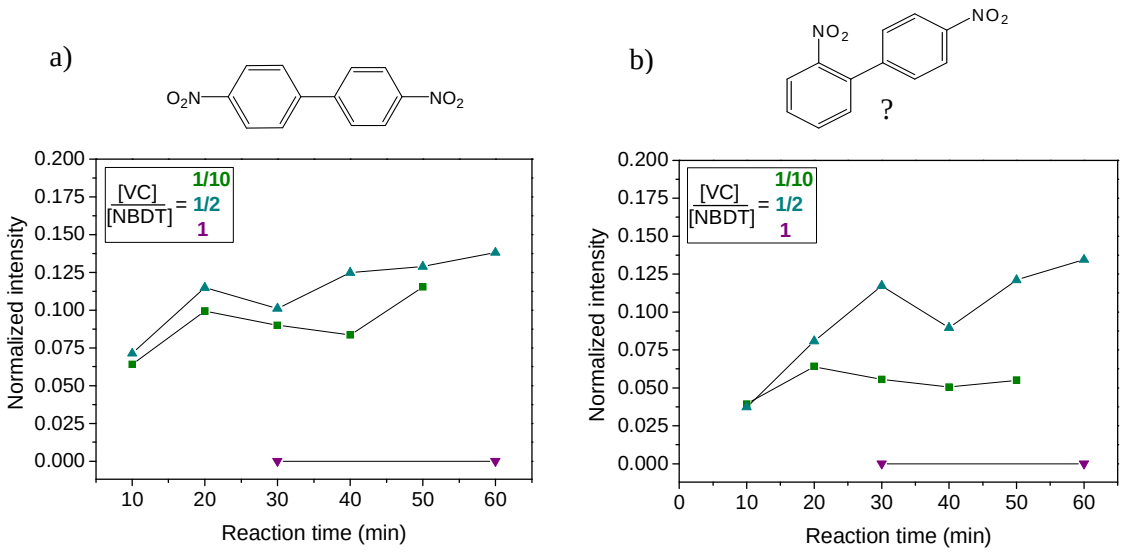

Figure 49 – Evolution with time of the GC-MS intensity (normalized according to all the identified compounds containing nitrobenzene moieties) of the main two molecules of interest a) 4,4'-dinitrobiphenyl and b) one of its structural isomer.

To conclude, from the nature of the compounds detected, we have demonstrated the very likely involvement of aryl radicals in the grafting for some experimental conditions as well as an obvious dependence of the reaction on the [VC]/[NBDT] ratio. In order to confirm these results, EPR using a spin-trap was performed.

IV.2.2.2 - Electron paramagnetic resonance (EPR)

The spin-trapping technique, widely applied in photochemistry[27, 28], polymer chemistry[29], biology and medicine[30, 31], is used for the detection and identification of short-lived free radicals. It is based on the addition of, commonly, nitroso or nitrone compounds, which gives rise to stable nitroxide radicals as a result of spin-trapping. This technique can also be applied in polymer research to study living anionic polymerization, alternating copolymerization or radical polymerization (herein ref[32]). Kunitake *et al.*[33] examined the radical polymerization of several monomers including methyl methacrylate initiated by the thermal decomposition of, in particular, azobis-isobutyronitrile (AIBN) with 2-methyl-2-nitrosopropane (MNP) as spin-trap. Moreover, a few teams investigated the spin-trapping of hydroxyl radicals[34] or aryl radicals[35, 36] aiming at defining the role of such species in genetic damaging such as in DNA, ribonucleic acid (RNA) and their components.

2-methyl-2-nitrosopropane (MNP) is a spin-trap of interest in this study because, as other nitroso traps, the EPR spectrum hyperfine splitting of the formed spin-adducts allows to determine unambiguously the structure of the trapped radical[25, 32, 36]. As many nitroso compounds, MNP is a dimer in the solid state. In order to act as spin-trap, its dissociation into monomer is required. That step may lead to some experimental difficulties detailed in appendix 3[37].

EPR spectra of solutions of NBDT, ascorbic acid and MNP as spin-trap (cf III.3.4.3) with various [VC]/[NBDT] ratios were recorded every 10 min for 60 min. A typical EPR spectrum of the MNP adduct (formed by the reaction of the spin-trap with a radical in solution) is shown in Figure 50. The simulation reveals that the spin-adduct is coupled to a nitrogen atom and two pairs of equivalent hydrogen atoms (identified as the ortho- and meta-protons in the aromatic ring). It is also possible to resolve an additional splitting due to paramagnetic nuclei in the para-position in the aromatic ring. Nitrogen and proton hyperfine splittings of the spin adducts are diagnostic parameters for the identification of the trapped-radicals. The hyperfine splitting constants (HFSCs) of these spin-adducts are given in Table 15. They are in accordance with MNP adducts of nitrophenyl radicals reported in the literature[36]. Thus, for the first time, the presence of aryl radicals in the redox-induced process is demonstrated. Moreover, those results also confirm that the oxidation of VC does not lead to the formation of $HA^{\bullet}$ (no corresponding spin-adduct detected) which excludes a diazonium salt reduction by a single electron pathway. Therefore, at this stage, it seems that the only possible reactions are the reduction of diazonium salts by ascorbic acid and/or ascorbate ion (first base) which in both cases involves a two-electron pathway (see II.3.2.2).

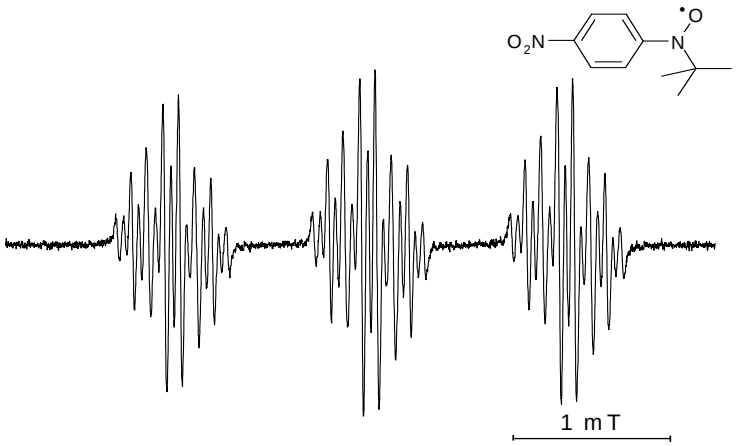

Figure 50 – Typical EPR spectrum of MNP adducts of nitro aryl radicals obtained in the case of NBDT (1 mM) reduction by VC (0.1 mM) in the presence of MNP (excess) and recorded 2 minutes after the addition of VC.

Table 15 – Hyperfine coupling constants of nitro aryl radicals MNP adducts.

	Hyperfine Splitting Constants (mT)	
	*a*N	*a*(others)
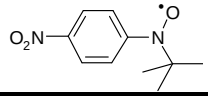	1.284	0.21 (2H); 0.097 (2H); 0.050 ($a_N NO_2$)

In order to establish a connection between the grafting of PNP layers on surfaces and the quantity of radicals formed with time, various ratios of [VC]/[NBDT] were tested and the reactions followed by EPR (Figure 51). It is important to point out that the concentration reported on Figure 51 is the concentration of the spin-adduct, a time-stable compound in the

timescale of our experiments. Thus, each measurement corresponds to the sum of all the radicals spin-trapped from the beginning of the experiment. All the kinetic curves in this figure can be decomposed in three steps: an initial rapid increase (the extrapolated curve at t=0 is clearly not null), after 2 minutes the reaction proceeds at a slower rate and finally, as it is obvious in the case of the ratio of 1/10, a saturation of the amplitude of the EPR signal is observed. We assume that the nitrophenyl radical creation as the reaction goes along is essential in the redox-induced process and occurs thanks to a slow reaction rate.

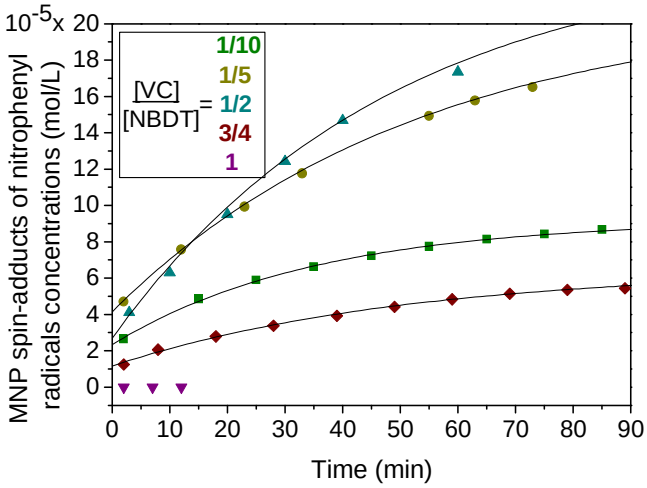

Figure 51 – Evolution of nitrophenyl radical MNP adduct concentration with time during the reaction of MNP (excess), NBDT (1 mM) and VC in the following ratios [VC]/[NBDT] 1/10 (■), 1/5 (●), 1/2 (▲), 3/4 (♦) and 1 (▼).

Another striking result from Figure 51 is that no MNP adducts is detected with [VC]/[NBDT]=1, which confirms the GC-MS results. Moreover, for a ratio 3/4, unexpectedly low amounts of trapped radicals are observed. A competition between the spin-trapping reaction and at least another reaction seems to occur. Several hypotheses can be proposed to explain the low amounts of MNP-adducts at the highest [VC]/[NBDT] ratios tested:

- First, the spin-adducts may be reduced directly by excess VC into the corresponding EPR-silent hydroxylamines, as already observed by Reszka *et al*[36].
- Second, dimerization of the aryl radicals may occur. Indeed, with the highest [VC]/[NBDT] ratios, excess aryl radicals are formed in solution and the dimerization (an order 2 reaction with respect to NBDT) may become predominant compared to the spin-trapping reaction (order 1). However, according to the GC-MS experiments previously described, this hypothesis is to be discarded. Indeed, no dimers from the reaction between two nitrophenyl radicals were identified for a [VC]/[NBDT] ratio of 1 whereas, after identical reaction time they were detected for lower ratios.
- Third, ascorbic acid may react with the diazonium salt in a non-redox way and form an adduct[1, 38, 39] by an inner-sphere electron transfer mechanism (see II.3.1.2). According to the literature, this leads to the 3-O-arenediazoascorbic acid formation (represented in Scheme 52). This compound belongs to the family of diazoether and displays an

absorbance maximum at λ_{max}=358 nm (yellow color). As mentioned in IV.2.1.1, whatever the [VC]/[NBDT] ratio, a drastic change in the color of the reactive solution is observed when adding ascorbic acid. The UV-visible spectrum of such a mixture [VC]/[NBDT] = 1 exhibits a maximum of absorbance at 354 nm which might speak for the diazoether formation (further experiments detailed in the next paragraph). Thus, it seems likely that the reaction which competes with the "direct" reduction of the diazonium salt by ascorbic acid is the formation of a diazoether adduct.

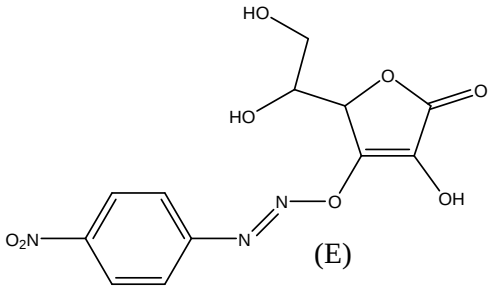

(E)

Scheme 52 – Chemical structure of the (E)-diazoether from the reaction between NBDT and VC. The (Z)-diazoether also exists but is not represented here.

By a rapid surface-solution comparison, we found that, in all cases, IR-ATR measurements seem in accordance with those EPR results. Indeed, aryl radicals were formed (since they were observed after spin-trapping) and a PNP layer was observed on gold surfaces. However, we could not find a monotonous relationship between the observed radical concentration (as estimated from the spin-trapping experiment) and the amount of nitrophenyl group of the final PNP film. Indeed, the aryl radicals actually experienced many termination chemical routes, including dimerization, in addition to their grafting on the gold surface. It is thus quite difficult to conclude on any "best" conditions leading to PNP film with the most nitrophenyl groups, although we observed PNP grafted films with higher amount of those groups for [VC]/[NBDT]=1/10 than for higher ratios. When stoichiometric amounts of NBDT and VC were used, no aryl radicals were detected by EPR whereas gold surfaces showed a very weak IR-ATR absorption at 1600, 1525 and 1350 cm^{-1}, characteristic of a PNP layer. Those signals may be attributed to the spontaneous grafting of diazonium salts on gold, as already described in chapter III.

IV.2.2.3 - UV-visible

In order to demonstrate the formation of a diazoether adduct in reactive solutions, UV-visible experiments were performed. Indeed, as mentioned above, such species have a characteristic absorption at 358 nm. From the EPR results, it seems that the ratio [VC]/[NBDT] has a strong influence on the presence of aryl radicals. Therefore, the absorption of the reactive solution was followed with time for various ratios (Figure 52). In the case of stoichiometric amounts of NBDT and VC, it is obvious that the diazonium salt (λ_{max}=258 nm) is "immediately" converted into another compound absorbing at 354 nm which is likely to correspond to the

(E)-diazoether (as it will be detailed below). Moreover, it is important to point out that the intensity of this absorption band is stable over 60 min. For the 1/5 and 1/10 ratios, it is more difficult to conclude since a large absorption band, increasing with reaction time, is observed in the 270 - 470 nm range. 4-nitrophenol certainly contributes to the signal since its main absorption peak is found at 318 nm. In addition, the diazoether probably takes part in the signal but its contribution does not give a peak as intense as in the case of ratio 1. Therefore, at maximum, the proportion of the diazoether compound is equal to the quantity of VC in solution which decreases for lower [VC]/[NBDT] ratios ([NBDT] constant). Indeed, the formation of the diazoether is based on an order 1 reaction regarding VC as well as NBDT and VC is the limiting reactant. The absorption below 500 nm could be explained by the presence of 4,4'-dinitroazobenzene and/or 4,4'-dinitrobiphenyl products in solution as observed in GC-MS measurements.

To summarize, the presence of the diazoether formation has definitely been demonstrated in the case of a [VC]/[NBDT] ratio of 1 whereas for the other ratios, these UV-visible experiments did not permit to clearly conclude. Therefore, the solutions have been characterized using electrospray ionization mass spectrometry (ESI-MS) which is a precise tool in the mass determination of compounds (although it only allows qualitative studies).

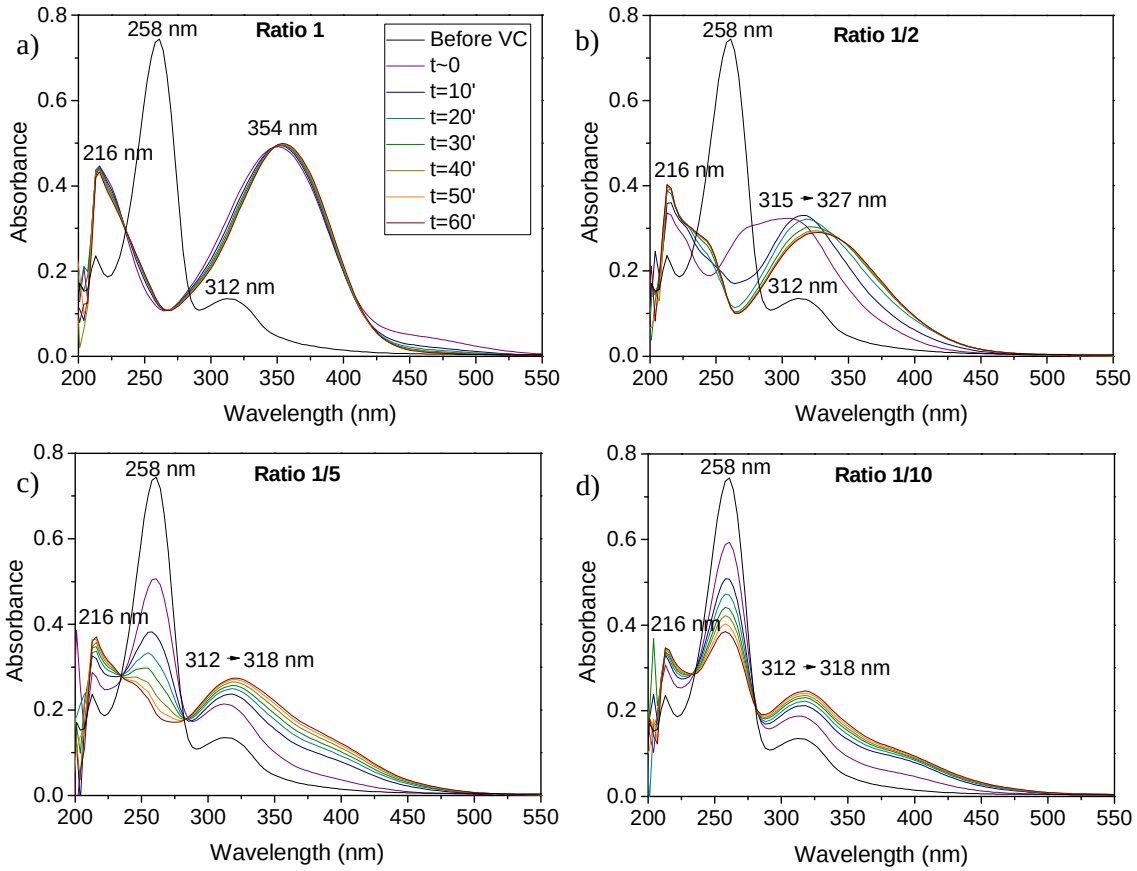

Figure 52 – Evolution of the UV-visible absorption of NBDT (50 µM) and VC ([VC]/[NBDT] ratios of a) 1, b) 1/2, c) 1/5 and d) 1/10) H_2O DI solutions with reaction time.

IV.2.2.4 - Electrospray ionization mass spectroscopy

As experiments were performed in a negative ionization mode (cf appendix 1), the main characteristic mass peak of the diazoether is expected to be found at 324 g/mol on the electrospray ionization mass spectrum. This was confirmed by injecting a diazoether (Figure 53a) synthesized in our laboratory from VC and NBDT following the procedure proposed by Doyle *et al.*[39] (cf appendix 2). The shape of this signal fits with the theoretical features predicted for a $C_{12}H_{10}N_3O_8$ organic compound (Figure 53b). Therefore, in order to monitor the diazoether formation, we will first follow the 324 g/mol mass peak for [VC]/[NBDT] = 1 and 1/10. However, the mass spectrum of NBDT alone gives a peak at a mass (324 g/mol) identical to the main one of the diazoether (Figure 53c) attributed to the presence of 4-nitrobenzene diazonium with two tetrafluoroborate counter-ions. Indeed the shape of signal fits with the predicted spectrum of a $C_6H_4N_3O_2B_2F_8$ compound (Figure 53d). Thus, if some NBDT remains in the solution (which will certainly be the case when working with the 1/10 ratio), it will be impossible to distinguish precisely the contribution of NBDT from the one of the diazoether. Therefore, experiments to test the presence of diazoether in the solution were carried out using 4-nitrobenzene diazonium perchlorate NBDP (see appendix 2 for its synthesis). In this case, the mass of the 4-nitrobenzene diazonium with two counter-ions is switched to 348 g/mol and can easily be differentiated from the diazoether signal.

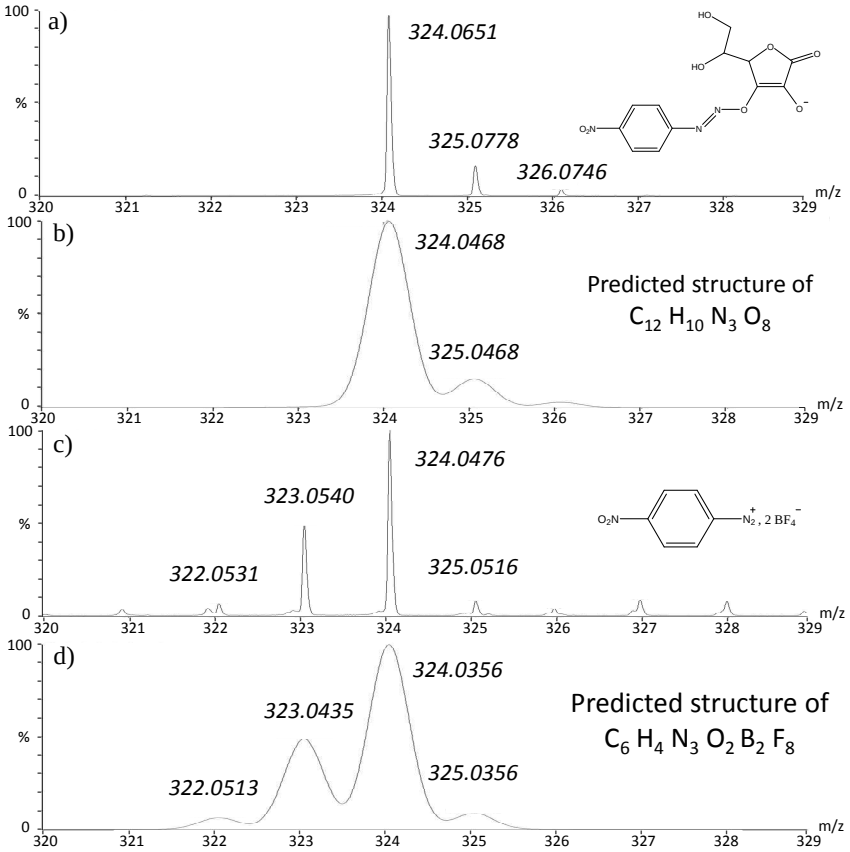

Figure 53 – Electrospray ionization mass spectra, zoomed in the 320 - 329 g/mol range, of a) reference diazoether, c) nitrobenzene diazonium ditetrafluoroborate and their corresponding predicted features respectively in b) and d).

The mass spectrum obtained after adding VC in stoichiometric amount to a NBDP solution is shown in Figure 54. The structure of the identified compounds is listed in Table 16. The presence of the diazoether and corresponding agglomerates as well as hydrogenated species demonstrates clearly the formation of a diazoether adduct from the reaction between the diazonium salt and ascorbic acid, which confirms the UV-visible results.

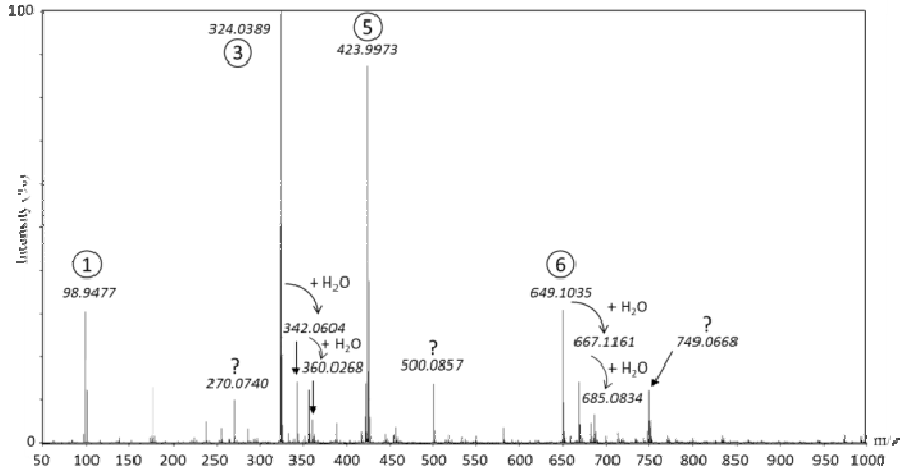

Figure 54 – Electrospray ionization mass spectrum of a NBDP H_2O solution after addition of VC in stoichiometric amount.

Table 16 – Main compounds identified in the electrospray ionization mass spectra of NBDP and VC solutions.

Compound	Mass	Structure
①	99 g/mol	ClO_4^-
②	138 g/mol	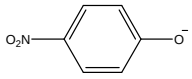
③	324 g/mol	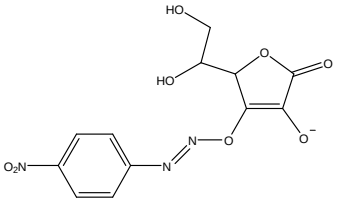
④	348 g/mol	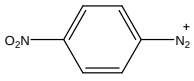 , 2 ClO_4^-
⑤	424 g/mol	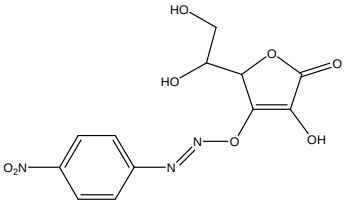 , ClO_4^-
⑥	649 g/mol	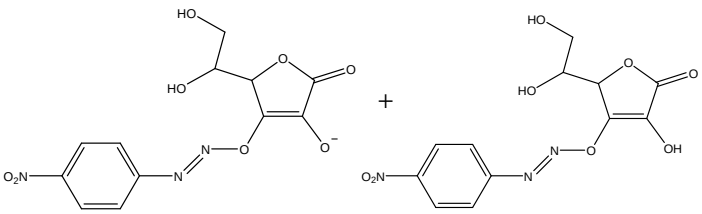

The [VC]/[NBDP] ratio of 1/10 was also tested (Figure 55). 4-nitrophenol is definitely present in the solution (compound 2 in Table 16). However, it cannot be determined whether it comes from the reaction of NBDP with VC, since it is already present in pure NBDP solutions. As in the previously studied case, diazoether and its derivative agglomerates were identified in the mass spectrum. Therefore, this result provides the first proof of the formation of the diazoether adduct even at low concentrations of VC. However, contrarily to those previous results, evidences of the existence of remaining diazonium salt, not linked to ascorbic acid, were found (compounds 4 in Table 16). This is not surprising since VC is the limiting reactant in this case.

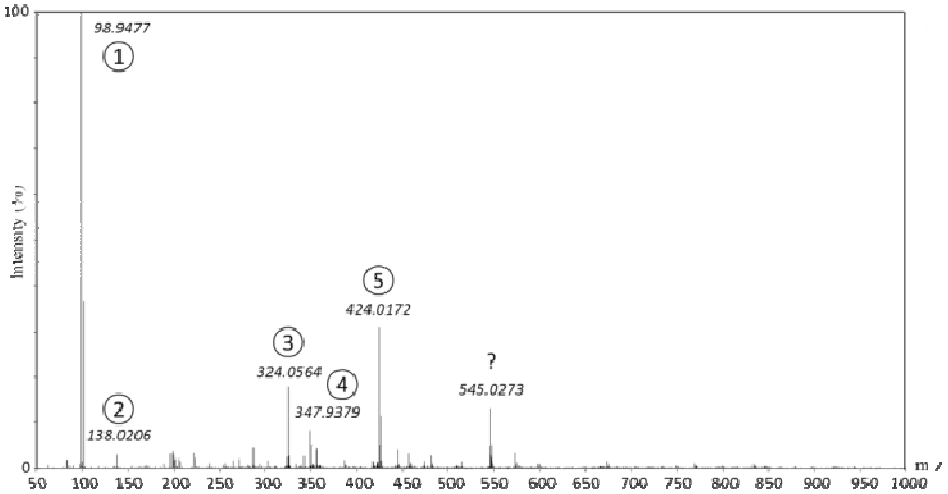

Figure 55 – Electrospray ionization mass spectrum of a NBDP H_2O solution after addition of VC ([VC]/[NBDP] = 1/10).

We have demonstrated the presence of the diazoether adduct in reactive solutions (whatever the [VC]/[NBDT] ratio). Let us now focus on its formation pathway and investigate if it can play a role in the grafting mechanism of diazonium salts on the surface of materials.

IV.2.2.5 - Formation of the diazoether and possible dediazoniation pathway

The β-nitrogen of aryldiazonium salts forms the centre of its electrophilic character[1]. Therefore, nucleophilic additions can occur. According to the nature of the atom of the nucleophile that provides the lone pair of electrons, *O*-, *S*-, *Se*-, *N*-, *P*- or *C*-coupling are reported[1]. The reaction of alkoxide or phenoxide ions (RO^-) on diazonium salts leads to the formation of diazoethers. The kinetic and mechanistic aspects of this *O*-coupling have been widely studied particularly in the case of reactions with alcoholic solvents (methanol[40], ethanol[40-42], butanol[43]). As represented in Scheme 53, this reaction can form the (Z)- and/or the (E)-diazoether. In the case of diazohydride[1] (R-φ-N_2-OH), it was found that the direct rearrangement of the (Z)- to the (E)-isomer is more consistent with the experimental data than a recombination after a primary dissociation of the (Z)-isomer into a diazonium ion. For other

diazoethers such as diazomethylether, no direct conversion of the (Z)- to the (E)-isomer has been found. The transformation occurs by an ionization-recombination mechanism. A three-phase mechanism was proposed to explain the whole reaction between the diazonium salt and the solvent. First, the (Z)-diazoether is formed extremely rapidly. Then, some of the (Z)-isomer decomposes to form dediazoniation products. Finally, the rest is converted into the (E)-diazoether[40]. The (Z)-diazoether was therefore considered as the kinetically determining product while the (E)-isomer was the thermodynamic product. This mechanism is very interesting since it shows that, in some cases, this *O*-coupling reaction can be an intermediate step in dediazoniation by an inner-sphere pathway which leads to the formation of aryl radicals.

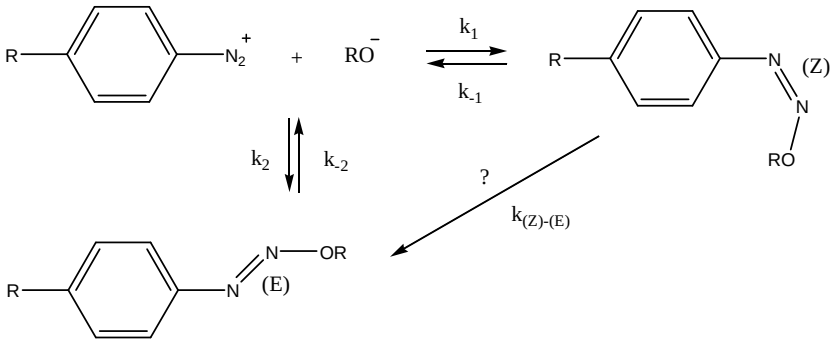

Scheme 53 – *O*-coupling of alkoxide or phenoxide ions (RO^-) on diazonium salts.

According to the literature of *O*-coupling reactions with alcoholic solvents[1, 6, 40], it seems that the diazoether is almost completely "protected" against dediazoniation if present as (E)-isomer. Therefore, only the (Z)-diazoether can undergo dediazoniation. Nevertheless, this behaviour is strongly depending on the solvent. The stability of the (Z)-adduct is critically dependent on the leaving group ability of RO^- and on the stability of the radical $RO^{\bullet}$, which is likely to be formed by dissociation of the diazoether. A few mechanisms based on the decomposition of (Z)-diazoether were proposed to explain the formation of dediazoniation products such as benzene. The dediazoniation by a homolytic pathway (Scheme 54) was found more probable than an anionic mechanism[1].

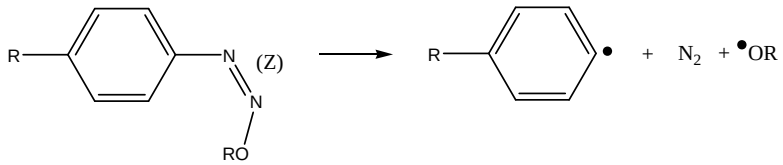

Scheme 54 – Dediazoniation pathway of the (Z)-diazoether.

The formation of diazoether by reaction of NBDT with ascorbic acid[38, 44, 45] was also reported (for the first time by Doyle *et al.*[39]). In contrast to diazoalkylether and in spite of the reducing properties of VC, it seems that this (E)-diazoether is stable and can be synthesized. Kinetics and mechanistic investigations[38] corroborated the dediazoniation pathway described above in the case of *O*-coupling reactions of diazonium salts with alcoholic solvent. Therefore, it is likely

that the ascorbic acid can carry out an inner-sphere electron transfer with diazonium salts, forming aryl radicals, through the decomposition of the (Z)-diazoether.

The UV-visible spectrum of the reference (E)-diazoether displays an intense absorption band around 354 nm corresponding to the $\pi \rightarrow \pi^*$ transition which is in accordance with the value found in the literature[39]. Therefore, since in the UV-visible experiments in water (Figure 52) we only observed one absorption band around this value, it is likely that we only formed the (E)--diazoether. No sign for the (Z)-diazoether was found. Indeed, if both diazoethers were present, two different absorption bands should be found. Similarly to what is observed for azobenzene, it is likely that the (Z)-isomer exhibits an absorption band at lower wavelength than the (E)--isomer since, due to steric effects, the π-system of this compound is less conjugated, which induces a higher gap value. Our lack of evidence for the transformation of the (Z)-diazoether into the (E)-isomer might be explained by a rapid conversion rate as well as the pH of the solution. Therefore, reactions with [VC]/[NBDT] ratio of 1 and 1/10 were followed for 10 min with a fast UV-visible spectrometer (one acquisition every 30 s) in H_2O and H_2SO_4 (pH = 2).

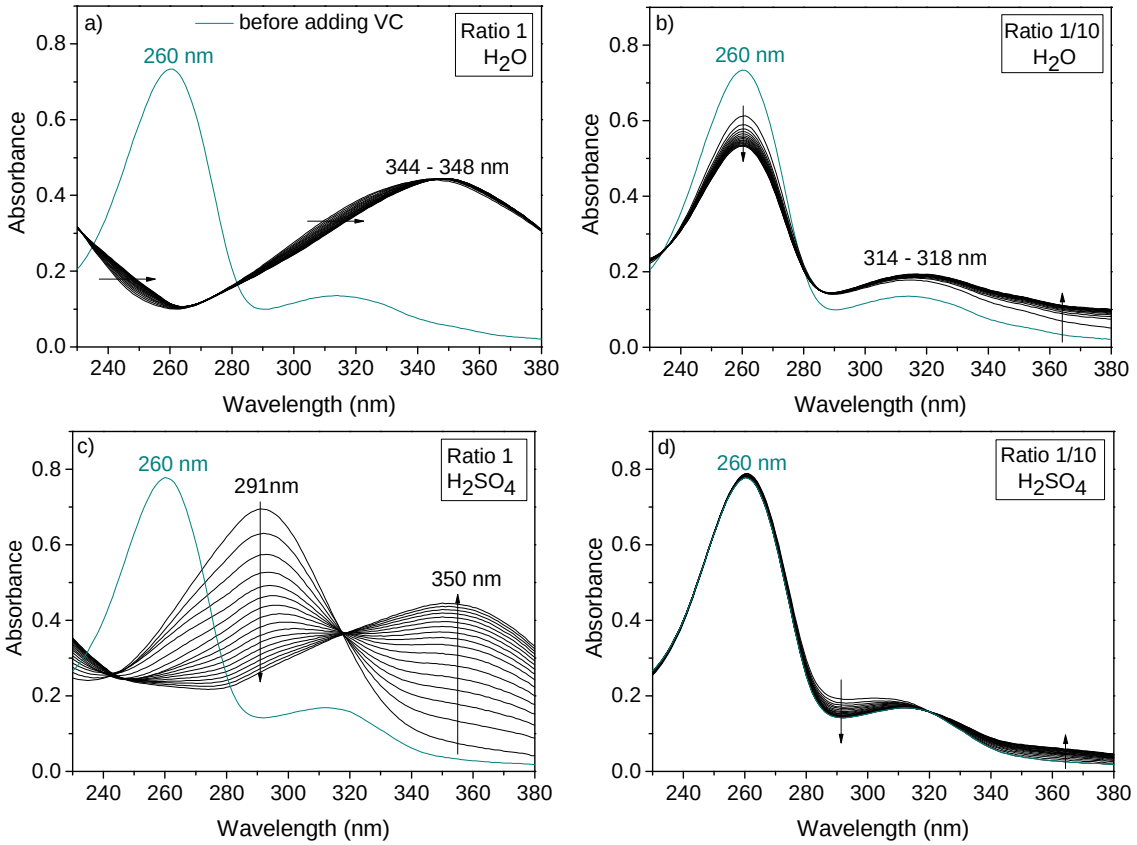

Figure 56 – Evolution over 10 min of the UV-visible absorption of NBDT (50 µM) and VC a) and b) in water and c) and d) in H_2SO_4 (pH = 2) for [VC]/[NBDT] ratios of respectively 1 and 1/10. A spectrum has been acquired every 30 s.

It is obvious that, for the ratio 1 (Figure 56a and Figure 56c), the pH has a great influence on the reaction. Indeed, only one absorption band at around 346 nm is observed in water during the whole 10 min of the study. In H_2SO_4 the starting solution mainly absorbs around 291 nm and

then its absorption shifts progressively towards 350 nm. The presence of an isosbestic point at 318 nm indicates a slow but entire conversion between the two colored compounds through an equilibrium. This behaviour could correspond to the fast formation of the (Z)-diazoether followed by its slow conversion into the (E)-isomer. Further experiments (not presented here) showed that this transformation lasts for 15 min. After the critical time, most of the first compound is converted into the second one. In the case of the ratio 1/10, this phenomenon is much more difficult to observe since only a small part of the diazonium salt is converted into the diazoether. However, by comparing the evolution of the absorption of the reactive solution in water and H_2SO_4 (Figure 56b and Figure 56d), it seems that in the latter case the signal is flattened in the 290 nm region which could correspond to the presence of the small amount of absorbing (Z)-diazoether. Hence, from these results, it seems that decreasing the pH of the solution slows down the conversion of the (Z)-diazoether into the (E)-isomer allowing us to observe the phenomenon with classical absorption spectroscopy. Even if it cannot be observed by this technique, the (Z) → (E) transformation certainly still occurs in H_2O DI but at a very high speed (almost instantaneously). Indeed, in H_2O, VC is mainly present as HA^- which is the compound needed for the *O*-coupling whereas, in acidic medium, it is in H_2A form. Therefore, the slow formation of the diazoether in H_2SO_4 could be due to the persistence of an equilibrium between H_2A and HA^-.

To conclude, it could be considered that aryl radicals detected by EPR measurements come from an intramolecular reaction between VC and NBDT followed by the dediazoniation of the (Z)-diazoether. Therefore, with view of the complexity of the reaction, several hypotheses concerning the mechanism of the VC-induced process can be made.

IV.2.3 - **Proposed mechanisms for the VC-induced grafting**

As previously discussed, we are aware that the results in terms of grafting obtained by surface analyses for the VC-induced process has to be considered carefully. First, it is likely that the phenomena occurring in solution do not directly reveal the grafting on surface. Only what happens near the surface of the substrate is relevant to explain the differences in terms of grafting. Second, only tendencies were determined. The spontaneous grafting of diazonium is probably still an important part of the observed grafting on surface even in presence of VC. However, as it will be seen in the next chapter concerning the grafting in presence of a vinylic monomer, VC plays a major role in the process. Therefore, proposing a possible mechanism in the “simple” case of the grafting of diazonium salts with VC is essential. According to EPR results and as expected, it is likely that the grafting process is based on the formation of aryl radicals that are able to graft on the surface of substrates. Prior to focus on how aryl radicals graft on materials, we will see how they can possibly be formed during this process.

IV.2.3.1 - Formation of aryl radicals

Relying on the literature, the several mechanisms discussed below were proposed in order to fit with the maximum of our experimental results. Indeed, it seems that aryl radicals can either be obtained by an outer- or an inner-sphere electron transfer mechanism.

An inner-sphere mechanism from the decomposition of (E)-diazoether

The simplest mechanism is to consider that there is no outer-sphere electron transfer mechanism but only the formation of the (E)-diazoether adduct between the ascorbate ion and the diazonium salt (inner-sphere)[46]. The mechanism is summarized in Scheme 55.

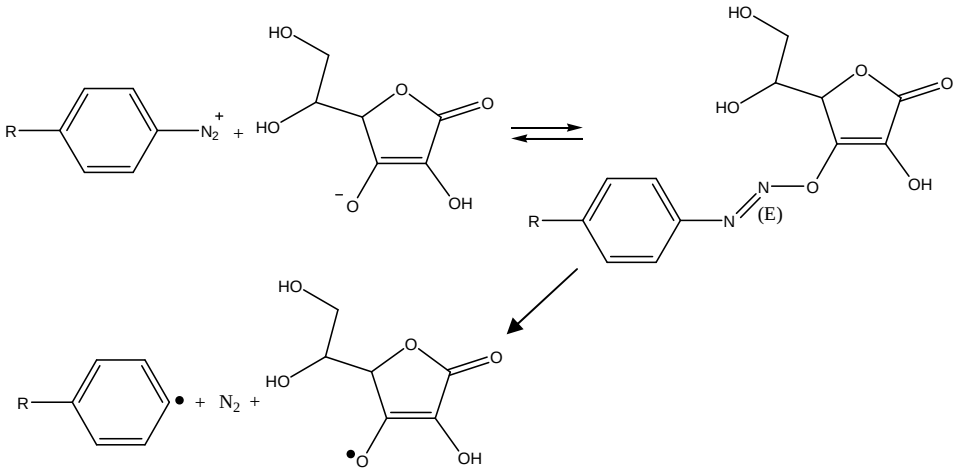

Scheme 55 – Inner-sphere mechanism from the decomposition of (E)-diazoether.

In this case, as in H_2O we could not observe the presence of the (Z)-diazoether, we assume that the (E)-diazoether is directly formed by adding VC in the diazonium salt solution. This is in good agreement with the change in color of the solution into a yellow mixture when adding VC (absorption band around 350 nm observed in UV-visible spectra). The formation of aryl radicals for [VC]/[NBDT] ratios of 1/10, 1/5, 1/2 and 3/4 will therefore be due to the decomposition of the (E)-diazoether. However, according to the literature, this reaction is not very likely. Moreover, the consumption of the (E)-diazoether in a reaction would involve a decrease in the absorption intensity of the UV-visible main peak of this compound with time. However, over 60 min, the absorption intensity around 354 nm seems either stable or to increase according to the ratio employed. To finish, it would not explain the fact that, for a ratio 1, no aryl radicals were observed since in this particular case it would mean that the decomposition of the (E)-diazoether cannot occur. In order to keep close to data given by the literature, we have proposed another mechanism considering that the decomposition into aryl radicals is undergone by the (Z)-diazoether.

A inner-sphere mechanism from the decomposition of (Z)-diazoether

In this mechanism, we assume that the (Z)-diazoether is formed (inner-sphere) from the reaction of ascorbate ion and diazonium salt. Rapidly, this compound decomposes to give aryl

radicals and transforms in the (E)-diazoether, as represented on Scheme 56. However, to fit with what was described in the literature, no decomposition of the (E)-diazoether is considered.

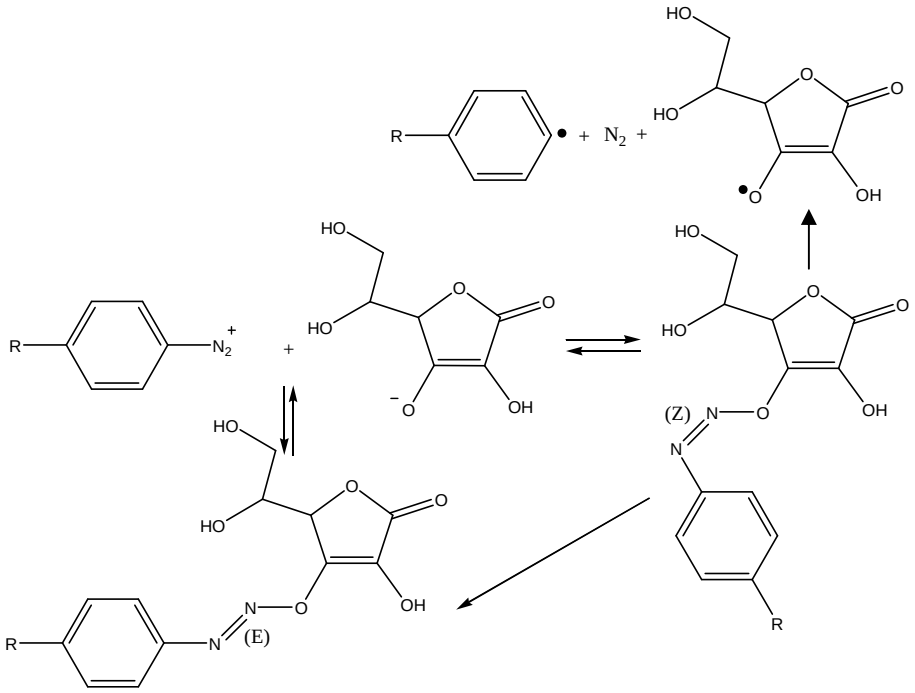

Scheme 56 – Inner-sphere mechanism from the decomposition of (Z)-diazoether.

In this case, by extrapolating what was observed in IV.2.2.5 in acidic media, we consider that the formation of the (Z)-diazoether is possible in H_2O although no direct evidence has been found. The (Z)-diazoether would be instantaneously formed and transformed in aryl radicals as well as the (E)-diazoether. This phenomenon could be in agreement with first, the rapid increase in the radical concentration observed by EPR in the first two minutes of the reaction for most of the ratios [VC]/[NBDT] tested and second, with the presence in UV-visible spectra of a component absorbing in the 300 - 400 nm region corresponding to the (E)-isomer. The slow but continuous formation of aryl radicals could be then attributed to the fact that the (Z)-diazoether formation is initially rapid but afterwards becomes slower and slower with the diminution in concentration of ascorbate ions. The transformation of this compound into radicals as well as into its isomer proceeds therefore during the whole reaction time. This slow formation of the (E)-diazoether can also partially explain the slight increase in absorption intensity in the 300 - 400 nm range with time. However, this would require that some ascorbate ions remain in solution for more than 60 min in order to form, by reaction with the diazonium salt, more (Z)-adduct during this period. This possibility was confirmed by ESI-MS measurements showing that ascorbic acid is still present even after a reaction time of 40 min for a [VC]/[NBDT] ratio of 1/2 (results not presented). Nevertheless, when using a ratio of 1/10, ESI-MS measurements did not allow detecting remaining ascorbate ions. The absence of radicals in the case of stoechiometric amounts of reactants could be attributed to very high

transformation rate of the (Z) into the (E)-diazoether, compound that cannot decompose into aryl radicals, due to the use of high concentration of ascorbate ions. However, our experiments do not permit to distinguish this mechanism from the one presented below.

A competition between an outer- and an inner-sphere mechanism

Similarly to the previously proposed mechanism (Scheme 56), we assumed that the reaction of VC on diazonium salt first forms the (Z)-diazoether adduct which can transform either into aryl radicals or into the (E)-diazoether (unable to decompose). On top of this reaction, we believe that the direct reduction of the diazonium salt by VC can still occur also leading to the formation of aryl radicals. This additional reaction is detailed in Scheme 57.

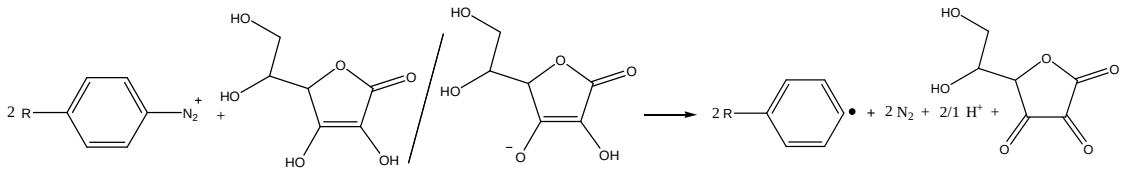

Scheme 57 – Outer-sphere electron transfer reaction entering in the mechanism based on competitive reactions between an outer- and an inner-sphere pathway.

This mechanism would therefore fit with experimental data the same way as for the mechanism described above. The only difference lies in the interpretation of the presence of radicals with time. In this case, we believe that the initial jump in concentration of aryl radicals and their slow formation with time is due to competitive reactions. The first reaction would still be the formation of the (Z)-diazoether from remaining ascorbate ions and its decomposition. The second would be based on a classical redox reaction between the diazonium salt and VC. Both reactions could lead to the slow formation of aryl radicals. However, the oxidation of VC during this redox reaction should form an oxidized product. No evidence of the presence of this compound was found in our experiments, but it is expected to be formed in very low amount.

Conclusion on the formation mechanism of aryl radicals

To our opinion, the last two mechanisms are the most likely to explain the formation of aryl radicals in the redox-induced process[b] since they fit the more experimental results and are in agreement with pathways already observed in the literature for other systems. However, we cannot reasonably decide between the exclusively inner-sphere electron transfer mechanism or the mixed outer- and inner-sphere mechanisms since we do not have clear evidence in favor of one or the other. Now, we have proposed mechanism for the formation of aryl radicals, it remains to explain how those aryl radicals graft onto materials and form an organic film.

[b] The term redox-induced will still be employed to describe the process in which the presence of ascorbic acid is required in order to form aryl radicals. However, when an inner-sphere electron transfer mechanism is proposed, this name is not perfectly adapted. Indeed, even if the diazonium salt is reduced and ascorbic acid is oxidized, the reaction is based on an intramolecular pathway.

IV.2.3.2 - Growth of the film

The mechanism for the formation of polyphenylene-like layers on substrates by the redox-induced process is based on an analogy with the proposed mechanism in the case of the construction of similar films by electrochemical reduction of aryl diazonium salts.

The most complete mechanism and probably the closest to the VC-induced one on gold was proposed by Combellas *et al.*[47] for the electrografting of *para*-substituted diazonium salts, including NBDT, in organic media on glassy carbon (Scheme 58). It consists in, first, the reduction of diazonium salt by electron transfer with the electrode and formation of an aryl radical. Then, this radical reacts with the surface of the electrode. Another aryl radical can attack the previously grafted aromatic ring which creates a cyclohexadienyle radical. To make possible the growth of the film, this cyclohexadienyle radical should be oxidized by transferring, for instance, an electron to a diazonium cation and producing H^+. The attack of the nitrophenyl radical is represented in *ortho* of the nitro group since some previous work from Combellas *et al.* [48, 49] on the influence of steric effects of the aromatic ring on the growth of the films showed that those aryl radicals mainly linked on the α-position of the NO_2. Overall, it seems that the grafting of polyphenylene-like films follows a chain radical mechanism equivalent to a "grafting from" pathway. To finish, this mechanism was recently completed by Doppelt[50] in order to explain the formation of azo bonds in the films, as detailed in III.3.1.3.

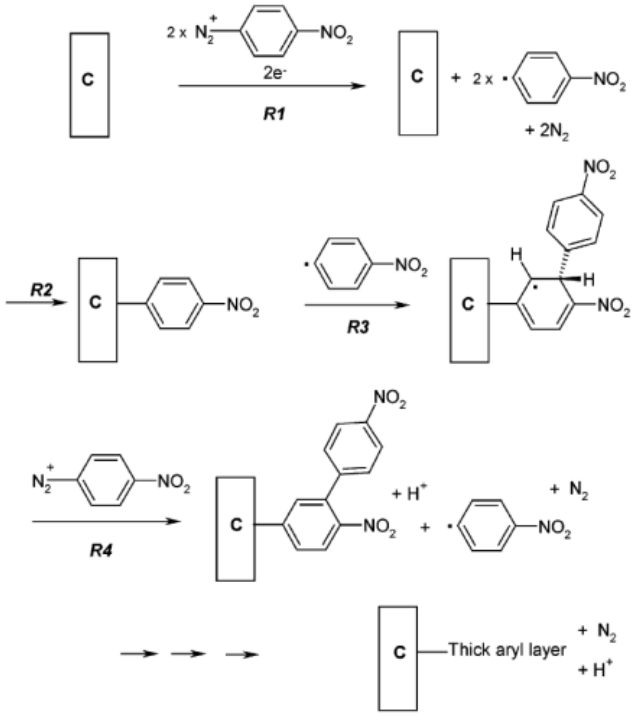

Scheme 58 – Mechanism of the electrografting of *para*-substituted diazonium salts, including NBDT, in organic media on glassy carbon extracted from the work of Combellas and coworkers[47].

In our case (chemical reduction of diazonium salt), the formation of aryl radicals is discussed in the previous paragraph and the growth of the film is likely to occur similarly to the electrochemical mechanism i.e. in three steps:

1. the attack of aryl radicals on the surface,
2. the attack of aryl radicals on already grafted aromatic rings,
3. the attack of diazonium cations on cyclohexadienyle radicals (formation of azo bridges).

However, at the same time, the spontaneous grafting process of diazonium salt can also take place, explaining particularly the presence of Au-N bonds at the interface film-substrate (see III.3.1). Therefore, it is likely that in the precise case of the grafting on NBDT on gold with VC, the resulting film comes from the combination of both processes: the spontaneous process and the electron transfer from VC process. Indeed, we cannot exclude that step 1 mentioned above does not really occur, and that aryl radicals are only capable of grafting on already attached aromatic rings (step 2) from the spontaneously formed film, but not directly on the gold surface. Considering this hypothesis, no general mechanism for the grafting on any type of materials can really be established, since it depends on the attachment way of the primer thin phenylene layer on the surface. The mechanism for this essential grafting could vary according to the substrate employed. For instance, in the case of reducing metals, the reduction of the diazonium salt by the substrate would lead to a rapid formation of aryl radicals and their grafting of the surface. Nevertheless, in other cases, aryl radicals might not be involved which is the case for substrates for which a spontaneous grafting is possible such as gold. To finish, direct diazonium coupling reactions with functions already present at the surface of substrates can also lead to the formation of a primer layer. The need for the primer phenylene layer would explain why, in some cases, pre-treatments of the substrate are required[51, 52]. On gold, the mechanism can therefore be roughly summarized as represented in Scheme 59.

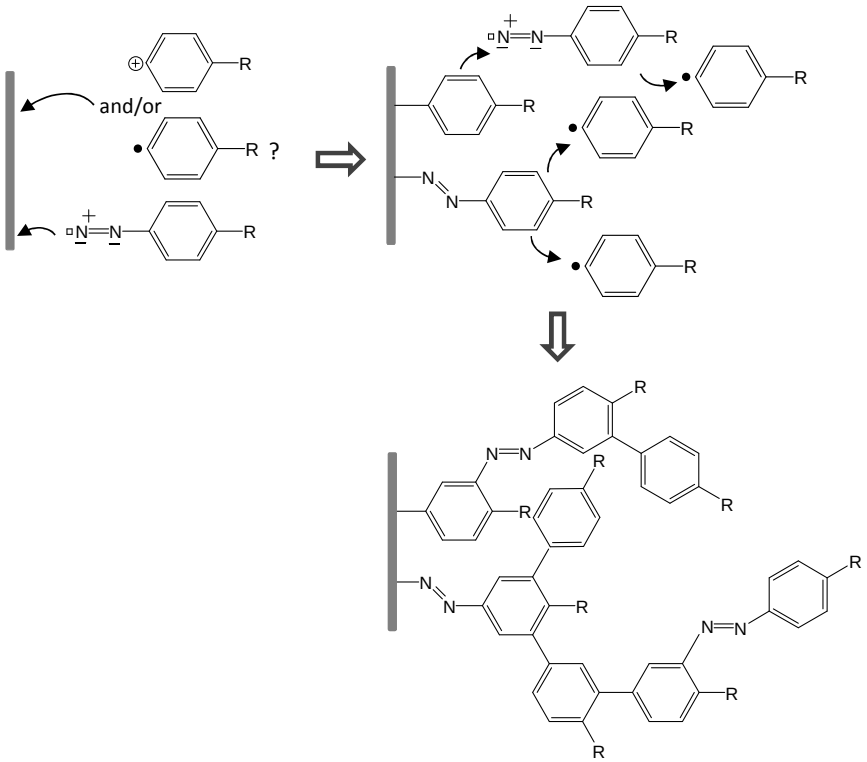

Scheme 59 – Mechanism proposed for the redox-induced grafting of diazonium salts on gold substrate.

IV.3 - **Comparison of the reducing agents**

To widen the study of the chemically-induced reduction of diazonium salts, we will compare the different graftings obtained according to the reducing agent used as well as the solvent. Then, we will draw a non-exhaustive list of working conditions for which each reducing agent is the most adapted.

IV.3.1 - **In terms of grafting efficiency**

The IR intensity values of the main characteristic band of polynitrophenylene films (ν^{s}_{NO2} = 1350 cm^{-1}) are summarized in Figure 57 according to the reducing agent (VC, H_3PO_2 and iron powder: a potential candidate, not presented here, to perform the reduction of diazonium salts) but also as a function of the solvent employed (acidic or neutral solutions). It is important to precise that the values presented here correspond to the grafting of 4-nitrobenzene diazonium salt tetrafluoroborate on gold substrates obtained with non-optimized experimental parameters (concentration, stirring, reaction time...). So, they are not to be considered as general rules of grafting. These values only prove that iron and H_3PO_2 are very efficient to promote the formation of the film in comparison to the values for the spontaneous grafting of diazonium salts. The efficiency of VC is clearly lower. However, its great influence on the reaction will be largely demonstrated in the next chapter when a vinylic monomer is added to the reaction mixture.

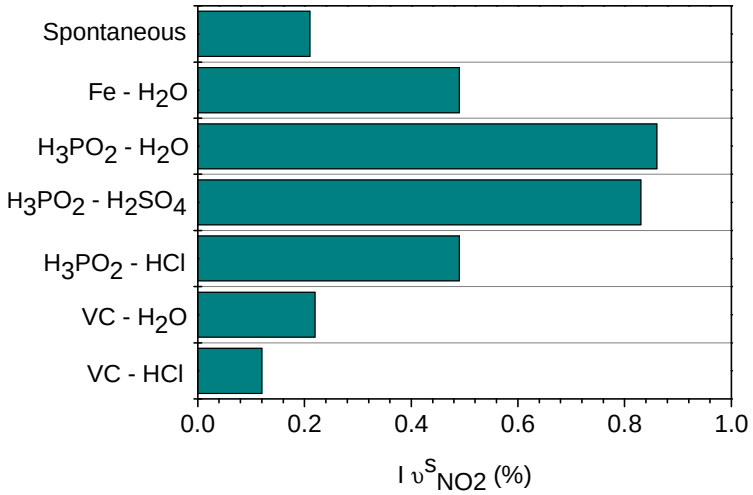

Figure 57 – IR intensity values of the ν^{s}_{NO2} = 1350 cm^{-1} band according to the reducing agent (VC, H_3PO_2 and iron) and as a function of the solvent employed.

IV.3.2 - **In terms of conditions to be used**

Whatever the application aimed, the use of basic medium is prohibited since the highest the pH is the less stable the diazonium salt. The direct reaction of diazonium salts with hydroxide ions is indeed well known[1]. Each reducing agent is more adapted to some experimental

conditions than others. Therefore, we will give basic clues on how to select the most suitable reducing agent considering a precise application.

Indeed, iron can *a priori* work at any pH. However, quantities of this reactant cannot be precisely evaluated since the powder grains are partially oxidized. Moreover, it is a magnetic compound which is unsuitable for mechanistic studies by EPR. To finish, as it acts in heterogeneous phase, remaining iron is likely to be found in the grafted films, which can be inappropriate particularly regarding biological applications. Concerning H_3PO_2, the reaction is performed in homogenous phase. However, the substrate itself should be safe at pH lower than 2. Besides, it cannot be used for EPR mechanistic investigations since the spin-traps employed are not stable in acidic media. To finish, ascorbic acid combines interesting properties of the two previously described reducing agents. As H_3PO_2, it works in homogeneous phase and as iron, at any pH. Moreover, the compound is well adapted to carry out EPR experiments and thus for studies on the understanding of the grafting mechanism.

To conclude, no general rules can be established. Only lines to direct the choice in reducing agent can be given. Moreover, these considerations do not replace a deep investigation to optimize the experimental conditions corresponding to the studied system: diazonium salt – reducing agent – solvent – substrate.

Summary

The redox-induced grafting of diazonium salts has been mainly used in the literature with H_3PO_2 as a reducing agent for the modification of carbon-based substrates. However, the mechanism of this grafting is still mainly unknown. It is likely that $H_2PO_2^-$ is the compound responsible for the reduction of diazonium salts, which explains why large excess of H_3PO_2 are generally used. This process has important potentialities since theoretically it would lead to the grafting of covalently bonded polyphenylene-like films on any type of materials (not only conducting or reducing substrates). In order to investigate this redox-induced grafting, the use of ascorbic acid as reducing agent has appeared essential to be able to perform EPR and detect the presence of expected aryl radicals. Therefore, even if the results in this particular case on surfaces could not bring precise elements in the understanding of the mechanism, the study of the reactive solutions has demonstrated the existence of aryl radicals and has revealed potential mechanisms for their formation. However, the mechanism in the case of VC seems more complex than when H_3PO_2 or iron are used as reducing agent for which a simple and direct redox reaction is very likely. Indeed, the existence of an inner-sphere electron transfer mechanism has been proved which is responsible for the presence of an intermediate diazoether adduct in solution. From this, two very probable mechanisms have been proposed: the first one exclusively based on an inner-sphere electron transfer mechanism and the second relying on

mixed outer- and inner-sphere mechanisms. Nevertheless, experimental results did not allow choosing between them. By analogy with electrochemical grafting of polyphenylene-like layers, a grafting mechanism of those aryl radicals has been presented.

It is important to underline that the process described in this chapter is already very powerful to provide many grafted primer layers on almost any kind of surfaces, suitable for further functionalization through reactions with the aryl groups or their para-substituents. However, the latter are limited by the necessary synthesis of the corresponding diazonium salts which stability is not very high. Hence, the polyphenylene grafted films obtained through the redox-induced grafting of diazonium salts cannot be an ubiquitous solution for the functionalization of surfaces Thus, the grafting of polymer films by use of a vinylic monomer (Graftfast^{TM} process), described in the next chapter, could widen the interest of the process. The study described in the present chapter has therefore constituted an intermediate mechanistic work with a view to understand the grafting mechanism of Graftfast^{TM}.

References

1. H. Zollinger, *Diazo chemistry I: Aromatic and Heteroaromatic coumponds*, VCH: Weinheim, New York, **1994**.
2. A. Mesnage, S. Esnouf, P. Jegou, G. Deniau, S. Palacin, *Understanding the Redox-Induced Polymer Grafting Process: A Dual Surface-Solution Analysis*, ***Chemistry of Materials***, **2010**, 22 (23), 6229-6239.
3. V. Mevellec, S. Roussel, L. Tessier, J. Chancolon, M. Mayne-L'Hermite, G. Deniau, P. Viel, S. Palacin, *Grafting polymers on surfaces: A new powerful and versatile diazonium salt-based one-step process in aqueous media*, ***Chemistry of Materials***, **2007**, 19 (25), 6323-6330.
4. M. Pandurangappa, N. S. Lawrence, R. G. Compton, *Homogeneous chemical derivatisation of carbon particles: a novel method for funtionalising carbon surfaces*, ***Analyst***, **2002**, 127 (12), 1568-1571.
5. M. Toupin, D. Belanger, *Spontaneous functionalization of carbon black by reaction with 4-nitrophenyldiazonium cations*, ***Langmuir***, **2008**, 24 (5), 1910-1917.
6. C. Galli, *Radical Reactions of Arenediazonium Ions - an Easy Entry into the Chemistry of the Aryl Radical*, ***Chemical Reviews***, **1988**, 88 (5), 765-792.
7. N. Kornblum, G. D. Cooper, J. E. Taylor, *The Chemistry of Diazo Compounds .2. Evidence for a Free Radical Chain Mechanism in the Reduction of Diazonium Salts by Hypophosphorous Acid*, ***Journal of the American Chemical Society***, **1950**, 72 (7), 3013-3020.
8. L. K. Skrunts, L. A. Kiprianova, A. F. Levit, I. P. Gragerov, *Kinetics and Mechanism of the Reaction of N,N,N',N'-Tetramethyl-Para-Phenylenediamine with Diphenyliodonium Chloride and Phenyldiazonium Fluoroborate*, ***Zhurnal Organicheskoi Khimii***, **1979**, 15 (8), 1645-1649.
9. G. G. Wildgoose, P. Abiman, R. G. Compton, *Characterising chemical functionality on carbon surfaces*, ***Journal of Materials Chemistry***, **2009**, 19 (28), 4875-4886.
10. G. G. Wildgoose, M. Pandurangappa, N. S. Lawrence, L. Jiang, T. G. J. Jones, R. G. Compton, *Anthraquinone-derivatised carbon powder: reagentless voltammetric pH electrodes*, ***Talanta***, **2003**, 60 (5), 887-893.
11. M. Pandurangappa, T. Ramakrishnappa, *Derivatization and characterization of functionalized carbon powder via diazonium salt reduction*, ***Journal of Solid State Electrochemistry***, **2008**, 12 (11), 1411-1419.
12. P. Abiman, G. G. Wildgoose, R. G. Compton, *A mechanistic investigation into the covalent chemical derivatisation of graphite and glassy carbon surfaces using aryldiazonium salts*, ***Journal of Physical Organic Chemistry***, **2008**, 21 (6), 433-439.
13. A. T. Masheter, G. G. Wildgoose, A. Crossley, J. H. Jones, R. G. Compton, *A facile method of modifying graphite powder with aminophenyl groups in bulk quantities*, ***Journal of Materials Chemistry***, **2007**, 17 (29), 3008-3014.
14. G. G. Wildgoose, H. C. Leventis, I. J. Davies, A. Crossley, N. S. Lawrence, L. Jiang, T. G. J. Jones, R. G. Compton, *Graphite powder derivatised with poly-L-cysteine using "building-block'' chemistry - a novel material for the extraction of heavy metal ions*, ***Journal of Materials Chemistry***, **2005**, 15 (24), 2375-2382.
15. P. Abiman, G. G. Wildgoose, R. G. Compton, *Investigating the mechanism for the covalent chemical modification of multiwalled carbon nanotubes using aryl diazonium salts*, ***International Journal of Electrochemical Science***, **2008**, 3 (2), 104-117.
16. M. Pandurangappa, T. Ramakrishnappa, *Spectroscopic and thermal characterization of carbon nanotubes functionalized through diazonium salt reduction*, ***Materials Chemistry and Physics***, **2010**, 122 (2-3), 567-573.
17. G. G. Wildgoose, N. S. Lawrence, H. C. Leventis, L. Jiang, T. G. J. Jones, R. G. Compton, *X-Ray photoelectron spectroscopy studies of graphite powder and multiwalled carbon nanotubes covalently modified with Fast Black K: evidence for a chemical release mechanism via electrochemical reduction*, ***Journal of Materials Chemistry***, **2005**, 15 (9), 953-959.
18. C. G. R. Heald, G. G. Wildgoose, L. Jiang, T. G. J. Jones, R. G. Compton, *Chemical derivatisation of multiwalled carbon nanotubes using diazonium salts*, ***ChemPhysChem***, **2004**, 5 (11), 1794-1799.

19. H. C. Leventis, I. Streeter, G. G. Wildgoose, N. S. Lawrence, L. Jiang, T. G. J. Jones, R. G. Compton, *Derivatised carbon powder electrodes: reagentless pH sensors*, ***Talanta***, **2004**, 63 (4), 1039-1051.

20. Y. P. Sun, K. F. Fu, Y. Lin, W. J. Huang, *Functionalized carbon nanotubes: Properties and applications*, ***Accounts of Chemical Research***, **2002**, 35 (12), 1096-1104.

21. B. I. Rosario-Castro, E. R. Fachini, J. Hernandez, M. E. Perez-Davis, C. R. Cabrera, *Electrochemical and surface characterization of 4-aminothiophenol adsorption at polycrystalline platinum electrodes*, ***Langmuir***, **2006**, 22 (14), 6102-6108.

22. L. Tessier, *Greffage de Films Organiques par Polymerisation Radicalaire Electro-amorcée en Milieu Aqueux Dispersé*, Thèse de l'Université Pierre et Marie Curie, Paris, **2009**.

23. S. S. C. Yu, E. S. Q. Tan, R. T. Jane, A. J. Downard, *An electrochemical and XPS study of reduction of nitrophenyl films covalently grafted to planar carbon surfaces*, ***Langmuir***, **2007**, 23 (22), 11074-11082.

24. A. F. Hegarty, *The Chemistry of Diazonium and Diazo Compounds*, Ed. S. Patai John Wiley & Sons, New York, **1978**.

25. K. J. Reszka, C. F. Chignell, *EPR and Spin-trapping Investigation of Free-Radicals from the Reaction of 4-Methoxybenzenediazonium tetrafluoroborate with Melanin and Melanin Precursors*, ***Journal of the American Chemical Society***, **1993**, 115 (17), 7752-7760.

26. C. Galli, *Stimulation by SN^{+2} or Ascorbic Acid on Diazonium Salts Reactions*, ***Tetrahedron Letters***, **1980**, 21 (47), 4515-4516.

27. P. Riesz, I. Rosenthal, *Photochemistry of Protein and Nucleic-Acid Constituents - Electron-Spin Resonance and Spin-Trapping with 2-Methyl-2-Nitrosopropane*, ***Canadian Journal of Chemistry***, **1982**, 60 (12), 1474-1479.

28. E. Rosa, A. Guerrero, M. P. Bosch, L. Julia, *EPR/Spin-trapping study of free radical intermediates in the photolysis of trifluoromethyl ketones with initiators*, ***Magnetic Resonance in Chemistry***, **2010**, 48 (3), 198-204.

29. F. Sun, S. L. Jiang, H. G. Du, *The photosensitive properties of polysiloxane acrylate resin containing tertiary amine groups*, ***Journal of Applied Polymer Science***, **2008**, 107 (5), 2944-2948.

30. Y. R. Chen, C. L. Chen, X. P. Liu, H. T. Li, J. L. Zweier, R. P. Mason, *Involvement of protein radical, protein aggregation, and effects on NO metabolism in the hypochlorite-mediated oxidation of mitochondrial cytochrome c*, ***Free Radical Biology and Medicine***, **2004**, 37 (10), 1591-1603.

31. M. R. Gunther, *Probing the free radicals formed in the metmyoglobin-hydrogen peroxide reaction*, ***Free Radical Biology and Medicine***, **2004**, 36 (11), 1345-1354.

32. B. Randy, J. F. Rabek, *Polymers: Properties and Applications 1: ESR spectroscopy in polymer research*, Springer-Verlag, Berlin, **1977**.

33. T. Kunitake, S. Murakami, *Study of Radical Polymerization by Spin Trapping: 1. Trapping of Initiating and Propagating Radicals*, ***Polymer Journal***, **1972**, 3 (2), 249.

34. M. Kuwabara, H. Ohshima, F. Sato, A. Ono, A. Matsuda, *Spin-Trapping Detection of Precursors of Hydroxyl-Radical-Induced DNA-Damage - Identification of Precursor Radicals of DNA Strand Breaks in Oligo(Dc)10 and Oligo(Dt)10*, ***Biochemistry***, **1993**, 32 (40), 10599-10606.

35. C. Hazlewood, M. J. Davies, B. C. Gilbert, J. E. Packer, *Electron-Paramagnetic-Resonance Studies of the Reaction of Aryl Radicals with Nucleic-Acids and Their Components*, ***Journal of the Chemical Society-Perkin Transactions 2***, **1995**, (12), 2167-2174.

36. K. J. Reszka, C. F. Chignell, *One-electron Reduction of Arenediazonium Compounds by Physiological Electron-donors Generates Aryl Radicals - an EPR and Spin-trapping Investigation*, ***Chemico-Biological Interactions***, **1995**, 96 (3), 223-234.

37. M. Kuwabara, S. Miyake, T. Jin, S. Sawamura, *Reactions and Rate Constants between Hydroxyl Radicals and the Dimer and Monomer of Spin Trap 2-Methyl-2-Nitrosopropane Determined by the Pulse-Radiolysis Method*, ***Journal of Physical Chemistry***, **1995**, 99 (38), 14078-14082.

38. U. Costas-Costas, E. Gonzalez-Romero, C. Bravo-Diaz, *Effects of ascorbic acid on arenediazonium salts reactivity: Kinetics and mechanism of the reaction*, ***Helvetica Chimica Acta***, **2001**, 84 (3), 632-648.

39. M. P. Doyle, C. L. Nesloney, M. S. Shanklin, C. A. Marsh, K. C. Brown, *Formation and Characterization of 3-O-arenediazoascorbic acids - New Stabme Diazo Ethers*, ***Journal of Organic Chemistry***, **1989**, 54 (16), 3785-3789.

40. T. J. Broxton, D. L. Roper, *Elucidation of Role of Syn-Arylazo and Anti-Arylazo Alkyl Ethers in Dediazoniation of Aryldiazonium Salts in Basic Alcoholic Solvents*, ***Journal of Organic Chemistry***, **1976**, 41 (12), 2157-2162.

41. A. Fernandez-Alonso, C. Bravo-Diaz, *Formation and Decomposition of Diazo Ether under Acidic Conditions. Effects of Ethanol Concentration, Acidity, and Temperature on the Ethanolysis of 4-Methylbenzenediazonium Ions*, ***Helvetica Chimica Acta***, **2010**, 93 (5), 877-887.

42. R. Pazo-Llorente, C. Bravo-Diaz, E. Gonzalez-Romero, *pH effects on ethanolysis of some arenediazonium ions: Evidence for homolytic dediazoniation proceeding through formation of transient diazo ethers*, ***European Journal of Organic Chemistry***, **2004**, (15), 3221-3226.

43. A. Fernandez-Alonso, M. J. P. Gallego, C. Bravo-Diaz, *Butanolysis of 4-methylbenzenediazonium ions in binary n-BuOH/H2O mixtures and in n-BuOH/SDS/H2O reverse micelles. Effects of solvent composition, acidity and temperature on the switch between heterolytic and homolytic dediazoniation mechanisms*, ***Organic & Biomolecular Chemistry***, **2010**, 8 (23), 5304-5312.

44. U. Costas-Costas, C. Bravo-Diaz, E. Gonzalez-Romero, *Micellar effects on the reaction between an arenediazonium salt and 6-O-octanoyl-L-ascorbic acid. Kinetics and mechanism of the reaction*, ***Langmuir***, **2004**, 20 (5), 1631-1638.

45. M. J. Pastoriza-Gallego, A. Fernandez-Alonso, S. Losada-Barreiro, V. Sanchez-Paz, C. Bravo-Diaz, *Kinetics and mechanism of the reaction between 4-hexadecylbenzenediazonium ions and vitamin C in emulsions: further evidence of the formation of diazo ether intermediates in the course of the reaction*, ***Journal of Physical Organic Chemistry***, **2008**, 21 (7-8), 524-530.

46. G. Schmidt, A. Filoramo, V. Derycke, J. P. Bourgoin, P. Chenevier, *Labile Diazo Chemistry for Efficient Silencing of Metallic Carbon Nanotubes*, ***Chemistry-A European Journal***, **2011**, 17 (5), 1415-1418.

47. C. Combellas, F. Kanoufi, J. Pinson, F. I. Podvorica, *Time-of-flight secondary ion mass spectroscopy characterization of the covalent bonding between a carbon surface and aryl groups*, ***Langmuir***, **2005**, 21 (1), 280-286.

48. C. Combellas, D. E. Jiang, F. Kanoufi, J. Pinson, F. I. Podvorica, *Steric Effects in the Reaction of Aryl Radicals on Surfaces*, ***Langmuir***, **2009**, 25 (1), 286-293.

49. C. Combellas, F. Kanoufi, J. Pinson, F. I. Podvorica, *Sterically hindered diazonium salts for the grafting of a monolayer on metals*, ***Journal of the American Chemical Society***, **2008**, 130 (27), 8576-8577.

50. P. Doppelt, G. Hallais, J. Pinson, F. Podvorica, S. Verneyre, *Surface modification of conducting substrates. Existence of azo bonds in the structure of organic layers obtained from diazonium salts*, ***Chemistry of Materials***, **2007**, 19 (18), 4570-4575.

51. A. Garcia, T. Berthelot, P. Viel, J. Polesel-Maris, S. Palacin, *Microscopic Study of a Ligand Induced Electroless Plating Process onto Polymers*, ***ACS Applied Materials & Interfaces***, **2010**, 2 (11), 3043-3051.

52. A. Garcia, J. Polesel-Maris, P. Viel, S. Palacin, T. Berthelot, *Localized Ligand Induced Electroless Plating (LIEP) Process for the Fabrication of Copper Patterns Onto Flexible Polymer Substrates*, ***Advanced Functional Materials***, **2011**, 21 (11), 2096-2102.

CHAPTER V

Graftfast™ process

The Graftfast™ process, recently developed in our laboratory, aims at functionalising any type of materials with polymers. In comparison to the redox-induced process previously presented, it widens the possibilities to tailor the surface properties of materials by increasing the range of functionalities that can be brought to the substrates. The Graftfast™ process is not restricted to commercial diazonium salts or aromatic primary amines but can be suitable for any vinylic monomer or monomers polymerising through a radical mechanism. Indeed, also based on a redox-induced reaction, it is likely that its mechanism also relies on the presence of radicals in solution. However, the mechanism of this Graftfast™ process has not been deeply studied and no experimental evidence of the radical mechanism originally proposed by Mévellec *et al*[1] had been obtained before the present work. Therefore, the purpose of this chapter is to determine a very likely mechanism based on experimental results for the grafting of PHEMA on gold. First of all, vinylic polymerization methods using diazonium salts will be examined. Then, the films will be characterized in terms of composition, structure, morphology, homogeneity and thickness. We will vary experimental parameters such as the ratios of the concentrations in reactants, the reaction time and the acidification of the solution in order to explore a wide range of grafting conditions. To finish, by combining surface with solution analyses, we will propose an explanation for the mechanism leading to the formation of polymer films on materials by the Graftfast™ process using ascorbic acid (VC) as reducing agent and we will deal with the possible modifications in mechanism according to the reducing agent considered.

V.1 - **Vinylic polymerisation utilising a diazonium salt**

The first use of diazonium salts in vinylic polymerisation was described in 1967 by Warson[2]. The author showed that the diazonium salt-hypophosphorous acid system is capable of acting as an initiator of the polymerisation of acrylonitrile in solution. The diazonium salt was present at 2 % of the molar concentration of acrylonitrile while a 5-fold excess of hypophosphorous acid as compared with the diazonium salt was used. The polymerisation of acrylonitrile in solution, accelerated by adding copper sulphate, was tested with various diazonium salts. The use of nucleophilic substituents on the benzene ring was found to reduce the efficiency of the polymerisation. An IR analysis and viscosity measurements revealed the presence of phosphorus in the resulting polymers. Therefore, according to those results, the author deduced that the hypophosphite radical ($H_2PO_2^{\bullet}$) was the initiator of polymerization. The reaction suggested to be responsible for the presence of $H_2PO_2^{\bullet}$ in solution was likely to involve the diazonium salt and particularly aryl radicals; but its formation remaineds unclear and several mechanisms were proposed (as represented in Scheme 60).

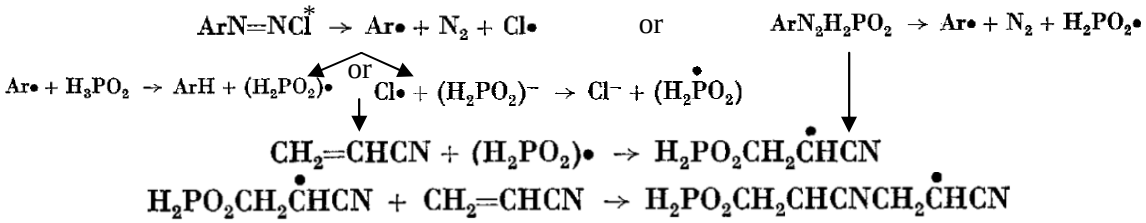

Scheme 60 – Proposed mechanisms for the initiation of acrylonitrile polymerization by hypophosphite radical extracted for Warson's work[2]. *This form would be due to the presence of Cl^- in acidic solutions.

Two techniques using diazonium salts in order to graft polymer chains on substrates were also reported: the SEEP process (electrochemical polymerization of vinylic monomer using diazonium salts) and an SI-ATRP process. They will not be described in details here since they have already been presented, respectively, in I.2.1.8 and I.2.2.2. Both methods are based on a first step consisting in the electrografting of diazonium salt as a primer-layer. Contrary to SEEP, SI-ATRP leads to the grafting of controlled polymer chains but it is a two-step process in which the formation of a polyphenylene-like film with an adequate function allows the subsequent ATRP step. Due to the first electrochemical step, both processes are limited to conducting materials. The Graftfast™ process overcomes these limitations since it is based on the redox-induced grafting of diazonium salts (described in the previous chapter) in presence of a vinylic monomer and thus can be theoretically suitable for any type of materials. Contrarily to the mechanism proposed by Warson described above[2], Mevellec *et al.*[1] suggested a mechanism similar to the one deeply investigated of the SEEP process[3] which could be split in four steps:

(1) The chemical reduction of the diazonium salt leading to the formation of the corresponding aryl radicals;
(2) The grafting of aryl radicals forming a polyphenylene-like layer in parallel with the initiation by those radicals of the radical polymerization of the vinylic monomer in solution;
(3) The interaction of the growing radical polymer chains with the PNP primer-layer to give a grafted "copolymer" film;
(4) The growth of the polymer film induced by the successive grafting of the growing radical chains on phenyl groups embedded in the already grafted film.

However, except for the first step for which evidences were recently found as detailed in chapter IV, this mechanism has not been demonstrated experimentally. Therefore, by a deep investigation of the composition and structure of the films, of the experimental parameters involved in the synthesis and of the composition of the solution, we will corroborate this mechanism and discuss its variations according to the reducing agent.

V.2 - Characterization of the Graftfast™ films

The grafting of polymer with the Graftfast™ process will be deeply studied. To start with, the grafted polymer will be characterised by classic surface analyses; the structure, homogeneity and conformity of the films will be examined and finally, the determination of the thickness of the films as well as of the degree of polymerization of grafted polymer chains will be discussed. Since ascorbic acid (VC) was shown to be a suitable reducing agent for the study of the grafting mechanism, experiments presented in this chapter will mainly be performed with VC.

V.2.1 - Typical films

As explained in II.3.3, we focused on the grafting of poly(hydroxyethyl) methacrylate PHEMA (represented in Scheme 61). This polymer is water soluble, easily identifiable by IR and XPS and does not contain nitrogen atoms, which permits to attribute all nitrogen detected to moieties from the diazonium salt. A typical resulting PHEMA film was analysed after the rinsing procedure described in II.3.5 and compared to a commercial PHEMA spectrum (Figure 58). The two spectra are very similar, particularly in the 1730 cm^{-1} absorption band (stretching vibration of C=O groups) meaning we actually grafted PHEMA on gold substrates by the Graftfast™ method. However, additional peaks in the Graftfast™ PHEMA grafted films are observed and, as in III.3.1 and IV.1.2, are attributed to NO_2 groups (1525 and 1350 cm^{-1}) meaning that nitrophenyl groups are also present in those films.

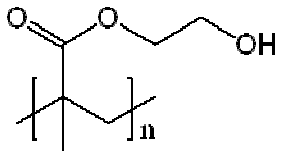

Scheme 61 – Poly(hydroxyethyl) methacrylate PHEMA (n denotes the degree of polymerisation).

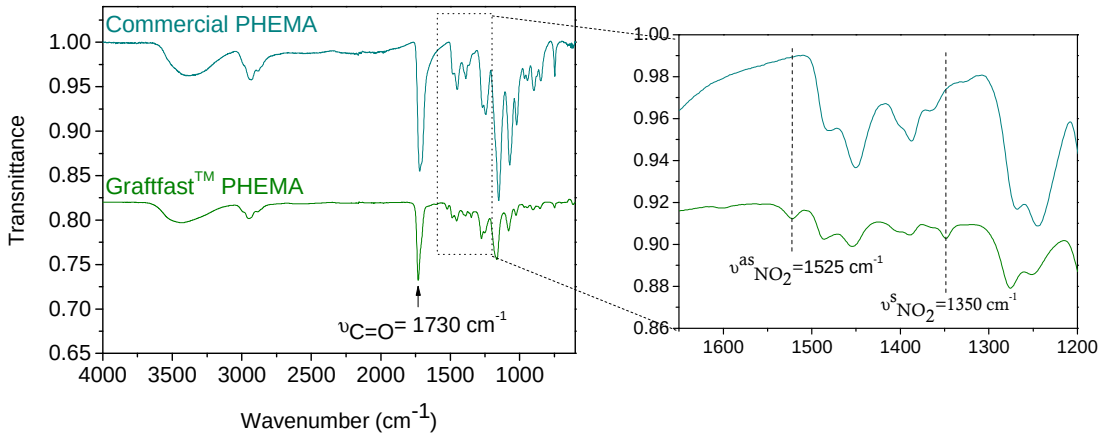

Figure 58 – Comparison of IR-ATR typical spectra of commercial PHEMA and a PHEMA film on a gold plate obtained by the Graftfast™ process (NBDT 0.046 M (1 eq), VC 1/10 eq, HEMA 15 eq, H_2O DI, 60 min) with a zoom in the 1200-1650 cm^{-1} region.

In addition, contact angle measurements (Figure 59) are in agreement with the presence of PHEMA on the gold surface since a classical value between 50-60° was found (instead of 99° for a pristine gold substrate). This value could also be typical of a polynitrophenylene-like layer as observed in IV.1.2. Therefore, a contact angle value in this range could also correspond to a mixed film containing PHEMA chains as well as nitrophenyl groups, as suggested by IR results.

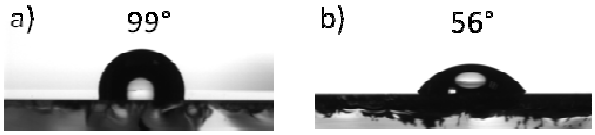

Figure 59 – Static water contact angle of a) pristine, b) PHEMA grafted (Graftfast™ process: NBDT 0.046 M (1 eq), VC 1/10 eq, HEMA 15 eq, H_2O DI, 60 min) gold plates.

XPS analyses were also carried out to characterise the grafted film. A typical survey spectrum as well as Au 4f, C 1s, O 1s and N 1s core level spectra are presented in Figure 60. The C 1s core level spectrum is composed of three main peaks. The peak centred at 285.0 eV corresponds to alkyl groups, -C-O- or -C-N- simple bonds appear at 286.6 eV and the peak at a higher binding energy (289.0 eV) is assigned to the carboxylate ester group COO confirming the grafting of PHEMA on the gold substrates. It is not surprising that the π - π^* shake-up satellite from benzene rings cannot be seen in our experiments since, as mentioned in appendix 5, it is likely that in comparison to PHEMA, aromatic rings are present in very low amounts in the polymer film. Therefore, C 1s spectra are only displayed with a maximum binding energy of 292 - 293 eV.

The O 1s spectrum displays three peaks attributed to single or double carbon-oxygen bonds. A ratio of 1 between all those contributions fits expectations for PHEMA.

In the N 1s core level analysis, we obtained a complex spectrum including nitro groups (NO_2) at 406.0 eV but also azo and amino groups gathered in a broad peak centred at 400 eV and a small Au-N contribution as detailed in III.3.1 which is characteristic of a PNP layer. Therefore, XPS results also demonstrate the presence of nitrophenyl groups inside the PHEMA films.

Finally, the Au 4f core level spectrum still shows the characteristic peaks of gold. This result is somewhat surprising. Indeed, according to profilometer thickness measurements (see V.2.3) the analysed Graftfast™ PHEMA grafted film is 23 ± 2 nm thick in average. However, the XPS technique only allows probing the outer 10-15 nm of the sample[4]. Therefore, no signal corresponding to the gold atoms should be detected.

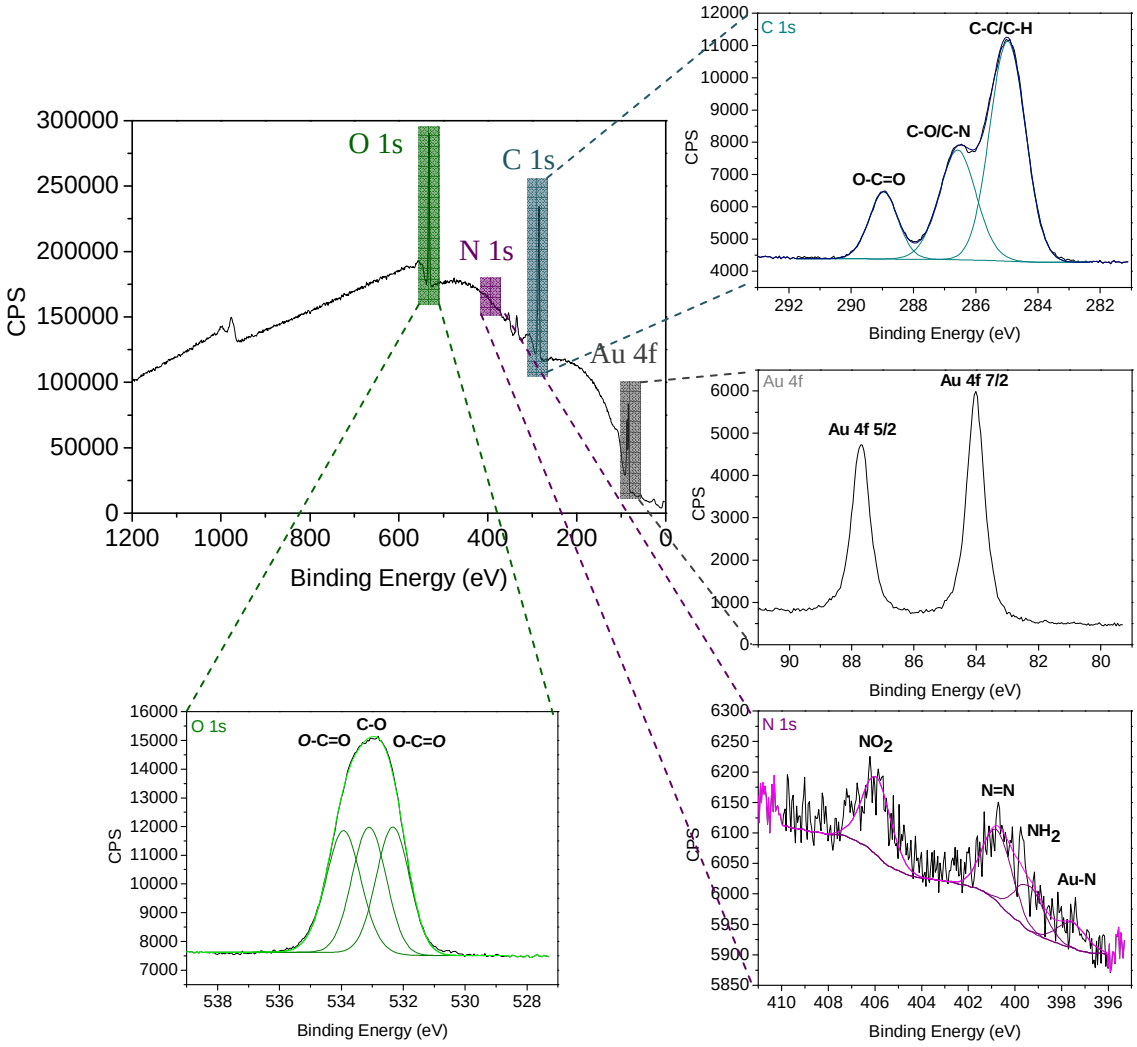

Figure 60 – XPS survey, C 1s, Au 4f, O 1s and N 1s core level spectra of a typical PHEMA film on a gold plate obtained by the Graftfast™ process (NBDT 0.046 M (1 eq), VC 1/10 eq, HEMA 5 eq, H_2O DI, 60 min).

In order, to understand this phenomenon, we compared the XPS area of the latter Au 4f 7/2 peak for two grafted PHEMA films of different thickness to pristine gold (Table 17). The area of this XPS peak is ten times smaller for the first PHEMA grafted film (Graftfast™ 1) than for the bare substrate. Moreover, the thicker the polymer film, the smaller the Au 4f 7/2 area. However, even for a 36 nm thick film, the signal of gold is still observed meaning that photoelectrons have found a way out the film and were collected on the detector. It is likely that this phenomenon is due to a low grafting density of the film or to its porosity.

Table 17 – Comparison of film thickness and Au 4f 7/2 area values of pristine and two PHEMA grafted gold substrates (Graftfast™ process: NBDT 0.046 M (1 eq), VC 1/10 eq, HEMA 5 eq (Graftfast™ 1) and 25 eq (Graftfast™ 2), H_2O DI, 60 min).

	Pristine gold	**Graftfast™ 1**	**Graftfast™ 2**
Thickness (nm)	-	23 ± 2	36 ± 3
Area Au 4f 7/2 (CPS.eV)	42170	4260	677

In addition to this difference on the Au 4f core level spectrum, by comparing two PHEMA grafted films of different thickness, a variation in the N 1s core level spectra was also noticed. The corresponding measurement is shown in Figure 60 for the 23 nm thick film and in Figure 61 regarding the 36 nm thick film. In the latter case, the amount of nitrogen is very weak to such an extent that it is almost impossible to accurately fit the signal with peaks. As XPS is sensitive to the outer part of the sample, the thicker the film, the less the interface film-substrate is probed. Therefore, we assumed that, similarly to what was concluded for the SEEP process, the interface film-substrate is richer in nitrogen (i.e. in moieties arising from the diazonium salt) than the bulk of the grafted film.

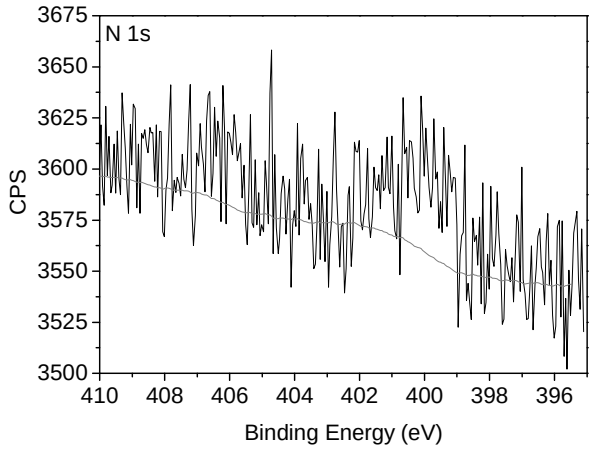

Figure 61 – N 1s core level spectrum of a PHEMA film on a gold plate obtained by the Graftfast™ process (NBDT 0.046 M (1 eq), VC 1/10 eq, HEMA 25 eq, H_2O DI, 60 min).

V.2.2 - **Structure of the films**

In order to confirm the localization of the nitrophenyl moieties in the film and to understand better the grafting mechanism of the Graftfast™ process, particular attention was paid in the determination of the film structure. A detailed analysis of the whole thickness of the film from the upper part (superficial) to inner part (interface area) was performed by ToF-SIMS experiments in abrasion mode. Indeed, the obtained ToF-SIMS depth profile gives the normalized intensity of the collected ionized fragments resulting from ion bombardment of the Graftfast™ film as a function of the abrasion time. Therefore, by identifying the fragments characteristic of nitrophenyl groups or PHEMA and by following their evolution according to the abrasion time, it is possible to determine the structure of the Graftfast™ films.

Various ions were detected on each negative ToF-SIMS spectra. The characteristic fragments of the nitrophenyl groups, the polymer or the gold substrate are summarized in Table 18.

Table 18 – Ions of interest detected in the negative Tof-SIMS abrasion spectra of a typical Graftfast™ PHEMA grafted on gold plates (NBDT 0.046 M (1 eq), VC 1/10 eq, HEMA 15 eq, H_2O DI, 60 min), their corresponding experimental mass and their attribution in the film.

Ion formula	Mass (m/z)	Fragment characteristic from	
$[NO]^-$	30.00	Nitrophenyl groups	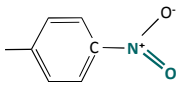
$[CNO]^-$	42.00	Nitrophenyl groups	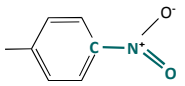
$[NO_2]^-$	46.00	Nitrophenyl groups	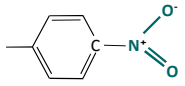
$[C_2H_5O_2]^-$	61.03	PHEMA	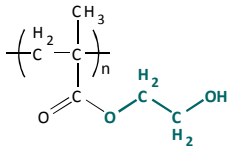
$[C_4H_5O]^-$	69.04	PHEMA	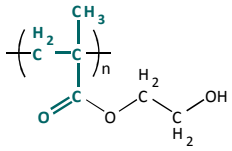
$[C_4H_5O_2]^-$	85.03	PHEMA	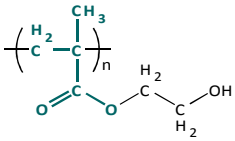
$[C_6H_4NO_2]^-$	122.02	Nitrophenyl groups	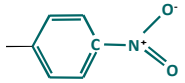
$[Au_2]^-$	393.94	Gold substrate	

For the sake of clarity, only the profiles of the most intense fragments characteristic of each different constituent of the film were plotted on Figure 62. Nitrophenyl moieties are represented by the fragment $[CNO]^-$, PHEMA by $[C_4H_5O_2]^-$ and the substrate by $[Au_2]^-$. An abrasion time of zero corresponds to the top of the film. The normalized depth profile of a Graftfast™ PHEMA film is presented in Figure 62a. When abrading the sample, three different phases are observed:

(1) First, there is an important decrease in the intensity of the fragment corresponding to the polymer. This phenomenon is due to charge effects from the bombardment with charged ions of a non-charged material and is therefore not significant.

(2) Then, the PHEMA fragments keep a constant intensity value until an abrasion time of around 70 s.

(3) After this abrasion time, the intensity of those fragments starts to decrease while the intensity of the nitrophenyl groups increases. This is followed by the increase of the signal of the fragment corresponding to gold meaning that the substrate is reached.

Contrary to fragments from PHEMA, the amount of the $[CNO]^-$ fragments from nitrophenyl groups increases just before the substrate is probed with a slope almost similar to the gold one.

This is consistent with the presence of a very thin PNP sub-layer near the interface film-substrate. However, nitrophenyl fragments are undoubtedly present is the entire film thickness since they were also detected in the top part of the films (intensity recorded at low abrasion times not null) but in lower amount than near the interface. Such observation can be in agreement with the initially proposed grafting mechanism. Indeed, the initiation of the HEMA polymerization by nitrophenyl radicals would spread nitrophenyl groups throughout the full polymer thickness up to the top of the film.

For comparison purpose, the normalized depth profile of a spin-coated PHEMA film on top of a thick PNP layer (obtained from a specific process under patent submission) is shown in Figure 62b. According to the repartition of the various fragments in the depth of the films, the outer of this sample is composed of PHEMA layer. Underneath, there is an intermediate zone made of a mix between PHEMA fragments and nitrophenyl groups. Then, a pure PNP layer is detected and the substrate is reached. This depth profile is quite similar to the Graftfast™ PHEMA profile in Figure 62a which confirms the structure of the Graftfast™ films. However, in the case of the Graftfast™ PHEMA film, it seems that there is not a clear separation between the PHEMA and the PNP layers. Indeed, the intensity of the PHEMA fragments is only null when the substrate is reached. Therefore, polymer chains are also present very close to the interface film-substrate but in smaller amount in comparison to the outer part of the films.

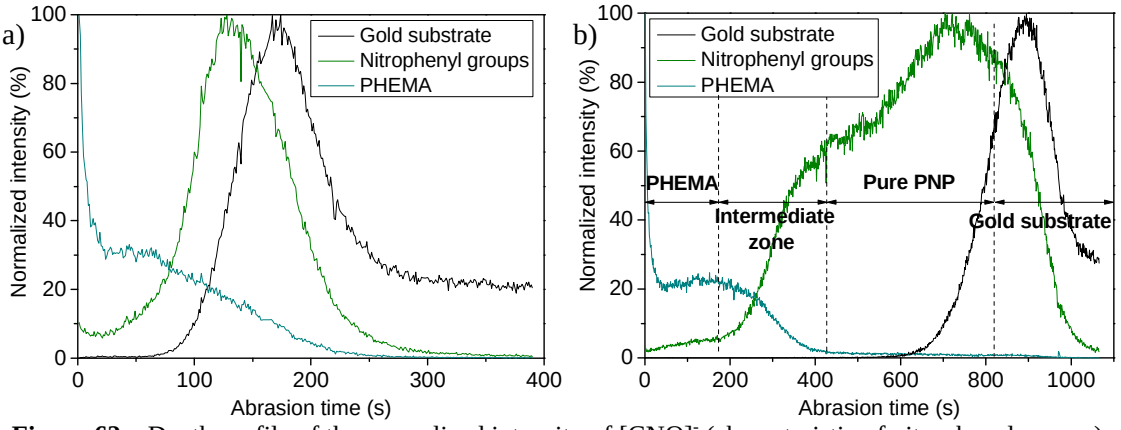

Figure 62 – Depth profile of the normalized intensity of $[CNO]^-$ (characteristic of nitrophenyl groups), $[C_4H_5O_2]^-$ (characteristic of PHEMA) and $[Au_2]^-$ (characteristic of the gold substrate), ions detected on the negative ToF-SIMS spectra of a) a typical Graftfast™ PHEMA grafted on gold plates (NBDT 0.046 M (1 eq), VC 1/10 eq, HEMA 15 eq, H_2O DI, 60 min) and b) a spin-coated PHEMA film on top of a PNP layer[a].

To summarize, according to the ToF-SIMS results, we have confirmed that the Graftfast™ PHEMA films are rich in nitrophenyl groups near the interface film-substrate but such moieties are also present in smaller amount up to the surface of the films (probably due to the fact that they initiate the polymerization). The polymer is found in the all depth of the film and mixes to

[a] Only qualitative comparison of those two profiles can be made. Moreover, for the sake of clarity, the spectra were normalized in intensity. Therefore, y-axes are not comparable.

nitrophenyl groups near the interface with the gold plate. The deduced structure of the Graftfast™ film is presented in Scheme 62[b] and is similar to the one of films obtained by the electro-induced process SEEP[5].

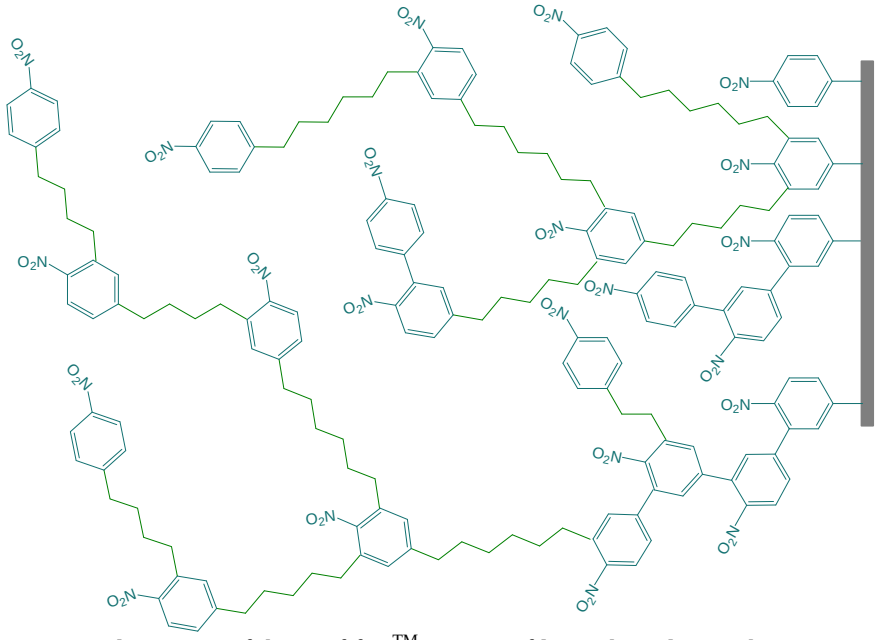

Scheme 62 – Proposed structure of the Graftfast™ PHEMA films. The polymer chains are represented in green and the nitrophenyl moieties in blue.

V.2.3 - **Morphology and conformity**

To go further in the characterization of the PHEMA films, AFM measurements were performed on a bare gold substrate and a Graftfast™ PHEMA film on gold.

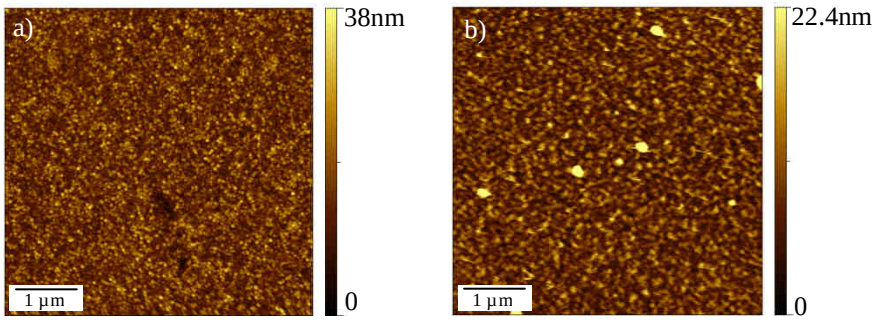

Figure 63 – 5 x 5 µm² AFM images of a) a pristine gold substrate and b) a Graftfast™ PHEMA on gold (NBDT 0.046 M (1 eq), VC 1/10 eq, HEMA 15 eq, H_2O DI, 60 min).

From the AFM images of a pristine gold plate (Figure 63a) and a PHEMA grafted film (Figure 63b), we calculated a roughness value of, respectively, 4.5 nm and 3.8 nm. This shows that the PHEMA layer is highly conform to the gold substrate and may, as in this case of a 35 nm thick film, slightly flatten it. Thus, Figure 63b confirms the conformity of the film to the

[b] All polymer chains are represented attached on an aromatic ring according to the results presented in V.4.3 on the importance of a primer PNP sub-layer on the grafting. For the sake of clarity, neither the degrees of polymerisation of the PHEMA chains nor the presence of amino or azo groups are taken into account.

substrate and gives also information on the morphology of the films. Indeed, this AFM image demonstrates the "grainy" morphology of the PHEMA grafted films. Similarly to what was observed by Tessier *et al.*[3] for electrochemically grafted PHEMA films, it is likely that the thicker the organic layer, the more flattened the initial morphology of the substrate, as illustrated by Scheme 63. The presence of high dots on the scanned area could be attributed (i) to dust on the substrate, (ii) to the presence of gold areas with a higher reactivity leading to the grafting of more polymer or (iii) simply remaining physisorbed polymer which was not discarded by the rinsing procedure.

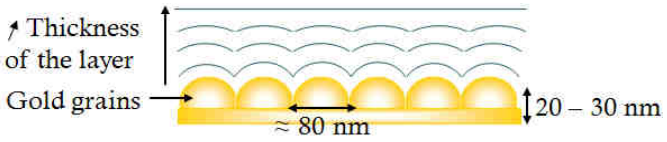

Scheme 63 – Scheme of the changes in morphology of the films due to the flattening effect induced by the increase of the polymer thickness, extracted from the work of Tessier[3].

V.2.4 - **Homogeneity**

The determination of the influence of experimental parameters on the films in order to investigate the mechanism will be mainly based on comparisons between IR intensities values of the stretching vibration of C=O groups. Therefore, it is important to evaluate the variations in IR absorption between values measured along the same substrate as well as on various substrates immersed in the same reactive solution.

First, by performing twelve measurements along the same PHEMA grafted film (Figure 64), an average intensity value of 7.5 ± 1.1 % was calculated. Therefore, the IR absorption value of a sample can be determined with a variation of plus or minus 15 %. As mentioned in IV.1.2.1, this discrepancy could be due to the variability of the ATR measurements but also to the homogeneity of the organic film itself. To get a better idea of the homogeneity of the PHEMA films, substrates were characterized at a smaller scale by IRRAS.

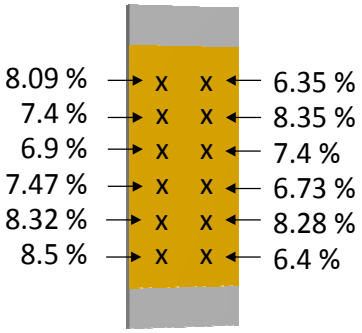

Figure 64 – Intensity of the $\nu_{C=O}$ absorption band from the IR-ATR analysis along the gold substrate (26 x 70 mm^2) of a PHEMA film grafted with the Graftfast™ process (NBDT 0.046 M (1 eq), VC 1/10 eq, HEMA 15 eq, H_2O DI, 60 min).

The IRRAS mapping, focused on the most intense band of the polymer (at 1730 cm^{-1}), is presented in Figure 65. It seems that, in this 17 x 4 mm^2 square, the IR intensities are very similar except in singular points. Indeed, each peak on the mapping represents a single point of

measurement for which more PHEMA is present. Such peaks are consistent with the dots that were observed by AFM (Figure 63b). However, they do not constitute the main part of the sample. Therefore, we can consider the grafting as homogeneous with a variation of ± 15 % on the IR values.

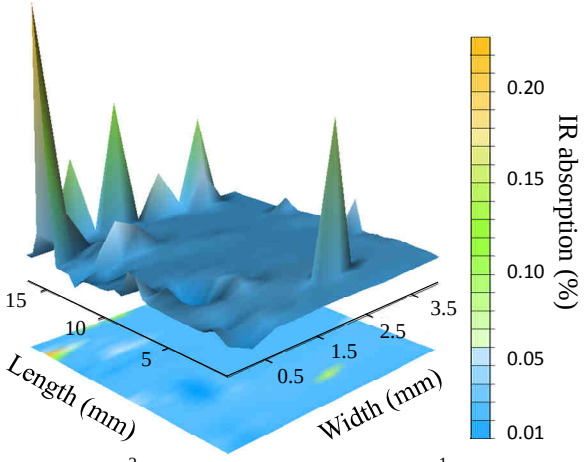

Figure 65 – IRRAS mapping (68 mm^2) of the $\nu_{C=O}$ band (1730 cm^{-1}) from a typical PHEMA layer grafted by Graftfast™ (NBDT 0.046 M (1 eq), VC 1/10 eq, HEMA 15 eq, H_2O DI, 60 min). A measurement was performed every 430 µm in both directions.

To finish, by analysing three different samples grafted at the same time and in the same reactive solution, we found out that the IR-ATR intensity average value was also obtained with a variation of ± 15 %. Thus, the same variation value on the IR measurements is reached when averaging various absorption values from the same sample or one IR value from three different samples. Therefore, in order to reasonably limit the number of measurements to characterize one experiment, for the rest of this work, we decided to perform IR measurements in the middle of three samples grafted simultaneously and to take the average value.

V.2.5 - **Reproducibility of the syntheses**

Let us now focus on the reproducibility of the process. In order to estimate the reproducibility of the experiments, the dispersion of the intensity values of $\nu_{C=O}$ was evaluated in the case of several PHEMA films grafted on gold, prepared in identical conditions over a year. These IR intensities as well as the average and the standard deviation of those data, calculated from the equation 5.1, are reported in Table 19.

The IR-ATR intensities are not constant from a Graftfast™ experiment to another one. If we consider the difference between the average and extreme values, for these experiments, the IR intensities are determined at plus or minus 44 %. Therefore, it seems that the process is poorly reproducible at least from a laboratory point of view. Such a dispersion of the values between theoretically “identical” samples could come from:

- the homogeneity of the film. As detailed in the previous part, the IR intensities are obtained with a variation of ± 15 %.

- a difference in reactivity of the gold plates. Indeed, the reactivity of the substrates can vary, for instance, according to their contamination, the time of storage, their preparation. In the latter case, the quality of the evaporated gold strongly depends on the parameters such as the cleanliness of the evaporation chamber and the cleaning of the glass plates.
- a variation in the reactants. In the case of ascorbic acid, the same batch was used during the whole work. However, the diazonium salt as well as the monomer came from different batches, because the consumption did not allow keeping the same one. Moreover, the purification of the diazonium salt by reprecipitation could provide batches of different purity.
- the atmosphere of the reaction. The diazonium salt is highly sensitive to temperature and light. Therefore, variations of such parameters could affect the synthesis. The humidity level in the air could also influence the reaction.
- the IR measurement. As mentioned in III.3.1, the IR-ATR measurements are sensible to the pressure applied on the sample and its contact with the diamond crystal[c]. Moreover, the determination of the intensity value depends on the base line of the spectrum.

$$\sigma = \sqrt{\frac{1}{n}\left(\sum_{i=1}^{n} x_i^2\right) - \bar{x}^2} \text{ with } \bar{x} = \frac{1}{n}\sum_{i=1}^{n} x_i \qquad (5.1)$$

Table 19 – Intensity value of $\nu_{C=O}$ band for Graftfast™ PHEMA films synthesized in identical conditions over a year (NBDT 0.046 M (1 eq), VC 1/10 eq, HEMA 15 eq, H_2O DI, 60 min).

Date (DD/MM/YY)	I $\nu_{C=O}$
15/12/09	8.05 %
26/01/10	7.61 %
23/04/10	5.99 %
31/05/10	4.5 %
30/06/10	5.28 %
24/09/10	5.4 %
06/10/10	8.75 %
15/10/10	10.19 %
03/11/10	5.4 %
14/01/11	9.76 %
Average $\bar{x}$	7.09 %
Standard deviation σ	1.9 %

In order to reduce such disparities in the IR intensities values, we tried to limit the effect of some of the parameters listed above. Comparisons will only be made between samples grafted on the same day, from the same reactants and on gold plates from the same evaporation batch. That way, we assume that the measurements are mainly influenced by the homogeneity of the

[c] This error is however already taken into account when calculating an average IR value from various samples.

films and the variability of the ATR measurements. Therefore, a variation of ± 15 % on the IR intensity values will be considered, as evaluated above.

V.2.6 - **Thickness of the films**

Beyond chemical characterizations of the polymer, it is also very important to determine the thickness of the grafted layers. Various techniques can be used to do so. First, the thickness of films can be evaluated from XPS data. It can also be reached by optical measurements with an ellipsometer and by mechanical measurements using a profilometer. To finish, as we will see that all those methods present drawbacks, we will propose another way to estimate the film thickness in the specific case of PHEMA based on the establishment of an abacus linking the IR intensity of the carbonyl band with the thickness measured by the previously described methods.

V.2.6.1 - Thickness calculations from XPS data

According to the equation (5.2), the thickness of thin films can be calculated from the decrease in intensity of the XPS gold signal observed between a pristine and a coated substrate.

$$\frac{I}{I_0} = e^{\left(-\frac{d}{\lambda \sin\theta}\right)} \quad \text{with} \quad \begin{array}{ll} I & \text{Intensity of the grafted sample (Au 4f 7/2)} \\ I_0 & \text{Intensity of the pristine sample (Au 4f 7/2)} \\ d & \text{Thickness of the organic layer} \\ \lambda & \text{Attenuation length of electrons} \\ \theta & \text{Angle of the XPS beam with the substrate} \end{array} \tag{5.2}$$

Since in all our experiments, XPS measurements were performed in normal incidence ($\theta = 90°$), the thickness of the layer is given by the following equation:

$$d = -\lambda \cdot Ln\frac{I}{I_0} \tag{5.3}$$

This formula was used by Whitesides and coll[6] for thickness determination of self-assembled monolayers (SAMs) of alkanethiols on Au(111) and values of λ were determined in this specific case ($\lambda = 42 \pm 1.4$ Å for a kinetic energy of photoelectrons of 1402 eV corresponding to Au 4f 7/2). However, applying this method to our films is not straightforward. First, since we are dealing with polyphenylene-like or polymer films, no value of the attenuation length of electrons was estimated for such films. Nevertheless, as a first approximation, for very thin PNP films λ values associated to alkanethiols layers could be used. However, this technique is limited to films thinner than approximately 10 - 15 nm (value corresponding to the maximum escape depth of electrons from the substrate).

To start with, we applied this method for the thickness calculation of pure polyphenylene-like films on gold as those formed in chapters III and IV. The Au 4f 7/2 intensity of a pristine gold substrate after abrasion of its surface in the XPS chamber to remove carbon and oxygen contamination was used as I_0. It was found that the thicknesses calculated for PNP

layers were identical to the one estimated in the case of a non-abraded pristine gold sample, i.e. identical to a contamination layer. Therefore, this method is not adapted for the determination of the thickness of PNP layers. It is neither efficient for the evaluation of thickness of PHEMA films. Indeed, as developed in V.2.1, the attenuation of the gold signal is unexpected for PHEMA films obtained by the Graftfast™ process since 36 nm thick films (profilometer measurement) can still display peaks corresponding to Au 4f 7/2. Therefore, the above formula will likely underestimate the thickness of the film. Moreover, films a lot thicker than 10 nm are often formed by the Graftfast™ process. To conclude, this technique based on XPS data is not suitable in our case for the thickness determination of neither PNP layer nor PHEMA films. Consequently, we focused on other methods and particularly profilometry.

V.2.6.2 - Thickness measurement by profilometry

Profilometry is a mechanical technique based on the variations in height, due to the profile of the surface, of a stylus in contact with the sample and moving along it. Often used to measure roughness of substrates, it could also be employed for thickness measurements when a "step" between the layer and the pristine substrate exists. Such configuration can be difficult to obtain since our sample are completely immersed in the reactive solution. Various techniques were tested in order to create this step. The method giving the best defined "step" consists in performing a manual straight "scratch" of the sample with a wooden stick. This removes the organic layer without, *a priori*, damaging the gold layer and forms a line potentially free of the polymer. A typical profile obtained by this technique to determine the thickness of the polymer film (35 ± 3 nm) is presented in Figure 66.

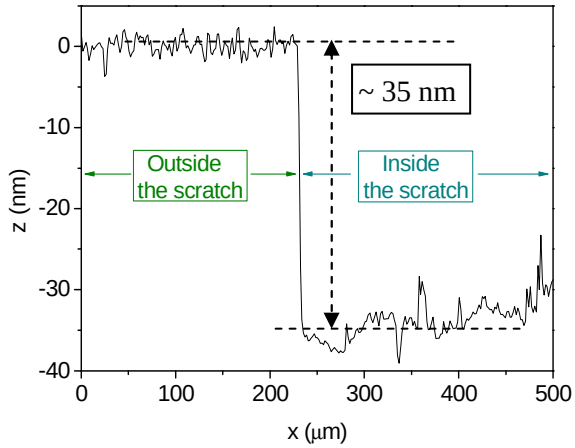

Figure 66 – Typical profile obtained with a profilometer of a PHEMA layer on gold in the area of the hand-made scratch (NBDT 0.046 M (1 eq), Iron, HEMA 15 eq, HCl 0.5 M, 60 min).

It is evident that the accuracy of those thickness measurements strongly depends on the formation of the "step". The thicker the film, the easier the creation of this step. However, remaining polymer inside the scratch is always of possibility and could lead to an underestimation of the thickness of the films. Therefore, small spot XPS measurements were performed inside and outside the scratch (Figure 67). From the higher intensity of the gold

signal inside the scratch, it is obvious that an important part of the organic film was removed from the substrate. Moreover, the area of total carbon is also strongly smaller when analysing the inside of the scratch, while nitrogen peaks only slightly diminuish. However, some nitrogen (in particular Au-N bonds representative of the interface film-substrate) were still detected inside the scratch as well as some carbon corresponding to the polymer (C=O band). Therefore, it seems that most of the polymer film is eliminated when scratching the sample. Nevertheless, similarly to the results of Charlier *et al.*[7] after the nanofriction of a PNP electrografted layer with an AFM tip, a small part of the organic film remains grafted, which induces an unmeasurable error in the thickness measurement.

Consequently the following question raised: in the case of the Graftfast™ PHEMA films, does it exist another method giving a more accurate thickness value of the films?

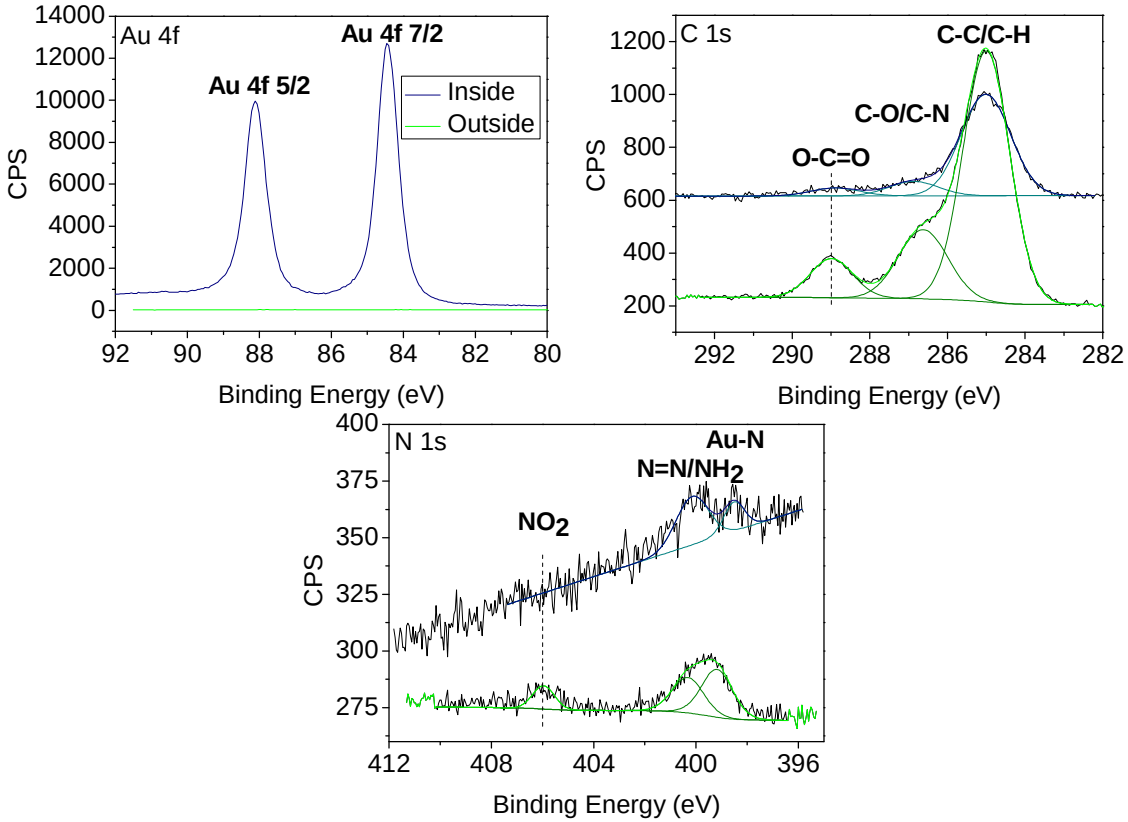

Figure 67 – Au 4f, C 1s and N 1s core level spectra outside and inside the scratch performed on a typical PHEMA film on a gold plate (NBDT 0.046 M (1 eq), Iron, HEMA 15 eq, HCl 0.5 M, 60 min).

V.2.6.3 - Thickness measurement by ellipsometry

Among the common method for thickness measurements, ellipsometry appeared as a potential candidate. It is an optical technique consisting in the analysis of the changes in polarisation of light upon reflection on a surface. Among the various applications of this characterization tool, thickness measurement was widely used in the case of “thin” films such as non-reflective layers, gold coatings and so on. This method is mainly suitable for substrates

composed of a small number of discrete and well-defined layers that are optically homogeneous and isotropic.

Thus, drawbacks of this technique for the thickness characterization of the Graftfast™ PHEMA films are quite obvious. First, those films are likely to be formed from a mix from PHEMA polymer chains and moieties from the diazonium salt. The refractive index of such a layer is unknown and no layer model has been established. Moreover, as detailed in V.2.4, the homogeneity of the polymer film might not be good enough for that method. To finish, the roughness of the gold substrate as well as the one of the film could be a problem for the measurement.

Ellipsometry experiments were performed (see appendix 1) using a layer model of a single organic layer on gold. Considering the factors of uncertainties in measurement mentioned above, the thicknesses of the films obtained by ellipsometry were not determined with a higher accuracy than those measured by profilometry (this could be for instance enhanced by defining a layer model closer to the reality of our films). Moreover, as we do not have the experimental apparatus in our laboratory, systematic thickness measurements of the grafted films are difficult. Therefore, we propose a method to quickly access the value of the thickness of the films by coupling ellipsometer and profilometer measurements with IR absorption intensities.

V.2.6.4 - IR intensity/thickness abacus for a rapid thickness determination

The IR-ATR technique is a non-quantitative method. However, the intensity of an absorption band, characteristic of the film (in our case $\upsilon_{C=O}$ at 1730 cm^{-1}), can be correlated to the thickness of the films *via* an abacus. To do so, Graftfast™ PHEMA films of various thicknesses were characterized by IR and profilometry/ellipsometry. The values are reported on the abacus in Figure 68. No values are presented for films thinner than 10 nm since both techniques are not suitable to measure such thicknesses.

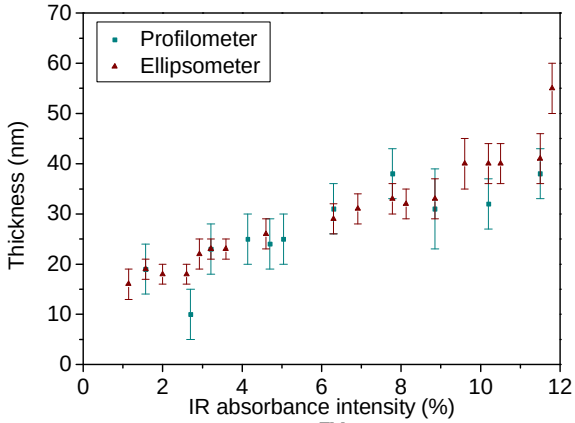

Figure 68 – IR intensity of the $\upsilon_{C=O}$ band for Graftfast™ PHEMA films of various thicknesses on gold (obtained in different conditions using VC[d]). The error bars indicate the uncertainties in measurement.

[d] No experimental data are presented for IR absorption intensity superior at 12 % i.e. thicker PHEMA films since in this work, we rarely obtained such films using ascorbic acid and in a reproducible way.

First of all, it is interesting to notice that the graphs obtained in the case of profilometry and ellipsometry experiments are very similar meaning that both techniques give close thickness values. This also indicates that this abacus is not dependent on the method chosen to measure the thickness of the PHEMA films. Besides, as it can be observed on this figure, for thickness values smaller than around 40 nm, it seems that there is a linear relationship between the IR intensity of the carbonyl band and the thickness of the polymer films. This result demonstrates that the comparison of the films in terms of thickness can reasonably be based on the measurement of the IR absorption intensity.

Therefore, in the rest of this chapter, the influence of the experimental parameters on the film growth i.e. on the film thickness will be achieved by directly comparing IR intensities of the $\upsilon_{C=O}$ IR band instead of thicknesses measured by ellipsometry (which cannot be daily performed in our laboratory) or profilometry (for which a scratch is required). Thus, the abacus (Figure 68) gives the correspondence between the IR intensity and the thickness of the film. This method is rapid, simple and can be systematically performed since IR is a common characterization tool. However, it is important to be aware of the limitations of this technique:

- The correlation between IR intensity and thickness is based on the assumption that there is no preferential orientation effect of the carbonyl groups in the films.
- This method is only suitable for the evaluation of relative thickness. The thickness values of two films can be compared one with the other but an absolute thickness value cannot be precisely determined.
- This technique is only suitable in the specific case of Graftfast™ PHEMA films on gold very probably obtained in presence of the same reducing agent since thickness values not fitting this linear relationship were determined for films synthesized with iron powder as reducing agent (see V.4.5.2 for a possible explanation).

V.2.7 - **Degree of polymerization of PHEMA grafted chains**

In order to fully characterize the Graftfast™ films, the last parameter to evaluate is the length of the PHEMA chains (molecular weight or degree of polymerization). To do so, two methods were used: size exclusion chromatography (SEC) and XPS. In the former case, the degree of polymerization of chains in solution can be potentially determined. Assuming that polymer chains formed in solution have the same characteristics as those grafted on the substrates, this method could give a rough idea of the value concerning grafted polymer chains on gold substrates. In the latter case, thanks to a few approximations, the degree of polymerization of grafted PHEMA chains was estimated.

V.2.7.1 - Size exclusion chromatography

To get information on the molar mass of the polymer by SEC, a calibration using standards of known molar mass has to be performed. However, SEC is a chromatography method based on the separation of macromolecules according to their hydrodynamic volume. Thus, a non-linear macromolecule would fill a higher volume than a linear macromolecule of identical molecular weight and be consequently eluted more rapidly in the column. Therefore, PHEMA standards of similar architecture of the polymer obtained by the Graftfast™ process are required. However, the architecture of the polymer in the case of the Graftfast™ process is unknown. Similarly to the probable grafting mechanism, it is likely that, in parallel to a classic polymerization pathway, growing polymer chains can potentially terminate onto nitrophenyl groups (present in the chain since they initiate the polymerization). Such phenomenon could lead to the formation of random non-linear polymer chains. Moreover, the mix composition of the polymer (due to presence of aromatic rings) can also affect the behaviour of the polymer in the SEC column. Therefore, no polymer standard mimicking the unidentified architecture and composition of the Graftfast™ PHEMA exists. Hence, the evaluation of the degree of polymerization of the Graftfast™ PHEMA is impossible. Only qualitative comparisons in signal intensity are relevant in the case of the study of the Graftfast™ solutions. Size exclusion chromatograms of a typical Graftfast™ solution at various reaction times are presented in Figure 69. The shorter polymer fragments take longer time to exit the column.

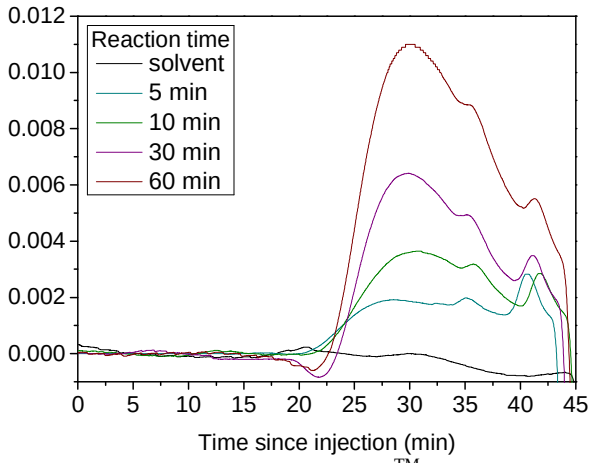

Figure 69 – Size exclusion chromatography of a Graftfast™ solution (NBDT 0.046 M (1 eq), VC 1/10 eq, HEMA 15 eq, H_2O DI) at various reaction time.

First of all, it is clear that whatever the solution analysed, there is a continuous distribution in polymer size. Moreover, all the molecular weights observed are already present after five minutes of reaction meaning that the polymerization in solution starts in the first 5 min of reaction. However, the detection is provided by a refractive index detector which measures the variation in refractive index of the analysed solution in comparison with a reference solution (mobile phase). Therefore, as polymer chains of different molecular weights are likely to have different refractive index values, they cannot be quantitatively compared. Only comparisons in

intensities of the polymer chains according to the reaction time can be made. It is obvious from Figure 69 that, as expected, whatever their molecular weight there is a linear increase in the number of polymer chains (growing or terminated) with reaction time. Particularly, the variations between 30 and 60 min reaction times indicate clearly that even the shortest polymer were created in the last 30 min of the reaction. This is an important observation since it proves that the solution is still "active" i.e. initiation of polymerization still occurs 30 min after the start of the reaction. Surprisingly for the longest reaction time no polymer chains with higher molecular weight than those observed at shorter reaction time were detected. This phenomenon is likely to be linked with the limited lifetime of growing radical chains in the medium (important number of termination reactions).

Therefore, thanks to SEC, polymerization in solution was demonstrated. Then, data on the « activity » of the solution were collected. Polymer chains are present in the first 5 min of the reaction but are also created in its last 30 min. However, we could not access the degree of polymerization of the PHEMA, grafted on the substrate or in solution. In order to estimate the number-average degree of polymerization (DP_n) of the Graftfast™ grafted PHEMA, we used an indirect method based on XPS results.

V.2.7.2 - Estimation of DP_n from XPS data

In this part, XPS data are used to estimate the degree of polymerization of grafted PHEMA. Indeed, as polymerization is initiated by nitrophenyl radicals, a PHEMA chain grafted on the substrate can be represented as in Scheme 64. Thus, grafted chains are composed of a nitrophenyl end (only entity bearing a nitrogen atom) and of n HEMA repeated units (each containing a carboxylate group). The degree of polymerization can therefore be estimated from equation 5.4 by calculating the ratio of the areas of carboxylate and nitro groups[e] (determined by XPS analysis).

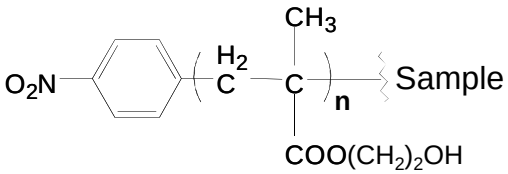

Scheme 64 – Representation of a PHEMA chain initiated by a nitrophenyl radical (n represents the average number of repeat units i.e. DP_n)

$$n = \frac{Area\ (COO)}{Area\ (NO_2 + NH_2)} \tag{5.4}$$

[e] As detailed in III.3.1.2, amino groups are likely to come from the degradation of nitro groups due to exposure to X-ray irradiation. Therefore, to take into account the entire amount of nitrogen from nitrophenyl groups, amino as well as nitro groups XPS contributions were added.

For samples obtained after a 60 min reaction time, the degree of polymerization of grafted PHEMA chains was estimated to range in average from 10 to 80[f]. Those DP_n values are likely to be underestimated. Indeed, in these calculations, we assumed that only one nitrophenyl moiety per grafted polymer chain was present in the film. However, depending on the thickness of the sample, the interface film-substrate, rich in nitrophenyl groups (see V.2.2), can be analysed by XPS. As it is impossible to dissociate nitrophenyl groups located in this area from nitrophenyl that have initiated the polymerization of grafted polymer chains, it overestimates the amount of nitrophenyl groups used in the equation 5.4. Moreover, the possibility of the grafting of nitrophenyl radicals directly onto the aromatic end of the polymer chains cannot be discarded. This would also lead to an overestimation of the amount of nitro groups in the films i.e. an underestimation of the DP_n of the PHEMA grafted chains. Besides, those DP_n values cannot be determined accurately since the nitrogen signal becomes less and less intense when analysing parts of the film which are more distant from the surface. Considering all these parameters, studies of the evolution of the degree of polymerization according to, for instance, reaction time or the [HEMA]/[NBDT] ratio were not performed.

V.3 - **Optimisation of the experimental parameters**

In this part, the influence of experimental conditions on the process will be investigated[g]. Ratios and concentrations of reactants will be optimized as well as the reaction time. Then, the efficiency of the usual rinsing procedure will be examined in this particular case of PHEMA films. To finish, the influence of gas bubbling and the acidification of the solution will be tested. The effect of those parameters on the Graftfast™ PHEMA films will be evaluated by comparing the IR intensity values of the $\nu_{C=O}$ band which, as previously detailed, is related to the thickness of the film. Beyond finding experimental parameters giving the thickest films, the study also aims at highlighting results which could be helpful in the understanding of the grafting mechanism.

V.3.1 - **Adjustment of concentrations of reactants**

Similarly to what was observed in the previous chapter, the value of the [VC]/[NBDT] ratio probably plays an important role in the synthesis. Moreover, it is likely that [HEMA]/[NBDT]

[f] According to those values, in some cases it would be more accurate to talk about oligomers and oligoradicals instead of polymers and macroradicals. However, in the rest of this work, we will carry on using the words polymer or polymer chains.

[g] As shown in appendix 6, even when no reducing agent is used, the temperature has an influence on the reaction. However, the mechanism involved remains unclear. Therefore, in order not to complicate the understanding of the Graftfast™ mechanism, we will not investigate the effect of the temperature during our experiments.

ratio and the NBDT concentration will also have an effect on the process. Therefore, their influences on the grafting of PHEMA films on gold were studied.

V.3.1.1 - Ratio [VC]/[NBDT]

The initial concentration of ascorbic acid in the solution was the first parameter to be optimized. The IR intensity values of the $\nu_{C=O}$ band according to the value of the [VC]/[NBDT] ratio are summarized in Table 20. It is clear that the lower the ratio, the higher the intensity value i.e. the thicker the PHEMA film. Therefore, as for the VC-induced process (chapter IV), a [VC]/[NBDT] ratio of 1/10 will be used for the rest of the study. Excess values of VC were not tested since stoichiometric amounts of reactants were already not giving any grafting of PHEMA.

Table 20 – IR intensity of the $\nu_{C=O}$ band of Graftfast™ PHEMA film according to the [VC]/[NBDT] ratio used (NBDT 0.046 M (1 eq), VC, HEMA 5 eq, H_2O DI, 60 min).

[VC]/[NBDT]	**1**	**3/4**	**1/2**	**1/5**	**1/10**
I $\nu_{C=O}$	0.33 %	0.88 %	1.2 %	1.4 %	2.66 %

V.3.1.2 - Ratio [HEMA]/[NBDT]

The [HEMA]/[NBDT] ratio is also likely to affect the synthesis of the Graftfast™ PHEMA films. The XPS area of carboxylate ester groups COO, the IR intensity of $\nu_{C=O}$ band and the thickness of the PHEMA films were followed to investigate the evolution of the grafting when varying the starting HEMA concentration (Figure 70).

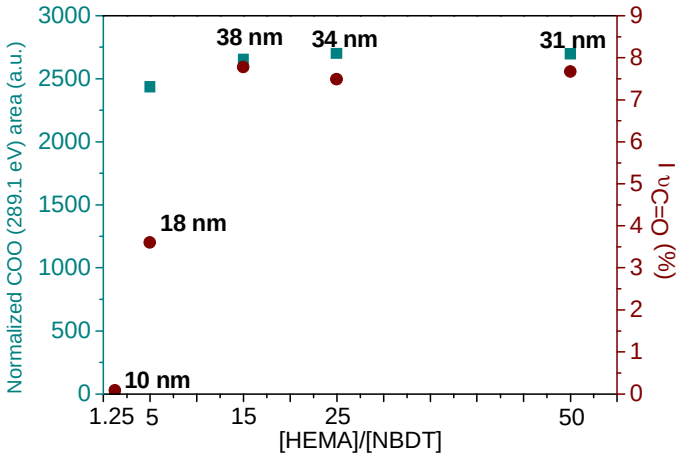

Figure 70 – XPS area of COO (blue), IR intensity of $\nu_{C=O}$ band (green) and film thickness (black, at ± 5 nm) of Graftfast™ PHEMA films as a function of the [HEMA]/[NBDT] ratio (NBDT 0.046 M (1 eq), VC 1/10 eq, HEMA, H_2O DI, 60 min).

It is interesting to notice that the variations of those three parameters with the HEMA starting concentration are parallel. It denotes that an increase in the IR intensity is mainly related to an increase in the film thickness and not in the film density. Moreover, the XPS measurements corroborate the IR results i.e. the presence of PHEMA films on the substrates is confirmed and thicker films are obtained for higher monomer concentrations. A 1.25-fold molar

excess of HEMA over the diazonium salt did not lead to any PHEMA grafting. However, from a [HEMA]/[NBDT] ratio of 15, a maximum value of the thickness of the PHEMA film was obtained. This critical value could correspond to a compromise between the termination rate of growing polymer chains on the surface and the physorption of polymer chains on the substrate. Indeed, the increase in the initial concentration of monomer simultaneously leads (i) to the formation of more growing polymer chains which can graft on the substrate and (ii) to more terminated polymer chains which can physisorb on the surface and block the growth of the film. Thus, the observed maximum thickness seems related to the amount of grafted and physisorbed chains. However, the latter parameter depends on the solubility of the polymer chains in the solvent. Particularly, experiments performed in monomer-rich aqueous solution may limit the physorption of the ungrafted polymer chains if the polymer chains are more soluble in the monomer than in water.

The presence of nitrophenyl moieties in the PHEMA structure was confirmed by IR-ATR and XPS. The thicker the PHEMA film, the higher is the IR absorption intensity of the characteristic bands of nitro and phenyl groups. The absorption intensity of the ν^{s}_{NO2} band for PHEMA polymer film was found higher than in the case of pure PNP films (respectively 0.78 % and 0.11 %). However, the thicker the PHEMA film, the smaller the XPS area of features from the nitrophenyl moieties (nitro and amino groups). The differences between IR and XPS measurements concerning the amount of nitrophenyl groups in the films can be attributed to a difference in analysed depth between those two techniques. Indeed, for IR-ATR measurements, this value depends on the wavelength of light, the refractive index of the crystal as well as of the sample and the incidence angle of the IR beam. The depth of penetration was calculated thanks to the equation 5.5 and found to range from 0.5 µm to 3 µm for respectively 4000 cm^{-1} to 600 cm^{-1}. Thus, in our case, the whole films are always analysed. On the contrary, XPS is only sensitive to the outer 10 - 15 nm of the coating. Therefore, we believe that, in the case of most PHEMA films, only a small amount of the nitrophenyl groups is detected by XPS in comparison to what is measured by IR because those moieties are mainly located near the interface film-substrate.

$$d_p = \frac{\lambda}{2\pi\sqrt{(n_1^2 \sin^2\theta_1 - n_2^2)}} \quad \text{with} \quad \begin{array}{ll} \lambda & \text{Wavelength of light} \\ \theta_1 & \text{Angle of incidence of the IR beam} \\ n_1 & \text{Refractive index of the crystal} \\ n_2 & \text{Refractive index of the sample} \end{array} \qquad (5.5)$$

To sum up the influence of the starting HEMA concentration, a 15-fold molar excess over NBDT corresponds to the lower HEMA concentration value giving thick PHEMA films. Therefore, in the rest of this study, the [HEMA]/[NBDT] ratio will be kept at 15.

V.3.1.3 - Concentration of NBDT

To finish with this study on the influence of the reactants concentrations, the concentration of the diazonium salt was varied. No concentration higher than 0.046 M was tested since we were limited by the solubility of NBDT in water. From the results reported in Table 21, it seems that the higher the NBDT concentration, the higher the IR intensity value of $\nu_{C=O}$ i.e. the thicker the PHEMA film. However, there is a critical NBDT concentration value, between 0.023 M and 0.01 M, from which almost no PHEMA grafting is observed. For lower concentrations than this critical value, the IR absorption spectrum corresponds to a PNP layer. Therefore, it is possible that, in those conditions, there was not enough polymer chains formed in solution to get them grafted on the substrate.

To conclude, it appeared that the thicker Graftfast™ PHEMA film on gold from NBDT and ascorbic acid are obtained using a NBDT concentration of 0.046 M, a [VC]/[NBDT] ratio of 1/10 and a [HEMA]/[NBDT] ratio of 15. Those optimized parameters will therefore be used in the rest of the study to make easier the evaluation of the influence of other experimental parameters on the grafting.

Table 21 – IR intensity of the $\nu_{C=O}$ band of Graftfast™ PHEMA film according to [NBDT] (NBDT 1 eq, VC 1/10 eq, HEMA 15 eq, H_2O DI, 60 min).

[NBDT]	**0.001 M**	**0.0046 M**	**0.01 M**	**0.023 M**	**0.046 M**
I $\nu_{C=O}$	0.21 %	0.11 %	0.67 %	8.9 %	10.19 %

V.3.2 - **Reaction time**

Another important parameter of the Graftfast™ process is the reaction time. Therefore, the grafting obtained for a reaction using the optimized concentrations determined in the previous part was followed with time. The IR intensity values were measured, after the usual rinsing procedure, at various reaction times in the case of two identical reactions carried out with 4-month time gap (since differences could be observed due to the lack of reproducibility of the experiments, see V.2.5). The results are presented in Figure 71.

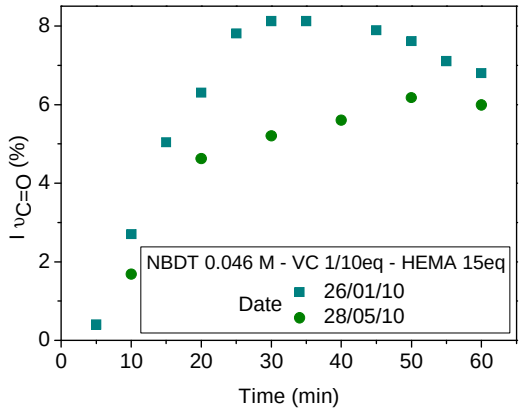

Figure 71 – IR intensity of the $\nu_{C=O}$ band of Graftfast™ PHEMA films synthesized in the same conditions but with a 4-month gap (NBDT 0.046 M (1 eq), VC 1/10 eq, HEMA 15 eq, H_2O DI) versus reaction time.

It is difficult to determine a general trend. Indeed, on the one hand, the first curve (green points) shows an initial linear increase of the amount of PHEMA on the substrate which then tends towards an asymptotic value after 60 min. As expected, the longer the reaction time, the more polymer chains are grafted until compounds in solution physisorb on the sample and block the access to the surface. On the other hand, the second curve (blue squares) also starts with a linear increase of the amount of grafted PHEMA but the maximum value is reached at around 30 min and is surprisingly followed by a decrease of the $\nu_{C=O}$ IR intensity. This behaviour is more difficult to explain. It could be due to our rinsing procedure which in the former case is not efficient enough to remove the entire non-grafted polymer or on the contrary damages the thick polymer films due to ultrasonication.

We therefore investigated the variations in grafting induced by the rinsing procedure. Simple water, ethanol, acetone rinsings were first performed. Then, a 5 min ultrasonication treatment was added (which corresponds to the typical rinsing procedure employed). To finish, on top of the previous rinsings, we investigated the effect of a treatment in a Soxhlet extractor (EtOH). The $\nu_{C=O}$ IR intensity values obtained after each procedure are reported on Figure 72.

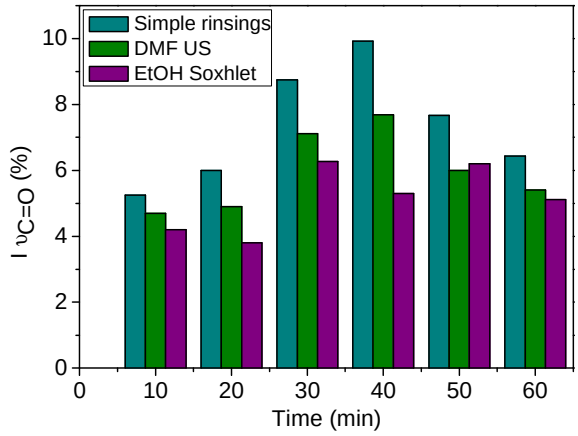

Figure 72 – IR intensity of the $\nu_{C=O}$ band of Graftfast™ PHEMA films (NBDT 0.046 M (1 eq), VC 1/10 eq, HEMA 15 eq, H_2O DI) as a function of the reaction time in the case of three different rinsing procedures: simple water, ethanol, acetone rinsings, + DMF US, + Soxhlet extractor.

As in the case of the data in blue in Figure 71, after simple rinsing and DMF US, a maximum of PHEMA grafting is observed around 30 - 40 min and is followed by a decrease. However, after the Soxhlet procedure, it seems that, considering the variations in measurement, a constant $\nu_{C=O}$ IR value is obtained from the reaction time. Over 50 min, the difference between the two latter rinsing procedures is not significant. DMF US on top of simple water, ethanol, acetone rinsing is therefore sufficient to remove all non-grafted polymer. Nevertheless, for reaction times of 30 min and 40 min, a relevant drop in IR intensity was detected between the latter two rinsings. This means that there is remaining physorbed polymer on the sample that can only be removed by a Soxhlet treatment. This behaviour could arise from differences in the cohesion of

the physisorbed polymer whether it contacts grafted PHEMA film or already physisorbed matter, which densities are likely to be different.

This study showed that the unexpected behaviour of some graftings with time could be explained in terms of rinsing procedure since a Soxhlet rinsing restores a "normal" trend. Moreover, it appears that a 60 min reaction associated to a typical rinsing procedure and a 30 min reaction coupled with a Soxhlet extractor (on top of a typical rinsing procedure) would give identical results. Therefore, for the sake of simplicity, a reaction time of 60 min and a typical rinsing procedure (water, ethanol, acetone rinsings followed by 5 min DMF US) will be employed for the rest of this chapter.

V.3.3 - **Gas bubbling**

As demonstrated in IV.2.2.2, the redox-induced process is based on the formation of aryl radicals from the reduction of the diazonium salt. In the Graftfast™ process, it is very likely that such reduction also occurs. Radicals are known to be sensitive compounds to the atmosphere of the reaction. On the contrary to inert atmospheres, oxidative atmospheres (O_2) can work as radical quencher. Therefore, the bubbling of the solution can have an impact on the grafting of PHEMA films. Argon, dinitrogen and air bubbling were examined and compared to a reaction performed without any bubbling. The variations detected on the $\nu_{C=O}$ IR intensity (Table 22) do not seem important enough to be attributed to an effect of the bubbling. Only the results obtained with air bubbling could be considered to slightly favor the grafting of PHEMA films, which is quite surprising since O_2 is a radical quencher. It is likely that the bubbling has an effect on the reactions occurring in solution but we did not study that aspect. No clear influence of any of the tested bubblings on the grafting i.e. on ending reaction on the surface was found. Therefore, for the rest of this study, no bubbling will be used.

Table 22 – IR intensity of the $\nu_{C=O}$ band of Graftfast™ PHEMA films (NBDT 0.046 M (1 eq), VC 1/10 eq, HEMA 15 eq, H_2O DI, 60 min) according to the nature of the gas bubbling of the solution.

	No bubbling	**Argon**	**N_2**	**Air**
I $\nu_{C=O}$ (%)	8.05 ± 1.2	7.65 ± 1.15	8.47 ± 1.27	9.4 ± 1.4

V.3.4 - **Acidification of the solution**

Last but no least experimental parameter investigated is the acidity of the solution. The effect of the pH of the solution and the nature of the acid used on the PHEMA grafting was tested. Experiments in acidic buffer solutions were also carried out and are presented in appendix 7.

First of all, the reaction was performed at various acidic pH using H_2SO_4 and HCl solutions. An experiment in H_2O DI was carried out in parallel for comparison purpose. The results presented in Figure 73 show that, whatever the pH of the solution, almost no PHEMA was grafted using HCl solutions. The interfering reaction forming chloroaryls from diazonium salt

and HCl (see II.3.1.3) could explain such behaviour. However, when using H_2SO_4 solutions, it seems that the more acidic the pH (down to pH of 1), the thicker the grafted films. Surprisingly, whatever the acid employed, no grafting was observed at pH lower than 1. The reason why such phenomenon occurred remains unclear. It could simply due to the very low amount of ascorbate ions in solution, which, according to the mechanism proposed for the VC-induced process in IV.2.3, is likely to be the compound responsible for the reduction of the diazonium salt. Indeed, at pH = 1, the concentration of ascorbate ions equals to 46 µM and at pH = 0.3 is five times lower.

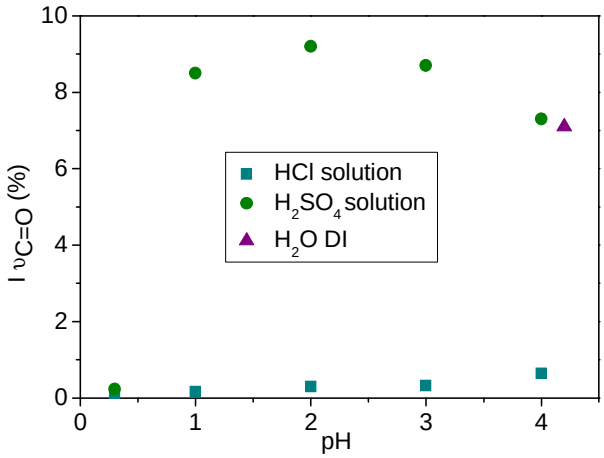

Figure 73 – IR intensity of the $\nu_{C=O}$ band of Graftfast™ PHEMA films (NBDT 0.046 M (1 eq), VC 1/10 eq, HEMA 15 eq, 60 min) according to pH and the nature of acid used (H_2SO_4 or HCl).

From the previous results, it is obvious that there is a strong influence of the nature of the acid. Therefore, the influence of five different acids on the Graftfast™ process was compared (Figure 74). Only reactions with HNO_3 and H_2SO_4 led to the grafting of PHEMA films. These results could be explained by the introduction of different counter-ions according to the acid used. Indeed, it is likely that some counter-ions stabilise more the diazonium ions than others which influence the ability of the diazonium salt to be reduced.

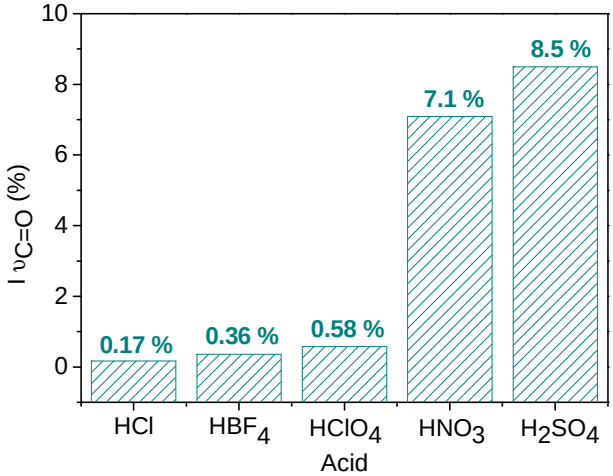

Figure 74 – IR intensity of the $\nu_{C=O}$ band of Graftfast™ PHEMA films (NBDT 0.046 M (1 eq), VC 1/10 eq, HEMA 15 eq, pH = 1, 60 min) according to the nature of acid used (HCl, HBF_4, $HClO_4$, HNO_3, H_2SO_4).

V.3.5 - **Conclusion on the effects of experimental parameters**

The experimental parameters have been optimized in the specific case of the grafting of PHEMA films on gold substrates using NBDT and ascorbic acid. The thicker PHEMA film in H_2O DI was obtained with:

- a NBDT concentration of 0.046 M,
- ten times less ascorbic acid than NBDT,
- a 15-fold molar excess of HEMA over the diazonium salt,
- no bubbling,
- a 60 min reaction time,
- a typical rinsing procedure (H_2O DI, ethanol, acetone rinsing and US 5 min in DMF).

A PHEMA film grafted in H_2SO_4 (pH = 2) with those parameters was found approximately 6 nm thicker than when synthesized in water DI. However, acidic conditions are not adapted for a mechanistic study (the spin-trap used in EPR experiments is not stable in acidic media). Therefore, with a view to study the grafting mechanism of the Graftfast™ process, all the following experiments will be performed in water DI. To finish, it is worth insisting on the fact that those optimized parameters are very likely to be exclusively adapted to this precise synthesis (NBDT, VC, HEMA, H_2O DI and gold substrates).

V.4 - Towards the understanding of the grafting mechanism

The study of the redox-induced process (chapter IV) as well as of the structure of the PHEMA films already brought information clarifying the grafting mechanism of the polymer films. However, lots of experimental proofs are still missing. Therefore, the last part of this chapter on the Graftfast™ process aims at (i) demonstrating the existence of radical polymer chains, (ii) defining the type of grafting involved in this mechanism, (iii) revealing the role of the primer PNP layer, (iv) proposing a grafting mechanism in accordance with our experimental results and to finish (v) discussing its variation according to the reducing agent.

V.4.1 - **Evidence of the existence of radical growing polymer chains**

As in the previous chapter, the Graftfast™ solutions (NBDT, VC and HEMA in H_2O DI) were investigated by EPR (using MNP as spin-trap).

A typical EPR spectrum is shown in Figure 75a. As previously illustrated, the interpretation of the hyperfine splittings is a powerful tool to determine the structure of the trapped-radicals. This EPR spectrum is analogous to the one obtained in IV.2.2.2 (case of the simple reduction of NBDT by VC) but shows an additional component. The simulation revealed that the spectrum is composed of a composite pattern: the main component is attributed to aryl radical adducts (Figure 75b); superimposed on this signal, a spectrum corresponding to a spin-adduct coupled

with only one nitrogen (with a hyperfine splitting constant of a_N = 1.62 mT) is observed. This latter is assigned to the spin adduct formed by the reaction of PHEMA chain propagation radicals with MNP (Figure 75c).

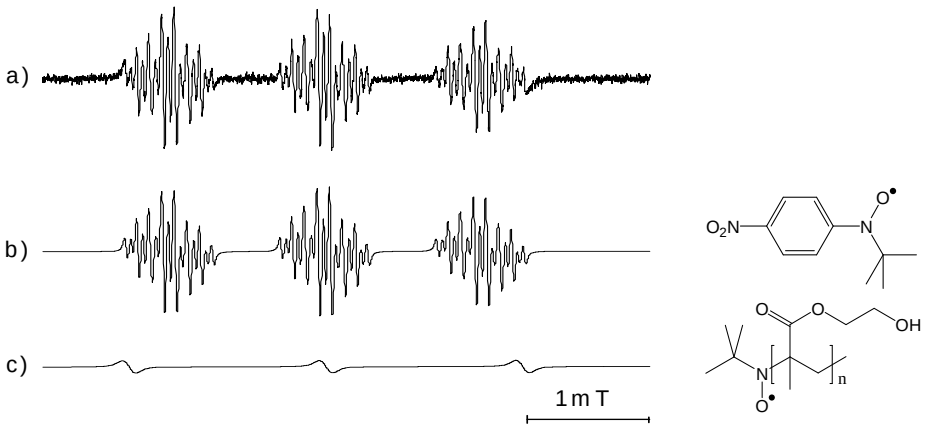

Figure 75 – a) Typical EPR spectrum of MNP adducts obtained in the case of NBDT (1 mM - 1 eq) reduction by VC (1/10 eq) in the presence of MNP (excess) and HEMA (1.25 eq) and recorded 2 minutes after the addition of VC; b) and c) decomposed spectra of MNP adducts of respectively aryl radicals and growing PHEMA chains. The corresponding spin-adducts formula are given on the right.

In order to make sure that the second spin adduct detected corresponds to the spin-trapping of growing polymer chains, we followed the effect of the introduction of MNP on the PHEMA grafting by IR-ATR. In comparison to typical Graftfast™ experiments (blue line in Figure 76), a drop in the $\nu_{C=O}$ IR intensity of 94 % is registered when the spin-trap is present in solution (green line in Figure 76). This result proves that the polymerization of HEMA occurs through a radical mechanism. Therefore, it is likely that the second spin adduct comes from the spin-trapping of growing PHEMA chains by MNP.

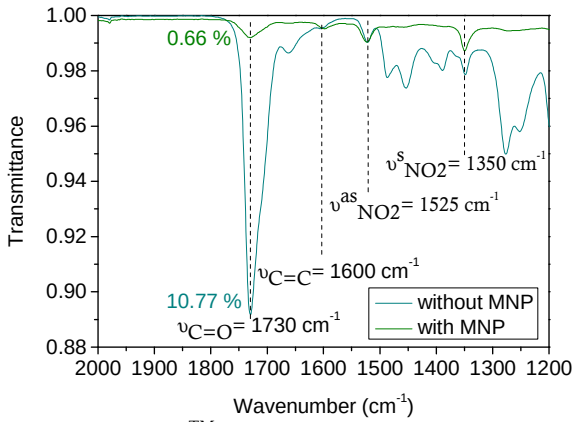

Figure 76 – IR-ATR spectra of Graftfast™ films obtained in presence or absence of an excess of the MNP spin-trap (NBDT 0.046 M (1 eq), VC 1/10 eq, HEMA 15 eq, 60 min).

The spin-trapping technique cannot give any information on the polymer degree of polymerization (DP). Indeed, whatever its value, the signal of the spin-adduct remains identical since only a nitrogen coupling is involved. Moreover, as we believe that the radical polymer chains formed in solution react very quickly with the MNP spin-trap preventing them to react with HEMA moieties and so to grow, DP are probably smaller than in a solution free of the

MNP spin-trap (conditions of normal Graftfast™ reaction). Nevertheless, the existence of aryl radicals and growing polymer chains during the Graftfast™ process is demonstrated.

Various HEMA concentrations were tested and the reactions followed by EPR. As two different spin-adducts were identified, we studied the evolution of their concentrations separately. Numerical simulations were employed for all spectra in order to determine the concentration of each spin-adduct: MNP adducts of nitrophenyl radicals and of radical polymer chains. The results are presented in Figure 77.

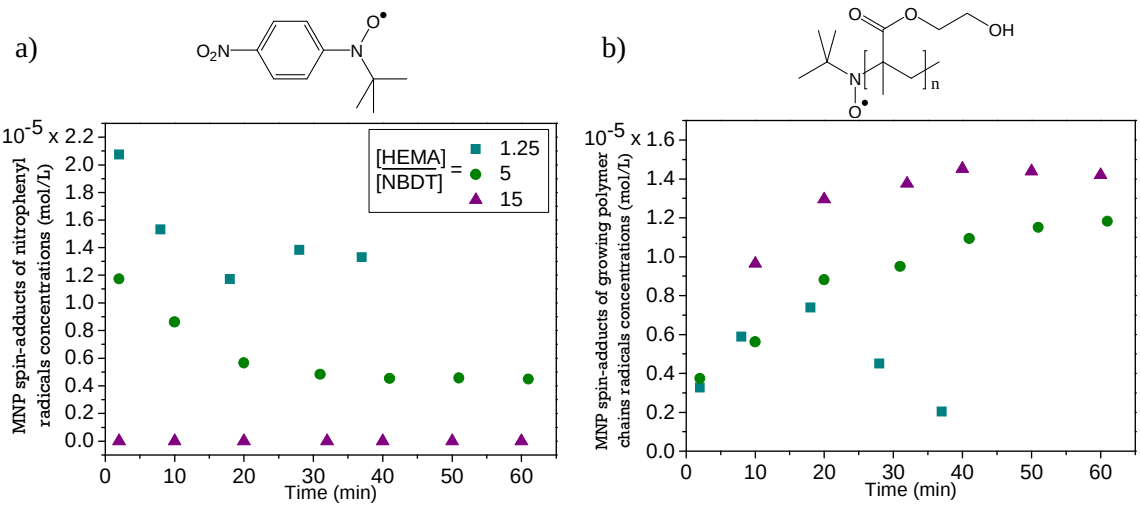

Figure 77 – Evolution MNP adduct concentration of a) nitrophenyl radicals and b) radical growing polymer chains with time in case of the reaction of MNP (excess), NBDT (1 mM - 1 eq) and VC (1/10 eq) and the following ratios [HEMA]/[NBDT] 1.25 (■), 5 (●), 15 (▲).

First of all, for some spectra shown in panels a) and b) in Figure 77, we observed a decrease in the concentration of the spin-adducts. As explained in IV.2.2.2, this can only be relevant to the spin-adduct reactivity so we will not go into quantitative interpretations. Indeed, nitroxide compounds are sensitive to carbonated radicals, which in this case could be the growing polymer chains or aryl radicals, to form alkoxyamines[8, 9]. All the reactions identified as likely to occur in this case are represented on Scheme 65.

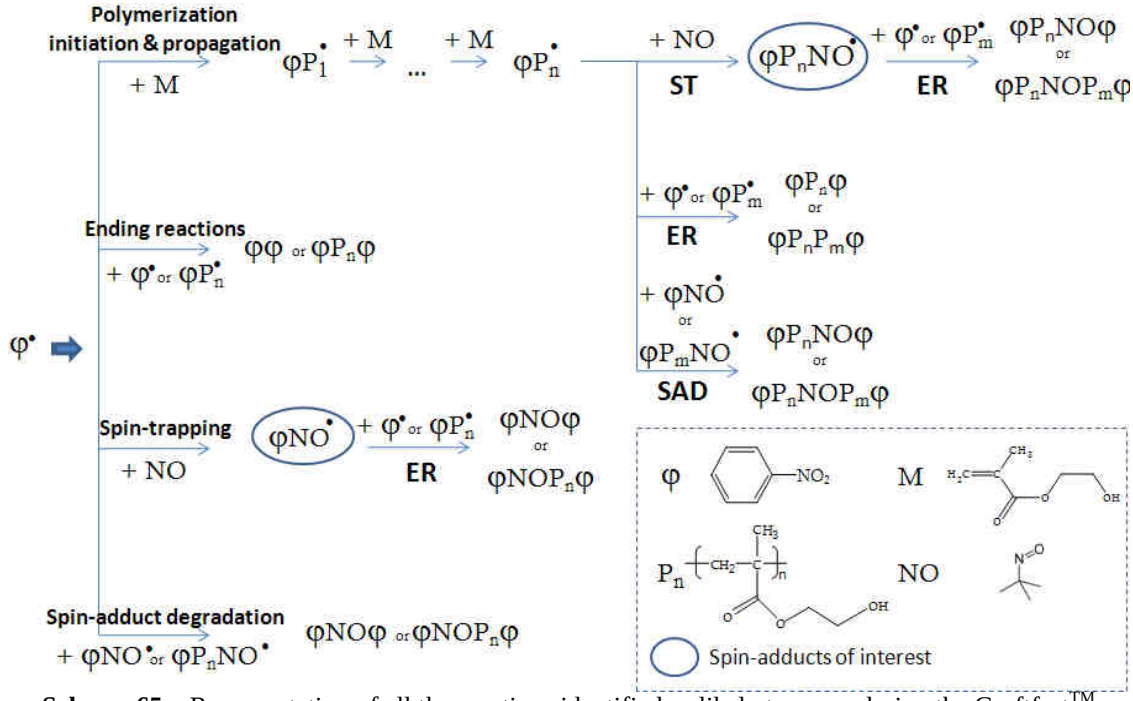

Scheme 65 – Representation of all the reactions identified as likely to occur during the Graftfast™ reaction (with NBDT, a reducing agent and HEMA) in presence of a MNP spin-trap. ER is an abbreviation for ending reactions, ST for spin-trapping and SAD for spin-adduct degradation.

Back to Figure 77, it seems that when the concentration of HEMA in the starting solution increased, less MNP adducts of aryl radicals were formed (degradation due to the reaction with growing polymer chains, see Scheme 65) and more MNP adducts of growing polymer chains were detected (degradation could also occur but globally there is an increase). This is in accordance with the assumed initiation of the HEMA polymerization by aryl radicals and an increase of the polymerization speed with the HEMA concentration. Indeed, the aryl radicals participating in the HEMA polymerization initiation cannot be spin-trapped (they do not contribute to the aryl radicals MNP adducts signal whereas the growing polymer chains initiated by those radicals can be spin-trapped and detected).

Over 40 min, the spin adducts concentrations seemed to reach constant values meaning either that they became stable and no more species are formed, or that their degradation exactly compensates their production. This phenomenon could be due to the fact that after 40 min, a lot less diazonium salt is reduced by ascorbic acid leading to the formation of less growing polymer chains, that is to say less species able to damage the spin-adducts.

Finally, the whole behavior of the curves obtained for [HEMA]/[NBDT] = 1.25 is difficult to explain. We assumed this is strongly related to the quantity of reactions involved in the process described in Scheme 65 and also to the relative rates of the reactions. However, the reason why less and less MNP adducts of growing polymer chains are observed after 20 min whereas more MNP adducts of aryl radicals are detected remains unclear.

A surface-solution comparison shows that the tendency highlighted by surface analyses is corroborated and finds explanation in this EPR study. Indeed, the surface analyses of the grafting of PHEMA films on gold substrates through the Graftfast™ process revealed the existence of a critical HEMA concentration value from which the PHEMA film thickness reaches a maximum (cf V.3.1.2). This result is confirmed by the following observation from EPR experiments: the more HEMA is introduced in solution, the more growing polymer chains are formed. Moreover, according to EPR measurements, for times longer than 40 min, only negligible amounts of growing polymer chains are formed. This result validates the observations made in V.3.2 indicating that the maximum thickness of film was obtained for a reaction ranging from 30 to 40 min before rinsing.

V.4.2 - **Grafting to/grafting from**

As mentioned in the first chapter, grafting methods of polymer brushes can be split in two types: (i) "*grafting to*" methods (moieties from the solution will graft onto the surface) and (ii) "*grafting from*" methods (in which the grafting proceeds by polymerization from the surface). The kind of grafting involved in the Graftfast™ process should therefore be determined.

In general, "grafting from" techniques require a first chemical step to immobilize polymerization initiators on the surface of the materials. However, cathodic electrografting is an exception since it is a "grafting from" technique with no preliminary step. Indeed, in this case, due to a cathodic potential, there is direct reduction of the monomer in an anionic radical which can graft on the surface and propagate the anionic active centre of polymerization.

Concerning the Graftfast™ process, initiators (aryl radicals) are formed in solution and no external energy is brought to the system to perform a direct reduction of the monomer. Therefore, it is likely that the Graftfast™ process occurs via a "*grafting to*" pathway. This hypothesis is in agreement with the detection of growing or terminated polymer chains by EPR and SEC. In order to verify this assumption, rotating disk electrode experiments were performed. Indeed, by this technique, Viel *et al.*[10] demonstrated that cathodic electrografting was a "*grafting from*" process. Since uniformly grafted polymer films were observed on the electrode even when rotating, they concluded that the film was growing from the surface. In the case of a "*grafting to*", chains formed in solution are likely not to be able to access the surface and graft when the electrode is rotating.

A typical Graftfast™ experiment was carried out using a gold rotating disk electrode (non-connected to a potentiostat) as substrate. Since the disk is only 2 mm in diameter, it was only analysed by XPS (Figure 78). When the substrate is immobile, a PHEMA film with the same characteristics as those obtained on flat gold substrates is formed. However, when it is rotating, the XPS area of the carboxylate (COO) band attributed to the PHEMA is divided by

three. According to the N 1s XPS spectra (not presented here), similar amounts of nitrophenyl groups are present on the gold disk whatever the rotation speed of the substrate. These results strongly suggest that the grafting of the polymer chains proceed *via* a "*grafting to*" in the Graftfast™ experiments. Remaining nitrophenyl groups and polymer on the surface of the rotating substrate could be attributed to the size of the grafted molecules. Indeed, the smaller the compounds, the more they can access the substrate even when it rotates.

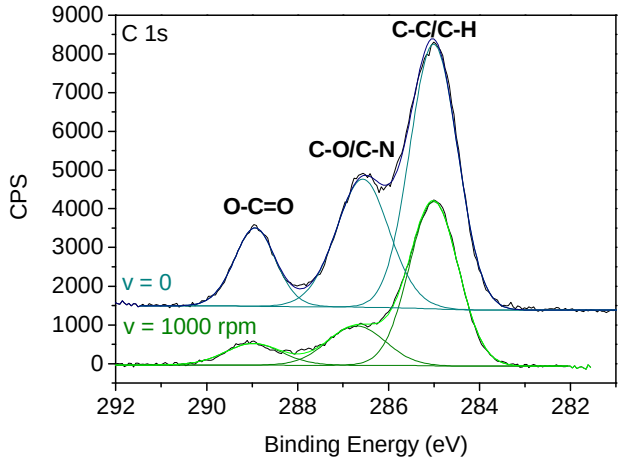

Figure 78 – C 1s core level spectra of rotating electrode gold disks grafted by Graftfast™ at a rotation speed of 0 and 1000 rpm (NBDT 0.046 M (1 eq), VC 1/10 eq, HEMA 15 eq, H_2O DI, 60 min).

V.4.3 - **Importance of the PNP primer-layer**

According to the very special structure of Graftfast™ films (rich in nitrophenyl groups at the interface film-substrate), it seems that the PNP layer plays an essential role in the grafting of the polymer chains on the substrate.

For once, the grafting experiment was performed in two steps: a first step consisting in the formation of a PNP layer and a second in which growing radical polymer chains was formed. More precisely, in the first step, a thick PNP film was synthesized in order to completely cover the gold surface. In the second step, iron powder was added to an acidic solution (HCl 0.5 M) containing only the HEMA monomer in order to start a radical polymerization. No diazonium salt (source of nitrophenyl groups) was present. According to the value of the Fe^{2+}/Fe redox potential ($E° = -0.44$ V), iron powder (unlike ascorbic acid) can reduce protons in solution which forms hydrogen radicals able to initiate the polymerization of the vinylic monomer. In order to evaluate the influence of the PNP primer-layer, the grafting of Sample 1 (achieved after the succession of those two steps) will be compared to the grafting obtained only after the second reaction on a bare gold substrate (Sample 2). The results are reported in Table 23.

Table 23 – IR intensity of the $\nu_{C=O}$ (1730 cm^{-1}) and ν^{s}_{NO2} (1350 cm^{-1}) bands after a 1st step leading to a thick PNP layer and a 2nd step for the PHEMA grafting (Iron 2 g, HEMA 4.8 mL, HCl 0.5 M 50.2 mL).

	Sample 1		**Sample 2**	
	$\nu_{C=O}$	ν^{s}_{NO2}	$\nu_{C=O}$	ν^{s}_{NO2}
1st step	-	2.92 %		
2nd step	10.14 %	3.1 %	0.64 %	-

According to the ν^{s}_{NO2} IR intensity value of sample 1 after the first step, it is obvious that a PNP layer was grafted on the gold plate. Then, after the second step the IR spectrum of the same sample exhibits a characteristic major absorption band at 1730 cm^{-1} related to the PHEMA carbonyl group. XPS and contact angle analyses (not presented here) also clearly indicate that a PHEMA film was grafted on the substrate. These results attest that the HEMA radical polymerization was effectively initiated by $H^{\bullet}$. However, on sample 2, almost no grafting of PHEMA is observed. It seems that growing radical oligomers formed in solution could not attach on the bare substrate. Therefore, although in the Graftfast™ process aryl radicals and growing radical chains are formed simultaneously in solution, the latter only grafted on the substrate when a primer PNP-layer is already present on the gold surface. This is supported by already described reactivity of alkyl radicals towards polycondensed aromatic rings[11] and it explains why final films are very similar to the ones obtained via the electroinduced process (SEEP). Moreover those results validate the hypothesis originally given by Mévellec *et al.*[1] i.e. the presence of nitrophenyl groups already grafted on the surface is essential in the Graftfast™ process and confirm that the Graftfast™ process follows a "*grafting to*" pathway.

V.4.4 - **Conclusion on the grafting mechanism of Graftfast™ with VC**

From all the results presented in this chapter, a grafting mechanism of PHEMA on gold substrate by the Graftfast™ process using VC as reducing agent can be proposed and is described in Scheme 66. It is important to underline that this is a simplified mechanism representing the main reactions leading to the construction of the films. Side reactions responsible for the presence of amino or azo groups in the films were voluntarily discarded in this scheme for sake of clarity, but are detailed respectively in III.3.1.2 and III.3.1.3.

Originally proposed by Mévellec *et al*[1], the mechanism of the Graftfast™ process relies on a key step which is the formation of aryl radicals (Scheme 66i) from the VC-induced reduction of the diazonium salt in solution (widely detailed in chapter IV). Indeed, those radicals have a double role. They can graft onto the substrate and form a primer-layer (rich in aromatic rings) essential for the subsequent grafting of polymer chains (Scheme 66ii); meanwhile they initiate the radical polymerization of the vinylic monomer in solution (Scheme 66iii). Finally, the growing radical polymer chains eventually graft by a "grafting to" pathway on the aromatic

rings present on the surface (Scheme 66iv) to form a grafted polymer films on the gold substrate.

The reason why the grafting of polymer varies according to experimental conditions is likely to be linked to the chemical reduction reaction (Scheme 66i). Indeed, this reaction forms the essential aryl radicals but, as mentioned in chapter IV, it is very sensitive to various parameters including the pH of the solution and, in the case of the reaction working with VC, to the ratio [VC]/[NBDT].

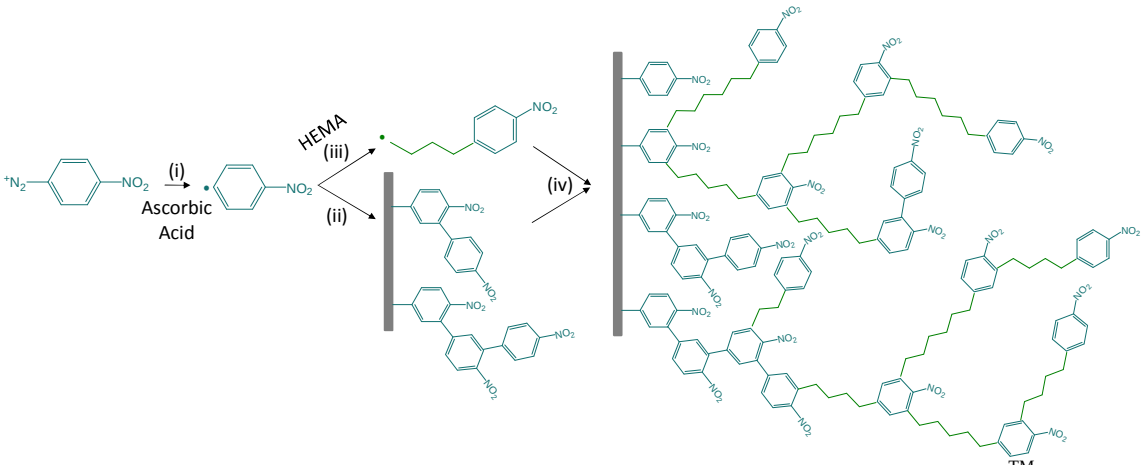

Scheme 66 – Simplified grafting mechanism of PHEMA onto gold substrate by the Graftfast™ process using ascorbic acid as reducing agent.

V.4.5 - **Is there any variation in mechanism with other reducing agents?**

As the first step of the mechanism is essential in the grafting, it is likely that according to the reducing agent used, variations in the grafting mechanism can occur. Therefore, the case of H_3PO_2 and iron powder were quickly investigated.

V.4.5.1 - With H_3PO_2

Concerning the use of hypophosphorous acid for the reduction of diazonium salts, it was shown that $H_2PO_2^-$ is likely to be the effective reducing agent (see IV.1.3.1). The reduction occurs through an outer-sphere electron transfer pathway which constitutes the first difference in mechanism in comparison to ascorbic acid. This chemical reduction produces aryl radicals but also $H_2PO_2^{\bullet}$. According to the Warson's work (presented in V.1), this compound could be responsible for the initiation of the polymerization of the vinylic monomer which would make a second difference with the mechanism observed when using ascorbic acid. Thus phosphorus-containing moieties should then be present in the final grafted film.

To confirm this hypothesis, a PHEMA film synthesized by the H_3PO_2-induced Graftfast™ process was characterized by XPS. The C 1s and N 1s XPS core level spectra (Figure 79) confirm the grafting of a PHEMA layer with features from nitrophenyl groups. By looking in details at the P 1s region, no specific signal is detected. Although XPS is only sensitive from 1 at.%, these results indicate clearly that no phosphorus atom is present in the film. Hence, the

direct initiation of the vinylic polymerization by $H_2PO_2^{\bullet}$ could only be a side-reaction. Thus, it is likely that, contrary to the mechanism proposed in 1967 by Warson, aryl radicals are responsible for the initiation of the radical polymerization of HEMA in solution. Therefore, except for the reduction mechanism pathway, the grafting mechanism of the VC or H_3PO_2-induced Graftfast™ process are very similar.

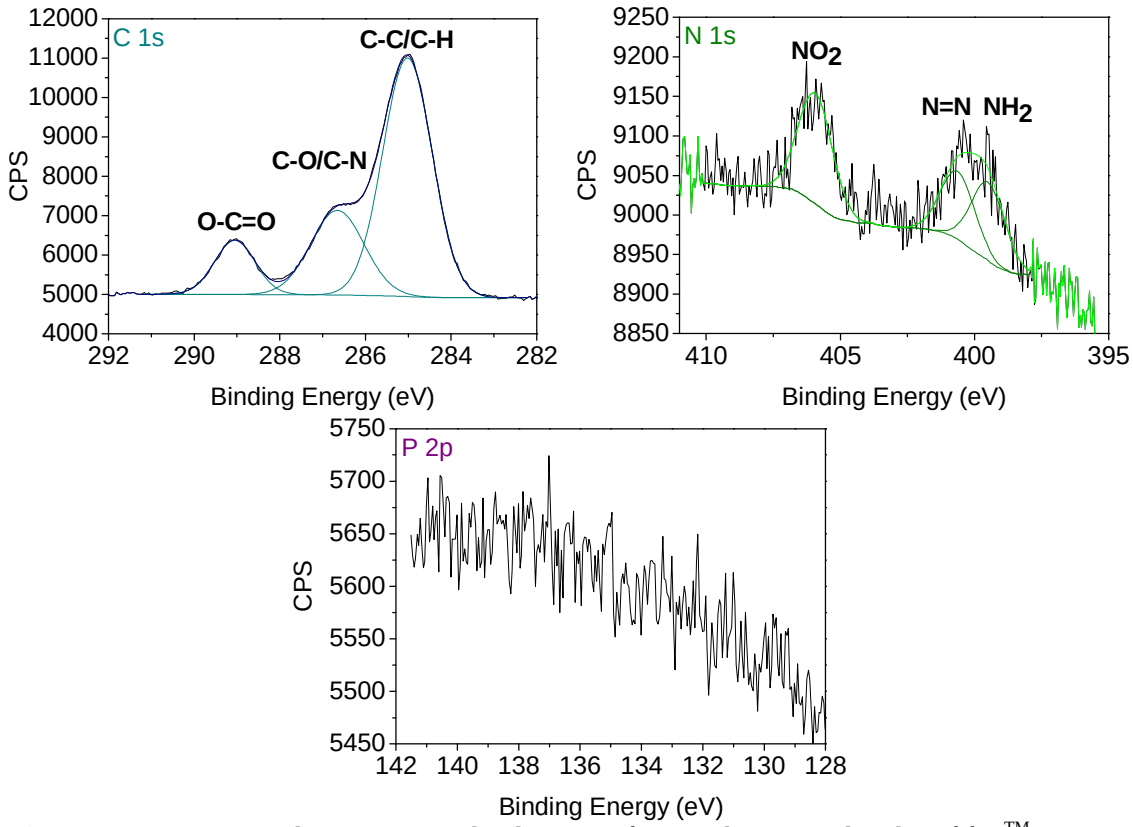

Figure 79 – C 1s, N 1s and P 2p XPS core level spectra of a typical H_3PO_2-induced Graftfast™ PHEMA film on a gold plate (NBDT 0.046 M (1 eq), H_3PO_2, HEMA 25 eq, H_2O DI, 60 min).

V.4.5.2 - With iron powder

When using iron powder as reducing agent, important variations in terms of grafting were observed according to the acidity of the solution. Results presented in Table 24 indicate clearly that the grafting reaction is favored in acidic medium in that case. Two reasons may explain that behaviour: (i) in acidic medium, the surface of the iron particles is constantly renewed by dissolution of the iron oxides formed upon the reduction of the diazonium salt or the protons; (ii) a variation in the grafting mechanism with the pH could occur.

Table 24 – IR intensity of the $\nu_{C=O}$ band of PHEMA films obtained by the Fe-induced Graftfast™ process (NBDT 0.046 M (1 eq), Iron 2 g, HEMA 25 eq, HCl 0.5 M or H_2O DI 47 mL, 60 min - non-optimized conditions).

	HCl 0.5 M	**H_2O DI**
I $\nu_{C=O}$ (%)	19.3	0.46

Indeed, on the one hand, as for the H_3PO_2-induced Graftfast™ process, the chemical reduction of diazonium salts with iron powder occurs *via* an outer-sphere electron transfer mechanism. On the other hand, unlike the process using H_3PO_2, the grafting mechanism of the iron-induced Graftfast™ process possibly varies from the one proposed when using VC.

As demonstrated in V.4.3, iron powder is suitable to reduce protons in acidic solution which leads to the formation of hydrogen radicals able to initiate the polymerization of a vinylic monomer. Such reaction is also supported by the observation of a lot of bubbles during the reaction, likely to be dihydrogen from the dimerisation of $H^{\bullet}$ in solution. Therefore, an additional succession of reactions takes place in the grafting mechanism of the Graftfast™ process when using iron (Scheme 67).

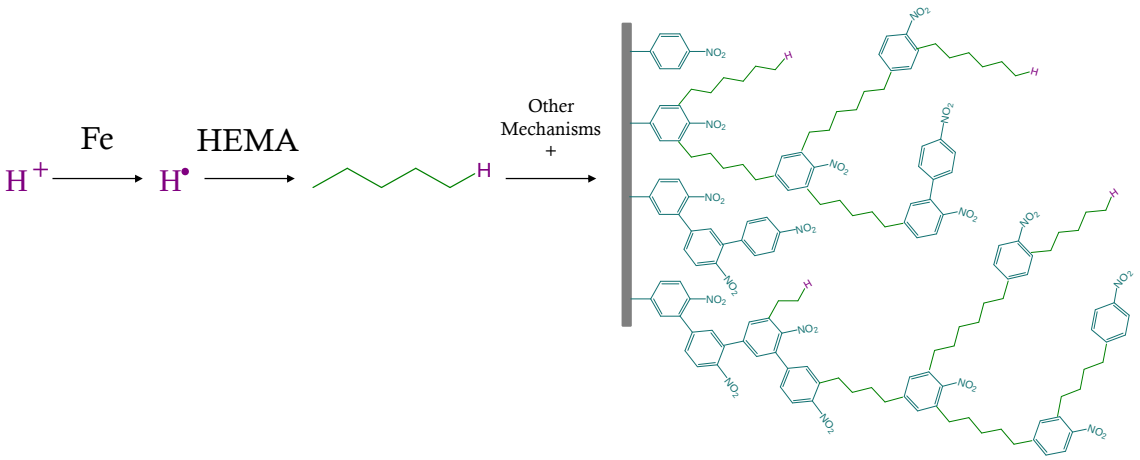

Scheme 67 – Additional reaction involved in the grafting mechanism of PHEMA onto gold substrate by the Graftfast™ process using iron powder as reducing agent.

This variation in mechanism also induces variations in the composition and structure of the films as clearly shown in the representation of the grafted films in Scheme 67:

- First, unlike nitrophenyl terminated chains, hydrogen terminated chains cannot be used as grafting sites for growing polymer chains. Thus, it is likely that those films are less dense than PHEMA films obtained with VC. This hypothesis is in agreement with the fact that, on the contrary to what is observed for VC-induced Graftfast™ process (see V.2.1), a remaining gold signal is still detected by XPS analysis for films up to 80 nm thick. Moreover, it could explain why some of the thicknesses and IR absorption values of PHEMA films obtained with iron powder are not fitting with the line formed by values obtained with VC on the IR intensity-thickness abacus established in V.2.6.4. Indeed, for identical IR intensities, PHEMA films synthesized with VC should be thinner than films obtained with iron powder. As IR intensities are characteristic of the amount of functional groups in the film, this would mean that iron-induced Graftfast™ PHEMA films are less dense than VC-induced ones.
- Second, it is not represented on Scheme 67 but more amino groups are detected in the films when iron powder is used than when VC is employed. This could be explained by

the reduction of nitrophenyl groups in primary amine by iron in concentrated HCl medium[12-14].

Summary

The Graftfast™ process is a functionalization method leading to the formation of polymer films on *a priori* any type of materials. It has a wide range of applications since it allows bringing new functionalities to materials surface. Based on the chemical reduction of diazonium salts, the better understanding of its grafting mechanism has appeared important in order to control the process.

First of all, the experimental conditions were optimized in the specific case of the grafting of PHEMA on gold plates using NBDT and VC. It has been demonstrated that, as in the previous chapter, an excess of diazonium salt over VC was favoring the grafting reaction. Moreover, a compromise on the monomer concentration (acting on grafting and physorption reactions of polymer chains) had to be found since almost no grafting was observed when [HEMA] was too low and a high amount of physisorbed polymer was obtained for high [HEMA] values. Besides, for unknown reasons, the grafting of PHEMA does not seem to occur at pH lower than 1 with this reducing agent and it is sensitive to the nature of the acid used. Finally, it has been confirmed that the thickness of the grafted films could be controlled with the reaction time. By looking in details to the composition of the films, to their structure but also to the composition of the reactive solutions, a grafting mechanism (close to the one originally proposed) has been established. As mentioned in the previous chapter, the reduction of diazonium salt by VC into aryl radicals occurs through an inner-sphere electron transfer pathway. Then, those radicals can simultaneously graft onto the substrate to form an essential primer-layer and initiate the radical polymerization of the vinylic monomer in solution. Finally, the growing radical polymer chains attach on the aromatic rings present on the substrate to form the grafted polymer film. Using H_3PO_2 or iron powder as reducing agent, the reduction mechanism switches from an inner-sphere to an outer-sphere electron transfer pathway. Moreover in the case of iron, the mechanism is a bit more complex than with VC or H_3PO_2 since hydrogen radicals from the reduction of protons in acidic solutions can also initiate and terminate the polymerization of the vinylic monomer.

The understanding of the Graftfast™ mechanism makes easier its application to various systems. However, it is likely that a variation in diazonium salt - reducing agent - solvent - substrate - polymer system from the one studied in this chapter will require a specific optimization of the experimental parameters. With those adaptations, the process is very powerful tool for the synthesis of surface functionalized materials. Particularly, the functionalization of TiO_2 nanoparticles with a final view to improve their integration in various environments will be investigated in the last chapter.

References

1. V. Mevellec, S. Roussel, L. Tessier, J. Chancolon, M. Mayne-L'Hermite, G. Deniau, P. Viel, S. Palacin, *Grafting polymers on surfaces: A new powerful and versatile diazonium salt-based one-step process in aqueous media*, ***Chemistry of Materials***, **2007**, 19 (25), 6323-6330.
2. H. Warson, *Initation of Vinyl Polymerisation Utilising a Diazonium Salt .1. Hypophosphorous Acid Redox System*, ***Makromolekulare Chemie***, **1967**, 105, 228-245.
3. L. Tessier, *Greffage de Films Organiques par Polymerisation Radicalaire Electro-amorcée en Milieu Aqueux Dispersé*, Thèse de l'Université Pierre et Marie Curie, Paris, **2009**.
4. D. Briggs, M. P. Seah, *Practical Surface Analysis - Vol 1: Auger and X-ray Photoelectron Spectroscopy*, John Wiley & Sons, **1990**.
5. L. Tessier, G. Deniau, B. Charleux, S. Palacin, *Surface Electroinitiated Emulsion Polymerization (SEEP): A Mechanistic Approach*, ***Chemistry of Materials***, **2009**, 21 (18), 4261-4274.
6. C. D. Bain, G. M. Whitesides, *Attenuation Lengths of Photoelectrons in Hydrocarbon Films*, ***Journal of Physical Chemistry***, **1989**, 93 (4), 1670-1673.
7. A. Ghorbal, F. Grisotto, M. Laude, J. Charlier, S. Palacin, *The in situ characterization and structuring of electrografted polyphenylene films on silicon surfaces. An AFM and XPS study*, ***Journal of Colloid and Interface Science***, **2008**, 328 (2), 308-313.
8. J. M. Catala, S. Jousset, J. P. Lamps, *Living/controlled radical polymerization of styrene mediated by nitroso compound: Kinetic and ESR studies*, ***Macromolecules***, **2001**, 34 (25), 8654-8656.
9. R. B. Grubbs, J. K. Wegrzyn, Q. Xia, *One-step synthesis of alkoxyamines for nitroxide-mediated radical polymerization*, ***Chemical Communications***, **2005**, (1), 80-82.
10. P. Viel, C. Bureau, G. Deniau, G. Zalczer, G. Lecayon, *Electropolymerization of methacrylonitrile on a rotating disk electrode at high spinning rate*, ***Journal of Electroanalytical Chemistry***, **1999**, 470 (1), 14-22.
11. M. Levy, M. Szwarc, *Methyl Affinities of Aromatic Compounds*, ***Journal of Chemical Physics***, **1954**, 22 (9), 1621-1622.
12. B. K. Lavine, G. Auslander, J. Ritter, *Polarographic studies of zero valent iron as a reductant for remediation of nitroaromatics in the environment*, ***Microchemical Journal***, **2001**, 70 (2), 69-83.
13. R. Mantha, N. Biswas, K. E. Taylor, J. K. Bewtra, *Removal of nitroaromatics from synthetic wastewater using two-step zero-valent iron reduction and peroxidase-catalyzed oxidative polymerization*, ***Water Environment Research***, **2002**, 74 (3), 280-287.
14. J. Werner, *Amination by Reduction*, ***Industrial and Engineering Chemistry***, **1948**, 40 (9), 1574-1583.

CHAPTER VI

Functionalization of Ti-based nanoparticles for their integration in sunscreen products

The development of a nano-object associating a novel Ti-based core, filtering both UVA and UVB radiation, with a shell bearing active functions would constitute an important breakthrough in the cosmetic field in comparison to products already present on the market of solar products. The synthesis of such a nanohybrid material is a real challenge and opportunity for the development of a sunscreen[a] since:

(i) Unlike all the others products on the market, it would be efficient in both the UVA and UVB domains without addition of any chemical additives (thanks to the properties of the mineral core);

(ii) It would be stable, well dispersed in the matrix, environment friendly and bring additional and original functions (thanks to a designated organic grafting of the mineral nanoparticles).

The elaboration of a suitable Ti-based mineral UV filter will not be experimentally investigated here. Indeed, the synthesis of nanoparticles is the core research interest of our partner: the "nanometric structures" group (CEA\IRAMIS\SPAM\LFP). This chapter reports a preliminary study consisting in evaluating the feasibility of a polymer grafting on TiO_2 nanoparticles. On the contrary of physisorption layers, a shell covalently grafted on the mineral core is more likely suitable for such applications since no release of undesired active species towards the living cells is expected. The Graftfast™ process has therefore appeared to be a convenient method for the elaboration of such polymer core-shell on TiO_2 nanoparticles. We will first present the context of the project and the scientific issues encountered for the development of new sunscreen products. We will show that TiO_2 and Ti-based nanoparticles synthesized by laser pyrolysis are good candidates for such applications. Then, we will present the currently core-shell nanoparticles. Finally, we will investigate the feasibility of the grafting of a biocompatible polymer (PHEMA) by the Graftfast™ process and give the first results on the stability of the resulting dispersions.

VI.1 - TiO_2 and Ti-based nanoparticles in cosmetics

Titanium dioxide is one of the most important inorganic products of the chemical industry. Its most common crystallographic forms are anatase (metastable product obtained at low temperatures) and rutile (thermodynamically stable product obtained at high temperatures). The worldwide interest for TiO_2 is due to its exceptional properties. Highly employed for various applications such as cosmetics[1] (particularly the rutile form for its interesting optical properties), pigment industries[2], solar cells[3, 4] and catalysis/photocatalysis for organic pollutants degradation[5] (especially the anatase form for its photocatalytic properties), TiO_2 has also started

[a] Sunscreen is a term describing any material which protects the skin from the effects of ultraviolet radiation.

to be used as films for the immobilization of biomolecules[6] and as nanoparticles in the field of hybrid materials[7-10].

Among those applications, we will focus in this project on the protection against UV radiations by integration of titanium dioxide nanoparticles into sunscreens. The reason why it has become a critical issue in the last few years will be presented. The needs to improve products already commercialized will be identified and a dual proposition will be made relying first on improvements in synthesis methods of Ti-based nanoparticles and second on modification of the surface of the nanoparticles.

VI.1.1 - **Issue of sunscreen products**

The correlation between solar exposure and the development of skin cancer is well known. UVB (290 – 320 nm) and UVA (320 – 400 nm) exposure are responsible for biological damage such as changes in DNA[11]. Particularly, UVA radiations were found to increase the rate of melanoma (one type of skin cancer) and they are also at the origin of the production of free radicals which cause damage to the cells and are responsible for skin ageing and occurrence of wrinkles. Sunscreen products decrease the penetration of UV radiation in the skin and therefore DNA damage. Therefore, efficient sunscreen should protect not only against UVB (as do most of them) but also against UVA. Even if the progression of skin cancer is slowing down, it was the cause of the death of around 1,400 people and 7,400 new cases of melanoma were detected in France in 2005 [12]. UVA rays account for up to 95 % of the UV radiation reaching the Earth's surface. Although they are less intense than UVB (Scheme 68), they penetrate further into the skin than UVB and are present with relative equal intensity during all daylight hours throughout the year[13]. However, many sunscreens do not block UVA radiation. Therefore, in addition to changing habits (including avoiding exposure between noon and 4 pm i.e. when UVB are the most intense and applying regularly an efficient protection cream), the improvement of the efficiency of sunscreens for the protection to UVA radiation is a real need and still a challenge.

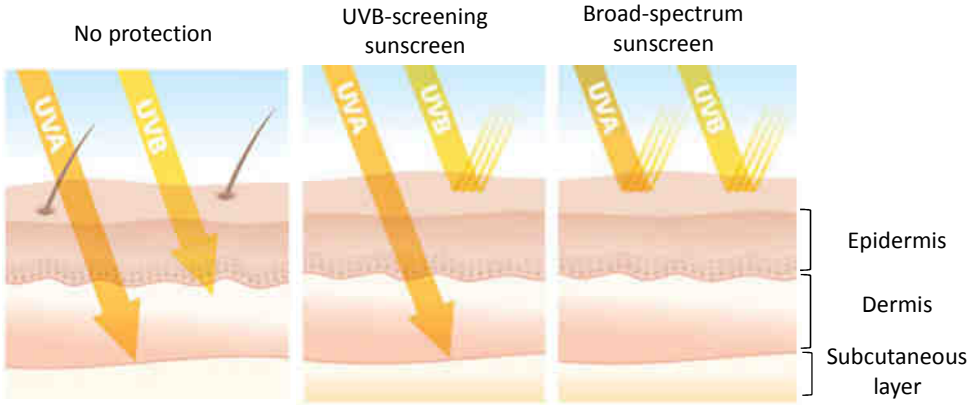

Scheme 68 – Penetration depth of UVA and UVB in the skin according to the protection used[13].

The formulations of current sunscreens contain two different types of UV filters: mineral filters (such as titanium dioxide, zinc oxide) and chemical filters (classified either in UVA filters e.g. benzophenones or UVB filters, e.g. salicylates). The sunscreen products of interest for this study are composed of TiO_2 nanoparticles. Indeed, unlike conventional TiO_2 particles which scatter visible light (sunscreen products containing such particles remain visible as a white film when applied on the skin), non-aggregated nanoparticles (20 – 50 nm[1]) scatter very little visible light and therefore appear transparent which makes them very suitable in the cosmetic field (Scheme 69).

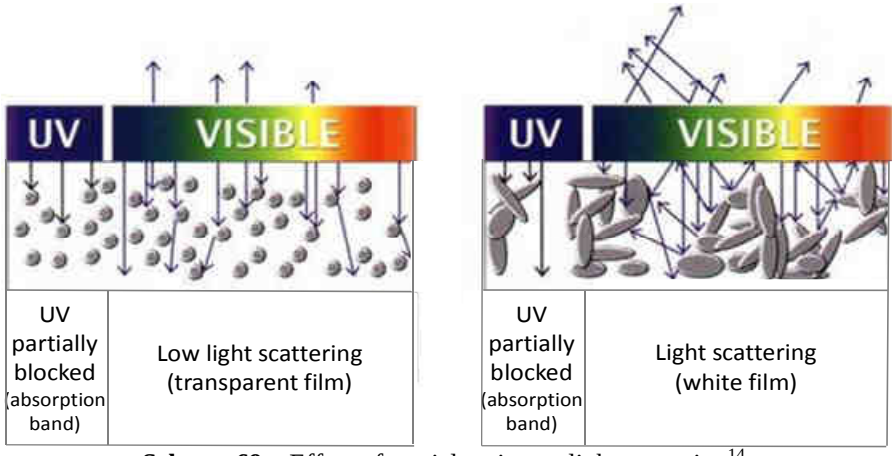

Scheme 69 – Effect of particles size on light scattering[14].

Besides, TiO_2 is an interesting material for such applications due to its optical properties. As represented in Scheme 70, it absorbs below 411 nm for titanium dioxide in a rutile phase (bandgap energy: 3.0 eV) and 384 nm for an anatase phase (bandgap energy: 3.2 eV) i.e. in the domain of UVB and UVA radiation. Nevertheless, in addition to the fact that the absorption in the UVA region is only partial concerning anatase, it appears that the absorption coefficient of UVA by TiO_2 nanoparticles is very low whatever the phase. Therefore, in order to get sunscreens protecting efficiently against UVB (thanks to TiO_2) but also UVA, in many cases chemical products are added in the cream. However, recent studies showed that such chemical filters can be harmful for the environment (for instance playing an important role in coral bleaching[15]) as well as for human health[16]. In this context, intensive research concerns the development of different ways to shift the optical gap of TiO_2 and Ti-based nanoparticles towards lower energies (below 3.0 eV) to extend the UV absorption zone of the mineral core to the visible (described in VI.1.2.2) and to remove the chemical filters used in the commercial creams.

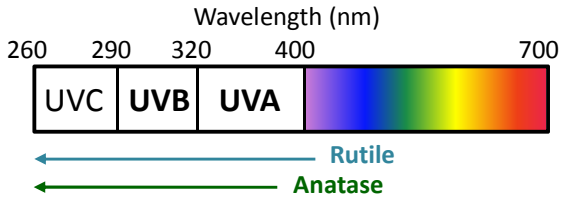

Scheme 70 – Absorption of UV and visible light of rutile and anatase phases of TiO_2.

Cosmetic creams are emulsions combining an organic phase (fatty esters or alcohols, paraffin oil or triglycerides) and an aqueous phase. Currently used particles, which exhibit highly hydrophilic surfaces, tend to concentrate in the aqueous part of the emulsions, which plays a significant role in the alteration of the properties of the sunscreen formulation. Therefore, a second challenge in the development of new UV filters lies in the synthesis of coated nanoparticles to obtain stable dispersions.

The tailoring of the surface chemistry of nanoparticles seems to be a key parameter in this context. More stable dispersions are likely to be reached by the synthesis of core-shell nanoparticles. Particularly a mix of hydrophilic and hydrophobic particles prepared separately or the synthesis of amphiphilic particles could stabilize the biphasic mixture. Moreover, the coating step could also be a way to bring additional and original properties to the nanoparticles such as moisturizers (titanium dioxide nanoparticles, which have high specific surface, induce dehydration problems), antioxidants (UV radiation causes oxidation reactions) and restructuring. This could turn out to be very promising since it would lead to sunscreens free of chemical additives. The coating of the TiO_2 nanoparticles could also appear essential since the main problem of mineral sunscreens is their potential photocatalytic activity. Indeed, the energy absorbed by the inorganic materials can induce the production of free radicals which in turn may promote the degradation of other components within the sunscreen formulation. As already employed in TiO_2-based commercial sunscreens, the coating of TiO_2 particles by an inert and passivating shell might be required to limit free radical generation and partially quench the photocatalytic activity of the mineral filter.

To sum up, in the context of preventing skin cancer, it seems that the development of organic/inorganic hybrid materials could be a real breakthrough. Properties of such materials clearly derive from the addition of both parts of the hybrid:

- The function of the nanoparticles will be the protection of skin against UV-light (efficient against UVA as well as against UVB),
- The function of the organic shell, obtained by a proper chemical functionalization, will be the improvement of the stability of the product, its biocompatibility, even a healthcare action and potentially the limitation of the photocatalytic activity of the nanoparticles.

Therefore, in the next parts, we will first see the existing synthesis methods for the formation of TiO_2 nanoparticles and particularly how the laser pyrolysis process is likely to play an important role in the improvement of the UV-filter properties of the Ti-based nanoparticles. Then, we will deal with the current synthesis methods to obtain core-shell nanoparticles (especially with polymeric coatings).

VI.1.2 - **TiO_2 and Ti-based nanoparticles**

To extend the UV protection range of TiO_2 and Ti-based nanoparticles, the gap of the material has to be shifted towards lower energies compared to currently used TiO_2 (rutile: 3.0 eV and anatase : 3.2 eV). This is likely to be achieved by changing slightly the composition of the nanoparticles during their formation. Therefore, prior to describe the possible ways to shift the band gap of the material, the synthesis methods of TiO_2 nanoparticles will be briefly presented with a strong emphasis on laser pyrolysis (process of interest in the project).

VI.1.2.1 - Synthesis methods

Numerous methods were developed for the synthesis of TiO_2 nanoparticles, which can be classified in chemical or physical methods. Due to the very high number of papers in the field, only a very succinct presentation will be given here.

For the production of TiO_2 materials, liquid phase synthesis methods (co-precipitation[17], solvothermal[18] or hydrothermal methods, electrochemical synthesis, sol gel synthesis[19, 20]) are efficient and versatile. TiO_2 nanoparticles could also be synthesized by high energy ball milling[21]. However, all these processes suffer from the same drawback: powders are produced by batches (whereas methods allowing continuous production are often preferred for industrial developments).

On the contrary, combustion as well as laser pyrolysis belong to the family of gas phase methods working in flow meaning that the collection of nanoparticles does not occur in the reaction zone, which allows continuous production. Combustion has been developed for years for the synthesis of TiO_2 nanoparticles for research[22, 23] and is the method used for ton production of common commercial powders (for example Evonik Degussa P25 from combustion of $TiCl_4$). Laser pyrolysis has also been used in research laboratories for production of TiO_2 nanoparticles (see for example Maskrot's work[24]). Since it is the synthesis method of the nanoparticles used in this chapter, its principle and advantages will be detailed below.

<u>Laser pyrolysis in more details</u>

As represented on Scheme 71, the laser pyrolysis method is based on the interaction in cross flow between a high power CO_2 laser beam and gaseous or liquid precursors (mainly titanium tetraisopropoxide TTIP for TiO_2 nanoparticle synthesis).

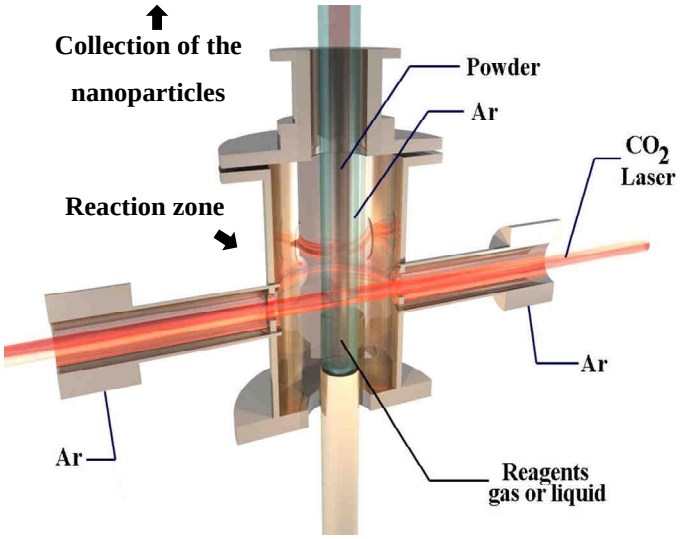

Scheme 71 – Reactive zone in laser pyrolysis process used for the continuous synthesis of TiO_2 nanoparticles.

The precursors are introduced in the reactor through a cylindrical nozzle and are confined in a laminar flow by a coaxial flow of neutral gas (when precursors are liquid they are introduced in the form of aerosol or vapor). The working pressure is constant and regulated through a valve controlling the pumping system. The pyrolysis reaction occurs with appearance of a flame at the intersection of the precursor flow and laser beam resulting from resonant energy transfer from laser to one or several components of the reactant mixture which are dissociated. Nanoparticles are formed through homogeneous nucleation and grow by collisions. The reaction is confined in a small volume by argon gas and therefore pollution due to interaction with the reactor cannot happen in this "wall less" reaction. When leaving the flame, the growth is quenched. Nanoparticles are collected on porous membranes inserted in the pumping system. The main drawback of this technique lies in the composition of the reactive mixture of precursors which has to contain at least one component absorbing the IR radiation of the laser.

Laser pyrolysis is an original synthesis technique for titanium oxide nanoparticles. It appears as a highly versatile method for the continuous synthesis of extremely pure and small particles with a narrow size distribution. The variable conditions of reaction (temperature, pressure, flow rate, composition of the solution of precursors…) are also an advantage as they allow synthesizing size-controlled nanoparticles with specific and original composition.

VI.1.2.2 - Shift of the optical gap towards lower energy

The most explored idea in order to shift the gap of the TiO_2 nanoparticles is to incorporate heteroatoms such as N[25], C[26], S[27] or F[28]. Another way is to use suboxide species TiO_{2-x} as widely described in the literature[29]. In this very active field, the laser pyrolysis is a very attractive synthesis method.

By this method, doped TiO_2 nanoparticles are easily obtained in a one-step reaction[24, 30] by simply mixing the precursors containing the dopants with the titanium precursor before the laser irradiation. For example, Maskrot *et al.*[24] presented the synthesis of complex products such as TiO_2 nanoparticles decorated with metallic particles (palladium, platinum and silver) while Pignon *et al.*[30] demonstrated the insertion of heteroatoms such as N in the structural organization of the nanoparticles (through the addition of NH_3 in the reactive mixture). The insertion of N allows shifting the gap in the zone of interest for this project[25] as represented on Figure 80 (red and blue spectra) and improves the absorption coefficient of the material as it has already been demonstrated[24, 31].

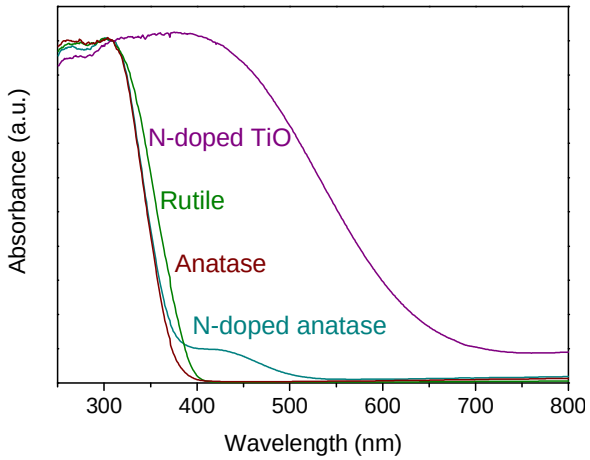

Figure 80 – Absorbance spectra of various Ti-based nanoparticles (rutile, anatase, N-doped anatase TiO_2 and N-doped TiO) synthesized by laser pyrolysis.

Another possibility to shift the optical gap is to obtain new metastable titanium oxide phases[32]. By working at high temperature (high laser power) and in presence of a reducing agent (NH_3 which is also partially incorporated in low amounts in the powder), stable powders containing a crystalline TiO phase have been synthesized as confirmed by the XRD diagrams presented in Figure 81 (green spectrum).

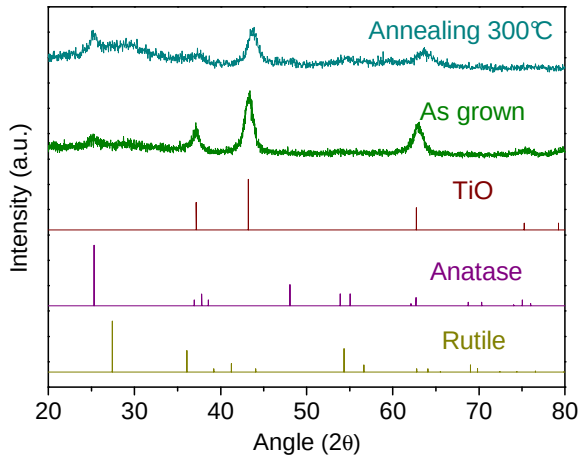

Figure 81 – XRD diagrams of N-doped TiO before and after a 300°C annealing under air. References are JCPDS: TiO 077-2170, Anatase 021-1272 and Rutile 21-1276.

This original structure is polluted by carbon coming from the titanium precursor decomposition. Carbon is removed while maintaining the TiO organization by simple soft annealing treatment under air. However, as illustrated by the blue spectrum in Figure 81, it can be noted that the annealing leads to the oxidation of a small part of TiO and that the resulting powder exhibits a strong shift of absorption towards the visible range (purple spectrum on Figure 80).

Work is currently in progress to fully understand the detailed process leading to such material and the origin of the shift observed in the optical gap but also to correlate the evolution of optical gap with stoichiometry, local organization and crystallization[33]. However, thanks to its original structure, TiO-based nanoparticles clearly show an extended absorption range (corresponding to a large shift of the optical gap of around 1 eV toward the visible range)[32] giving thus a full filtering of the UVA and UVB. We have no knowledge of a gap shift as large as this one in the literature. For comparison, Figure 82 gives the UV absorption profiles of several commercial products including Optisol™ (claimed as the best TiO_2-based filtering on the market).

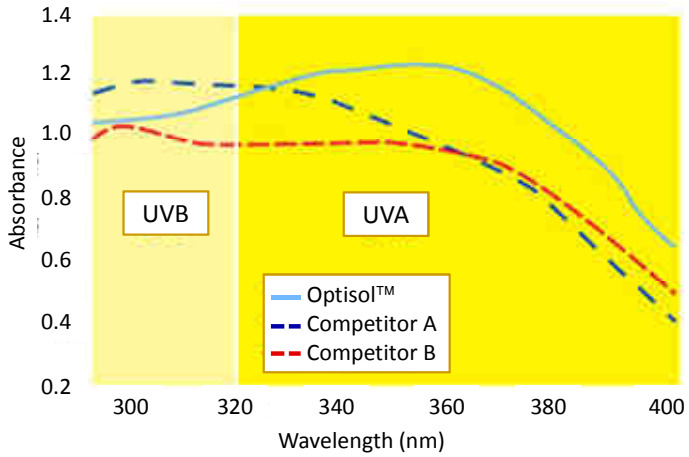

Figure 82 – Absorption profiles of Optisol™ and other competitor materials[34].

The potential health effects/hazards of Optisol™ in comparison with other commercially available titanium dioxide nanoparticles were tested by Park *et al.*[11]. The authors came to the same conclusion as those expressed in the Nanoderm Final report[35] which states: "…we do not expect any health effects for the topical application of sunscreens containing TiO_2 nanoparticles (especially when coated) on healthy skin which are related to the particulate state". Nevertheless, as deeply discussed in the work of Serpone *et al.*[1], the penetration of TiO_2 materials in the skin, their role in the generation of highly oxidizing radicals as well as their capacity to induce DNA damages have also been widely studied but no clear conclusions was obtained.

VI.1.3 - **Core-shell nanoparticles**

Current commercial sunscreens are mixtures of TiO_2 particles coated by an inert shell with a polymer matrix that contains, in particular, the additives required for UVA screening. Indeed, the synthesis of an inert capping of the TiO_2 nanoparticles has appeared as a major issue considering the potential photoactivity of the TiO_n core (especially photocatalysis for an anatase TiO_2 phase) or a possible bad tolerance of the skin to the material. This core-shell structure prevents any contact of the TiO_2 nanoparticles with the skin making the shell act as a photoactivity shield. Encapsulation of TiO_2 nanoparticles in inorganic substances (especially SiO_2 since silica is biocompatible, has low cost and mild fabrication process) was performed by well-established processes (for instance polyelectrolytes[36] and sol-gel[37]). For organic/inorganic nanohybrid structures, it can be obtained by using a two-step method consisting in performing classical siloxane chemistry followed by typical polymer grafting[38, 39].

For other applications than sunscreens, several approaches concerning the direct grafting of polymer onto TiO_2 nanoparticles have been reported in the literature. Such polymer shell could on its own play a double role: isolate the TiO_2 core from the skin to limit the photocatalysis of the material (replacing SiO_2 capping) and be a primer layer for the attachment of additives. For instance, the radical graft polymerization of vinyl monomers was successfully achieved on the surface of TiO_2 nanoparticles by employing radiation[40], high frequency discharge plasma[41] or by introducing trichloroacetyl[42], azo[42, 43] or peroxyester[44] initiating groups in order to initiate the polymerization. The grafting of TiO_2 nanoparticles was also reached using usual polymerization initiators with a prior grafting of coupling agents on the nanoparticles such as acrylic acid chloride[43], butyltitanate[45], phosphorus-containing compounds[9, 46] or more commonly double bonds-terminated silyl products[10, 47, 48]. Most of the cited works focused on the grafting of methacrylate polymers (in particular poly(methyl methacrylate) PMMA). Few teams dealt with the grafting of poly(styrene) PS[9, 41, 43, 46], poly(ethyleneterephtalate) PET[7, 8] or poly(tetraethylene glycol malonate) PTEGM[49] according to the applications of the final nanocomposite. However, all those polymerization processes, already successfully used for the surface modification of TiO_2 nanoparticles, going from free radical polymerization[42, 44, 47] (including controlled ones such as SI-ATRP[50], RAFT[43, 51] or NMP[46]) to in situ polycondensation[7, 8] generally involve: a two-step reaction or long reaction time or heating/cooling or controlled atmosphere or organic solvents.

VI.2 - **Grafting of Ti-based nanoparticles by the Graftfast™ process**

To improve stability and control the dispersion of TiO_2 nanoparticles in various environments, the organic modification of the surface of the nanoparticles could be efficient since it would help preventing aggregation of the particles and improving their affinity for

solvents. Our proposal here is to rely on a covalent grafting process to functionalize the surface of the nanoparticles with a stable and robust polymer shell to obtain stable and long living dispersions which could be used in sunscreen products.

Let us remind that a solar cream is a biphasic emulsion and the UV filter (i.e. the nanoparticles) must be equally dispersed in the aqueous phase as well as in the oily phase. To achieve a stable emulsion, it could be necessary to graft hydrophobic functions (e.g. fatty ester) giving the dispersion in the oily phase as well as hydrophilic functions (e.g. polyol) giving the dispersion in aqueous phase.

The use of the Graftfast™ process seems suitable for such purpose. Indeed, it is wet chemistry and an environment friendly process. It has already been successfully applied to various nano-objects such as carbon nanotubes and it also allows the grafting of polymer mixtures and copolymers which is convenient for multiple functionalizations of the nanoparticles.

As mainly investigated and employed on flat substrates, various improvements for the grafting of Ti-based nanoparticles will however have to be brought to this process particularly regarding the individual functionalization of the particles and their purification.

First, in this part, we will present a preliminary study aiming at showing the feasibility of the grafting of Ti-based nanoparticles by a polymer. This work will be mainly performed using N-doped anatase TiO_2 nanoparticles synthesized by laser pyrolysis of 9.6 ± 3 nm in diameter (size measured by XRD)[b]. Although those nanoparticles have potentially a photocatalytic activity, no inert shell will be synthesized prior to the polymer grafting. Indeed, we believe that the grafted polymer could play the same role as this inert shell i.e. preventing any contact between the nanoparticles and the skin cells. The grafting of poly(hydroxyethyl)methacrylate (PHEMA) onto those nanoparticles will be investigated since from previous studies we have a deep understanding of the grafting of this polymer by the Graftfast™ process. Moreover, it is biocompatible and it is likely to keep the hydrophilicity of the nanoparticles.

Second, the efficiency of the polymer grafting to insure good dispersion and stability of nanoparticles in water will be tested.

[b] Adjustments of the experimental parameters of the grafting were initially performed on commercially available TiO_2 nanopowder Evonik Degussa P25 (80 % anatase and 20 % rutile) with a mean diameter of 25 nm. TEM images of those nanoparticles will be presented since the corresponding characterisations on the N-doped Ti-based nanoparticles have not been made yet.

Even if N-doped TiO is the final material of interest in this study, tests on the feasibility of the grafting were carried out on N-doped TiO_2 nanoparticles since it is an abundant material. The grafting of N-doped TiO nanoparticles was also achieved but will not be presented here since preliminary results are similar than those on N-doped TiO_2 nanoparticles but these powders have not been yet fully characterized.

VI.2.1 - **PHEMA grafting on N-doped TiO_2 nanoparticles**

Similarly to experiments performed on planar substrates, the concentrations in the various reactants were: [NBDT] = 0.046 M (1 eq), [VC] 1/10 eq, [HEMA] 15 eq. Typically, we worked on TiO_2 dispersions of 0.8 mg/mL (with a final solution volume of 10 mL). However, to be suitable for the grafting on nanoparticles, the process required some adjustments.

First, ultrasonication (US) was used to maintain a good dispersion and avoid aggregation of the nanoparticles both before and during the reaction. On the contrary of the observations of Pinson and coll.[52] regarding the grafting of diamond nanoparticles in neutral or acidic media using US, we found that, in our case, US was not contributing to the grafting process. Therefore, we concluded that only the typical parameters of the Graftfast™ synthesis (reducing agent, solvent, reaction time, concentrations…) could influence the reaction.

Unlike planar substrates, nanoparticles could not be easily removed from the solution after the desired reaction time. Therefore, another modification when compared to the classical reaction lied in the method for stopping the reaction, for purifying and collecting the nanoparticles of the Graftfast™ reaction. Indeed, in this modified protocol, a volume of ethanol corresponding to at least the initial volume of the reactive solution was added to stop the reaction. The suspension was then washed by a few centrifugation – redispersion cycles (3000 rpm for 20 min) first with ethanol to remove free polymer chains and unreacted monomer, then with dimethyl formamide (DMF) to remove the ungrafted polyphenylene moieties and finally with water to eliminate DMF. Afterwards, the solvent was eliminated and the TiO_2 nanoparticles treated with the Graftfast™ process were either dried in air for a few hours or redispersed in a solvent according to the characterization aimed. Since the particles were rinsed by US in good solvents of the polymer, the remaining polymer at the surface of the nanoparticles is considered to be strongly grafted.

To evaluate the feasibility of the grafting of PHEMA on N-doped TiO_2 nanoparticles, the coating, the composition and the chemical structure of the nanoparticles were investigated. Thanks to the determination of the amount of PHEMA on the grafted nanoparticles as well as an estimation of the polymerization degree of the grafted polymer chains, the surface coverage of polymer on the nanoparticles was estimated. Finally, the influence of the grafting on the morphology of the nanoparticles was examined.

VI.2.1.1 - Characterizations of the core-shell nanoparticles

The N-doped TiO_2 nanoparticles (blue spectrum in Figure 80) grafted with PHEMA by the Graftfast™ process were first studied by infrared spectroscopy. Their IR spectrum is compared to the corresponding untreated TiO_2 nanoparticles (N-doped TiO_2) in Figure 83. The untreated N-doped TiO_2 nanoparticles only absorb at 3340 cm^{-1} (which corresponds to the stretching vibration of the surface hydroxyl groups or the absorption of water), at 1640 cm^{-1} (zoom in

Figure 83) which can be attributed to the bending vibration of the H-O-H bonds of adsorbed water and show a strong and broad peak in the 800-600 cm^{-1} region corresponding to the lattice vibrations of TiO_2 nanoparticles[50]. In the grafted N-doped TiO_2 product (GF- N-doped TiO_2), a new peak at 1717 cm^{-1} appears. It is due to the stretching vibration of C=O groups contained in the polymer indicating the presence of grafted PHEMA onto TiO_2 nanoparticles. Moreover in accordance with the mechanism widely discussed in the previous chapter, the GF- N-doped TiO_2 spectrum (magnification in the 1000-2000 cm^{-1} region in Figure 83) also exhibits two weak absorption bands at 1525 and 1350 cm^{-1} which are attributed to, respectively, the asymmetric and symmetric stretching of aryl-NO_2 groups, characteristic of nitrobenzene moieties. However, the weak peak at 1600 cm^{-1} typical of the presence of phenyl groups cannot be clearly identified. Only a shoulder in the peak at 1640 cm^{-1} (absorption of the TiO_2 nanoparticles) is observed.

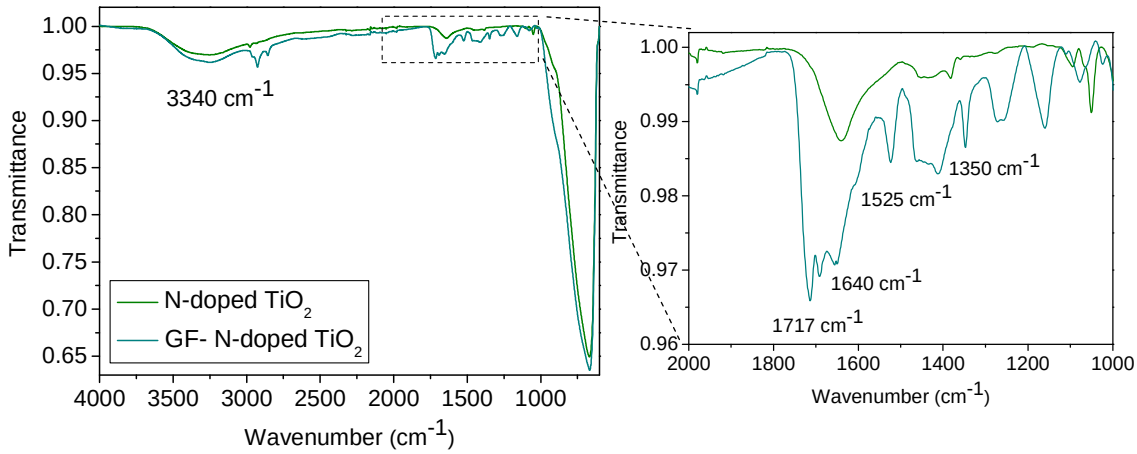

Figure 83 – IR spectrum of the PHEMA grafted N-doped TiO_2 nanoparticles (GF- N-doped TiO_2) compared to the corresponding untreated nanoparticles with a zoom in the 1000-2000 cm^{-1} region.

The IR comparison in Figure 84 shows a good correspondence between the new bands present in the GF-N-doped TiO_2 spectrum and the characteristic bands of a commercial PHEMA particularly at 1720 cm^{-1} (stretching vibration of C=O groups) which confirms the grafting of PHEMA onto TiO_2 nanoparticles.

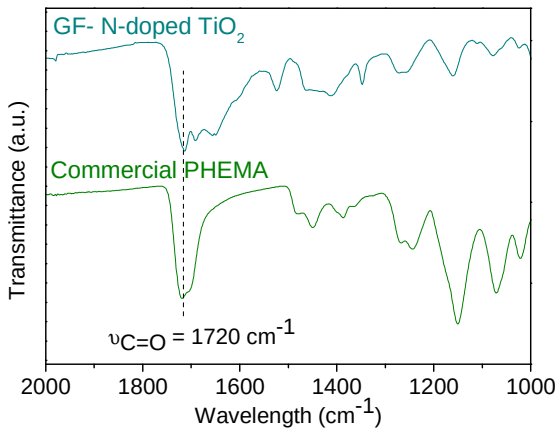

Figure 84 – IR spectrum of the PHEMA grafted N-doped TiO_2 nanoparticles compared to commercial PHEMA (20000 g/mol).

XPS analyses were also carried out in order to confirm the efficient grafting of PHEMA onto N-doped TiO_2 nanoparticles. First, Figure 85 shows typical survey scans of untreated and grafted N-doped TiO_2 nanoparticles. Unlike the C 1s peak (centred at 285 eV), the main Ti 2p and O 1s peaks (centred at respectively 459 and 530 eV) are attenuated in the spectra of the grafted nanoparticles, with respect to the pristine ones. This is a first XPS evidence of the occurrence of a coating.

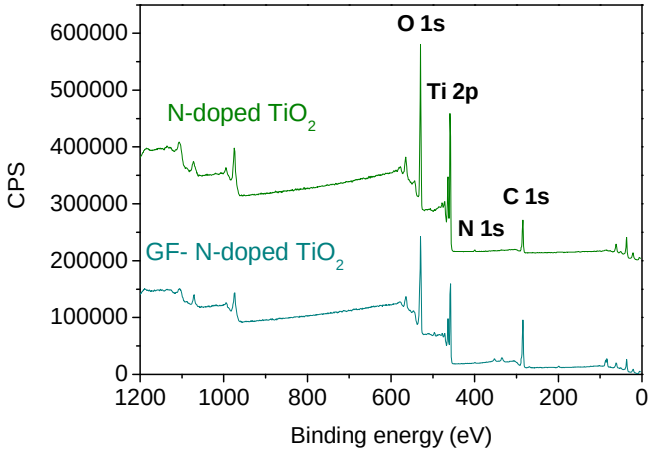

Figure 85 – Typical XPS survey scans of untreated and PHEMA grafted N-doped TiO_2, respectively noted N-doped TiO_2 and GF- N-doped TiO_2.

To investigate the chemical composition of the coating, XPS analyses in the C 1s region were performed. A typical C 1s core level spectrum of untreated N-doped TiO_2 nanoparticles (Figure 86) is composed of three main peaks. The first contribution adjusted at 285.0 eV corresponds to C-C/C-H bonds. The peak at 286.5 eV is due to -C-O- or/and -C-N- simple bonds. The last peak at a higher binding energy (288.8 eV) is assigned to carboxylate groups COO.

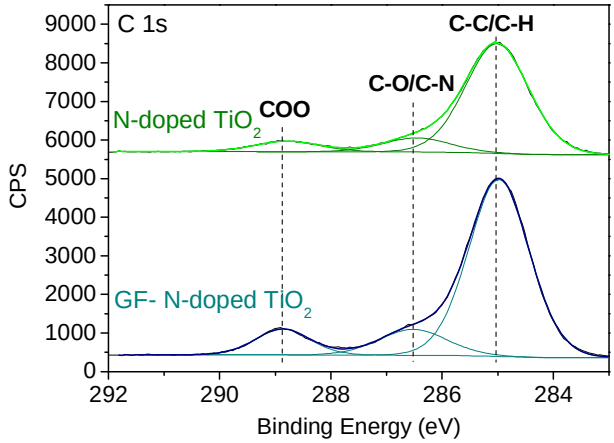

Figure 86 – Typical XPS C 1s core level spectrum of untreated and PHEMA grafted N-doped TiO_2, respectively noted N-doped TiO_2 and GF- N-doped TiO_2.

All those contributions in the C 1s spectrum are classically observed and attributed to surface contamination of pristine TiO_2 nanoparticles. The C 1s signal of GF- N-doped TiO_2 nanoparticles (Figure 86) is different from the one of pristine nanoparticles. The peak-fitting

parameters of functional groups in the C 1s region are summarized in Table 25. The contributions of C-O/C-N simple bonds and carboxylate ester groups O-C=O are higher in the GF- N-doped TiO_2 than in the untreated nanoparticles. This is due to the presence of the characteristic groups in the grafted polymer which confirms the grafting of PHEMA on N-doped TiO_2 nanoparticles.

Table 25 – Contribution (in %) of functional groups to C 1s region from untreated and PHEMA grafted N-doped TiO_2 (respectively noted N-doped TiO_2 and GF- N-doped TiO_2).

	C-C/C-H (285.0 eV)	**C-O/C-N** (286.5 eV)	**O-C=O** (288.8 eV)
N-doped TiO_2	81	11	8
GF- N-doped TiO_2	77	12.7	10.3

The N 1s core level in untreated and grafted TiO_2 nanoparticles was also analysed. Figure 87 reveals that both types of nanoparticles contain nitrogen which is not surprising since they were doped with this element. Unfortunately, the two spectra are very similar. In the pristine nanoparticles, three peaks at 399.4 eV, 400.3 eV and 401.8 eV are observed and are assigned to the doping and surface contamination of the nanoparticles. It is very difficult to attribute accurately those peaks to functional groups in the nanoparticles. However, regarding the spectrum of the GF- N-doped TiO_2, we assume that the observed peaks can be assigned in the same way as when considering the grafting of polymer films on flat surfaces (see the previous chapters for more details). Therefore, the first peak at 399.3 eV is likely to correspond to NH_2 groups, the second peak at 400.2 eV is assigned to N=N bonds (azo groups) while the third peak at 401.8 eV is attributed to NH_3^+. Obviously, the likeliness of the species present on the surface on both the pristine and grafted nanoparticles (amines, ammoniums) prevents an unambiguous use of the N1s XPs analysis.

The main difference between those two spectra nevertheless lies in the attenuation in intensity of the N 1s signal of grafted nanoparticles in comparison to untreated TiO_2. Such as for the Ti 2p and O 1s signals, this phenomenon could be explained by the presence of a coating at the surface of the grafted nanoparticles. Indeed, due to this shell, the core of the material as well as its surface would be less probed during the XPS analysis and therefore the N 1s signal would decrease. Moreover, unlike carbon, only low amounts of nitrogen are brought by the polymer film (N/C ≈ 2 % in a 35 nm PHEMA film on a planar gold substrate), which possibly do not compensate the attenuation of the signal due to the coating.

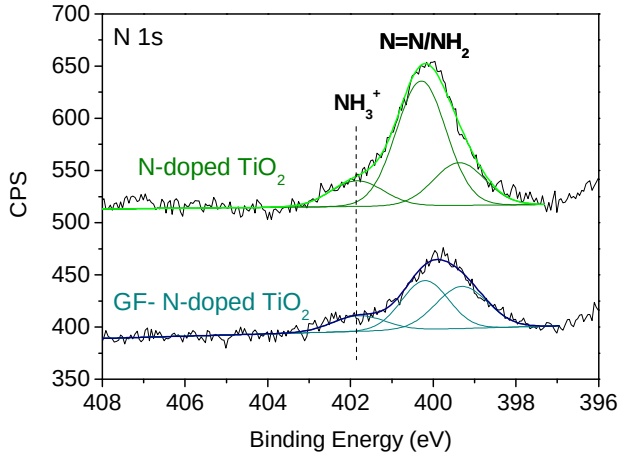

Figure 87 – Typical XPS N 1s core level spectrum of untreated and PHEMA grafted N-doped TiO_2, respectively noted N-doped TiO_2 and GF- N-doped TiO_2.

Finally and surprisingly in the grafted nanoparticles, no peak around 406 eV standing for the presence of NO_2 groups from nitrobenzene moieties in the film can be observed in Figure 87. The absence of NO_2 contribution could be explained either by their complete degradation into amine due to exposure to X-ray irradiation during the XPS analysis (see III.3.1.2) or by an unclear action of the N-doped TiO_2 nanoparticles. Indeed, in parallel to the grafting of the nanoparticles of interest, other types of Ti-based nanoparticles with various anatase/rutile ratios were grafted including N-doped TiO nanoparticles and undoped TiO_2 nanoparticles. In a general way, we observed that, in contrast to all the N-doped nanoparticles (Figure 87), the N 1s spectrum of grafted undoped TiO_2 (Figure 88) displays a component at a higher binding energy (405.9 eV) assigned to nitro groups which clearly demonstrates the presence of an organic shell grafted onto the TiO_2 nanoparticles. Therefore, there is a possible but unexplained involvement of the nature of the nanoparticles in the reduction of the nitro groups into amines.

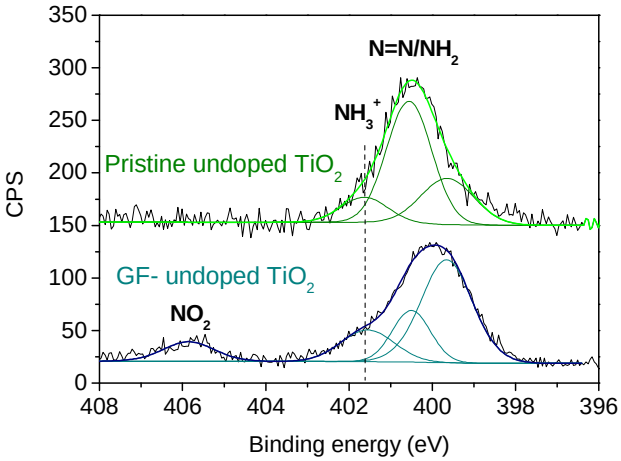

Figure 88 – Typical XPS N 1s core level spectrum of untreated and PHEMA grafted undoped TiO_2 (85 % anatase, 15 % rutile), respectively noted TiO_2 and GF - TiO_2.

To summarize, thanks to IR and XPS analyses, we have demonstrated the successful grafting of a PHEMA shell on N-doped TiO_2 nanoparticles. The analyses have also confirmed that the composition of the grafted film is very similar to the one obtained for PHEMA films on flat

surfaces which validates the grafting mechanism proposed. To go further in the study of the polymeric shell, we will now focus on the estimation of the surface coverage of polymer chains on the nanoparticles surface.

VI.2.1.2 - Estimation of the surface coverage of the nanoparticles

To evaluate the grafting density of grafted TiO_2 nanoparticles, we will combine an estimation of the degree of polymerization (DP) of the polymer determined from XPS with an estimation of the amount of polymer grafted on the nanoparticles.

For the estimation of the DP of the grafted polymer, we used the technique based on XPS data described in V.2.7.2. Typically, the area ratio between carbonyl groups from the polymer and amino/nitro groups from the aryl moieties leads to an estimation of the DP of the polymer. As previously mentioned, the XPS spectrum of N-doped TiO_2 nanoparticles does not display the characteristic component of NO_2 groups. Therefore, undoped TiO_2 nanoparticles were used for this study. However, since the pristine nanoparticles already show a large peak at the same energy as amino groups (Figure 88), we only took into account the area of nitro groups in the calculation. Therefore, it is very likely that we overestimated the DP value. The observed XPS carbon-nitrogen ratio, i.e. $(C=O)/(NO_2)$, allowed us to estimate a degree of polymerization of grafted PHEMA chains of 38 ± 20 units.

Then, thermogravimetric analysis was used to estimate the amount of polymer grafted on the undoped TiO_2 nanoparticles surface. Figure 89 shows that the polymer starts to decompose at 250°C and is completely decomposed around 500°C[c]. The observed weight loss from 200 to 500 °C indicates that the grafted polymer represents 4.06 wt.% of the GF-TiO_2 nanoparticles total weight. From this result, the number of repeating structural units composing PHEMA on the surface of TiO_2 nanoparticles can be estimated. Disregarding nitrophenyl moieties composing the coating, assuming that TiO_2 nanoparticles are individual, that the weight loss can entirely be attributed to the degradation of the polymer and considering that TiO_2 nanoparticles have a density of 3.9 g/cm^3, we calculated that the TiO_2 nanoparticles are covered by 1.5 ± 0.4 units/nm^2 in average. However, in this calculation, we also did not take into account the aggregation of the nanoparticles which could provide a higher value. To conclude, TGA gives an average coverage ratio of 1 to 2 HEMA units per nm^2.

[c] The data are only given from 200 °C since at lower temperatures the weight of the sample fluctuates. These variations, always reported when using this TGA apparatus, come from the introduction of the argon flow in the system which leads to buoyancy on the sample and occur until equilibrium is established.

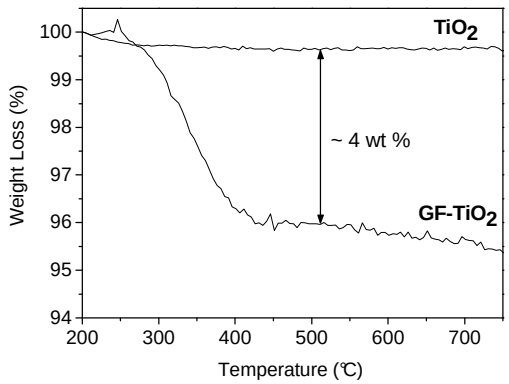

Figure 89 – TGA of pristine and PHEMA grafted (GF-TiO_2) TiO_2 nanoparticles (85/15 anatase/rutile).

This result is in agreement with the low grafting density of polymer chains already indicated by XPS from the attenuation (but not complete extinction) of the Ti 2p signal in the survey scans of grafted nanoparticles (Figure 85) as well as the estimated polymer length of 38 ± 20 units. Combined together, the two estimations detailed above indicate that there are approximately 1.5/38 = 0.04 polymer chains composed of ca. 38 monomer units per square nanometer grafted at the surface of the undoped TiO_2 nanoparticles[d]. Therefore we showed evidence that the polymer is not grafted at full surface density on the nanoparticle.

VI.2.1.3 - Morphology of the grafted nanoparticles

Finally using TEM, we tried to observe the grafted polymer around the nanoparticles. The comparison between untreated P25 TiO_2 nanoparticles (Figure 90a) and the corresponding grafted nanoparticles (Figure 90b) can neither demonstrate the presence of the polymer grafting around the nanoparticles nor lead to a conclusion on the effect of the grafting on the prevention of the nanoparticles aggregation. Thus, we decided to negatively stain the TEM grid containing the PHEMA grafted P25 TiO_2 nanoparticles to enhance electron contrast between the polymer and the nanoparticles. The result of the staining is shown in Figure 90c. The dark grey areas correspond to the polymer which coats the nanoparticles. Therefore, these TEM pictures demonstrate that the polymer was successfully grafted onto the TiO_2 nanoparticles. It also shows that the morphology of the nanoparticles remains relatively unchanged after grafting.

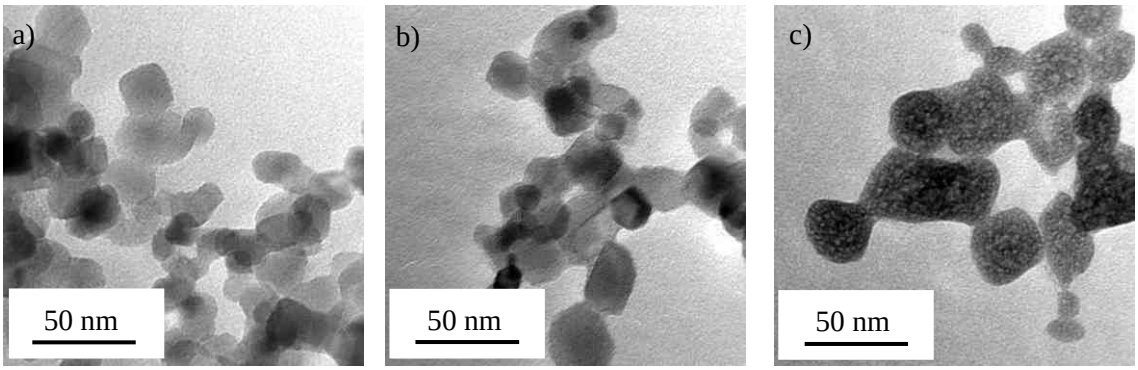

Figure 90 – TEM images of a) untreated P25 TiO_2 nanoparticles b) PHEMA grafted P25 TiO_2 nanoparticles and c) PHEMA grafted P25 TiO_2 nanoparticles negatively stained with uranyl acetate.

[d] Considering the approximations made, this value is likely to be overestimated.

VI.2.2 - **First test on the stability of the TiO_2 dispersion**

The primary purpose of the grafting of the nanoparticles is to enhance the stability of their dispersion in their environment of use. Therefore, the first test consisted in evaluating the effect of the PHEMA grafting on the stability in water of a dispersion of grafted N-doped TiO_2 nanoparticles. This experiment was performed using a turbidimeter. The measurements of the intensity of the transmitted light over the entire height of the flask containing the nanoparticles suspension with time give information on the stability of the dispersion.

The turbidimetry graphs recorded for two days in the case of dispersions in water of pristine and PHEMA-grafted N-doped TiO_2 nanoparticles (4 mg/mL) are reported in Figure 91.

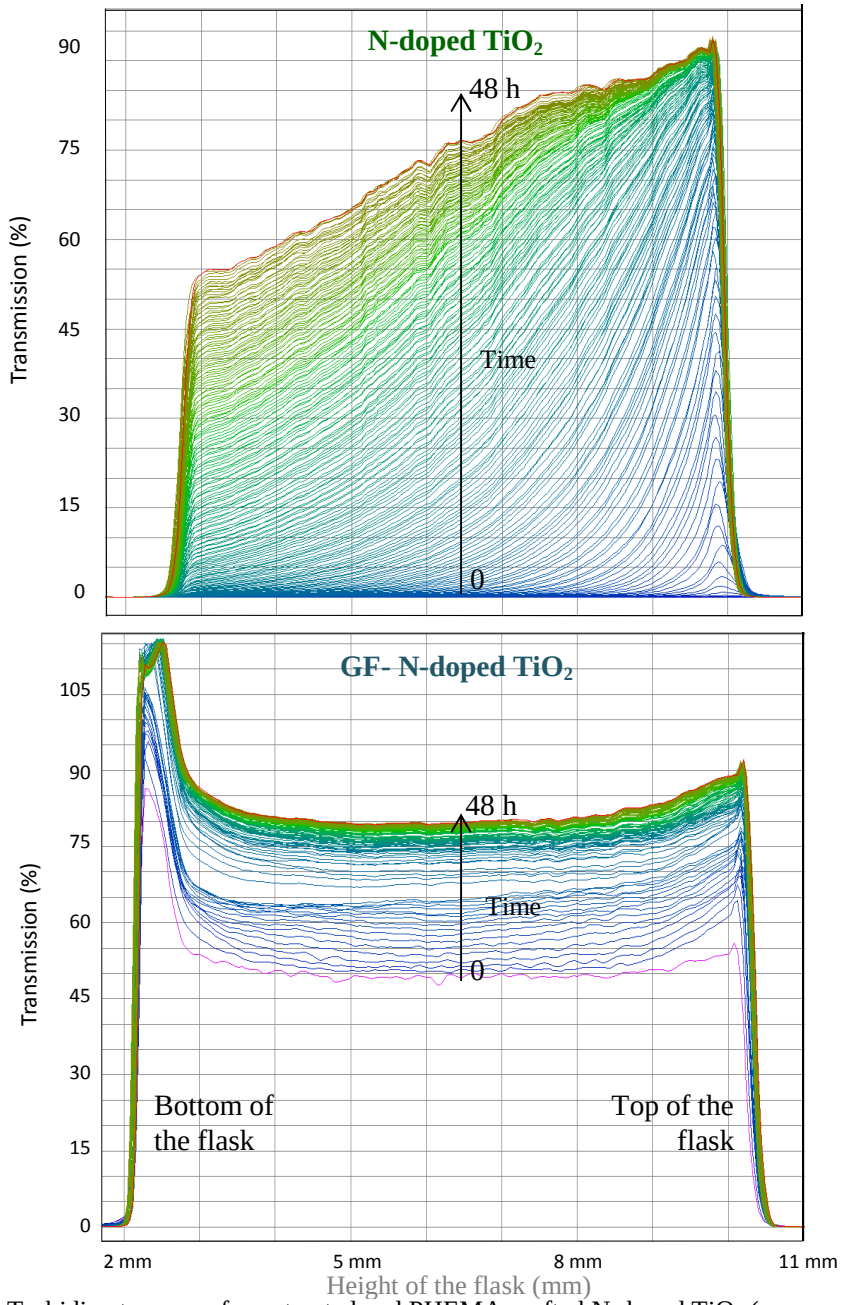

Figure 91 – Turbidimetry scans for untreated and PHEMA grafted N-doped TiO_2 (a scan every 2 min in the first half hour and then a scan every 30 min for 2 days; only one in two scans are displayed for the sake of clarity; start scan: purple and end scan: red).

Concerning ungrafted nanoparticles (N-doped TiO_2), we observed a faster increase of the light transmission at the top of the flask than at the bottom over the two days of analysis. This is classical of the sedimentation of TiO_2 nanoparticles from the top towards the bottom of the flask. Therefore, the suspension of pristine N-doped TiO_2 nanoparticles is not stable at all over the two days of analysis. We believe that if carrying out the analysis for a longer time, we should reach a transmission close to 100 % everywhere in the sample. Regarding the PHEMA-grafted nanoparticles, the behaviour is very different. The transmission increased homogeneously and constantly along the flask (except at the bottom where the transmission is always higher than in the rest of the suspension[e]). After two days, the transmission seemed to reach a stable maximum of transmission (80 % in the middle of the flask). The reason why all the transmission values are higher in this case than for the pristine nanoparticles will be explained further.

In order to compare precisely the two samples, data giving the evolution with time of the transmission at three different heights of the flask were extracted (Figure 92).

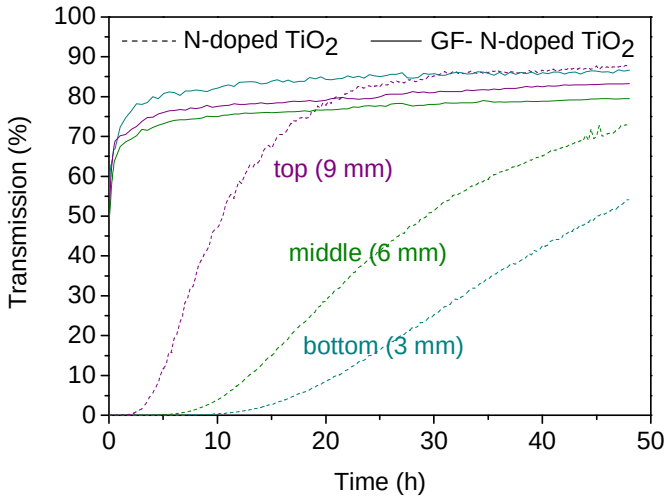

Figure 92 – Transmission of the suspension in water (4 mg/mL) of untreated (dashed lines) and PHEMA grafted N-doped TiO_2 nanoparticles as function of time and the position of the measurement in the sample (bottom: blue lines, middle: green lines and top: purple lines).

First of all, from the three curves represented in dashed on Figure 92, the phenomenon of sedimentation from the top to the bottom of the flask as well as the instability of the suspension of pristine N-doped TiO_2 nanoparticles are obvious. Contrary to this dispersion, we clearly noticed that, whatever the analysed part in the sample, the suspension containing the grafted nanoparticles evolves rapidly in the first 5 min of analysis and then very slowly after, reaching a quasi-stable transmission value. Therefore, we believe that if we could decrease the concentration in nanoparticles down to the one remaining after the two days of analysis, we

[e] The transmission intensity values over 100 % in the case of the grafted nanoparticles, at the end of the measurement at the bottom of the flask, remain unexplained.

would obtain a more stable suspension with time. However, if the transmission values of the GF- N-doped TiO_2 suspension are already fairly stable with time (increase of 30 % transmission in the middle of the flask instead of 70 % for N-doped TiO_2), they are always higher than for the suspension of pristine nanoparticles. We assume that this phenomenon is not related to the stability of the suspensions and could be explained by the following reasons:

- A possible difference in TiO_2 nanoparticles concentration between the two samples. Indeed, the untreated and grafted nanoparticles were dispersed at 4 mg/mL in water. However, the mass of polymer grafted nanoparticles is higher than for the pristine ones. Therefore, it is likely that less TiO_2 nanoparticles are present in the suspension of grafted nanoparticles, hence a higher initial transmission value.
- An effect of the agglomeration of the nanoparticles. As represented on Scheme 69, the more agglomerated the nanoparticles or the bigger, the more they scatter light. Therefore, the less they transmit it. Thus, if the pristine nanoparticles are initially more agglomerated than the grafted ones, they should transmit less light.
- An effect of the polymer shell. TiO_2 nanoparticles are already highly hydrophilic due to their important amount of OH groups on their surface. It is likely that the polymer grafting masks those functional groups and do not bring a sufficient amount of hydrophilic groups to compensate this coverage. Moreover, the Graftfast^{TM} process does not lead to the grafting of homopolymers but of statistical copolymers containing the monomer and aryl groups. It is worth noting that this behaviour might have an effect on the hydrophilic/hydrophobic properties of the polymer grafts. Particularly, some aryl groups are terminating the polymer chains and therefore are potentially located at the surface of the nanoparticles.

To summarize, it seems that the PHEMA grafting on the nanoparticles has improved the stability of their dispersion in water. We assume that a more stable dispersion could be obtained by optimizing the thickness of the polymeric shell and by using lower concentrations in nanoparticles.

Summary

By this preliminary work (recently published[53]), we have demonstrated the efficiency of the organic modification by a simple “green process” of TiO_2 nanoparticles with interesting optical properties (including N-doped TiO_2 and N-doped TiO nanoparticles, displaying an extended absorption towards visible light). We have characterized the grafted polymer in terms of chemical composition, confirmed the grafting mechanism proposed in the previous chapter, evaluated the surface coverage of the nanoparticles (0.04 polymer chains of 38 units per nm^2) and showed that this method does not change the morphology of the nanoparticles. We finally presented the first test on the stability of the dispersion of the grafted nanoparticles in water

showing that an enhanced stability of the nanoparticles suspension due to the PHEMA grafting. However some work still needs to be done to improve this parameter.

To go further in a potential use of those grafted nanoparticles in sunscreens, the reactivity of these nanopowders will have to be studied particularly their photocatalytic activity. An important step will also consist in the co-grafting with two (or more) different kinds of polymers with different hydrophilic properties to insert the nanoparticles in solar creams (biphasic emulsion). The polymers composing the shell remain to be fully determined according to the precise environment in which the nanoparticles will be dispersed as well as the nature of the active molecules to be attached on the nanoparticles.

This surface modification process opens the way for a large number of applications requiring polymer grafted TiO_2 nanoparticles or other type of nano-objects. Particularly, the final TiO_2 innovative product could certainly be developed in much larger fields than cosmetics: glass UV filter, photovoltaics... Indeed, in the field of energy, photovoltaic cells based on TiO_2 nanoparticles with an increased specific surface area and extended absorption zone obtained by a low cost approach could compete with the products currently used.

References

1. N. Serpone, D. Dondi, A. Albini, *Inorganic and organic UV filters: Their role and efficacy in sunscreens and suncare product*, ***Inorganica Chimica Acta***, **2007**, 360 (3), 794-802.

2. A. P. del Pino, P. Serra, J. L. Morenza, *Coloring of titanium by pulsed laser processing in air*, ***Thin Solid Films***, **2002**, 415 (1-2), 201-205.

3. M. Gratzel, *Photoelectrochemical cells*, ***Nature***, **2001**, 414 (6861), 338-344.

4. B. Oregan, M. Gratzel, *A Low-Cost, High-Efficiency Solar-Cell Based on Dye-Sensitized Colloidal TiO_2 Films*, ***Nature***, **1991**, 353 (6346), 737-740.

5. O. K. Varghese, M. Paulose, T. J. LaTempa, C. A. Grimes, *High-Rate Solar Photocatalytic Conversion of CO_2 and Water Vapor to Hydrocarbon Fuels*, ***Nano Letters***, **2009**, 9 (2), 731-737.

6. X. Chen, S. J. Dong, *Sol-gel-derived titanium oxide/copolymer composite based glucose biosensor*, ***Biosensors & Bioelectronics***, **2003**, 18 (8), 999-1004.

7. M. El Fray, A. R. Boccaccini, *Novel hybrid PET/DFA-TiO_2 nanocomposites by in situ polycondensation*, ***Materials Letters***, **2005**, 59 (18), 2300-2304.

8. K. Q. Han, M. H. Yu, *Study of the preparation and properties of UV-blocking fabrics of a PET/TiO_2 nanocomposite prepared by in situ polycondensation*, ***Journal of Applied Polymer Science***, **2006**, 100 (2), 1588-1593.

9. M. N. Tchoul, S. P. Fillery, H. Koerner, L. F. Drummy, F. T. Oyerokun, P. A. Mirau, M. F. Durstock, R. A. Vaia, *Assemblies of Titanium Dioxide-Polystyrene Hybrid Nanoparticles for Dielectric Applications*, ***Chemistry of Materials***, **2010**, 22 (5), 1749-1759.

10. J. P. Zou, Y. Zhao, M. J. Yang, Y. Dan, *Preparation and characterization of polystyrene/titanium dioxide composite particles containing organic ultraviolet-stabilizer groups*, ***Journal of Applied Polymer Science***, **2007**, 104 (5), 2792-2798.

11. B. Park, P. A. Martin, C. Harris, R. Guest, A. Whittingham, P. Jenkinson, *Preliminary in vitro investigation of the potential health effects of Optisol (TM), a nanoparticulate manganese modified titanium dioxide UV-filter used in certain sunscreen products*, ***Nanotoxicology***, **2009**, 3 (2), 73-90.

12. ***Sources Relaxnews***, **June 2008**

13. Skin Cancer Fundation, *Understanding UVA and UVB*, http://www.skincancer.org/understanding-uva-and-uvb.html.

14. Primtjetcolor, *Laques et encres pour imprimantes et traceurs*, http://www.primjetcolor.com.pl/special_lacquers_ns_fr.html.

15. R. Danovaro, L. Bongiorni, C. Corinaldesi, D. Giovannelli, E. Damiani, P. Astolfi, L. Greci, A. Pusceddu, *Sunscreens cause coral bleaching by promoting viral infections*, ***Environmental Health Perspectives***, **2008**, 116 (4), 441-447.

16. K. M. Hanson, E. Gratton, C. J. Bardeen, *Sunscreen enhancement of UV-induced reactive oxygen species in the skin*, ***Free Radical Biology and Medicine***, **2006**, 41 (8), 1205-1212.

17. Y. B. Xie, C. W. Yuan, *Characterization and photocatalysis of Eu3+-TiO2 sol in the hydrosol reaction system*, ***Materials Research Bulletin***, **2004**, 39 (4-5), 533-543.

18. M. Kang, *Synthesis of Fe/TiO_2 photocatalyst with nanometer size by solvothermal method and the effect of H_2O addition on structural stability and photodecomposition of methanol*, ***Journal of Molecular Catalysis a-Chemical***, **2003**, 197 (1-2), 173-183.

19. J. Livage, M. Henry, C. Sanchez, *Sol-gel chemistry of transition-metal oxides*, ***Progress in Solid State Chemistry***, **1988**, 18 (4), 259-341.

20. C. Guillard, B. Beaugiraud, C. Dutriez, J. M. Herrmann, H. Jaffrezic, N. Jaffrezic-Renault, M. Lacroix, *Physicochemical properties and photocatalytic activities of TiO_2-films prepared by sol-gel methods*, ***Applied Catalysis B-Environmental***, **2002**, 39 (4), 331-342.

21. S. Begin-Colin, G. Le Caer, E. Barraud, O. Humbert, *Mechanically activated synthesis of ultrafine rods of HfB2 and milling induced phase transformation of monocrystalline anatase particles*, ***Journal of Materials Science***, **2004**, 39 (16-17), 5081-5089.

22. H. K. Kammler, S. E. Pratsinis, *Carbon-coated titania nanostructured particles: Continuous, one-step flame-synthesis*, ***Journal of Materials Research***, **2003**, 18 (11), 2670-2676.

23. W. J. Stark, S. E. Pratsinis, A. Baiker, *Heterogeneous catalysis by flame-made nanoparticles*, ***Chimia***, **2002**, 56 (10), 485-489.

24. H. Maskrot, Y. Leconte, N. Herlin-Boime, C. Reynaud, E. Guelou, L. Pinard, S. Valange, J. Barrault, M. Gervais, *Synthesis of nanostructured catalysts by laser pyrolysis*, ***Catalysis Today***, **2006**, 116 (1), 6-11.

25. R. Asahi, T. Morikawa, T. Ohwaki, K. Aoki, Y. Taga, *Visible-light photocatalysis in nitrogen-doped titanium oxides*, ***Science***, **2001**, 293 (5528), 269-271.

26. H. Irie, Y. Watanabe, K. Hashimoto, *Carbon-doped anatase TiO_2 powders as a visible-light sensitive photocatalyst*, ***Chemistry Letters***, **2003**, 32 (8), 772-773.

27. T. Umebayashi, T. Yamaki, S. Yamamoto, A. Miyashita, S. Tanaka, T. Sumita, K. Asai, *Sulfur-doping of rutile-titanium dioxide by ion implantation: Photocurrent spectroscopy and first-principles band calculation studies*, ***Journal of Applied Physics***, **2003**, 93 (9), 5156-5160.

28. T. Yamaki, T. Sumita, S. Yamamoto, *Formation of TiO_2-xFx compounds in fluorine-implanted TiO_2*, ***Journal of Materials Science Letters***, **2002**, 21 (1), 33-35.

29. A. Teleki, S. E. Pratsinis, *Blue nano titania made in diffusion flames*, ***Physical Chemistry Chemical Physics***, **2009**, 11 (19), 3742-3747.

30. B. Pignon, H. Maskrot, V. G. Ferreol, Y. Leconte, S. Coste, M. Gervais, T. Pouget, C. Reynaud, J. F. Tranchant, N. Herlin-Boime, *Versatility of laser pyrolysis applied to the synthesis of TiO_2 nanoparticles - Application to UV attenuation*, ***European Journal of Inorganic Chemistry***, **2008**, (6), 883-889.

31. N. Herlin, H. Maskrot, B. Pignon, *Procédé de synthèse de nanoparticules de TiCON et TiON par pyrolyse laser*, FR070328, **2007**.

32. P. Simon, B. Pignon, B. Miao, S. Coste-Leconte, Y. Leconte, S. Marguet, P. Jegou, B. Bouchet-Fabre, C. Reynaud, N. Herlin-Boime, *N-Doped Titanium Monoxide Nanoparticles with TiO Rock-Salt Structure, Low Energy Band Gap, and Visible Light Activity*, ***Chemistry of Materials***, **2010**, 22 (12), 3704-3711.

33. P. Simon, *Synthèse de nanoparticules d'oxydes de titane par pyrolyse laser : étude de la structure cristallographique et des propriétés optiques et électroniques*, Thèse de l'Université de Paris Sud (ED471), Paris, **2011**.

34. Oxonica, *About OPTISOL™ UV Absorber*, http://www.oxonica.com/materials/materials_optisol.php.

35. NANODERM, *Quality of skin as a barrier to ultra-fine particles*, QLK4-CT-2002-02678. Final report, **2007**.

36. Y. A. Ren, M. Chen, Y. Zhang, L. M. Wu, *Fabrication of Rattle-Type TiO2/SiO2 Core/Shell Particles with Both High Photoactivity and UV-Shielding Property*, ***Langmuir***, **2010**, 26 (13), 11391-11396.

37. O. K. Park, Y. S. Kang, *Preparation and characterization of silica-coated TiO2 nanoparticle*, ***Colloids and Surfaces a-Physicochemical and Engineering Aspects***, **2005**, 257-58, 261-265.

38. J. C. Chen, M. Hu, W. D. Zhu, Y. P. Li, *Synthesis of well-defined structurally silica-nonlinear polymer core-shell nanoparticles via the surface-initiated atom transfer radical polymerization*, ***Applied Surface Science***, **2011**, 257 (15), 6654-6660.

39. J. A. Zhang, N. N. Liu, M. Z. Wang, X. W. Ge, M. Y. Wu, J. J. Yang, Q. Y. Wu, Z. L. Jin, *Preparation and Characterization of Polymer/Silica Nanocomposites via Double In Situ Miniemulsion Polymerization*, ***Journal of Polymer Science Part a-Polymer Chemistry***, **2010**, 48 (14), 3128-3134.

40. B. Jiang, X. T. Zu, F. Y. Tang, Z. H. Wu, J. Lu, Q. R. Wei, X. D. Zhang, *Surface modification on nanoscale titanium dioxide by radiation: Preparation and characterization*, ***Journal of Applied Polymer Science***, **2006**, 100 (5), 3510-3518.

41. S. F. Zhong, Q. R. Ou, Y. D. Meng, *High frequency discharge plasma induced grafting of polystyrene onto titanium dioxide powder*, ***Journal of Wuhan University of Technology-Materials Science Edition***, **2007**, 22 (2), 303-306.

42. Y. Shirai, K. Kawatsura, N. Tsubokawa, *Graft polymerization of vinyl monomers from initiating groups introduced onto polymethylsiloxane-coated titanium dioxide modified with alcoholic hydroxyl groups*, ***Progress in Organic Coatings***, **1999**, 36 (4), 217-224.

43. B. J. Lowes, A. G. Bohrer, T. Tran, D. A. Shipp, *Grafting of polystyrene "from" and "through" surface modified titania nanoparticles*, ***Polymer Bulletin***, **2009**, 62 (3), 281-289.

44. N. Tsubokawa, H. Ishida, *Graft-Polymerization of Vinyl Monomers by Peroxyester Groups Introduced onto the Surface of Inorganic Ultrafine Particles*, ***Polymer Journal***, **1992**, 24 (8), 809-816.

45. G. H. Li, *Surface Modification and Characterizations of TiO_2 Nanoparticle*, ***Surface Review and Letters***, **2009**, 16 (1), 149-151.

46. R. Matsuno, H. Otsuka, A. Takahara, *Polystyrene-grafted titanium oxide nanoparticles prepared through surface-initiated nitroxide-mediated radical polymerization and their application to polymer hybrid thin films*, ***Soft Matter***, **2006**, 2 (5), 415-421.

47. H. Xu, J. X. Shi, T. Sun, *Polymethylmethacrylate-grafted titanium dioxide nanoparticles prepared via radical polymerization*, ***Journal of Advanced Materials***, **2008**, 40 (1), 27-32.

48. L. Zan, Z. S. Liu, J. C. Zhong, Z. G. Peng, *Organic modification on TiO_2 nanoparticles by grafting polymer*, ***Journal of Materials Science***, **2004**, 39 (9), 3261-3264.

49. C. Deng, P. F. James, P. V. Wright, *Poly(tetraethylene glycol malonate) titanium oxide hybrid materials by sol-gel methods*, ***Journal of Materials Chemistry***, **1998**, 8 (1), 153-159.

50. X. W. Fan, L. J. Lin, P. B. Messersmith, *Surface-initiated polymerization from TiO_2 nanoparticle surfaces through a biomimetic initiator: A new route toward polymer-matrix nanocomposites*, ***Composites Science and Technology***, **2006**, 66 (9), 1198-1204.

51. B. Hojjati, P. A. Charpentier, *Synthesis and kinetics of graft polymerization of methy methacrylate from the RAFT coordinated surface of nano-TiO_2*, ***Journal of Polymer Science Part a-Polymer Chemistry***, **2008**, 46 (12), 3926-3937.

52. C. Mangeney, Z. Qin, S. A. Dahoumane, A. Adenier, F. Herbst, J. P. Boudou, J. Pinson, M. M. Chehimi, *Electroless ultrasonic functional ization of diamond nanoparticles using aryl diazonium salts*, ***Diamond and Related Materials***, **2008**, 17 (11), 1881-1887.

53. A. Mesnage, M. Abdel Magied, P. Simon, N. Herlin-Boime, P. Jegou, G. Deniau, S. Palacin, *Grafting polymers to titania nanoparticles by radical polymerization initiated by diazonium salt*, ***Journal of Materials Science***, **2011**, 46 (19), 6332-6338.

CONCLUSION

We have just described a recently developed chemical anchoring process induced by diazonium salts for the functionalization of any type of surfaces by organic layers and particularly polymer films. The aim of this work was to study the different parameters of this aqueous process as well as the structure of the films in order to propose a grafting mechanism according to the composition of the solution (i.e. in presence or absence of a reducing agent and with or without a vinylic monomer in solution). We have also evaluated the feasibility of its application for the functionalization of TiO_2 nanoparticles with a view to use them in sunscreen products.

We have highlighted the industrial interests for surface functionalization by organic coatings and we have emphasized the role of diazonium salts as a coupling agent in the improvement of some processes leading to the formation of polymer films (cathodic electrografting, surface-initiated polymerizations, and so on…). In this context, the very versatile approach (working in ambient conditions, in water and forming strongly grafted and stable organic films) has proven to overcome some of the limitations generally encountered by competing techniques, in particular the use of organic solvents.

By using the spontaneous reaction of diazonium salts with some specific substrates, we have demonstrated the formation of a covalent substrate-film interface bond in a very precise case (on nickel plates in acetonitrile). Surprisingly, we have also observed the spontaneous grafting of diazonium salts on gold. The most probable mechanisms have been tested and we have concluded in favor of the involvement of complementary mechanisms which are the direct reaction of diazonium cations with the gold surface, as well as a cationic mechanism leading to the formation of aryl cations able to graft on the substrate. However, to date, the mechanism is still subject to debate in the scientific community.

Then, with a view to obtain thicker polyphenylene films, the introduction of a reducing agent in solution has been investigated. In this system, we have demonstrated for the first time the presence of aryl radicals in solution, and thus confirmed the involvement of a redox-induced process leading to the reduction of diazonium salts into aryl radicals. Similarly to electrochemical processes, once formed these aryl radicals are able to graft on the substrate and on already grafted aryl moieties leading to thin polyphenylene films. However, unlike electrochemical procedures, due to its redox nature, this process can be potentially applied to any type of materials. Moreover, we have evidenced that contrary to other reducing agents, ascorbic acid reduces the diazonium salt via an inner-sphere electron transfer mechanism which explains the peculiar experimental conditions used and notably the choice in the concentration ratio of reducing agent and diazonium salt.

In order to access a wider range of organic coatings, a vinylic monomer has been added to the reactive solution (Graftfast™ process). In addition to a specific concentration of reducing agent, we have also found that a compromise on the monomer concentration has to be made. We have managed to confirm the control of the thickness of the grafted films with the reaction time. Thanks to a dual surface-solution analysis, we have established a very likely "*grafting to*" mechanism based on the double role of aryl radicals involving the formation of a primer layer by their grafting on the substrate (providing the covalent link between the surface and the polymer chains) as well as the initiation of the polymerization of the vinylic monomer. The oligomer radical chains in solution can then react on the aromatic rings present on the surface, their successive addition leading to the thickening of the film. However, some work still needs to be done to understand the sensitivity of the reaction to pH as well as the acid used and to confirm or invalidate the correlation of this phenomenon with the use of VC.

Although this work attempted to cover the subject, for the sake of simplicity in the understanding of the grafting mechanism, we have restricted this work to very specific conditions (mainly commercial diazonium salts with ascorbic acid and HEMA on gold plates). Therefore, it would be interesting to test other systems (diazonium salt / reducing agent / aqueous solvent / substrate / polymer) from the one studied in this work. Particularly, working with other substrates or with insoluble monomers in emulsion would confirm the versatility of the process and widen the range of its applications. However, it is likely that according to the system studied, an optimization of the experimental parameters would be required since variations in mechanism and reactivity could occur. Besides, a better understanding of the one-pot reaction (formation of the diazonium salt simultaneously to its grafting) as well as an exploration of a larger variety of experimental conditions (to date, reaction principally carried out with iron powder) would become essential since applications using this system are expanding.

These redox-induced anchoring processes in particular Graftfast™ are very promising and have already been used for various applications for instance:

- cation exchange membranes[1],
- self-adhesive surfaces[2],

[1] X. T. Le, P. Viel, P. Jegou, A. Garcia, T. Berthelot, T. H. Bui, S. Palacin, *Diazonium-induced anchoring process: an application to improve the monovalent selectivity of cation exchange membranes*, ***Journal of Materials Chemistry***, **2010**, 20 (18), 3750-3757.

[2] P. Viel, X. T. Le, V. Huc, J. Bar, A. Benedetto, A. Le Goff, A. Filoramo, D. Alamarguy, S. Noel, L. Baraton, S. Palacin, *Covalent grafting onto self-adhesive surfaces based on aryldiazonium salt seed layers*, ***Journal of Materials Chemistry***, **2008**, 18 (48), 5913-5920.

- immobilization of DNA and proteins[3],

- effluent treatment[4],

- composite materials[5],

- electroless plating onto polymers[6]: offering a chromium free alternative method applicable for the formation of patterned surfaces and to polymers usually non-accessible by traditional metallization process.

Recently and as presented in this work, it has also been successfully applied to TiO_2 nanoparticles with specific optical properties making them an interesting material in sunscreen products. The morphology of the nanoparticles remained unchanged after the polymer grafting while the stability of the dispersion of the grafted nanoparticles in water has been enhanced. However, the stability has to be even more improved and it remains to investigate the conservation of the optical properties of the TiO_2 nanoparticles after the grafting and to test the photocatalytic activity of the powder.

[3] T. Berthelot, A. Garcia, L. Xuan Tuan, J. El Morsli, P. Jegou, S. Palacin, P. Viel, *''Versatile toolset'' for DNA or protein immobilization: Toward a single-step chemistry*, ***Applied Surface Science***, **2011**, 257 (8), 3538-3546.

[4] X. T. Le, P. Viel, A. Sorin, P. Jegou, S. Palacin, *Electrochemical behaviour of polyacrylic acid coated gold electrodes: An application to remove heavy metal ions from wastewater*, ***Electrochimica Acta***, **2009**, 54 (25), 6089-6093.

[5] A. Gohier, F. Nekelson, M. Helezen, P. Jegou, G. Deniau, S. Palacin, M. Mayne-L'Hermite, *Tunable grafting of functional polymers onto carbon nanotubes using diazonium chemistry in aqueous media*, ***Journal of Materials Chemistry***, **2011**, 21 (12), 4615-4622.

[6] A. Garcia, T. Berthelot, P. Viel, J. Polesel-Maris, S. Palacin, *Microscopic Study of a Ligand Induced Electroless Plating Process onto Polymers*, ***ACS Applied Materials & Interfaces***, **2010**, 2 (11), 3043-3051.

A. Garcia, J. Polesel-Maris, P. Viel, S. Palacin, T. Berthelot, *Localized Ligand Induced Electroless Plating (LIEP) Process for the Fabrication of Copper Patterns Onto Flexible Polymer Substrates*, ***Advanced Functional Materials***, **2011**, 21 (11), 2096-2102.

A. Garcia, *Ligand Induced Electroless Metal Plating of Polymers*, Thesis of the Ecole Polytechnique, **2011**.

APPENDIXES

Appendix 1
Laboratory apparatus

1. Analysis techniques

AFM

AFM images were obtained in tapping mode using a commercial AFM (Molecular Imaging PicoSPMLe) controlled with a PicoScan 2100 controller (Scientec, France) placed in an acoustic box on a floating table to avoid vibrations during measurements. Pyramid-shaped AFM tips in silicon were mounted onto a 225 µm-length cantilever vibrating at a resonance frequency of approximately 75 kHz and with a spring constant of 3 $N.m^{-1}$. Data were treated with Gwyddion software.

Contact angle

Contact angle measurements were made on a system from Apollo Instruments by delivering a 2 µL drop of ultra-pure water (H_2O MQ 18 MΩ) at a 1 µL/s speed from a microsyringe onto the sample mounted on an illuminated horizontal stage. The image of the static water droplet was captured by a video camera and the SCA20 software. Six measurements were taken for each sample and the average water contact angle was calculated.

Electrospray ionization mass spectroscopy *(CEA/DEN/DANS/DPC/SECR/LSRM)*

ESI-MS analyses were carried out using a LCTXE premier from Waters in a negative ionization mode with a ToF analysis. A flow rate of 10 µL/min H_2O:MeOH 50:50 v/v was employed. A dinitrogen flow rate of 10 mL/min was set up at the cone level and a 350 mL/min one at the desolvatation level. The desolvatation and source temperatures were respectively 200 °C and 100°C. The capillary and the cone voltages were respectively 2500 V and 20 V.

Sample preparation: MeOH was added to the reaction medium after the desired reaction time in order to stop the reaction and to reach a H_2O:MeOH 50:50 v/v solution (compatible with the column).

Ellipsometry *(CEA/DSM/IRAMIS/SPEC/GMOB)*

The thickness of the films was determined by spectroscopic ellipsometry, using a SOPRA ES3G ellipsometer. The light beam allowed getting a 2 x 2 mm^2 footprint on the sample. The optical constants, used for computation of the film thickness, of the bare gold substrates were extracted from the literature and the refractive index of the polymer layer was 1.45 according to typical values usually employed for organic films. The major sources of uncertainty lay in the difference of the substrate from ideal bulk metal, from its roughness as well as from the inhomogeneity of the polymer film and its dual composition.

EPR *(CEA/DSM/IRAMIS/LSI)*

EPR spectra were recorded at the X band (9.4 GHz) on a Bruker ER-200D EPR spectrometer equipped with a high sensibility cavity. EPR measurements were performed at room temperature using a flat quartz aqueous cell. The typical instrument settings were: microwave power 2 mW, gain 10^5, modulation amplitude 0.1 G, time constant 81.92 ms. Hyperfine splitting constants and spectra deconvolution were determined by means of an automated simulation program using the Levenberg-Marquardt method. For all the spectra Lorentz line shapes were assumed. Radical concentrations were calculated from a 5 mM 4-hydroxyTEMPO water solution.

Sample preparation: detailed in appendix 3.

GC-MS *(CEA/DEN/DANS/DPC/SECR/LSRM)*

For gas chromatography - mass spectroscopy analyses, a GC-ToF (GCT premier) from Micrommas (Manchester, UK) was used with the software MassLynx (version 4.1). Electron impact ionization was employed with energies of 70 eV (source temperature 200 °C). The capillary column (SLB-5ms from Sigma Aldrich) was apolar, of 30 m length, 0.25 mm diameter and with a 0.25 µm film thickness. A helium constant flow rate of 1.1 mL/min was running across the column. The injection syringe was always washed in MeOH and then water prior to injecting the solution of interest in the spectrometer in a splitless mode. The program temperature of the oven was the following: start at 100 °C then 20 °C/min until a temperature of 300 °C was reached and finally a 10 min stage at 300 °C. The temperatures of injection and of the interface were both 250 °C.

Sample preparation: In order to analyse all the compounds present in solution or formed during the reaction (including precipitates) and to « stop » the reaction, ACN was added after the desired reaction time. A dilution in water was then performed to reach concentrations of maximum 4.10^{-4} M in diazonium salts and inject solutions of ACN:H_2O 1:10 v/v.

IR-ATR

Infrared spectra were obtained on a Bruker VERTEX 70 spectrometer equipped with ATR (Attenuated Total Reflection) Pike-Miracle device (equipped with a synthetic diamond crystal deposited on a KRS-5 (thallium-bromo-iodide) lens). The detector was a MCT (Mercury-Cadmium-Telluride) working at liquid nitrogen temperature. The spectra were obtained *via* the OPUS software after 256 scans at 2 cm^{-1} resolution between 600 and 4000 cm^{-1} with a background at air. The base line of the spectra is automatically adjusted. The contributions from H_2O (3100-3300 cm^{-1}, liquid and gas from the detector), CO_2 (2300 cm^{-1}, gas) and ATR crystal (2000-2200 cm^{-1}, diamond) were subtracted.

IRRAS

IR-mappings were obtained with a Bruker Hyperion 2000 microscope purged with dinitrogen and equipped with a MCT detector. The sample moves thanks to a motorized plate. Whatever the analysed surface, spectra (600-4000 cm^{-1}) were acquired after 126 scans at a 6 cm^{-1} resolution. The data are integrated on the absorption band of interest (1350 cm^{-1} in the case of a PNP layer and 1730 cm^{-1} in the case of a PHEMA film).

NMR *(CEA/DSV/iBiTec-S/SCBM)*

^{1}H-NMR spectra were recorded at room temperature on a Bruker AVANCE DRX 400 operating at 400 MHz.

Profilometer

The thickness of the sample was measured with a Dektak 3030 ST profilometer using a lateral resolution of 50 µm able to measure steps between 10 nm and 400 µm. Typically, a scan length of 500 µm at a low stylus speed with a 2 mg force was used.

SEC *(CEA/DEN/DANS/DPC/SECR/LSRM)*

Size exclusion chromatography analyses were performed on a liquid chromatography system (METROHM) using a high performance column (Superdex 75 10/300 from Tricorn). Therefore, the stationary phase was made of composite of cross-linked agarose and dextran (13 µm average particle size). The mobile phase was made of 10 mM of ammonium acetate in H_2O DI to avoid interaction between the stationary phase and the compounds of interest. The detection was provided by a refractive index detector (RI Bischoff 8120).

Sample preparation: after the desired reaction time, a volume of ACN/H_2O equal to four times the volume of the reactive solution was added (final solution composed of ACN:H_2O 20:80 v/v) in order to stop the reaction and solubilise all the polymer. Then, these samples were injected in a liquid chromatography system for a SEC analysis.

TEM *(CEA/DSV/iBiTec-S/SB2SM)*

TEM images were obtained with a Philips CM12 electron microscope. For the visualization of the polymer on the TiO_2 nanoparticles a negative staining was performed by exposing the grids to a droplet of a 2 wt.% uranyl acetate solution in water for 1 min. The grids were tapped dry with a piece of filter paper to remove the excess of stain and air-dried before TEM measurements.

TGA *(CEA/DSM/IRAMIS/SPAM/EDNA)*

Differential thermogravimetric analyses were carried out on a simultaneous TGA-DSC analyser Netzsch STA 449 C under a flow of argon and with the following temperature program: 20 to 800 °C at 10°C/min.

ToF-SIMS *(Alchimer SA*)

The instrument for ToF-SIMS analyses was an ION TOF IV from *ION TOF*. Depth profiles were obtained working in negative ionization mode. A Cs^+ ion beam (500 V) was used in addition of the Au_3^+ primary ions beam (energy of 25 keV on a 150 x 150 μm^2 surface) for the abrasion of a 750 x 750 μm^2 zone of the sample. Acquiring time was depending on the thickness of the sample.

Turbidimeter *(CEA/DSM/IRAMIS/SPAM/EDNA)*

The turbidimetry analyses were performed on a Turbiscan Lab expert apparatus from Formulaction. A scan was recorded every 1h. Prior to the characterisation, the suspensions of nanoparticles were sonicated with a US probe for 30 min.

UV-visible

UV-visible spectra were recorded with a Perkin Elmer - Lambda 650 spectrometer with a tungsten-halogen and deuterium lamps and a R955 photomultiplier detector (resolution 190 - 900 nm). Data were collected *via* the Perkin Elmer UV win lab explorer software. When fast measurements were required a Perkin Elmer - Lambda 900 spectrometer able to work at 500 nm/min was used.

XPS

X-ray photoemission spectroscopy (XPS) analyses were performed with a Kratos Axis Ultra DLD using a high-resolution monochromatic Al-Kα line X-ray source at 1486.6 eV and a power of 150 W. Fixed hemispheric analyser pass energy of 20 eV was used for core level scans and 160 eV for survey. The photoelectron take-off angle was always normal to the surface, which provided an integrated sampling depth of approximately 15 nm for a polymeric material. The area analysed was 700 x 300 μm^2. A survey spectrum and core-level spectra of C1s (282 - 292 eV), O1s (526 - 538 eV) and N1s (396 - 409 eV) regions were systematically recorded. The energy scale of the instrument was calibrated by setting Au $4f_{7/2}$ = 84.0 eV, $Ag3d_{5/2}$ = 368.7 eV, $CuL_3M_{4,5}M_{4,5}$ = 567.9 eV and Cu $2p_{3/2}$ = 932.65 eV. When charging phenomena occurred, we used a charge neutralizer (Kratos's system). On the spectra, the charge was counterbalanced by adjusting:

- in the case of gold substrates, the Au $4f_{7/2}$ level of the pristine gold substrate (reference sample always analysed if the charge neutralizer was employed) at 84.0 eV and by applying this shift to all the samples studied in the same batch,
- in the case of TiO_2 nanoparticles, the carbon-carbon bond energy of the contamination of untreated TiO_2 at 285.0 eV.

For small spot analyses, the pass energy of the analyser was 40 eV for core level scans. The area analysed was a spot of 110 µm in diameter. Data were acquired with Vision 2 software and treated with Avantage software.

2. Other apparatus

Electrochemistry

EG&G potentiostats (Princetron Applied Research) model 263A and 273A were used for, respectively, electrochemical measurements and removal of the oxide from the substrates.

Probe sonicator

The probe sonicator used for the dispersion of nanoparticles as well as during reactions was an Autotune Series High Intensity Ultrasonic Processor 750 W model (Fisher Bioblock Scientific). The probe was a 3 mm titanium-coated conic microprobe. To avoid the warming of the reactive solution, the system was placed in 5 °C cooled water.

Rotating disk electrode

A rotating disk electrode system, model 636 (EG&G Princeton Applied Research), was used for investigating reaction mechanisms. The electrode was made of conductive stainless steel disks polished and coated with 150 µm of pure gold (by vacuum evaporation, see below) embedded in an inert non-conductive polymer (PTFE). It was attached to an electric motor in order to control precisely the rotating rate of the electrode. Since the reaction studied was not electrochemical, the rotating disk electrode was not connected to a potentiostat.

Spin coating

The deposition of organic films was achieved using a spin coater from Laurell Technologies (model WS-400B-6NPP Lite).

Sputtering deposition

Sputter deposition was performed, from an Alcatel apparatus, on glass plates (RS France), cleaned beforehand, under vacuum with a diode/radio frequency system from nickel (Marz 99.995 %) and platinum (Marz 99.99 %) targets.

Ultrasonic cleaner

An ultrasonic cleaner (VWR), with a 1L tank capacity and able to deliver a maximum power of 80 W was used in the rinsing procedure of the substrates.

Vacuum Evaporation

Gold substrates were obtained by vacuum evaporation in a Balzers BAK 600 evaporator of chromium (to enhance gold adhesion on glass) and pure gold (99.99 % from Williams Advanced Materials) at room temperature on 37 x 6 mm² glass plates supplied by RS France (homemade cut from 76 x 26 mm^2 glass plates). Prior to evaporation, the glass plates were rinsed 10 min under ultrasonication in water, ethanol and acetone successively. The thickness of the deposited layers was monitored in-situ by using a quartz crystal microbalance. This technique was also used for the deposition of gold on silicon and stainless steel substrates.

Appendix 2
Chemical syntheses

1. Reprecipitation of NBDT

The commercial nitrobenzene diazonium tetrafluoroborate (Scheme 1) was purified by precipitation in cold diethyl ether.

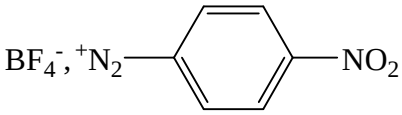

Scheme 1 – Nitrobenzene diazonium tetrafluoroborate (NBDT).

The yellow NBDT powder (Figure 1a) was dissolved, at room temperature and under stirring, in the minimum amount of acetonitrile. The mixture was then poured slowly into ice-cold diethyl ether to precipitate the diazonium salt. The precipitate was filtered through a Büchner funnel, washed with cold diethyl ether and dried, at room temperature, in a vacuum desiccator for 1h. Finally, the white powder (Figure 1b) was kept in a closed vial in the fridge.

Figure 1 – Images of the NBDT powder a) before and b) after the reprecipitation procedure.

The powder before and after reprecipitation were characterized by IR-ATR (Figure 2). The two spectra are identical displaying in particular the characteristic absorption band of the diazonium group (N_2^+) at 2306 cm^{-1} as well as the two characteristic bands of nitro groups at 1538 cm^{-1} (ν^{as}_{NO2}) and 1355 cm^{-1} (ν^{s}_{NO2}).

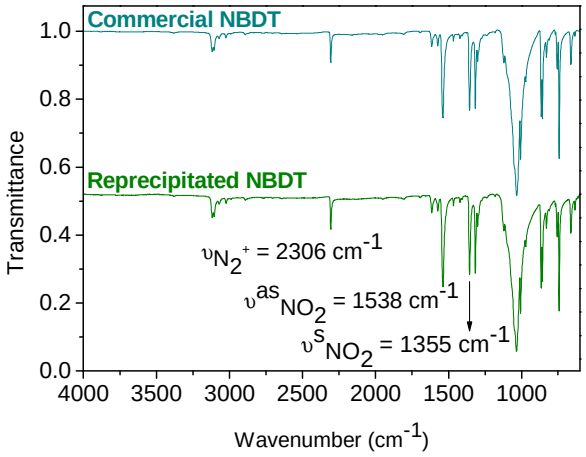

Figure 2 – IR-ATR spectra of NBDT before and after the reprecipitation procedure.

NBDT was also characterized by NMR. The compounds before and after reprecipitation gave the same results.

^{1}H NMR (400 MHz, CD_3CN, δ, ppm):

- before reprecipitation: 8.74 (d, $^{3}J_{HH}$ = 9.2 Hz, 2H), 8.62 (d, $^{3}J_{HH}$ = 9.6 Hz, 2H);
- after reprecipitation: 8.75 (d, $^{3}J_{HH}$ = 9.6 Hz, 2H), 8.62 (d, $^{3}J_{HH}$ = 9.2 Hz, 2H).

2. Syntheses of diazonium salts

Most of the diazonium salts used in this work (3Cl, CF_3, SCH_3, COOH) were synthesized by the following procedure. As an example, we will detail the procedure used for the synthesis of 4-thiomethylbenzene diazonium tetrafluoroborate (Scheme 2).

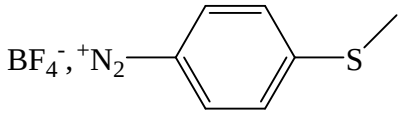

Scheme 2 – 4-thiomethylbenzene diazonium tetrafluoroborate.

The diazonium salt was prepared from the corresponding amine. In a typical synthesis, 1.1 equivalents of $NOBF_4$ were added in a closed round-bottom flask containing a solution of 4-(thiomethyl)aniline dissolved in the minimum amount of acetonitrile at -40 °C. The mixture was stirred for 30 min under argon flow at -40°C and then warmed to room temperature and poured slowly in ice-cold diethyl ether to precipitate the diazonium salt. The salt was filtered through a Büchner funnel and washed with diethyl ether. The diazonium salt was stored at -18 °C prior to use.

The synthesized 4-thiomethylbenzene diazonium tetrafluoroborate was then characterized by IR (Figure 3) and NMR. The IR spectrum clearly shows the characteristic band of diazonium groups at 2250 cm^{-1} as well as a few other bands testifying of the presence of thiomethyl group in the compound (1415 cm^{-1}: ν^{as}_{CH3}, 1333 cm^{-1}: ν^{s}_{CH3}) and of the nature of the counter-ion (ν_{BF4-} = 1050 & 1020 cm^{-1}).

^{1}H NMR (400 MHz, CD_3CN, δ, ppm): 8.51 (d, $^{3}J_{HH}$ = 9.6 Hz, 2H), 7.74 (d, $^{3}J_{HH}$ = 9.2 Hz, 2H), 2.67 (s, 3H, SC*H*$_3$).

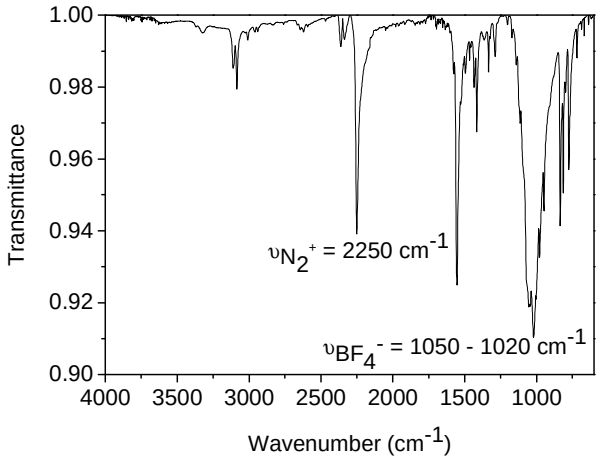

Figure 3 – IR-ATR spectrum of 4-thiomethylbenzene diazonium tetrafluoroborate.

Concerning 4-nitrobenzene diazonium perchlorate, the synthesis procedure used was different. Indeed, 2 equivalents of amine (4-nitroaniline) were mixed with 1 equivalent of $NaNO_2$ in an ice-cold flask. Then 2-3 mL of $HClO_4$ were added and the solution was stirred for 30 min. The precipitate was filtered through a Büchner funnel and softly dried at ambient air.

The IR spectrum of the synthesized product is presented in Figure 4. It is very similar to the spectrum of 4-nitrobenzene diazonium tetrafluoroborate (see Figure 2) except for the IR absorption band attributed to the counter-ion at 620 and 1065 cm^{-1} standing for ClO_4^- (instead of 1050 and 1020 cm^{-1} for BF_4^-).

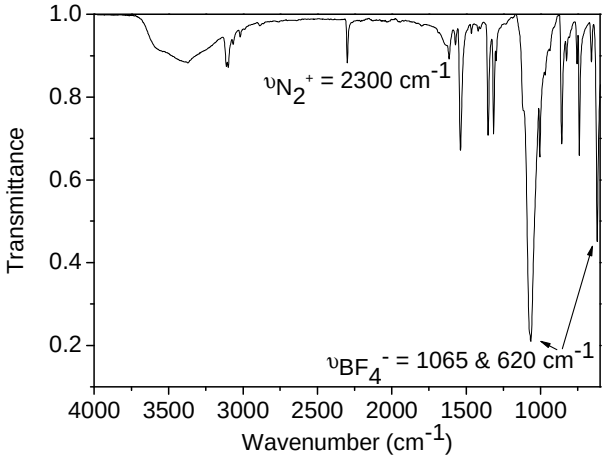

Figure 4 – IR-ATR spectrum of 4-nitrobenzene diazonium perchlorate.

3. Formation of the diazoether

Stoichiometric amounts of freshly reprecipitated NBDT and ascorbic acid were mixed in a H_2O DI. After a 15 min reaction time, the diazoether was precipitated in ether. The powder was collected in a Büchner funnel, dried at ambient air prior to be kept in a closed vial in the fridge.

The UV-visible spectrum of this synthesized compound, presented in Figure 5, displays an intense absorption band at 354 nm. Moreover, the corresponding IR spectrum (Figure 6) is consistent with the presence of nitro, phenyl, alcohol as well as carbonyl groups.

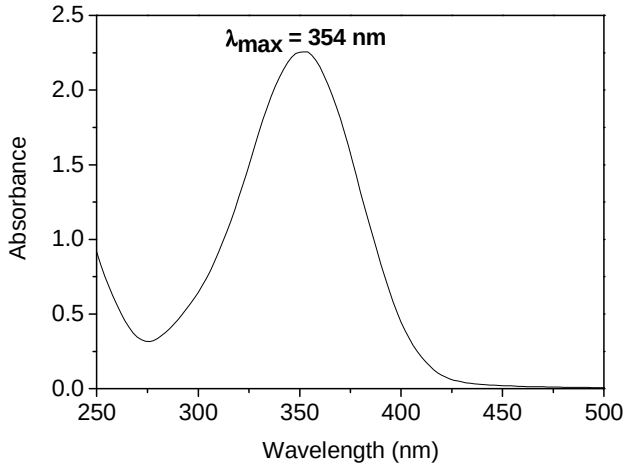

Figure 5 – UV-visible of the diazoether from the reaction of NBDT with VC.

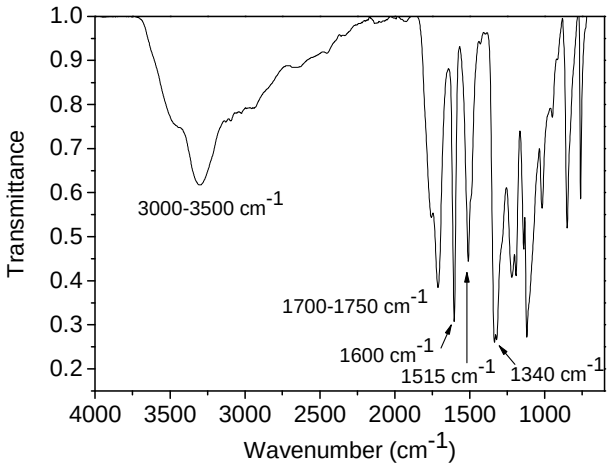

Figure 6 – IR spectrum of the diazoether from the reaction of NBDT with VC.

Therefore, according to the literature, it seems that the diazoether represented on Scheme 3 was successfully synthesized. Besides, the molar mass of the synthesized compound, determined by electrospray ionization mass spectroscopy, corresponds to the one of the diazoether. However, in view of the complexity of the NMR spectrum of this molecule (not shown here), it is likely that the synthesized diazoether contains impurities. This is not too much of a problem since only qualitative studies will be made using the molecule.

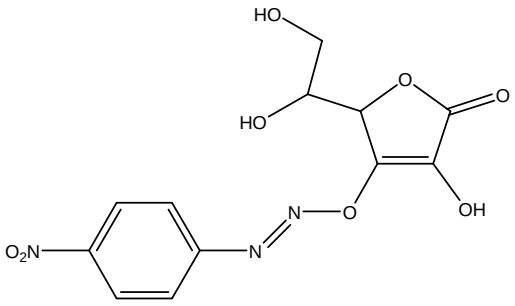

Scheme 3 – Synthesized diazoether from the reaction of NBDT with VC.

Appendix 3
EPR experimental details

With a view to detect and identify short lived free radicals, EPR experiments have been performed using a spin-trap. The compound of interest as a spin-trap is the monomer of the 2-methyl-2-nitrosopropane (MNP) dimer. The MNP solution was prepared, at room temperature, in a nitrogen flow glove box (oxygen free atmosphere) by dissolving about 0.2 g of the MNP dimer in 50 mL of DI water previously bubbled 10 min with argon gas. Then, the solution was stirred overnight in a closed vial at room temperature in the dark to dissolve as much MNP dimer powder as possible and to reach stable monomer-dimer equilibrium (approximately 10 h after dissolution[1]).

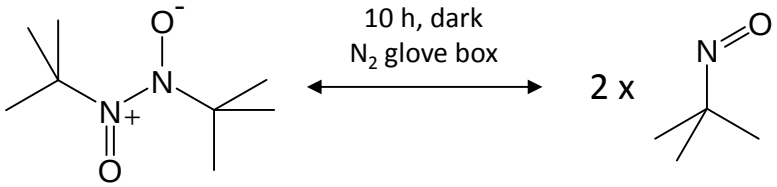

Scheme 1 – Reaction of the formation of the MNP spin-trap in solution.

This spin-trap solution is very sensitive to temperature, light, oxygen and stable for a limited period of time. Thus, it is easily understandable that the spin-trap solution was prepared just before its use and stored for no more than a day in the dark fridge. The equilibrium of the MNP dimer (colorless liquid) and monomer (blue liquid) in aqueous solution imposes to perform a measurement in order to evaluate the MNP monomer concentration in solution.

A simple method using UV/vis spectrometry adapted from literature[2] was used to find out the MNP monomer concentration in solution. Kuwabara *et al.*[3] determined a molar absorbance coefficient of $\varepsilon_{662\ nm} = 10 \pm 5\ M^{-1}.cm^{-1}$ for this compound. As illustrated by Figure 1, the concentration of MNP solutions used, based on the absorbance values at 662 nm, was 2 mM in average (always within the 1 mM – 5 mM range).

[1] M. Kuwabara, S. Miyake, T. Jin, S. Sawamura, *Reactions and Rate Constants between Hydroxyl Radicals and the Dimer and Monomer of Spin Trap 2-Methyl-2-Nitrosopropane Determined by the Pulse-Radiolysis Method*, ***Journal of Physical Chemistry***, **1995**, 99 (38), 14078-14082.

[2] T. Ohkuma, Y. Kirino, T. Kwan, *Some physicochemical properties of 2-methyl-2-nitrosopropane, phenyl N-tert-butyl nitrone, 5,5-dimethylpyrroline-N-oxide, and 2,5,5-trimethylpyrroline-N-oxide and the feasibility of their use as spin traps in aqueous solution*, ***Chemical & Pharmaceutical Bulletin***, **1981**, 29 (1), 25-28.

[3] M. Kuwabara, W. Hiraoka, S. Sawamura, M. Katayama, *Reactions and Rate Constants between Hydrated Electrons and the Monomer and Dimer of 2-Methyl-2-Nitrosopropane Determined by the Pulse-Radiolysis Method*, ***Journal of the American Chemical Society***, **1991**, 113 (10), 3995-3997.

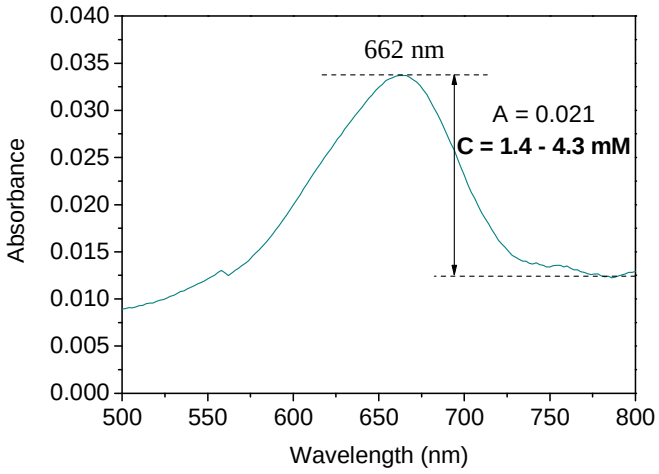

Figure 1 – UV-visible spectrum of a MNP solution before EPR experiments from which the concentration in spin-trap is determined.

To make sure that all the radicals formed can be spin-trapped, an excess of MNP spin-trap versus the diazonium salt was employed during EPR experiments. Therefore NBDT concentration of 1 mM was always used and the concentrations of ascorbic acid and HEMA (in the case of the Graftfast^{TM} process) were adjusted functions of [NBDT].

Appendix 4

Indirect measurement of [NBDT]

For experimental reasons, an indirect measurement of the concentration in diazonium salt can be required. According to the literature[1], the NEDA (N-(1-naphthyl) ethylene diamine dihydrochloride) reacts, in acidic water, specifically with diazonium salts. This diazo coupling reaction[2] with NBDT leads to the formation of a stable azo compound characterized by its maximum absorbance λ_{max} at 545 nm and a corresponding extinction coefficient at room temperature in water of ε_{545}=53,560 $cm^{-1}M^{-1}$. Therefore, by measuring the absorption of this reaction product, the concentration in diazonium salt can be determined.

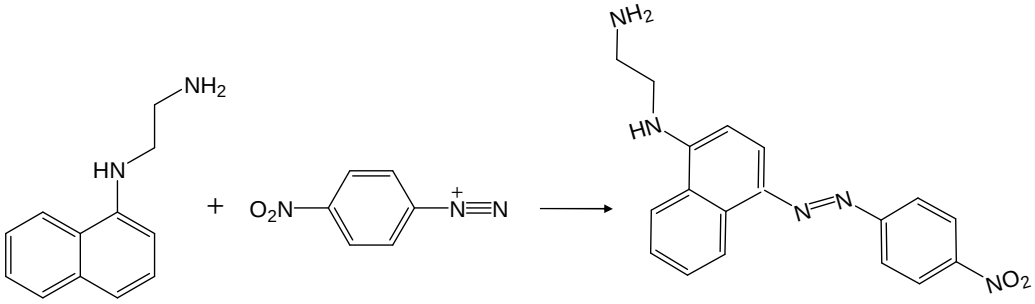

NEDA NBDT N-(1-naphtyl-4-diazo-4nitrobenzene) ethylenediamine

Scheme 1 – Diazo coupling reaction leading to the formation of an adduct detectable by UV-vis.

This indirect method is particularly efficient to measure the [NBDT] with time without working in diluted solutions (usually used so that the concentrations fit directly with the range of values acceptable for direct UV-visible measurements). Moreover, contrary to direct UV-visible measurements, with this technique we are not limited by the acquisition time of the spectrometer. A small amount of the reactive solution was taken and diluted in water (to reach concentrations suitable for UV-visible measurements) prior to the addition of an excess of NEDA powder. A strong change in color was observed (from transparent to purple) testifying of the diazo coupling reaction. Finally, the sample was analysed by an UV-visible spectrometer to determine the absorbance of the sample from which the concentration in diazonium salt was calculated.

[1] T. J. Novitsky, *Diazo-coupling option with Pyrochrome Chromogenic LAL*, ***Associates of Cape Cod Incorporated***, **1998**, 16 (2).

[2] F. A. Carey, R. J. Sundberg, *Chimie Organique Avancée*, Tome 1. Structure moléculaire et mécansimes réactionnels, DeBoeck Université, **1996**.

Appendix 5
Shake-up satellite

It is well-known that benzene rings, for instance in polystyrene films[1], give an XPS peak at high binding energy called π-π* shake-up satellite. This peak is due to shake-up excitations taking place in the π orbitals of the benzene rings. Simultaneously to the ejection of the photoelectron from the 1s orbital, an electron is promoted from an occupied π bonding orbital on the benzene ring to an unoccupied π* antibonding orbital.

Organic films synthesized spontaneously, by a chemically induced process or by the Graftfast™ method all contain benzene rings from the aromatic diazonium salt as demonstrated by the IR and XPS detection of the groups borne by the aromatic rings (mainly nitro in our case) and the detection, uniquely by IR, of the stretching vibration of aromatic carbon double bonds. Therefore, the presence of this shake-up satellite in the XPS C 1s core level spectra of those films was investigated.

From the spectra a and b in Figure 1, it is clear than no π-π* shake-up satellite is present in the 292 eV region for respectively spontaneous PNP films and Graftfast™ PHEMA films.

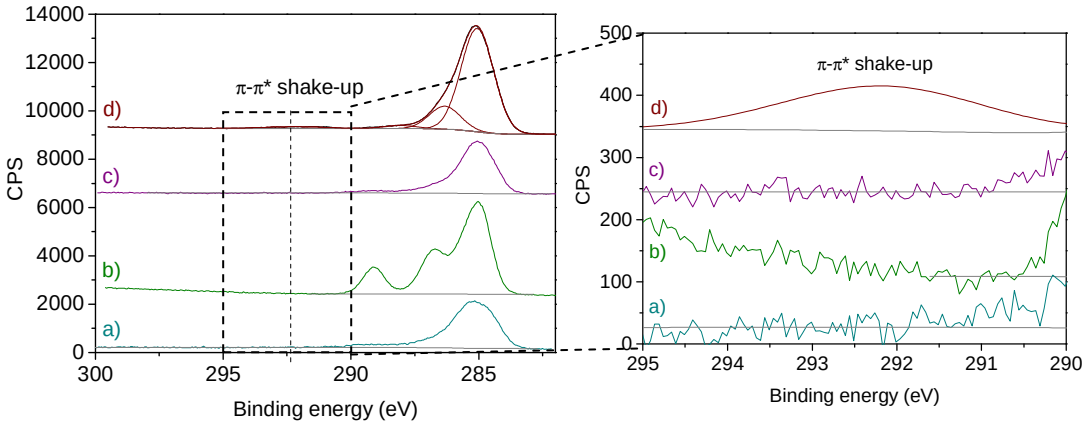

Figure 1 – C 1s core level spectra of a) a spontaneous PNP film (NBDT 0.046 M, H_2O DI, 60 min) and b) a PHEMA film (NBDT 0.046 M, VC 1/10 eq, HEMA 15 eq, H_2O DI, 60 min) c) a SAM of nitrobenzenethiol and d) a thick PNP film on gold with a zoom in the 290 - 295 eV region.

In order to understand why we are not able to observe this peak, a SAM of nitrobenzenethiol (containing a low amount of benzene rings) and a thick PNP film (containing an important amount of aromatic moieties) were analysed by XPS (Figure 1 c and d). The shake-up satellite was only detected in the latter case. Therefore, similarly to the SAM, it is very likely that this

[1] G. Beamson, D. Briggs, *High Resolutin XPS of Organic Polymers*, John Miley & Sons, **1992**.

S. Gam-Derouich, B. Carbonnier, M. Turmine, P. Lang, M. Jouini, D. Ben Hassen-Chehimi, M. M. Chehimi, *Electrografted Aryl Diazonium Initiators for Surface-Confined Photopolymerization: A New Approach to Designing Functional Polymer Coatings*, ***Langmuir***, **2010**, 26 (14), 11830-11840.

Plasma polymerization of polystyrene, http://www.docstoc.com/docs/23284495/XPS-case-study.

peak cannot be detected in the case of the spontaneous or induced grafting of PNP films as well as Graftfast™ PHEMA films due to the very low amount of benzene rings in the films. In particular, concerning Graftfast™ (co)polymer films, the signal can also be difficult to observe in accordance with the relative amounts of the two precursors in the reacting mixture.

To conclude, the π-π* shake-up satellite can be observed but only in the case of films containing an important amount of benzene rings. Therefore, in this work, we will consider that we only display the XPS C 1s spectra up to 292 eV and focus on the feature at lower binding energies.

Appendix 6
Influence of the temperature

The temperature is well known to be responsible for the degradation of diazonium salts in solution. In order to evaluate the role of the temperature in the polymer grafting, reactions in temperature but without any reducing agent were performed. From the results presented in Figure 1, it is clear that, from 35°C, the amount of grafted polymer linearly increases with temperature. This strong effect of the temperature on the grafting fits perfectly with the value of 45°C found by DSC for the decomposition of the NBDT diazonium salt in water. These experiments are also in agreement with the results obtained in III.3.4.2 showing that the higher the temperature (beyond 40°C), the more efficient the spontaneous grafting of diazonium salt on the substrate. However, the precise mechanism of such phenomenon remains unclear. Only further experiments, for example EPR with a heated analysis cell, could allow us to clarify this grafting mechanism.

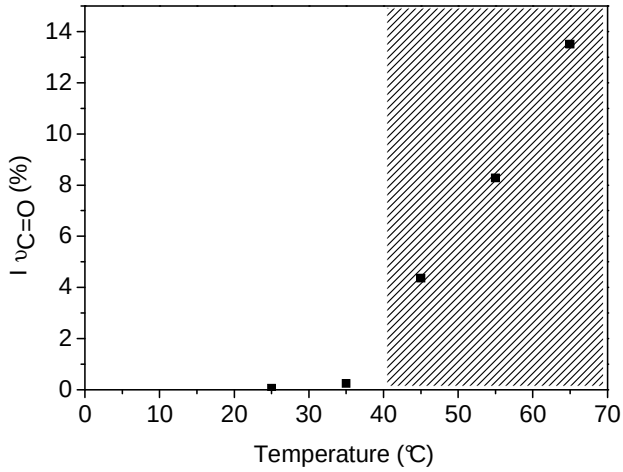

Figure 1 – Intensity of the $\nu_{C=O}$ absorption band from the IR-ATR analysis of the PHEMA films obtained after 1h immersion of gold plates in 0.046 M NBDT, HEMA 15 eq, H_2O DI as a function of the temperature.

The temperature seems to have an effect on the grafting of both diazonium salt and polymer even when no reducing agent is present in solution. Therefore, this parameter will not be investigated in more details since it is likely that it would only complicate the grafting mechanism and not bring any additional information in the understanding of the Graftfast™ mechanism.

Appendix 7
Graftfast™ in buffer solutions

The solvent used in the Graftfast™ process was identified as a parameter having a potential influence on the grafting of polymer. In addition to simply changing the nature of the solvent, we also examined the effect of buffer solutions. Since the diazonium salt reacts with organic acids, phosphate buffer solutions of pH = 2.1 (H_3PO_4/KH_2PO_4) and 7.2 (KH_2PO_4/K_2HPO_4) were tested.

The reactions of NBDT with VC in presence of HEMA performed in buffer solutions were followed with time. The corresponding results giving the variations of the intensity of absorption of the polymer film at 1730 cm^{-1} are shown on Figure 1 in parallel with the results obtained for similar reactions performed in H_2O DI (pH = 5.5) or H_2SO_4 (pH = 2). The reactions performed in phosphate buffer solution of pH = 7 and in H_2O DI give very similar results. Surprisingly, in comparison with the reaction in H_2SO_4 pH = 2, the reaction performed in phosphate buffer solution of pH = 2 gives very high absorption values. Moreover, these values are also a lot higher than those obtained at higher pH with does not really fit with the proposed mechanism. Indeed, the mechanism is based on the formation of the diazoether from ascorbate ion which can eventually decompose and give aryl radicals. Therefore at acidic pH, this reaction should not occur. These phenomenon could potentially be explained by a modification of the counter-ion of the diazonium salt.

To sum up, we have observed an unexpectedly thick PHEMA films when working in buffer solutions but this behaviour remains very unclear.

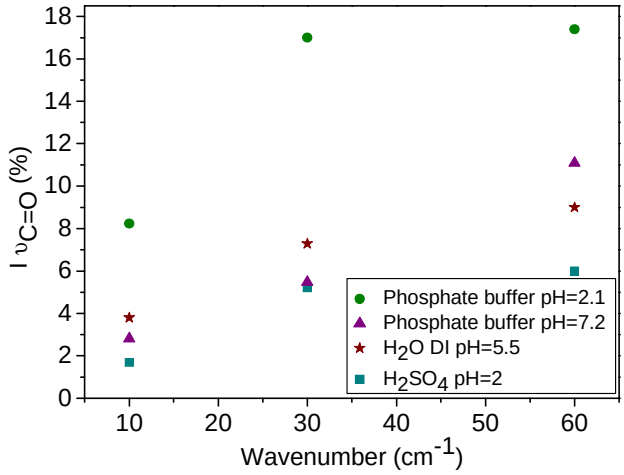

Figure 1 – IR intensity of the $\nu_{C=O}$ band of Graftfast™ PHEMA films (NBDT 0.046 M (1 eq), VC 1/10 eq, HEMA 15 eq, 60 min) with reaction time and according to the solvent used (H_2O DI, H_2SO_4 10^{-3} M, phosphate buffer solution of pH 2.1 and 7.2).

Abstract

In this work, three surface functionalization processes have been studied: the spontaneous grafting from diazonium salts, the chemically induced grafting from diazonium salts and the chemically induced grafting from diazonium salts in presence of vinylic monomers (which is Graftfast™). These processes work at room temperature, atmospheric pressure, in aqueous medium and without any external energy source ("green" chemistry). They lead to the formation of organic films (in particular polymer films in the case of the Graftfast™ process), stable, strongly grafted and with a controlled thickness (chemically activated processes). Contrary to diazonium salt electrografting methods, the reaction can occur on any type of substrate from insulators to conductors including nanomaterials. The so-modified surface can show new properties (for instance water-repellency or protection against corrosion) which is of a major interest in some industrial fields.

The main objective of this work was to understand the grafting mechanism of those processes, especially of the Graftfast™ process, by studying the chemical composition of the films, their structure as well as the composition of the reactive solution. As for classical radical chain polymerization, the mechanism can be split in three steps: initiation, propagation, termination. The polymerization is initiated by aryl radicals in solution coming from the chemical reduction of the diazonium salts (outer-sphere or inner-sphere mechanism according to the reducing agent used). In parallel, aryl radicals can graft to the surface of the substrate and form an essential polyphenylene primer-layer. The propagation stops when the growing polymer chains react on the aromatic rings already grafted on the substrate (termination step). It results an aryl groups/polymers mixed structure of the films. The Graftfast™ process has been notably tested with a view to improve the dispersion of nano-objects in water in the framework of a preliminary study on sunscreens containing TiO_2 nanoparticles.

Key words: Surface functionalization, radical polymerization, aryldiazonium salts, redox activation, polymer films, titanium dioxide nanoparticles.

Résumé

Au cours de ce travail, trois procédés de fonctionnalisation de surface à partir de sels de diazonium ont été étudiés, à savoir : un procédé spontané, un procédé activé chimiquement et le procédé appelé Graftfast™ (activation chimique en présence de monomères vinyliques). Ces procédés, dits de chimie verte, fonctionnent à température ambiante, pression atmosphérique, en milieu aqueux et sans apport extérieur d'énergie. Ils conduisent à la formation de films organiques (notamment de polymères dans le cas du procédé Graftfast™) stables, greffés de manière covalente et d'épaisseur contrôlée (procédés activés chimiquement). Contrairement aux méthodes d'électrogreffage de sels de diazonium, ces procédés peuvent s'appliquer à tout type de substrats allant des isolants aux conducteurs en passant par les nanomatériaux. Le substrat ainsi modifié peut présenter de nouvelles propriétés (par exemple d'hydrophilie, de protection contre la corrosion, …) ce qui est d'un intérêt majeur dans certaines problématiques industrielles.

L'objectif majeur de ce travail a été de comprendre les mécanismes réactionnels de ces trois procédés et plus particulièrement du procédé Graftfast™ en étudiant la composition chimique des films, leur structure mais aussi la composition des solutions réactionnelles. Comme pour une polymérisation radicalaire en chaîne conventionnelle, le mécanisme réactionnel du procédé Graftfast™ (cas le plus complexe) procède en trois étapes : amorçage, propagation, terminaison. La polymérisation est amorcée par les radicaux aryles en solution, issus de la réduction chimique des sels d'aryldiazonium (mécanisme en sphère interne ou en sphère externe selon le réducteur chimique). Parallèlement, les radicaux aryles peuvent se greffer à la surface du substrat et former une sous-couche d'accroche de polyphenylene jouant un rôle essentiel dans la construction des films. La propagation s'achève lorsque les chaînes polymères en croissance réagissent par des réactions de transfert sur les noyaux aromatiques déjà greffés sur le substrat (étape de terminaison). Les films obtenus sont alors de structure mixte : groupements aryles, polymères. Ce procédé a notamment été testé dans le but d'améliorer la dispersion des nano-objets dans l'eau, dans le cadre d'une étude préliminaire sur les crèmes solaires à base de nanoparticules de dioxyde de titane.

Mots clés : Fonctionnalisation de surface, polymérisation radicalaire, sel de diazonium aromatique, activation redox, films polymères, nanoparticules de dioxyde de titane.